

Final Report

FDOT Contract No.: BDK75-977-41

UF Contract No.: 91977

Field Testing of Jet-Grouted Piles and Drilled Shafts



Principal Investigators: Michael C. McVay

David Bloomquist

Primary Researcher: Sudheesh Thiyyakkandi

Department of Civil and Coastal Engineering
Engineering School of Sustainable Infrastructure and Environment
University of Florida
P.O. Box 116580
Gainesville, Florida 32611-6580

Developed for the



Project Managers: Rodrigo Herrera, P.E., Peter Lai, P.E. (Retired)

January 2014

DISCLAIMER

The opinions, findings, and conclusions expressed in this publication are those of the authors and not necessarily those of the Florida Department of Transportation or the U.S. Department of Transportation.

Prepared in cooperation with the State of Florida Department of Transportation and the U.S. Department of Transportation.

SI (MODERN METRIC) CONVERSION FACTORS (from FHWA)

APPROXIMATE CONVERSIONS TO SI UNITS

SYMBOL	WHEN YOU KNOW	MULTIPLY BY	TO FIND	SYMBOL
LENGTH				
in	inches	25.4	millimeters	mm
ft	feet	0.305	meters	m
yd	yards	0.914	meters	m
mi	miles	1.61	kilometers	km

SYMBOL	WHEN YOU KNOW	MULTIPLY BY	TO FIND	SYMBOL
AREA				
in²	square inches	645.2	square millimeters	mm ²
ft²	square feet	0.093	square meters	m ²
yd²	square yard	0.836	square meters	m ²
ac	acres	0.405	hectares	ha
mi²	square miles	2.59	square kilometers	km ²

SYMBOL	WHEN YOU KNOW	MULTIPLY BY	TO FIND	SYMBOL
VOLUME				
fl oz	fluid ounces	29.57	milliliters	mL
gal	gallons	3.785	liters	L
ft³	cubic feet	0.028	cubic meters	m ³
yd³	cubic yards	0.765	cubic meters	m ³

NOTE: volumes greater than 1000 L shall be shown in m³

SYMBOL	WHEN YOU KNOW	MULTIPLY BY	TO FIND	SYMBOL
MASS				
oz	ounces	28.35	grams	g
lb	pounds	0.454	kilograms	kg
T	short tons (2000 lb)	0.907	megagrams (or "metric ton")	Mg (or "t")

SYMBOL	WHEN YOU KNOW	MULTIPLY BY	TO FIND	SYMBOL
TEMPERATURE (exact degrees)				
°F	Fahrenheit	5 (F-32)/9 or (F-32)/1.8	Celsius	°C

SYMBOL	WHEN YOU KNOW	MULTIPLY BY	TO FIND	SYMBOL
ILLUMINATION				
fc	foot-candles	10.76	lux	lx
fl	foot-Lamberts	3.426	candela/m ²	cd/m ²

SYMBOL	WHEN YOU KNOW	MULTIPLY BY	TO FIND	SYMBOL
FORCE and PRESSURE or STRESS				
Lbf[†]	poundforce	4.45	newtons	N
kip	kip force	1000	pounds	lbf
lbf/in²	poundforce per square inch	6.89	kilopascals	kPa

APPROXIMATE CONVERSIONS TO SI UNITS

SYMBOL	WHEN YOU KNOW	MULTIPLY BY	TO FIND	SYMBOL
LENGTH				
mm	millimeters	0.039	inches	in
m	meters	3.28	feet	ft
m	meters	1.09	yards	yd
km	kilometers	0.621	miles	mi

SYMBOL	WHEN YOU KNOW	MULTIPLY BY	TO FIND	SYMBOL
AREA				
mm ²	square millimeters	0.0016	square inches	in ²
m ²	square meters	10.764	square feet	ft ²
m ²	square meters	1.195	square yards	yd ²
ha	hectares	2.47	acres	ac
km ²	square kilometers	0.386	square miles	mi ²

SYMBOL	WHEN YOU KNOW	MULTIPLY BY	TO FIND	SYMBOL
VOLUME				
mL	milliliters	0.034	fluid ounces	fl oz
L	liters	0.264	gallons	gal
m ³	cubic meters	35.314	cubic feet	ft ³
m ³	cubic meters	1.307	cubic yards	yd ³

SYMBOL	WHEN YOU KNOW	MULTIPLY BY	TO FIND	SYMBOL
MASS				
g	grams	0.035	ounces	oz
kg	kilograms	2.202	pounds	lb
Mg (or "t")	megagrams (or "metric ton")	1.103	short tons (2000 lb)	T

SYMBOL	WHEN YOU KNOW	MULTIPLY BY	TO FIND	SYMBOL
TEMPERATURE (exact degrees)				
°C	Celsius	1.8C+32	Fahrenheit	°F

SYMBOL	WHEN YOU KNOW	MULTIPLY BY	TO FIND	SYMBOL
ILLUMINATION				
lx	lux	0.0929	foot-candles	fc
cd/m ²	candela/m ²	0.2919	foot-Lamberts	fl

SYMBOL	WHEN YOU KNOW	MULTIPLY BY	TO FIND	SYMBOL
FORCE and PRESSURE or STRESS				
N	newtons	0.225	poundforce	lbf
kPa	kilopascals	0.145	poundforce per square inch	lbf/in ²

*SI is the symbol for International System of Units. Appropriate rounding should be made to comply with Section 4 of ASTM E380. (Revised March 2003)

TECHNICAL REPORT DOCUMENTATION PAGE

1. Report No.	2. Government Accession No.	3. Recipient's Catalog No.	
4. Title and Subtitle Field Testing of Jet-Grouted Piles and Drilled Shafts		5. Report Date January 2014	
		6. Performing Organization Code	
7. Author(s) Michael C. McVay, David Bloomquist, and Sudheesh Thiyyakkandi		8. Performing Organization Report No.	
9. Performing Organization Name and Address University of Florida – Dept. of Civil and Coastal Engineering Engineering School of Sustainable Infrastructure & Environment 365 Weil Hall – P.O. Box 116580 Gainesville, FL 32611-6580		10. Work Unit No. (TRAIS)	
		11. Contract or Grant No. BDK75-977-41	
12. Sponsoring Agency Name and Address Florida Department of Transportation 605 Suwannee Street, MS 30 Tallahassee, FL 32399		13. Type of Report and Period Covered Final Report 02/02/2011 – 3/01/14	
		14. Sponsoring Agency Code	
15. Supplementary Notes			
16. Abstract A field study of deep foundations supporting high mast lighting and signage was undertaken in typical Florida soils. Three drilled shafts (48 in x12 ft and two 48 in x18 ft) and two jet-grouted piles (28 in x18 ft) were constructed in Keystone Heights, and subject to axial as well as combined lateral with torsional loading. In the case of combined loading, a heavy-duty mast arm equivalent to FDOT's E7-T6 type was placed on the top of each foundation and loaded with a crane. In situ as well as laboratory data were collected for the sand, silt, and clay layers to measure properties in order to predict capacities (axial and torsional) based on FDOT (ω) and FHWA (β and rational) methods. In the case of the axially loaded drilled shafts, FHWA's rational approach agreed the closest to measured results, followed by FHWA's β method (<20% difference); however, for combined loading (lateral and torque), FHWA's β method was the closest (<12% difference), followed by rational approach (<40% difference). It was noted under combined loading that the short shaft underwent lateral and rotational failure, and one of the longer shafts had rotation failure in combination with nonlinear lateral response. Both of the jet-grouted piles were side grouted, followed by tip grouting to have lateral dimensions similar to the drilled shafts. The piles could not be failed axially with top-down testing due to pullout failure of the 40-ft reaction shafts. Under combined loading, the jet-grouted piles had 3 times the capacity of the drilled shafts (<3 ⁰ of rotation) when loading was stopped (capacity of mast arm). A Statnamic axial capacity of 1000 kip was obtained for one of the piles, of which 450 kip was skin friction. Both torsional and axial skin friction of the piles were predicted based on pressuremeter testing, as well as observed grout pressures during construction. A comparison with similar capacity drilled shafts showed that the jet-grouted piles were 20% to 40% more economical.			
17. Key Words Jet-grouted pile, Drilled shaft, Top-down load test, Mast arm, Combined torsion-lateral load test, Lateral load test, Statnamic load test, Skin, Tip, and Total Resistance		18. Distribution Statement No restrictions.	
19. Security Classif. (of this report) Unclassified	20. Security Classif. (of this page) Unclassified	21. No. of Pages 309	22. Price

ACKNOWLEDGMENTS

The researchers would like to thank the Florida Department of Transportation (FDOT) for the financial support to carry out this research, as well as the input of the project managers for its successful outcome. In addition, this research would not have been completed without the help of the State Materials Office (SMO). SMO officials were kind enough to conduct all the in situ tests (SPT, CPT, DMT, PMT), laboratory tests (classification tests, direct shear test, UU test, etc.), CSL tests on drilled shafts, as well as noise and vibration monitoring during jetting and grouting. They also provided water for pile jetting and grouting and offered assistance with all the load test program. The researchers are thankful to FDOT District 2 engineers for allowing use of their site for the test program and conducting the drilled shaft inspection. The researchers would like to recognize Applied Foundation Testing, Inc., for performing grouting and Statnamic load testing without being charged for their service and equipment. Finally, the researchers are grateful to Loadtest, Inc. (Gainesville, FL), for lending various instruments (digital levels, string pots, in-place inclinometers, etc.) for axial, lateral, and combined lateral-torsional load testing.

EXECUTIVE SUMMARY

This research reports on a 2 ½-year field study of deep foundations that support FDOT's high mast lighting, signage, etc., which are subject to (1) axial and (2) combined lateral and torsional loading. In urban areas, the typical foundation of choice has been drilled shafts (reduced vibration and noise); however, a new jet-grouted pile system was also evaluated. It has a number of distinct advantages: (1) the reinforced precast concrete member eliminates the quality uncertainty issues inherent in cast-in-place drilled shafts; (2) jetting minimizes noise and vibration of driven piles installation; (3) grouting maximizes the skin and tip resistance; and (4) tip grouting of the pile not only increases tip resistance, but provides a proof test from which higher LRFD ϕ factors may be used in design. Of interest with jet-grouted piles was (1) constructability, (2) capacity vs. design resistance and (3) cost vs. conventional drilled shafts. Additionally, a revised FDOT design method for drilled shaft foundations subject to torque and lateral loading was also evaluated based on measured drilled shaft field response.

This research started with the design of two 28-in square x 18-ft-deep (with two 48-in diameter side grout zones) jet-grouted piles to sustain the lateral and torsion loading for an FDOT E7-T6 mast arm assembly under a design wind speed of 130 mph. A similar size drilled shaft (4-ft diameter x 18 ft deep), as well as a shorter shaft (4-ft diameter x 12 ft deep) was also designed for comparison with similar loading and soil condition. Next, all the foundations (jet-grouted and drilled shafts) were installed by an FDOT-approved contractor (Reliable Constructors, Inc., Mount Dora, FL). Then a heavy-duty mast arm was designed and constructed for the combined torsion and lateral load testing of piles/shafts. Subsequently, testing was performed on the foundations by applying a lateral load on the mast arm by pulling with a crane.

In the case of the jet-grouted piles, the reaction system (4 ft diameter x 40-ft-deep drilled shafts) used for the static top-down load testing was found not able to reach the ultimate capacity of jet-grouted piles. Consequently, a Statnamic load test was conducted on one of the jet-grouted piles to obtain the ultimate axial resistance (1200 kip). Similarly, the combined torsion and lateral loading of both piles had to be stopped before reaching the failure state due to the capacity of the crane's winch cable and/or the structural capacity of mast arm assembly.

The top-down load testing showed that the axial capacity of jet-grouted pile was more than three times that of drilled shafts with the same diameter and length. Similarly, the torsional resistance of the piles was found to be more than 2.5 times of the ultimate torsional capacity of the drilled shafts. The study also considered the effect of loading sequence on the axial and torsional response of the jet-grouted piles (i.e., first axial, then torsion on pile 1 and vice versa on pile 2). However, it was observed that the influence of prior loading was negligible, if any, in both axial and torsional loading scenario. The estimate of axial or torsional side resistance for the jet-grouted pile was found to be in general agreement with the predictions based on (1) K_g method, (2) pressuremeter method, or (3) construction tip grout pressure data.

Combined torsion and lateral load testing of three drilled shafts (two 4-ft diameter x 18 ft deep and one 4-ft diameter x 12 ft deep) was conducted to validate FDOT and FHWA design approaches. For all the shafts, the test was continued until failure; the shorter shaft (12 ft deep) failed by combined rotation and translation; whereas 18-ft-deep shafts had a rotational mode of failure. A comparison of measured torsional resistance with FDOT design methods revealed that the revised method overpredicts the torsional capacity by 25-45%. O'Neill and Hassan's (1994) beta (β) method is found to predict the torsional resistance very well, while the rational method (Brown et al., 2010) predictions were in the range of 1.2 to 1.7 times the measured values.

In addition to the axial and torsional resistance, the lateral resistance of jet-grouted pile was also found to be greater than that of a similarly sized drilled shaft. It is believed that the greater lateral stiffness of the pile was attributed to the increased stiffness of soil surrounding the pile due to grouting, as well as stiffness contribution of the pile cap. Finally, a cost of comparison of jet-grouted piles vs. equivalent capacity drilled shafts revealed that the jet-grouted piles vary from 30% to 80% the cost of a drilled shaft with similar load resistance.

It was also found that FDOT Index No. 17743, which calls for a 4-ft diameter x 18-ft-long drilled shaft to support an E7-T6 mast arm subject to 130 mph wind speed, was unconservative. However, a similarly dimensioned jet-grouted pile under small rotations ($< 3^\circ$) was capable of supporting the E7-T6 mast arm assembly at 140 mph wind speeds. Consequently, based on capacity as well as cost, the research supports the use of jet-grouted piles for FDOT pole/mast arm structures in typical Florida soils (silts and+ sands).

TABLE OF CONTENTS

	<u>page</u>
DISCLAIMER	ii
SI (MODERN METRIC) CONVERSION FACTORS (from FHWA).....	iii
TECHNICAL REPORT DOCUMENTATION PAGE	v
ACKNOWLEDGMENTS	vi
EXECUTIVE SUMMARY	vii
LIST OF TABLES	xiv
LIST OF FIGURES	xvii
1. INTRODUCTION	1
1.1 Background.....	1
1.2 Objective and Supporting Tasks.....	3
1.2.1 Construction of reaction drilled shafts and test drilled shafts	4
1.2.2 Combined torsion and lateral load testing on drilled shafts	4
1.2.3 Top-down axial compression testing of the 4 ft x18 ft drilled shaft	5
1.2.4 Design and construction of jet-grouted piles.....	5
1.2.5 Field installation of jet-grouted piles.....	6
1.2.6 Combined torsion and lateral load testing on jet-grouted piles.....	6
1.2.7 Top-down axial compression testing of the jet-grouted piles	7
1.2.8 Lateral load testing on drilled shaft and jet-grouted pile.....	7
1.2.9 Cost comparison of jet-grouted piles vs. drilled shafts	8
1.2.10 Statnamic load testing of jet-grouted pile.....	8
2. LITERATURE REVIEW	9
2.1 Past Studies on Jet-grouted Piles	9
2.2 Foundation for Mast Arm Assemblies Supporting Highway Signs and Signals.....	18
2.3 Unit Skin Friction of Drilled Shafts Using In Situ Test Results.....	24
2.3.1 SPT-Based methods.....	25
2.3.1.1 O’Neill and Hassan (1994) method.....	25
2.3.1.2 Rational method (Brown et al., 2010).....	26
2.3.2 Alpha (α) method for cohesive soils.....	27
2.3.4 CPT based direct methods	28
2.3.4.1 Aoki and Velloso's method	29
2.3.4.2 LCPC method.....	29
2.3.4.3 UIUC method (Alsamman 1995).....	30
2.4 Methods for Estimating Torsional Capacity of Drilled Shafts	32
2.5 Estimation of Lateral Capacity of Drilled Shafts	34

3. SOIL EXPLORATION AT THE TEST SITE.....	36
3.1 In Situ Tests	39
3.1.1 Standard penetration test	39
3.1.2 Cone penetration test	40
3.1.3 Pressuremeter test.....	42
3.1.4 Dilatometer test	44
3.2 Laboratory Tests and Soil Classification.....	45
3.3 Estimation of Soil’s Unit Weight	48
3.4 Estimation of Angle of Internal Friction	50
4. DESIGN AND CONSTRUCTION OF REACTION AND TEST DRILLED SHAFTS.....	54
4.1 Structural Design of Drilled Shafts.....	54
4.2 Design and Fabrication of Embedded Pipe and Flange Section.....	57
4.3 Construction of Reaction Drilled Shafts.....	62
4.3.1 Construction of reinforcing cages, attachment of Dywidag bars, and instrumentation	62
4.3.2 Shaft excavation, reinforcing cage placement, and concreting	66
4.4 Construction of Test Drilled Shafts	71
4.4.1 Instrumentation installed in test drilled shafts.....	71
4.4.2 Shaft excavation	74
4.4.3 Placement of reinforcement cage, concrete, embedded pipe and flange section, and Dywidag bars	76
4.5 Cross-Hole Sonic Logging (CSL) Tests on Test Drilled Shafts.....	80
5. DESIGN AND CONSTRUCTION OF JET-GROUTED PILES.....	84
5.1 Structural Design of the Precast Pile Section	84
5.2 Design and Fabrication of Grout Delivery and Jetting Systems.....	85
5.3 Construction of Precast Piles.....	89
5.4 Preparation of Precast Piles for Jetting.....	94
5.4.1 Flushing of each grout delivery systems to ensure proper function.....	94
5.4.2 Testing the membrane	95
5.4.3 Attaching top and bottom side grout membranes.....	96
5.4.4 Attaching nozzles for jetting/tip grouting system	99
5.4.5 Testing of nozzles to ensure uniform water distribution at tip	99
5.5 Jetting of Piles.....	100
5.6 Design and Construction of Concrete Cap for Jet-Grouted Piles	103
5.6.1 Design of concrete cap	103
5.6.2 Construction of concrete cap.....	107
5.7 Side Grouting of Jetted Piles	111
5.8 Tip Grouting of the Piles	115
5.9 Analysis of Noise and Vibration Data.....	119
5.9.1 Measured noise.....	120
5.9.2 Measured ground surface vibration.....	125

6. AXIAL TOP-DOWN LOAD TESTS ON A DRILLED SHAFT AND JET-GROUTED PILES	129
6.1 Top-Down Static Load Testing of Drilled Shaft	129
6.2 Top-Down Static Load Testing of Jet-grouted Piles	135
6.2.1 Axial load test on jet-grouted pile 1	136
6.2.2 Load test on jet-grouted pile 2	140
6.3 Statnamic Load Testing of Jet-grouted Pile 1	145
6.4 Prediction of Unit Skin Resistance of Jet-grouted Pile	147
6.4. 1 Kg method	147
6.4.2 Using in situ pressuremeter test data	149
6.4.3 Using the measured tip grout pressure	152
6.5 Comparison of the Axial Response of Jet-grouted Piles and Drilled Shafts	154
7. COMBINED TORSION AND LATERAL LOAD TESTS ON DRILLED SHAFTS AND JET-GROUTED PILES	155
7.1 Design and Fabrication of Mast Arm – Pole System and Connections	155
7.2 Combined Torsion and Lateral Load Testing of Drilled Shafts	157
7.2.1 Combined torsion and lateral load test on TS1	157
7.2.1.1 Setting of mast arm – pole assembly on top of shaft	158
7.2.1.2 Application of lateral load on mast arm at an eccentric distance of 35 ft	162
7.2.2 Combined torsion and lateral load test on TS2 (4-ft diameter x 18 ft long)	164
7.2.3 Combined torsion and lateral load test on TS3 (4-ft diameter x 18 ft long)	171
7.2.4 Comparison of measured and predicted torsional resistance of the test shafts	174
7.3 Combined Torsion and Lateral Load Testing of Jet-GROUTED Piles	177
7.3.1 Combined torsion and lateral load test on JP2	177
7.3.2 Combined torsion and lateral load test on JP1	182
7.3.3 Comparison of measured and predicted torsional resistance of jet-grouted pile	185
7.4 Comparison of the Axial Response of Jet-grouted Piles and Drilled Shafts	186
8. LATERAL LOAD TEST ON DRILLED SHAFT AND JET-GROUTED PILE	189
8.1 Test Setup, Instrumentation, and Loading	189
8.2 Analysis of Results	190
9. COST COMPARISON OF JET-GROUTED PILES VS. DRILLED SHAFTS	193
9.1 Jet-grouted Pile Construction Costs	193
9.2 Drilled Shaft Construction Costs	196
10. SUMMARY AND CONCLUSIONS	198
REFERENCES	206
APPENDIX A: SOIL EXPLORATION DATA	213

APPENDIX B: STRUCTURAL DESIGN OF DRILLED SHAFTS, EMBEDDED PIPE AND FLANGE SECTION, AND CSL RESULTS.....	219
APPENDIX C: STRUCTURAL DESIGN OF PRECAST PILE AND CONCRETE CAP	240
APPENDIX D: PREDICTION OF SKIN RESISTANCE OF DRILLED SHAFT	259
APPENDIX E: PREDICTION OF TORSIONAL RESSITANCE OF DRILLED SHAFTS AND JET-GROUTED PILES	272

LIST OF TABLES

<u>Table</u>	<u>page</u>
Table 2-1. Mast arm type and corresponding drilled shaft dimensions used in Florida.....	20
Table 2-2. α values for different soil types	29
Table 2-3. Friction coefficient, α_{LCPC} (Bustamante and Gianeselli, 1982).....	30
Table 2-4. Equations for f_s (after Alsamman, 1995).....	32
Table 3-1. Pressuremeter limit pressures for jet-grouted pile locations	44
Table 3-2. Unit weight estimation at the test piles and shafts locations using different approaches.....	51
Table 3-3. Correlations for peak friction angle prediction	52
Table 3-4. Shear parameters at the test piles and shafts locations	53
Table 4-1: Moments and load on the foundation top for E7-T6 mast arm assembly at a wind speed of 206 mph.....	55
Table 4-2. Design capacity of 24-in diameter x 0.625-in-thick HSS pipe.....	58
Table 4-3. Measured range of properties of bentonite slurry.....	67
Table 4-4. Measured properties of fresh concrete	69
Table 4-5. 28 th day compressive strength	70
Table 4-6. Measured range of properties of bentonite slurry (test shafts).....	75
Table 4-7. Properties of new concrete mix	77
Table 4-8. Measured properties of fresh concrete	77
Table 4-9. Measured 28 th day compressive strength (test shafts).....	79
Table 5-1. Estimation of required jet pipe diameter	88
Table 5-2. Properties of the concrete mix	92
Table 5-3. Measured properties of concrete	92
Table 5-4. Comparison of measured and predicted grout pressures.....	115
Table 5-5 Comparison of the measured and predicted tip grout pressures.....	118

Table 5-6. Limiting velocity suggested by AASHTO Designation R8-81	126
Table 6-1: Unit skin frictions for each segment.....	133
Table 6-2. Comparison of the measured vs. the predicted values	135
Table 6-3. Side resistance using K_g method.....	151
Table 6-4. Estimation of side resistance using the pressuremeter test data	151
Table 6-5. Side resistance using sustained tip grout pressures	153
Table 6-6. Comparison of measured and predicted skin resistance.....	153
Table 6-7: Comparison of unit skin frictions for jet-grouted pile vs. drilled shafts	154
Table 7-1. Dimensions of arm and pole.....	156
Table 7-2. Maximum vertical displacement at the top of shaft	162
Table 7-3. Comparison of measured and predicted torsional resistance	175
Table 7-4. Comparison of measured and predicted torsional resistance	186
Table 7-5. Comparison of forces and moments on the foundation during the load tests	188
Table 9.1. Material cost for the construction of two jet-grouted piles.....	194
Table 9.2. Labor cost for the construction of two jet-grouted piles.....	195
Table 9.3. Pile jetting service cost for two jet-grouted piles	195
Table 9.4. Grouting service cost for two jet-grouted piles	195
Table 9-5. Construction cost for two 4-ft diameter x 18-ft-deep drilled shaft.....	197
Table 9-6. BDR cost estimate for equivalent drilled shaft.....	197
Table 10-1. Comparison of forces and moments on the foundation during the load tests	204
Table D-1. Aoki and Velloso's α values for different soil types	265
Table D-2. LCPC Friction coefficient	267
Table D-3. UIUC equations for unit skin friction.....	270
Table E-1. Torsional resistance using K_g method.....	289
Table E-2. Torsional resistance using pressuremeter data.....	289

Table E-3. Torsional resistance using sustained tip grout pressures290

LIST OF FIGURES

<u>Figure</u>	<u>page</u>
Figure 2-1. Schematic of jet-grouted pile with grout delivery and jetting systems	11
Figure 2-2. Grout delivery systems for the top and bottom zones of pile	13
Figure 2-3. Jet nozzles and side grout membranes attached to piles	13
Figure 2-4. Excavated 16-in-square x 20-ft-long jet-grouted pile	14
Figure 2-5. Mohr’s circle at the failure state (McVay et al., 2009; Thiyyakkandi et al., 2013a)	15
Figure 2-6. Chart for grout vertical stress coefficients, K_g (Source: Thiyyakkandi et al., 2013a)	16
Figure 2-7. Mast arm structures supporting highway signs, signals, and luminaries	19
Figure 2-8. Coordinate system (ref: FDOT Mathcad program: DrilledShaft v2.0).....	19
Figure 2-9. Torque to lateral load ratio for different single mast arm structures.....	21
Figure 2-10: Variation of lateral load capacity with torque to lateral load ratio for different L/D ratios (source: McVay et al., 2003; Hu et al., 2006)	23
Figure 2-11. Design curves for f_s (after Alsamman, 1995).....	31
Figure 2-12. Soil pressure diagram proposed by McVay et al. (2003).....	35
Figure 3-1. Test layout.....	37
Figure 3-2. Location of various in situ tests along with the location of shafts and piles.....	38
Figure 3-3. SPT blow count (N) profiles at the test site	40
Figure 3-4. q_c profiles at the test site	41
Figure 3-5. Shear wave velocity (m/s) profile at the test site	42
Figure 3-6. Pressure-volume curves from PMT at 8.5 ft for two jet-grouted piles	43
Figure 3-7. Pressure-volume curves from PMT at 16 ft for two jet-grouted piles	43
Figure 3-8. Pressure-volume curves from PMT at 16 ft and 24.5 ft for RS2	44
Figure 3-9: Graphical presentation of some of the DMT results	46

Figure 3-10. Typical grain size distributions for different soil at the site.....	47
Figure 3-11. Soil moisture content profiles for all the borings.....	47
Figure 3-12. Soil classification (USC) and N_{60} at the location of jet-grouted piles	48
Figure 3-13. Soil classification (USC) and N_{60} at the location test drilled shafts	49
Figure 4-1. Longitudinal section and cross-section of test drilled shafts with reinforcement details	56
Figure 4-2. Alternative support structure (FDOT project BDK75-977-04, Cook et al., 2010).....	58
Figure 4-3. Assumed linear interaction between torsion and flexure for concrete breakout.....	59
Figure 4-4. Longitudinal, cross-sectional, and isometric view of embedded pipe and flange section	61
Figure 4-5. Fabricated embedded pipe and flange section	62
Figure 4-6. Construction of reinforcing cage.....	63
Figure 4-7. Schematic of reaction drilled shafts with reinforcement and Dywidag bars	64
Figure 4-8. Reinforcing cage with Dywidag bars.....	65
Figure 4-9: Instrumentation on RS2	65
Figure 4-10. Excavating hole for drilled shaft construction	67
Figure 4-11. Desanding the bentonite slurry.....	67
Figure 4-12. Bailing bucket used for cleaning the excavation bottom	68
Figure 4-13. Setting rebar cage in the excavation.....	68
Figure 4-14. Concrete placement.....	69
Figure 4-15. Forming the shaft top with the use of a template	70
Figure 4-16. Schematic of test drilled shaft TS1	72
Figure 4-17. Schematic of test drilled shafts TS2 and TS3	73
Figure 4-18. Location of sister-bar strain gauges in TS2.....	74
Figure 4-19: Completely instrumented test shafts TS2 and TS3	75
Figure 4-20. Lowering reinforcing cage to excavation.....	76

Figure 4-21. Installation of embedded pipe and flange section	78
Figure 4-22. Installation of Dywidag cage within pipe and flange section	79
Figure 4-23. Test site with reaction and test drilled shafts.	80
Figure 4-24. CSL testing setup for test shaft	81
Figure 4-25. Typical CSL results for the test shafts (TS3).....	81
Figure 5-1. Cross-section of precast pile component with reinforcement details.....	85
Figure 5-2. Schematic diagram of jet-grouted pile	86
Figure 5-3. Grout delivery systems for side grouting.....	87
Figure 5-4. Jetting system for jet-grouted pile.....	88
Figure 5-5. Formwork for precast piles	89
Figure 5-6. Reinforcement cage with grout delivery systems, jetting system, and instrumentation	90
Figure 5-7. Reinforcement cage within the formwork ready for concrete placement.....	91
Figure 5-8. Concrete placement.....	93
Figure 5-9. Flushing the grout delivery systems.....	94
Figure 5-10. Failure envelope for direct shear tests on membrane-soil interface.....	95
Figure 5-11. Tension test of membrane strip	96
Figure 5-12. Membrane seamed for side grout zone	97
Figure 5-13. Attaching membrane to pile.....	98
Figure 5-14. Pile after attaching the grout membranes.....	99
Figure 5-15. Pile after attaching nozzles.....	99
Figure 5-16. Nozzle testing.....	100
Figure 5-17. Pile jetting	101
Figure 5-18. Pulling out the casing after jetting and soil backfilled.....	102
Figure 5-19. Schematic of precast concrete cap-pile connection	103
Figure 5-20. Longitudinal and cross-sectional views of concrete cap-pile connection.....	104

Figure 5-21. Longitudinal section and cross-section of concrete cap with reinforcement details	105
Figure 5-22. Formwork for concrete cap	107
Figure 5-23.: Reinforcement cage for concrete cap.....	108
Figure 5-24. Anchor bolt welded to 3.5-in diameter x 3/4-in-thick bearing plate	108
Figure 5-25. Reinforcement cage for caps ready for concrete placement	109
Figure 5-26. Concrete placement for caps	110
Figure 5-27. Precast cap placement and grouting.....	111
Figure 5-28. Grout mixing	112
Figure 5-29. Grout pressure and displacement measurement.....	112
Figure 5-30a. Pile 1, top membrane, measured side grout pressure vs. grout volume	113
Figure 5-30b. Pile 1, bottom membrane, measured side grout pressure vs. grout volume.....	113
Figure 5-30c. Pile 2, Top membrane, measured side grout pressure vs. grout volume	114
Figure 5-30d. Pile 2, Bottom membrane, measured side grout pressure vs. grout volume	114
Figure 5-31. Ground surface crack (pile 2: top bag).....	114
Figure 5-32. Grout mixing and pumping	116
Figure 5-33. Grout pressure and displacement monitoring	116
Figure 5-34. Tip grout pressure versus grout volume pumped.....	117
Figure 5-35. Pile head displacement versus grout volume pumped	118
Figure 5-36. Instrumentation for noise and vibration measurement.....	119
Figure 5-37. Location of construction equipment and vibration and noise monitors.....	121
Figure 5-38. Noise measurement for Pile-2.....	122
Figure 5-39. Noise measurement during pile jetting process	122
Figure 5-40. Location of grout pump and vibration and noise monitors for side grouting	124
Figure 5-41 Noise measurement during side grouting.....	124
Figure 5-42 Noise measurement during tip grouting.....	124

Figure 5-43. Peak particle velocity measurement for pile 2	126
Figure 5-44. Peak particle velocity during jetting process	127
Figure 5-45. Peak particle velocity measurement during side and tip grouting	128
Figure 6-1. Setting reaction beam girders on the top of reaction support stands.....	130
Figure 6-2. Load test setup for the 4-ft diameter x18-ft-long drilled shaft (TS2)	131
Figure 6-3. Hydraulic jack, load cell, digital dial gauges, mirrored scale with wire line reference, and data acquisition using National Instruments device	132
Figure 6-4. Measured strain at various levels within the drilled shaft.....	133
Figure 6-5. Load distribution along the shaft.....	134
Figure 6-6. Load vs. displacement response of the drilled shaft	135
Figure 6-7. Load test setup with all instrumentation	136
Figure 6-8. Pile displacement monitoring instrumentations	137
Figure 6-9. Measured strain at different depths	138
Figure 6-10. Load distribution along the jet-grouted pile 1	139
Figure 6-11. Load-displacement response for the jet-grouted pile	140
Figure 6-12. Test setup for top-down testing of jet-grouted pile 2	141
Figure 6-13. Load distribution along the jet-grouted pile 2.....	143
Figure 6-14. Load-displacement response of JP2.....	144
Figure 6-15. Comparison of load-displacement response of pile 1 and 2	144
Figure 6-16. 500-ton Statnamic testing on jet-grouted pile 1	145
Figure 6-17. Dynamic forces in the jet-grouted pile.....	146
Figure 6-18. Dynamic and static resistance of jet-grouted pile 1.	147
Figure 6-19. Deformed mesh after grouting and displacement profile during top-down loading of jet-grouted pile.....	149
Figure 6-20. Estimation of residual stress from pressuremeter expansion curves.....	152
Figure 6-21. Total load-displacement response of jet-grouted piles and drilled shaft.....	154

Figure 7-1. Arm-pole connection with dimensions	156
Figure 7-2. New mast arm assembly.....	157
Figure 7-3. Setting mast arm assembly on the top of shaft using a crane.....	159
Figure 7-4. Schematic of string pot arrangement.....	159
Figure 7-5. String pot arrangement at the site.....	160
Figure 7-6. Digital level and invar staffs for vertical deformation monitoring	160
Figure 7-7. Axial load vs lateral displacement during the application of dead wt. of mast arm assembly.....	161
Figure 7-8. Applying lateral load to mast arm.....	163
Figure 7-9. Torque vs. rotation during combined torsion and lateral load test.....	164
Figure 7-10. Test shaft after load test	164
Figure 7-11. Total station for rotation and translation measurement.....	166
Figure 7-12. String pot layout and support system.....	167
Figure 7-13. Placement of digital dial gauges	168
Figure 7-14. Combined torsion and lateral loading on the 18-ft-long drilled shaft (TS2).....	168
Figure 7-15. 20-kip capacity load cell used for the test.....	169
Figure 7-16. Torque vs. rotation response of TS2	170
Figure 7-17. Lateral load vs. resultant lateral displacement response of TS2	170
Figure 7-18. Lateral load vs. overturning response of TS2	171
Figure 7-19. Torsional crack and gap after loading.....	171
Figure 7-20. Torque vs. rotation response of drilled shaft.....	172
Figure 7-21. Lateral load vs. resultant lateral displacement response for drilled shaft	173
Figure 7-22. Torque vs. rotation responses for TS2 and TS3.....	173
Figure 7-23. Lateral resistance reduction factor due to torsion for L/D ratio = 3.....	176
Figure 7-24. String pot layout and support system.....	178
Figure 7-25. Application of lateral load on the arm by pulling with a crane.....	179

Figure 7-26. Torque vs. displacement response for JP2	180
Figure 7-27. Lateral displacement components during the load test	180
Figure 7-28. Lateral load vs. resultant lateral displacement	181
Figure 7-29. Torsional cracks and gaps after loading and unloading	182
Figure 7-30. Torsion test on JP 1	182
Figure 7-31. Torque vs. rotation response for jet-grouted pile 1	183
Figure 7-32. Lateral load vs. lateral displacement	184
Figure 7-33. Torque vs. rotation responses for piles 1 and 2	184
Figure 7-34. Lateral load vs. lateral displacement responses JP1 and JP2	185
Figure 7-35. Torque-rotation response of jet-grouted piles and drilled shafts	187
Figure 8-1. Lateral load test setup	190
Figure 8-2. In-place inclinometer installation in the test shaft	191
Figure 8-3. Displacement profile for drilled shaft	191
Figure 8-4. Lateral load vs. lateral displacement responses	192
Figure 10-1. Pile jetting	200
Figure 10-2. Total load-displacement response of jet-grouted piles and drilled shaft	201
Figure 10-3. Comparison of load-displacement response of JP1 and JP2	202
Figure 10-4. Torque-rotation response of jet-grouted piles and drilled shafts	203
Figure 10-5. Lateral load vs. lateral displacement of jet-grouted pile vs. drilled shaft	204
Figure A-1. CPT boring data near JP1	213
Figure A-2. CPT boring data near TS2	214
Figure A-3. Soil classification and uncorrected SPT blow counts at the location of RS1	215
Figure A-4. Soil classification and uncorrected SPT blow counts at the location of RS2	216
Figure A-5. Soil classification and uncorrected SPT blow counts at the location of RS3	217
Figure A-6. Soil classification and uncorrected SPT blow counts at the location of RS4	218

Figure B-1. ACI stress block diagram for 48-in diameter drilled shaft	219
Figure B-2. Concrete breakout failure for embedded pile and flange section in torsion	226
Figure B-3. CSL test results for Test shafts; (a) TS1, and (b) TS2.....	239
Figure C-1. ACI stress block diagram for precast pile	241
Figure C-2. Three dimensional view of concrete cap – pile connection	246
Figure C-3. Concrete breakout failure of anchors in shear	250
Figure C-4. Concrete pryout failure of anchors in shear	252
Figure D-1. Soil properties for the skin resistance prediction of TS2	259
Figure E-1. Soil properties for the torsional resistance prediction of TS1	272
Figure E-2. Soil properties for the torsional resistance prediction of TS2	278

CHAPTER 1 INTRODUCTION

1.1 Background

Jet-grouted precast pile is a new generation of deep foundation, recently developed by the Florida Department of Transportation. The construction of the new pile is accomplished in four distinct stages: (1) Construction of precast concrete pile and preparation for jetting; (2) Jetting of the pile into ground using pressurized water; (3) Side grouting of the pile; and lastly, (4) tip grouting. The use of jetting and grouting techniques overcome the inherent disadvantages of currently used deep foundations. Specifically, the jetting minimizes the noise and vibration as opposed to hammer-driven installation of conventional driven pile; the reinforced precast concrete member eliminates the quality uncertainty issues inherent in cast-in-place drilled shafts and continuous flight auger (CFA) piles; and side and tip grouting significantly improves skin and tip resistance. In addition, tip grouting also provides a proof test from which higher load and resistance factor design (LRFD) ϕ factors may be used in design.

The jet-grouted pile incorporates its own jetting/tip grouting system, i.e., nozzles to minimize water use. In cases of surface limestones or marls, an auger may be used to create the hole. With respect to the grouting system, jet-grouted pile's unique attributes include a novel grout delivery and pressure monitoring system that allows for multiple grouting sessions to ensure specified grout pressures and volumes are achieved adjacent to the pile. In addition, by incorporating micro-fine fly ash, the improved mix design results in an excellent bond of the grout to the pile. Multiple semi-rigid membrane sections attached around the perimeter of the pile confine the grout flow, cause radial expansion of the grout zone and ensure a good bond between grout and pile, i.e., no mixing of grout and soil. In addition, the radial expansion of the

grout develops very high radial stress next to the pile and thus increases the axial and torsional side resistance of the pile.

FDOT research BD545-31 tested small jet-grouted piles (6-in×6-in x 8 ft and 8-in×8-in x 8 ft) in the FDOT's 12 ft \emptyset x 35 ft deep test chamber filled with loose to medium dense Florida silty sands. The piles developed 65 kip & 110 kip of axial capacity or 1.2 ksf of unit skin friction at 5 ft depth vs. 0.62 ksf for driven piles. Moreover the excavated piles showed excellent grout coverage and bonding along entire length of the pile. Also tested was a large pile, 16-in×16-in by 20 ft precast concrete jet-grouted pile which was capable of resisting 450 ft-kip of torque or 1.6 ksf of shear resistance, and the axial top-down load test showed 300 kip of resistance at 0.1-in pile head displacement.

The results of FDOT research showed that jet-grouted piles are an attractive alternative to both driven piles and drilled shaft for FDOT structures (i.e., signage, lighting, walls, etc.). Even though the piles have been tested in a large test chamber environment, they need to be tested under typical field conditions to validate construction as well as design estimates of torsion and axial resistance. In addition, the axial and torsional resistances of the new piles need to be compared with similar sized drilled shafts in the same field condition. It is also of interest to study the influence of test sequence on the axial and torsional resistance of the pile (i.e., 1st torsion test, then axial test and vice-versa) in order to obtain an adequate level of confidence in the constructability and applicability of the pile.

Concurrently, with recent jet-grouted pile research, the FDOT revised the design approach for drilled shaft supporting Mast Arms (FDOT, 2011). An important change was the introduction of the torsional resistance based on the "omega" method. For granular soils, a constant "omega value" ($\omega_{\text{fdot}}=1.5$) is used unlike the FHWA Beta method (O'Neill and Reese,

1999), which uses a depth dependent β value. Note the embedment depth for pole-mast arm foundation is determined as the maximum of the depth to resist overturning (function of lateral loads and moments) and the depth to resist torsion. However, past FDOT laboratory research (i.e., centrifuge study, BC354-09) has revealed that even though the torsional resistance of the shafts was not influenced by lateral load, the shafts' lateral resistance was reduced significantly by torsion. Since the tests were carried out on 30 ft mast arms (i.e., not the longest one; 78 ft), as well as no full scale data on such foundations (i.e., construction issues) are available, full scale field testing is required for further verification. In addition, the static load testings of drilled shafts will identify the actual soil-structure interaction as well as failure mode for verifying the revised design approach and/or modifying the methodology, if necessary.

1.2 Objective and Supporting Tasks

The primary objective of this research was testing the new jet-grouted piles and drilled shafts under typical construction practices and in Florida soil conditions with typical design loads, which includes axial, lateral, and combined torsion and lateral. The specific objectives are as follows:

- Validate design and constructability by performing full scale field installation and load testing (axial, lateral, and combined torsion and lateral) of two identical jet-grouted piles
- Obtain combined torsion and lateral load response of drilled shafts and verify FDOT's revised design approach for drilled shafts supporting Mast arm structures
- Compare axial, lateral, and combined torsion and lateral load response of jet-grouted pile vs. drilled shaft
- Cost comparison of jet-grouted piles vs. drilled shafts

In case of foundation for a standard FDOT Mast arm assembly, the eccentric self-weight of the structure develops axial load and bending moment about the axis perpendicular to arm and the wind loading generates torsion, lateral load, and bending moment about the arm axis

(function of pole height). Consequently, the actual loading scenario could only be simulated by the use of a full scale Mast arm structure. Accordingly, one of FDOT's longest Mast Arm assemblies E7-T6 type (78-ft long; Index No. 17743) was considered for this research. FDOT Design Standards (Index No. 17743) prescribe a 4-ft diameter x 18 ft long drilled shaft to support an E7-T6 Mast Arm assembly. Due to location, FDOT borrow pit in Keystone Heights, Florida was used for the full scale test program.

The following are the specific tasks that were performed as part of the research:

1.2.1 Construction of reaction drilled shafts and test drilled shafts

Four 4 ft x 40 ft and two 4 ft x 55 ft reaction shafts, two 4-ft x 18 ft test drilled shafts and one 4 ft x 12 ft test drilled shaft were constructed for the research. The construction of reaction and test drilled shafts were performed by third party vendor: Reliable Constructors Inc. Due to water table location, the wet construction method with bentonite slurry was used for all the shaft construction. Forty-foot reaction shafts were used to provide resistance during the axial top-down load testing of jet-grouted piles and an 18 ft deep drilled shaft. Two 4 ft diameter x 55 ft deep reaction shafts were used for the FDOT's concurrent research project: BDK-75-977-46.

1.2.2 Combined torsion and lateral load testing on drilled shafts

Combined torsion and lateral load testing of three drilled shafts: two 4 ft x18 ft drilled shafts and one 4 ft x 12 ft drilled shaft, were conducted to identify the actual soil-structure interaction and failure mechanism. The measured results were compared with FDOT's revised design approach as well as other prediction methods reported in literature. Note that two test shafts were of the same size (4 ft diameter x 18 ft deep) to study the influence of prior top-down loading on the torsional resistance of the shaft. Specifically, one 18 ft deep drilled shaft was subjected to top-down load testing before torsion test. Two different length shafts (18 ft and 12

ft) were used to facilitate the verification of the adequacy of a constant ω_{fdot} (1.5, independent of depth) in the FDOT's revised design approach. Test was performed using a heavy duty full-scale mast arm assembly attached to the top of shaft. The lateral load was applied in increments on the mast arm at an eccentric distance of 35 ft from the pole by pulling with a crane. Applied load, and rotation and translation of shaft were monitored throughout the load test. The tests were continued until the failure of shafts. The measured torsional resistance was subsequently compared with predicted values based on representative Florida design approaches.

1.2.3 Top-down axial compression testing of the 4 ft x18 ft drilled shaft

Axial top-down testing of one of the 4 ft x18 ft drilled shafts was also performed. Reaction drilled shafts, along with FDOT load test girders and 1000 ton jack and load cell were used to test the axial capacity of the drilled shaft. The strain gauges installed at various levels within the shaft were continuously monitored during the test and used to separate out skin resistance and tip resistance contributions. The focus of this test was to compare the drilled shaft response to the jet-grouted pile behavior. The test result (skin resistance) was also be used to verify the applicability of various SPT and CPT based prediction methods in typical Florida soil.

1.2.4 Design and construction of jet-grouted piles

Two identical jet-grouted piles were designed and constructed at the test site for axial, lateral, and combined torsion and lateral load test program. The structural element of the pile was 28 in square x 19.5 ft long (18 ft embedment depth) reinforced concrete member. The expected final diameter of membrane (side grout bulb) was 48-in. The standard two membrane system with both an inlet and exit ports for the grout delivery system was considered in conformity with previous research. Sister-bar stain gauges were placed at various levels within piles to separate out skin and tip resistance from total resistance, estimate bending along pile if any, etc. After the

curing, the precast piles were prepared for field installation (i.e., attaching membranes, nozzles, etc.).

1.2.5 Field installation of jet-grouted piles

After construction of the pre-cast pile with jetting, and grout delivery system, the membranes were attached and piles were jetted into the ground at the test site. Water was recirculated throughout the jetting process to minimize the water loss (e.g., percolation, surface flow). The piles were supported in vertical position using a crane and lowered as penetration occurred. After the installation of jet-grouted piles, reinforced concrete cap was placed / constructed at the top of each pile. A precast concrete cap was chosen for one of the jet-grouted piles and a cast-in place cap for the other. This concrete cap was required for transferring the forces and moments from the mast arm structure to the pile during the torsion test. The concrete cap was designed to meet various standard code requirements (ACI 318-08, AASHTO LRFD, AISC 360-05, etc.). After the installation of concrete caps, the piles were grouted in place. First side grouting was performed and after hydration, tip grouting on the piles were performed. One of the advantages of the jet-grouted pile is that tip grouting of the pile tip will always mobilize the axial unit skin friction along the pile shaft. Grout pressure, grout volume pumped, upward displacement of pile, and strain at different levels within the pile were continuously monitored during the grouting process. Noise and ground surface vibration measurement were also undertaken during both jetting and grouting operation.

1.2.6 Combined torsion and lateral load testing on jet-grouted piles

Combined torsion and lateral load testing of jet- grouted piles were performed to determine their response in typical Florida conditions and loading scenarios. Test setups for the jet-grouted piles were the same as that for drilled shafts. The testing sequence was different for

the two piles to identify the influence of loading sequence on the behavior of the piles. That is, for one piles, the torque test was performed before axial load test and for the other vice-versa. The results were compared to predictions based on measured in situ/laboratory soil properties.

1.2.7 Top-down axial compression testing of the jet-grouted piles

Static top-down testing of jet-grouted piles were performed to validate their axial capacity and design estimates in typical soil condition. The test set up for the static top-down testing was the same as that for drilled shaft. One pile was subjected to axial test before torsion and the other only after torsion test to estimate the influence of prior torsional loading on the axial resistance. The pile strains, applied load, and pile top displacement were monitored during the tests. The strain gauge data were used to estimate skin and tip contribution to the total resistance. The measured resistance was then compared with earlier design values. However, the ultimate capacity of both piles could not be obtained from the static load tests due to the pullout failure of reaction drilled shaft. A Statnamic load test on one of the jet-grouted piles was required to determine the ultimate capacity of the pile.

1.2.8 Lateral load testing on drilled shaft and jet-grouted pile

After torsion and axial load testing of drilled shafts and jet-grouted piles, lateral load testing of one of the drilled shafts (4 ft x18 ft) and a jet-grouted pile was performed. The testing of jet-grouted pile and drilled shaft was performed simultaneously using a combined loading/reaction system with dywidag bars. The load was applied at one end (jet-grouted pile) using an hydraulic jack and the applied load was measured using a load cell installed at the other end (drilled shaft). The results were then used to compare the response of jet-grouted piles vs. Drilled shaft.

1.2.9 Cost comparison of jet-grouted piles vs. drilled shafts

To assist with the implementation, a cost comparison of the manufacture and installation of jet-grouted piles vs. drilled shafts was undertaken. The comparison considered all costs: direct costs (labor and materials), and indirect costs (rental, size of equipment, mobilization, demobilization, and cleanup). Since the jet-grouted pile has significantly higher axial and torsional resistance compared to a similar sized drilled shaft, the cost of jet-grouted pile was compared with an equivalent drilled shaft (i.e., similar axial and torsional resistance).

1.2.10 Statnamic load testing of jet-grouted pile

The ultimate capacity or even the Davisson capacity of the side and tip grouted drilled shaft could not be determined from the static top-down load test due to the pullout failure of reaction drilled shafts. FDOT engineers decided that another load test should be performed on the pile to assess its capacity for design purposes. Accordingly, Applied Foundation Testing performed a 500 ton Statnamic Load Test on jet-grouted pile. The ultimate static capacity of the pile was deduced from the measured dynamic force, acceleration data, and strain gauge data. The static load-displacement response was subsequently compared with that of similar sized drilled shafts.

CHAPTER 2 LITERATURE REVIEW

This Chapter reviews past studies on jet-grouted piles and drilled shafts relevant to this research project. Specifically, previous research on the individual and group response of jet-grouted piles, the design methodology for the piles in cohesionless soils, and the behavior of drilled shafts supporting mast arm structures under combined torsion and lateral loading are presented. Different methods used in this study for predicting the ultimate unit skin, torsional, and lateral resistance of drilled shafts utilizing field/ laboratory soil tests data are also discussed.

2.1 Past Studies on Jet-grouted Piles

Jet-grouted piles are a new foundation type recently developed by FDOT and UF utilizing different proven deep foundation installation and improvement techniques (McVay et al. 2009; Lai et al., 2010; McVay et al., 2010; and Thiyyakkandi et al., 2013a). Four distinct stages are involved in the construction of the pile: (1) construction of precast pile with jetting and grout distribution systems (1) jetting of prefabricated pile with the aid of pressurized water; (2) side grouting of the pile; and (3) tip grouting.

Pressurized water jetting is an effective method for installing piles near existing structures, which eliminates the issues of noise and vibrations associated with dynamic pile driving operations (Tsinker, 1988, Gunaratne et al., 1999, Gabr et al., 2004). Jetting assists pile installation in the following ways: (1) the jetting pressure erodes the soil at the tip of the pile; (2) jetting will increase local pore water pressure and hence decrease effective stress, resulting in easier pile penetration; (3) the upward flow of water brings cuttings to the surface as well as lubricates the pile (relieve skin friction) and assists with its downward movement (Tsinker, 1988). Equation (2-1) is the flow rate equation to estimate the water requirements for jetting into sandy soil proposed by Shestopal (1959).

$$\frac{Q}{D} = [530(d_{50})^{1.3}l^{0.5}] + C\pi lk \quad (2-1)$$

Where,

Q = flow rate (m³/hr)

D = pile diameter or width (m)

d_{50} = average size of sand particles (mm)

l = desired submerged length of pile (m)

C = 0.1 for dry sand and 0.017 for saturated sand stratum

$k = (\sum k_n l_n) / l$ = average permeability coefficient (m/ day)

Gunaratne et al. (1999) identified that the lateral load capacity of a jetted pile is considerably less than that of driven pile due to the soil disturbance (stress relief) due to the jetting process. Gabr et al. (2004) has found that pile insertion rate increases with increase in flow velocity for a given flow rate.

Deep foundation grouting has been successfully employed worldwide for the last five decades (Gouvenot and Gabiax, 1975; Stocker, 1983; Bruce, 1986; Plumbridge and Hill, 2001; Mullins et al., 2001; McVay et al., 2009; and Thiyyakkandi et al., 2013b). However most of the past studies were focusing on tip grouting and their effectiveness in improving the tip resistance of deep foundations (Mullins et al., 2001, 2004 and 2006; Ruiz, 2005; Duan and Kulhawy, 2009; Youn and Tonon, 2010; Dapp and Brown, 2010, Dai et al., 2010, Thiyyakkandi et al., 2013b). Joer et al. (1998) developed an apparatus for pile-soil interface grouting. McVay et al. (2009) identified that side grouting of a pile using single-pipe delivery system similar to one developed by Joer et al. (1998) has the following drawbacks: (1) no regrouting possible; (2) very poor bonding between the grout and pile as the grout flows along the least resistant path. Typical

grout mixes used for grouting are cement, sand, and water. Micro-fine materials (e.g., fly ash, bentonite, etc.) are also used to partially replace cement and improve pumpability through small diameter grout delivery pipes.

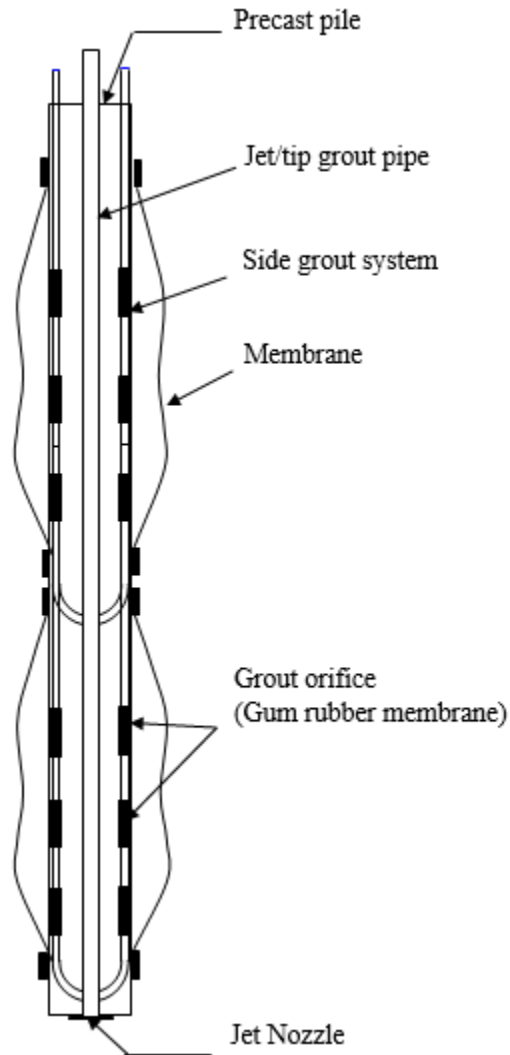


Figure 2-1. Schematic of jet-grouted pile with grout delivery and jetting systems

Figure 2-1 shows the schematic of the jet-grouted pile with grout distribution and jetting systems from McVay et al. (2009). Separate grout distribution systems are used for side and tip grouting. As shown in Figure 2-1, two side grout zones are generally considered along the pile length with their own pipe network for each zone. However, more side grout zones can be

included depending on the length of pile. Each of the side grout pipes has an entry and an exit (U-shaped) to allow staged grouting (Figure 2-2). The grout exits the pipe network through a series of holes drilled into the bottom half of each grout pipe. Note that each pair of holes are covered with gum rubber membranes, which allows the exit of grout under certain minimum pressure and seals the holes while cleaning the pipe network with water for regrouting. A center jetting pipe is used to provide pressurized water at the tip of the pile for jetting/ pile installation. The central pipe is later used for tip grouting. In the case of larger size (width) piles, the jet pipe can be branched off into four or five pipes at bottom for the uniform distribution of water at tip. The nozzle at the end of the jet pipe (Figure 2-3) increases the water velocity as well as minimizes the water consumption during jetting. The nozzle also prevents sand or fines ingress into the jet pipe after jetting, and thus avoiding possible grout blockage during subsequent tip grouting. Most importantly, each side grout zone is surrounded by a high tensile strength membrane attached to the pile, which prevents the grout flow along the weakest path and causes radial expansion of the grout zones by providing confinement. Recall that such radial expansion results in the major principal stress oriented along the horizontal/radial direction. The membranes also prevent the grout-soil mixing and improve the grout-pile interface bonding (McVay et al., 2009; Thiyyakkandi et al., 2013a). Previous studies have shown that the piles have very high axial and torsional resistances (McVay et al., 2009; Lai et al., 2010). It has been reported that the unit skin friction of a jetted and grouted pile is about 5 times that of similar sized drilled shafts (Thiyyakkandi et al., 2013a). Figure 2-4 shows the photograph of the excavated 16-in-square x 20-ft-long jet-grouted pile (McVay et al., 2009; Lai et al., 2010).



(Source: FDOT Report BD545)

Figure 2-2. Grout delivery systems for the top and bottom zones of pile



Small-scale pile



Full-scale pile

(Source: FDOT Report BD545)

Figure 2-3. Jet nozzles and side grout membranes attached to piles



(Source: FDOT Report BD545)

Figure 2-4. Excavated 16-in-square x 20-ft-long jet-grouted pile

Thiyyakkandi et al. (2013b) proposed a design methodology for the jet-grouted piles in cohesionless soils based on the experimental data and finite element modeling. The methodology includes the prediction of the expected grout pressures, the unit skin friction, and the load-displacement response of the piles. According to which, the cylindrical cavity limit pressures and spherical cavity limit pressures at representative depths can be used as reasonable predictors of the expected grout pressures during side and tip grouting respectively.

The approach for estimating unit skin friction was developed based on the stress state adjacent to the pile during the different stages (such as during grouting, after grouting, and axial loading) captured from the experimental study and FEM analysis (Thiyyakkandi et al., 2013a). Since the side grouting resembles a cylindrical cavity expansion, the radial stress (σ_r) becomes the major principal stress and the circumferential or hoop stress (σ_θ) becomes the minor principal stress during grouting. The hoop stress (σ_θ) is close in magnitude to the intermediate or vertical (σ_z) stress. The Mohr circle (σ_1 and σ_3) corresponding to this stress state touches the critical state

failure envelope for the soil. However, the stress state around the pile changes due to elastic unloading immediately after grouting. The elastic unloading causes the radial and vertical stresses to decrease and the hoop stress to increase. Consequently the radial stress becomes the major principal stress and the vertical stress becomes the minor principal stress. The Mohr's circle at this stage is below the failure envelope. Subsequent axial loading diminishes the horizontal stress adjacent to the pile as the principal planes rotate until the failure occurs along vertical plane (Figure 2-5). Recall that the horizontal stress is no longer principal stress. However the magnitude of the minor principal stress is not significantly altered by the mobilization of side resistance during axial loading, i.e., it's approximately equal to the residual vertical stress (σ'_{vg}) after grouting. Shown in Figure 2-5 the Mohr's circle at the failure state and Equation (2-2) gives the magnitude of ultimate unit skin friction for the pile (McVay et. al, 2009; and Thiyyakkandi et al., 2013a).

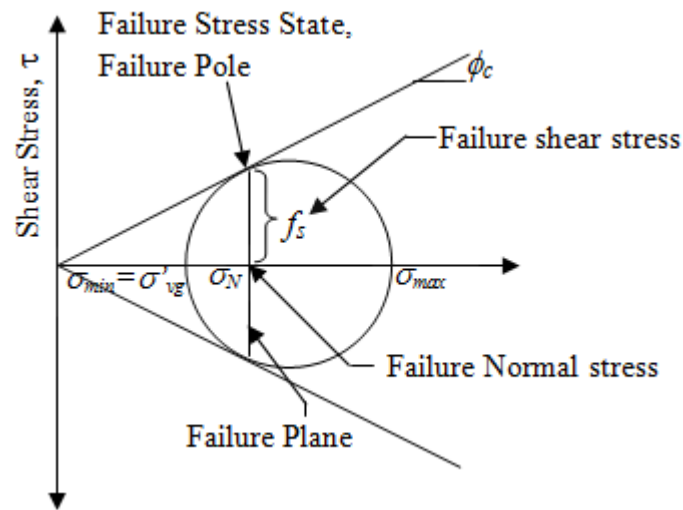


Figure 2-5. Mohr's circle at the failure state (McVay et al., 2009; Thiyyakkandi et al., 2013a)

$$f_s = \sigma'_{vg} \left[\frac{\sin \phi_c}{1 - \sin \phi_c} \right] \sin(90 - \phi_c) \quad (2-2)$$

Where, f_s - ultimate unit skin friction; ϕ_c – critical state friction angle; and σ'_{vg} - vertical effective stress (σ'_{vg}) at the grout-soil interface, which is expressed (Equation 2-3) in terms depth (h), buoyant weight (γ') and the grout vertical effective stress coefficient, K_g .

$$\sigma'_{vg} = K_g \sigma'_{v0} = K_g \gamma' h \quad (2-3)$$

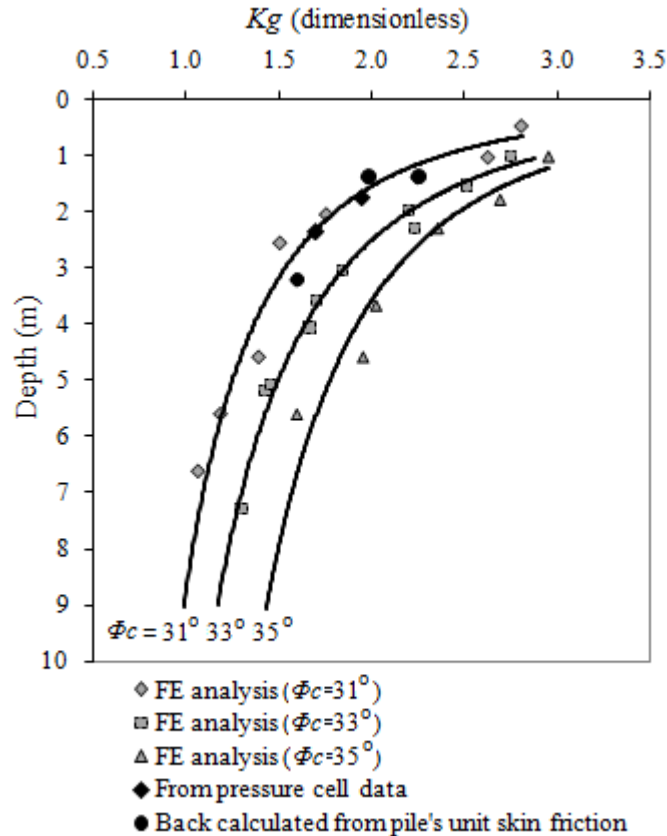


Figure 2-6. Chart for grout vertical stress coefficients, K_g (Source: Thiyyakkandi et al., 2013a)

Figure 2-6 presents the chart for the grout vertical stress coefficients, K_g , for various depths and friction angles (Thiyyakkandi et al., 2013a). Thiyyakkandi et al. (2013a) also suggested a method for predicting the load-displacement response of the pile using the load transfer approach (T-Z and Q-Z curves) following McVay et al. (1989). The load transfer

Equations (2-4, 2-5; McVay et al., 1989) and the ultimate unit tip resistance, q_b , Equation (2-6; Randolph et al. 1994) are given below:

$$T-Z \text{ curve: } Z = \left(\frac{\tau_0 r_0}{G} \right) \left[\ln \left[\frac{r_m - \beta}{r_0 - \beta} \right] + \left[\frac{\beta \cdot (r_m - r_0)}{(r_m - \beta)(r_0 - \beta)} \right] \right] \quad (2-4)$$

$$Q-Z \text{ curve: } Z = \frac{Q(1-\nu)}{4R_0 G \left(1 - Q \frac{R_t}{Q_f} \right)^2} \quad (2-5)$$

$$q_b = [1 + \tan \phi_c \tan(45 + \phi_c/2)] P_L \quad (2-6)$$

Where,

r_0 = radius of pile after grouting (or block radius for group)

r_m = radius of influence zone = $2.5\rho L(1-\nu)$ (Randolph and Wroth, 1978)

L = length of pile

ν = Poisson's ratio

ρ = ratio of G at $L/2$ to G at tip

τ_0 = shear stress on pile-soil interface,

G = shear modulus

$$\beta = r_0 \tau_0 \cdot \frac{R_f}{\tau_{\max}}$$

R_f = ratio of failure shear stress to its ultimate

R_0 = radius of tip bulb (or radius of block foot print for group)

Q = mobilized tip load

R_t = ratio of failure to ultimate tip resistance

Q_f = ultimate tip load

q_b - Ultimate unit tip resistance

P_L - Spherical cavity limit pressure

McVay et al. (2010) conducted the group testing of jet-grouted piles at typical $3D$ spacing (D -precast pile width/diameter) in the large test chamber environment and found that the groups behaves as a single block with uniform displacements within the group footprint during the top-down loading. The side and tip grouting of adjacent piles significantly improves the confining stress and the relative density (hence the shear modulus) of the soil mass within the

group. Consequently very little shear strain is developed within the group with the large shear strain occurring outside the group with the group failing as a single block. The methodology suggested by Thiyyakkandi et al. (2013a) for the single piles was found to reasonably predict the axial load–displacement responses of jet-grouted pile groups (McVay et al., 2010).

All the previous experiments were performed in the large FDOT test chamber. Therefore the capacity as well as the prediction methods for piles had to be verified under typical field conditions at full scale. In addition axial, lateral, and combined torsion and lateral resistance of the pile had to be compared to similar sized drilled shafts in the same field scenario at failure (hurricane) design loads.

2.2 Foundation for Mast Arm Assemblies Supporting Highway Signs and Signals

Based on observed hurricane extreme events, FDOT has moved towards using the cantilever Mast arm structures for supporting highway signs, signal, and luminaries (Figure 2-7) near the coast. In current practice, drilled shaft foundations are used to support such structures. The drilled shaft for a Mast arm structure needs to be designed to safely carry the large torsion and lateral loads developed during a hurricane (high wind velocity) in addition to the moment due to the eccentric dead weight of the structure itself. Specifically, the self-weight of the structure develops axial load, V_y and moment, M_z (about the axis perpendicular to arm) on the foundation. The loading on the Mast arm assembly (wind loading; e.g., hurricane) will produce torsion (T or M_y), lateral load, V_z , and bending moment about the arm axis, M_x (function of pole height). The orientation of the coordinate system considered here is shown in Figure 2-8.



Figure 2-7. Mast arm structures supporting highway signs, signals, and luminaries

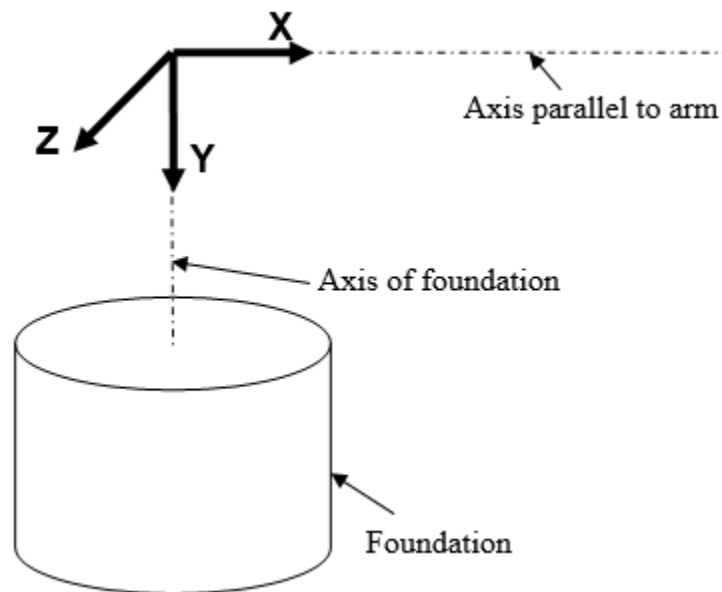


Figure 2-8. Coordinate system (ref: FDOT Mathcad program: DrilledShaft v2.0)

The dimensions of Mast arm assembly (i.e., pole height, arm length, etc.) vary depending on the number of lanes at the highway intersection. Details of the different combinations (Pole type and Arm type) of Mast arm assemblies and the supporting drilled shafts used by FDOT are listed in FDOT Design Standards Index No: 17743. Table 2-1 presents the arm length, pole

height and the drilled shaft dimensions for the different types of single Mast arm assemblies currently used in Florida. FDOT has developed a MathCAD spread sheet (Mastarm v4.3) to determine the forces and moments on the top of the foundations for different Mast arm assemblies under different wind velocities, which is downloadable from the software section of FDOT’s Structures Design website. Estimation of lateral load and torque on the top of foundation for different types of Mast arm assemblies using the Mastarm v4.3 indicates that the ratio of torque to lateral load (unit-ft or m) is nearly constant for any wind velocities above 40-60 mph. Figure 2-9 shows the torque/lateral load ratio vs. wind speed for different types of single Mast arm assemblies. It is evident that the wind loading on a Mast arm structure can be simulated by applying a lateral load on the arm at an eccentric distance (standoff distance) equal to the corresponding torque/lateral load ratio.

Table 2-1. Mast arm type and corresponding drilled shaft dimensions used in Florida

Mast arm assembly type	Arm length (ft)	Pole-Arm connection elevation (ft)	Drilled shaft Dimensions	
			Diameter (ft)	Length (ft)
D1-S1	36	22	3.5	13
D3-S2	46	22	4	13
D5-S3	60	22	4	15
D6-S4	70.5	22	4.5	17
D7-S6	78	22	4.5	15
E1-T1	36	22	3.5	12
E3-T2	46	22	3.5	14
E5-T3	60	22	4	15
E6-T4	70.5	22	4	19
E7-T6	78	22	4	18
F1-W1	36	22	3.5	12
F3-W2	46	22	3.5	14
F5-W3	60	22	4	15
F6-W4	70.5	22	4	19
F7-W6	78	22	4	18

(Source: FDOT Index No: 17743 and FDOT MathCAD spreadsheet: Mastarm v4.3)
D, E, F – Arm type; S – Pole type

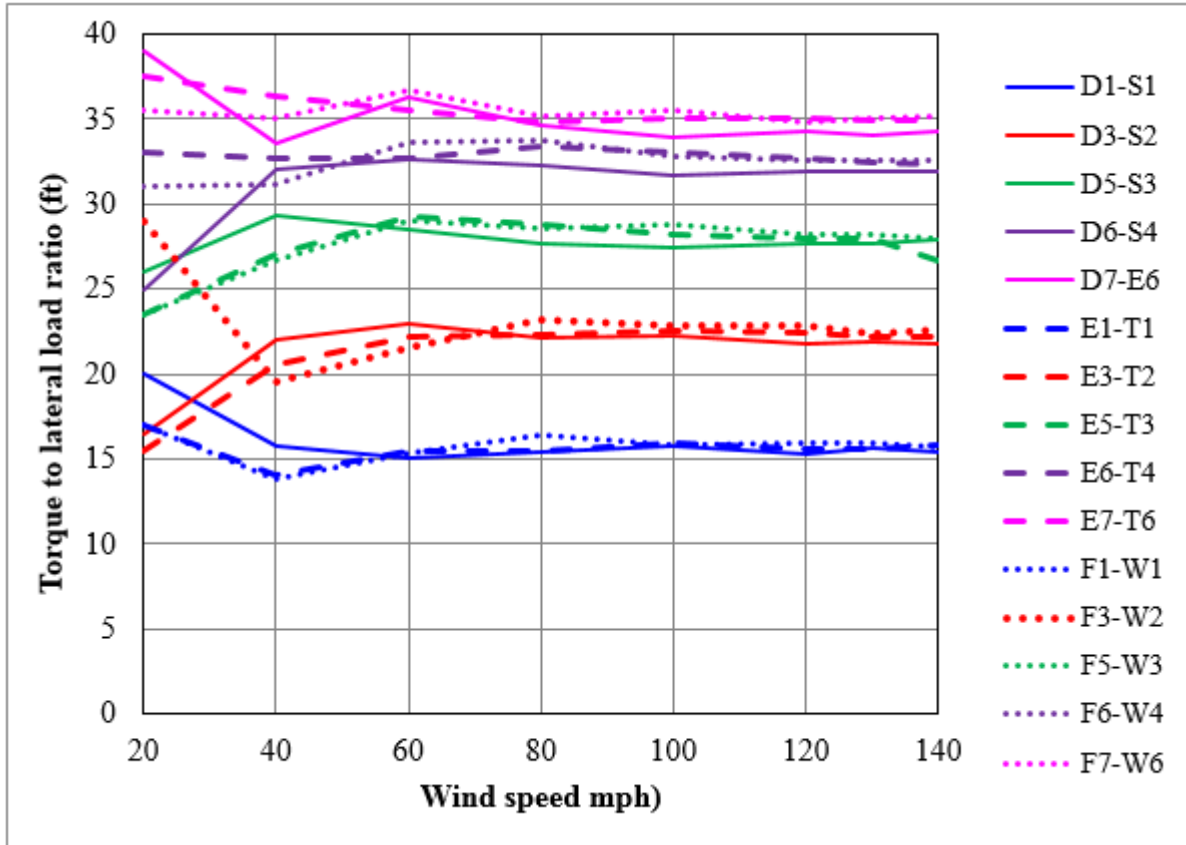


Figure 2-9. Torque to lateral load ratio for different single mast arm structures

Previous field (Tawfiq, 2000) and centrifuge testing (McVay et al., 2003; Hu et al., 2006) of drilled shaft foundations with Mast arm structures identified that the foundations need to be designed for coupled torque-lateral load scenario. Specifically, Tawfiq (2000) conducted three full-scale torsional load tests on drilled shafts constructed using different methods (dry hole, and wet hole with slurry). The drilled shaft constructed using the dry hole method did not fail (i.e., not fully mobilized), whereas the one constructed using wet hole with thick slurry failed at very low torque. The study concluded that the FDOT design methods were conservative and the torsional resistance of the shaft is influenced by the lateral displacement of the shaft caused by the lateral load. Tawfiq (2000) suggested a method to predict the torsional resistance of drilled shaft as a function of lateral displacement using the Subgrade reaction method (Reese and

Matlock, 1956; and Matlock and Reese, 1960). Further field testing was required to confirm repeatability of the results and capture the actual soil-structure interaction to aid the development of an adequate design approach.

McVay et al. (2003) performed centrifuge testing of high mast arm/cantilever signal structures supported on drilled shafts as a part of FDOT research project BC354-09. The tests were conducted at three different length-to-diameter ratios ($L/D = 3, 5, \text{ and } 7$) in both dry and saturated cohesionless soil conditions. Lateral load was applied at one of the three locations: (1) on the pole; (2) at mid-mast arm; and (3) at the mast arm tip. The study showed that laterally loaded short shafts ($L/D \leq 3$) failed due to the soil failure; on the other hand, long shafts ($L/D \geq 7$) failed because of the limited moment capacity of the shaft section (McVay et al., 2003; Hu et al., 2006). The experimental study also revealed that the torsional resistance of the shaft was not influenced by lateral load; whereas the lateral capacity was significantly influenced by the applied torsion and found to be a function of torque-to-lateral-load ratio. A reduction of 50% was observed for high torque to lateral load ratio. Figure 2-10 displays the variation of lateral load capacity with torque to lateral load ratio for different L/D ratios (McVay et al., 2003; Hu et al., 2006). A method to predict the ultimate lateral capacity was suggested using the free earth support approach (Hu et al., 2006). The method is briefly described in Section 2-5 of this chapter. Though the centrifuge model tests can model the stress state, foundation geometry, and different loading conditions appropriately, they fail to incorporate the effect of soil grain size. For that reason, the findings from the centrifuge study require further validation by performing full-scale field tests before implementation.

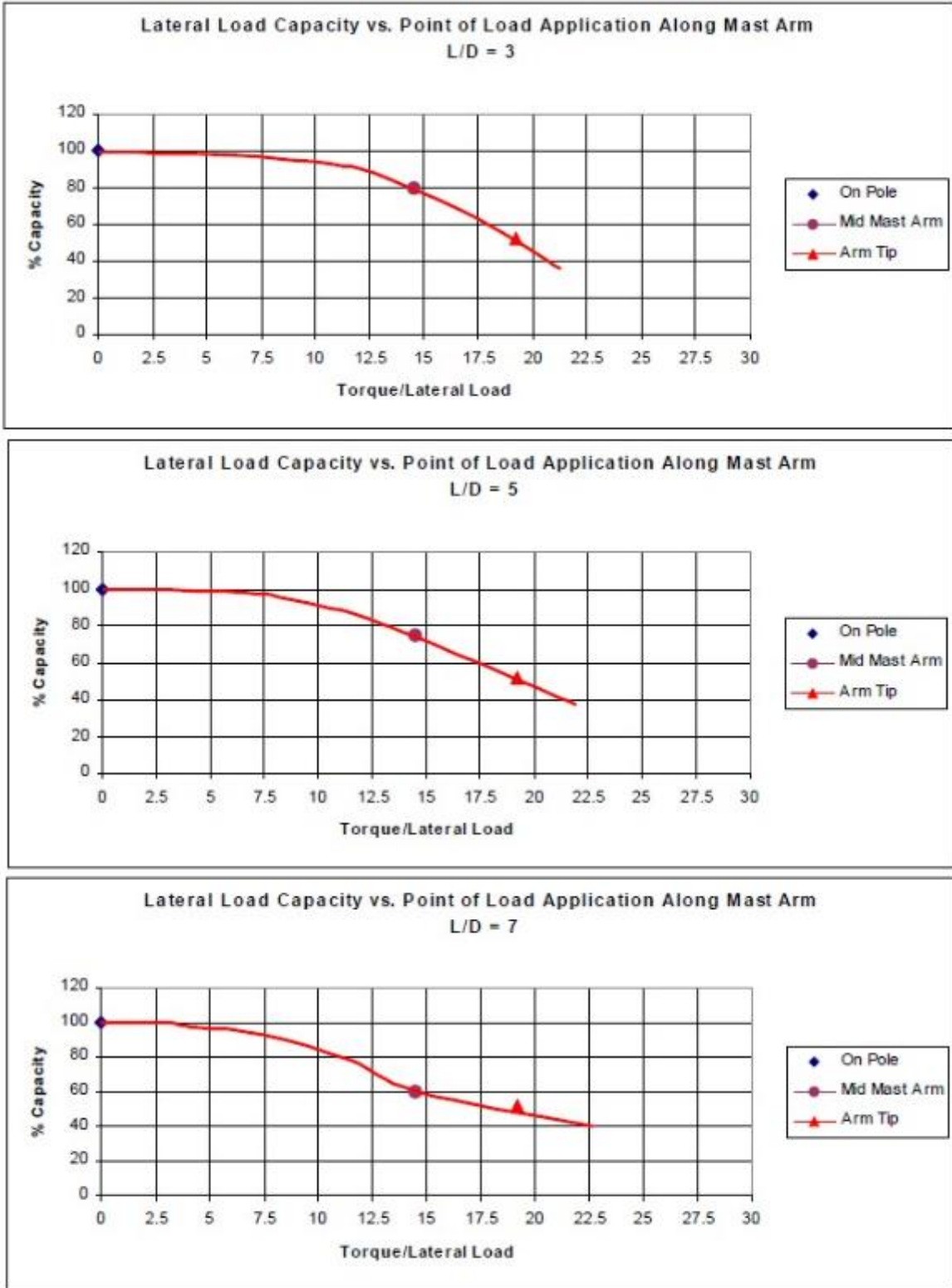


Figure 2-10: Variation of lateral load capacity with torque to lateral load ratio for different L/D ratios (source: McVay et al., 2003; Hu et al., 2006)

Even though past studies suggest that the foundation for such structures should be designed for a coupled case of torque and lateral load, the current practice is still to treat the lateral and torsional load separately due to the lack of further validation. The lateral capacity is estimated using Brom's solution, or p-y curve approach, or continuum analysis (FEM). The lateral load analysis using one of the above methods decides the required shaft diameter and the minimum embedment depth. Then the torsional capacity of the foundation with the minimum embedment depth is compared with design torque. If the design torque exceeds the estimated torsional capacity, the embedment depth is increased.

The majority of failures during the past hurricane events were found to be at the anchor bolt connection between the pole and drilled shafts, with little evidence of the foundation failure (i.e., no shaft-soil interface failure). Consequently, FDOT reviewed the methodology that had been used for determining the embedment depth (FDOT Design Standards), and had the opinion that the method was over conservative. Accordingly, FDOT revised the design approach for economic considerations. The revised approach is known as 'OMEGA (ω)' method, which is discussed later in this chapter. A MathCAD spreadsheet (Drilled Shaft v2.04) based the revised design method is available in the software section of FDOT's Structures Design website. Still, the adequacy of the revised approach had to be verified by observing the field performance of drilled shafts designed using the new approach.

2.3 Unit Skin Friction of Drilled Shafts Using In Situ Test Results

The unit skin friction of drilled shafts in general can be estimated using indirect and direct methods. For indirect methods, the required soil parameters are angle of internal friction, ϕ , coefficient of lateral earth pressure (K), etc., for cohesionless soils and undrained shear strength, S_u for cohesive soils from in situ or laboratory soil tests. Direct methods use empirical

correlations based on in situ soil tests. The most commonly used in situ tests used for the pile design are Standard Penetration Test (SPT) and Cone Penetration test (CPT). There are a large number of methods available for predicting the unit skin resistance of drilled shafts. The methods used in this research are briefly described below:

2.3.1 SPT-Based methods

Based on Coulomb's friction law, unit skin friction (f_s) on a pile/drilled shaft in granular cohesionless materials can be represented as:

$$f_z = \sigma'_{hz} \tan \delta_z = K_z \sigma'_{vz} \tan \delta_z = \beta_z \sigma'_{vz} \quad (2-7)$$

$$\beta_z = K_z \tan \delta_z \quad (2-8)$$

Where, z - depth below ground surface; σ'_{hz} - horizontal effective stress at depth z ; K_z - coefficient of lateral pressure; σ'_{vz} - vertical effective stress at depth z ; δ - interface friction angle at depth z .

Two different beta (β) methods discussed by Brown et al. (2010) are used in this study. The first method is the depth dependent beta method (O'Neill and Hassan method, 1994) and the second is the rational method (Brown et al., 2010).

2.3.1.1 O'Neill and Hassan (1994) method

O'Neill and Hassan method uses a β value, which solely a function of depth, but independent of the soil strength and in situ stress state, except the modification when $N_{60} < 15$. Note, this β value as a function of depth was back-calculated from the field test data. The latest FHWA manual for drilled shaft (Brown et al. 2010) refers to it as 'O'Neill and Reese (1999) method'. The following expressions can be used to estimate β :

For sandy soils:

$$\beta = 1.5 - 0.135\sqrt{z} \quad \text{for } N_{60} > 15, 0.25 \leq \beta \leq 1.2$$

$$\beta = \frac{N_{60}}{15} (1.5 - 0.135\sqrt{z}) \quad \text{for } N_{60} < 15$$
(2-9)

For gravelly sand and gravels:

$$\beta = 2 - 0.06(z)^{0.75} \quad \text{for } N_{60} > 15, 0.25 \leq \beta \leq 1.8$$

$$\beta = \frac{N_{60}}{15} (2 - 0.06(z)^{0.75}) \quad \text{for } N_{60} < 15$$
(2-10)

2.3.1.2 Rational method (Brown et al., 2010)

The rational method uses more fundamental approach to estimate β value. Specifically coefficient of horizontal soil stress (K) and shaft-soil interface angle (δ) are first estimated, which are then combined to obtain the β value. The procedure and equations for estimating unit skin friction using this method are as follows,

- 1) Interface friction angle (δ) is assumed to be equal to the effective stress friction angle of the soil; i.e., $\delta = \phi'$.
- 2) It is assumed that no stress change around shaft occurs due to installation process; i.e., coefficient of lateral stress, $K = K_0$ (coefficient of earth pressure at rest)
- 3) Determine K_0 using the Equation (2-11):

$$K_0 = (1 - \sin \phi') OCR^{\sin \phi'} \leq K_p \quad (2-11) \quad \text{Mayne and Kulhawy (1982)}$$

$$OCR = \frac{\sigma'_p}{\sigma'_v}$$

$$K_p = \tan^2 \left(45 + \frac{\phi'}{2} \right)$$

Where OCR – over-consolidation ratio; K_p – coefficient of passive earth pressure; σ'_p – effective vertical pre-consolidation pressure, which can be obtained by,

For sand or silty sand to sandy silt:

$$\frac{\sigma'_p}{P_a} \approx 0.47(N_{60})^m \quad (2-12) \quad (\text{Mayne, 2007})$$

$m = 0.6$ for clean quartzitic sand; 0.8 for silty sand to sandy silt

For gravelly soils:

$$\frac{\sigma'_p}{P_a} = 0.15N_{60} \quad (2-13) \quad (\text{Kulhawy and Chen, 2007})$$

Where, P_a - atmospheric pressure in the same units as σ'_p

4) Substituting Equation (2-11) into Equation (2-8) yields,

$$\beta = (1 - \sin \phi') \left(\frac{\sigma'_p}{\sigma'_v} \right)^{\sin \phi'} \tan \phi' \leq K_p \tan \phi' \quad (2-14)$$

2.3.2 Alpha (α) method for cohesive soils

This is the well-known method used for drilled shafts in cohesive soils (Brown et al., 2010). According to this method unit skin friction is given by,

$$f_z = \alpha s_{uz} \quad (2-15)$$

Where, s_{uz} – undrained shear strength at depth z ; α - coefficient relating unit skin with undrained shear strength. The value of α is as follows:

$\alpha = 0$, between the ground surface and a depth of 5ft or the depth of seasonal moisture change, whichever is greater.

$\alpha = 0.55$, along remaining portion of shaft for $(s_u/P_a) \leq 1.5$

$\alpha = 0.55 - 0.1 \left(\frac{s_u}{P_a} - 1.5 \right)$, along remaining portion of shaft for $1.5 \leq (s_u/P_a) \leq 2.5$

2.3.4 CPT based direct methods

Past studies by several investigators (Briaud and Tucker, 1988; Tand and Funegard, 1989; Sharp et al., 1988, Lee and Salgado, 1999) have reported that the CPT based prediction methods are normally better than other in situ test based methods for the axial capacity of deep foundations. This is due to the quasi-static nature of the cone penetration test, where a cylindrical penetrometer is pushed in to the ground, which is similar to a static pile load test. Although both cone tip resistance (q_c) and cone sleeve friction (f_{cs}) have been used to predict the unit skin friction, the expressions based on cone tip resistance are most common. General expressions for unit skin friction in terms of q_c and f_{cs} can be expressed as:

$$f_{si} = c_{si} \cdot q_{ci} \quad (2-16)$$

$$f_{si} = c_{sfi} \cdot f_{csi} \quad (2-17)$$

Where c_{si} and c_{sfi} are the reduction coefficients to convert q_{ci} and f_{csi} respectively to unit skin friction for layer i . The need for such reduction coefficient is to take account of the influences of scale effect, loading rate, and the difference of the pile/shaft installation (driving, drilling hole, etc.). The basic difference in the CPT based methods suggested by various investigators is the different values for reduction coefficients (c_s and c_{sf}). In this research, three different methods were used for the predictions, which are described below:

2.3.4.1 Aoki and Velloso's method

Aoki and Velloso (1975) proposed an Equation (2-18) for unit skin friction by correlating the load test results with CPT data at the locations. In the equation, α is the shaft resistance factor depending soil type as given in Table 2-2 and F_2 is function of foundation type. For bored pile (or drilled shafts) F_2 is in the range of 6.0-7.0.

$$f_{si} = \frac{\alpha}{F_2} \cdot q_{ci} \quad (2-18)$$

Table 2-2. α values for different soil types

Soil Type	α (%)	Soil Type	α (%)	Soil Type	α (%)
Sand	1.4	Silt	3.0	Clay	6.0
Silty sand	2.0	Sandy silt	2.2	Sandy clay	2.4
Clayey silty sand	2.4	Clayey sandy silt	2.8	Silty sandy clay	2.8
Clayey sand	3.0	Clayey silt	3.4	Silty clayey	4.0
Silty Clayey sand	2.8	Sandy clayey silt	3.0	Sandy silty clay	3.0

2.3.4.2 LCPC method

LCPC method is the most common CPT method used for estimating deep foundation capacity. This method is suggested by Bustamante and Gianselli (1982), which considers different pile installation methods and soil types. Several researchers (Briaud et al., 1989, Milovic and Milovic, 1993) validated the adequacy of the method for different piles/shafts in different types of soils. Euro-code also recommends this method for pile design. Bustamante and Frank (1997) updated this method with minor changes. The method suggests equations for both side and tip resistance of the piles/shafts in terms of cone resistance (q_c). The expression for unit skin friction can be written as:

$$f_{si} = \frac{q_{ci}}{\alpha_{LCPC}} \quad (2-19)$$

Where, α_{LCPC} is the LCPC friction coefficient and their values for bored piles (drilled shafts) are given in Table 2-3. The value of α_{LCPC} depends on pile and soil types. Table 2-3 also presents maximum recommended f_s values for different soil type.

Table 2-3. Friction coefficient, α_{LCPC} (Bustamante and Gianceselli, 1982)

Nature of Soil	q_c/P_a	α_{LCPC}		Maximum f_s/P_a	
		IA	IB	IA	IB
Soft clay and mud	< 10	30	30	0.15	0.15
Moderately compact clay	10 to 50	40	80	0.35 (0.8)	0.35 (0.8)
Silt and loose sand	≤ 50	60	150	0.35	0.35
Compact to stiff clay and compact chalk	> 50	60	120	0.35 (0.8)	0.35 (0.8)
Soft chalk	≤ 50	100	120	0.35	0.35
Moderately compact sand and gravel	50 to 120	100	200	0.8 (1.2)	0.35 (0.8)
Weathered to fragmented chalk	> 50	60	80	1.2 (1.5)	0.8 (1.2)
Compact to very compact sand and gravel	> 120	150	300	1.2 (1.5)	0.8 (1.2)

Type IA – Plain bored piles, mud bored piles, hollow auger bored piles, cast screwed piles, piers, barrettes, and micropiles installed with low injection pressure

Type IB – Bored piles with steel casing and driven cast piles

P_a - reference stress = 100 kPa. (Bracketed value is used only in the case of careful execution and minimum soil disturbance due to construction)

2.3.4.3 UIUC method (Alsamman 1995)

Alsamann (1995) at University of Illinois at Urbana- Champaign (UIUC) developed correlations for unit skin and tip resistance of drilled shafts using 95 full-scale load test results and the corresponding CPT data. Figure 2-11 shows the design curves for unit skin friction as a function of cone penetration resistance (q_c) for gravelly sand/gravel, sand/silty sand and cohesive soils. Separate curves are suggested for mechanical and electrical cones (Figure 2-11). As shown in the Figure 2-11, f_s values are nearly the same irrespective of the type of cone (mechanical or

electrical) and hence the same set of correlations given in Table 2-4 can be used for both types of cones.

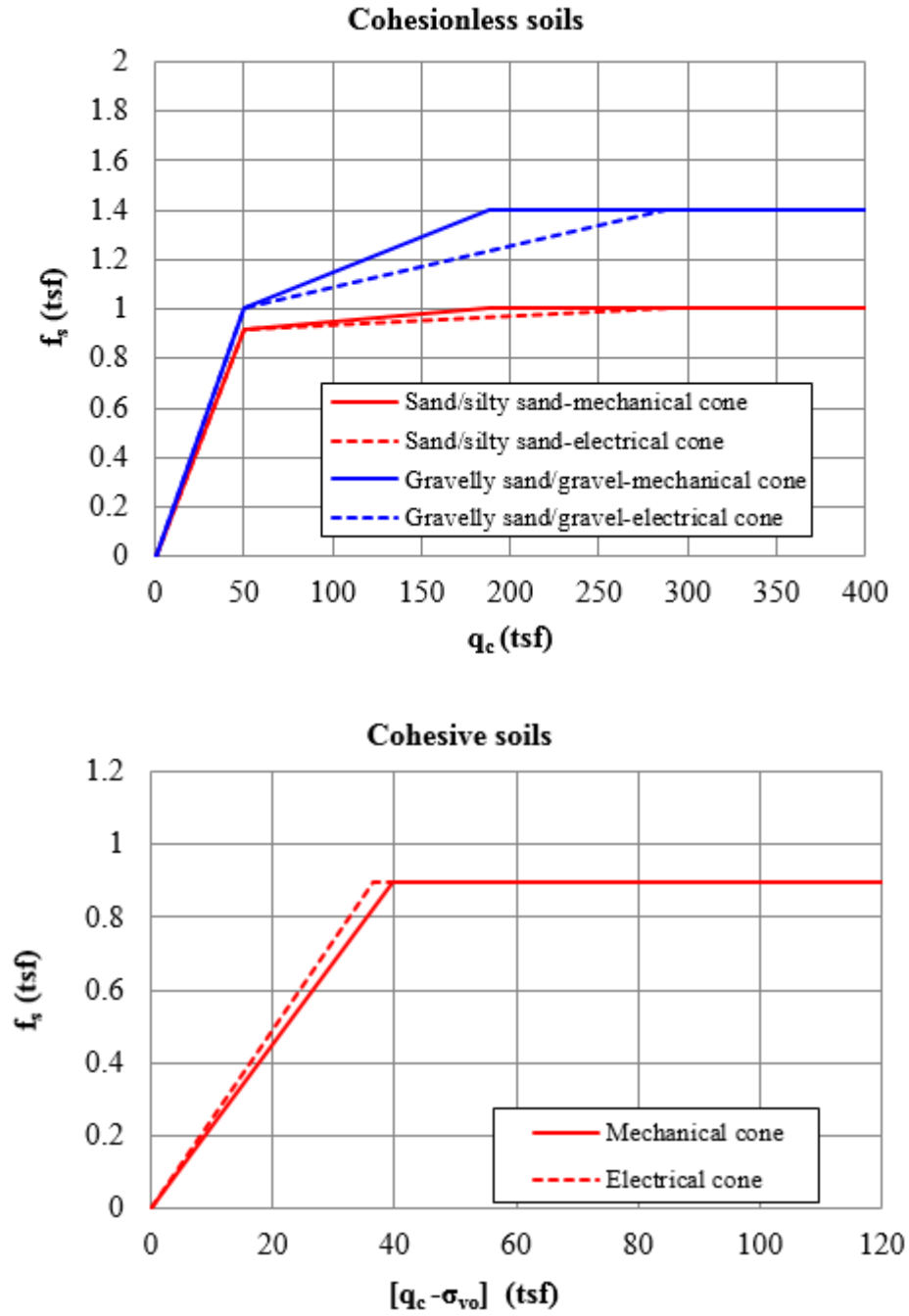


Figure 2-11. Design curves for f_s (after Alsamman, 1995)

Table 2-4. Equations for f_s (after Alsamman, 1995)

Soil type	Ultimate unit skin f_s (tsf)
Gravelly sand / Gravel	$f_s = 0.02 q_c$ for $q_c \leq 50$ tsf $f_s = 0.0019 q_c + 0.9 \leq 1.4$ for $q_c \geq 50$ tsf
Sand / silty Sand	$f_s = 0.015 q_c$ for $q_c \leq 50$ tsf $f_s = 0.0012 q_c + 0.7 \leq 1.0$ for $q_c \geq 50$ tsf
Clay	$f_s = 0.023 (q_c - \sigma_{vo}) \leq 0.9$

2.4 Methods for Estimating Torsional Capacity of Drilled Shafts

Although both side and tip of a drilled shaft contribute to its torsional capacity, the major contribution is from the side resistance (skin friction). Since anomalies may still exist at the shaft tip even after cleanout, increased use of post tip grouting has been observed. Generally, torsional resistance from a shaft's tip should only be accounted when the engineer is confident about the shaft-soil contact at the tip (i.e., no debris or anomalies). Assuming that the diameter of shaft is uniform throughout the length, the torsional resistance due to skin (side) can be expressed as:

$$T_s = \frac{\pi D^2}{2} \int_0^L f_{sz} dz \quad (2-20)$$

Where, f_{sz} – torsional unit skin friction; D - diameter of the shaft; and L - length of the shaft.

Tip contribution of torsional resistance can be obtained using the following equation:

$$T_t = \pi \left(\frac{D}{2}\right)^2 L \gamma_{conc} \left(\frac{D}{3}\right) \tan \delta \quad (2-21)$$

Where, γ_{conc} – unit weight of concrete (in submerged condition use submerged unit weight);

δ – Interface friction angle at tip.

The total nominal torsional resistance is given by

$$T_n = T_s + T_t \quad (2-22)$$

It is reasonable to assume that torsional unit skin friction is equal to the axial unit skin friction (Hu et al., 2006) based on Coulomb friction law and hence the axial unit skin friction predicted using the various methods discussed in previous Section (Section 2.3) could be used to estimate skin contribution of torsional resistance.

As mentioned earlier, FDOT recently revised the methodology for estimating the torsional resistance of drilled shafts supporting Mast arm structures in granular soils, i.e., Equations (2-20) through (2-22) with the following approximations:

- 1) In Equation (2-21), $\delta = \phi_{\text{soil}}$
- 2) In Equation (2-20),

$$f_{sz} = \sigma'_{vz} \omega_{FDOT} \quad (2-22)$$

Where, ω_{FDOT} – load transfer ratio where allowable rotation may exceed 10^0 .

Initially a constant ω_{FDOT} value of 1.5 irrespective of soil properties and depth was used to consider the simultaneous overturning and torsional loads. However based on the results of the first full-scale combined torsion and lateral load test performed in this research, FDOT re-revised the methodology by changing ω_{FDOT} value as shown in Equation 2-23, which is called as “FDOT re-revised methodology” in this report. For cohesive soil, α method is used for obtaining f_{sz} in Equation (2-20).

$$\begin{aligned} \omega_{FDOT} &= 1.5 && \text{for } N_{60} > 15 \\ \omega_{FDOT} &= 1.5 \left(\frac{N_{60}}{15} \right) && \text{for } 5 < N_{60} < 15 \end{aligned} \quad (2-23)$$

2.5 Estimation of Lateral Capacity of Drilled Shafts

In this study, the ultimate lateral capacity of drilled shaft was estimated using the free earth support approach proposed by McVay et al. (2003) and Hu et al. (2006). The method uses the free earth support pressure distribution (Teng, 1962) and the ultimate value of the soil pressure variation with depth as characterized by Reese et al. (1974). Figure 2-12 shows the assumed soil pressure distribution. A reduction factor (R_m) was introduced to adjust the soil pressure [$S_p(x)$], i.e., $R_m S_p$, (Figure 2-12) in case the bending moment reaches the moment capacity of the shaft section. Note that once the shaft's moment capacity is reached, lateral resistance is fixed and in such cases full soil resistance (passive state) may not be mobilized. The magnitude of R_m and ultimate lateral capacity are obtained by considering the force and moment equilibrium along with the moment capacity of the shaft. In the case of coupled torsion and lateral loading, another reduction factor (R_T) obtained from Figure 2-9 (McVay et al., 2003; Hu et al., 2006) was used to further adjust the lateral capacity due to the influence of torque [i.e., new soil pressure = $R_T R_m S_p(x)$; Figure 2-12]. Recall that previous centrifuge study (Hu et al., 2006) provided R_T factors up to a maximum torque to lateral load ratio (eccentric distance) of 21ft only. McVay et al. (2003) also developed a MathCAD spreadsheet to estimate the lateral capacity based on this approach.

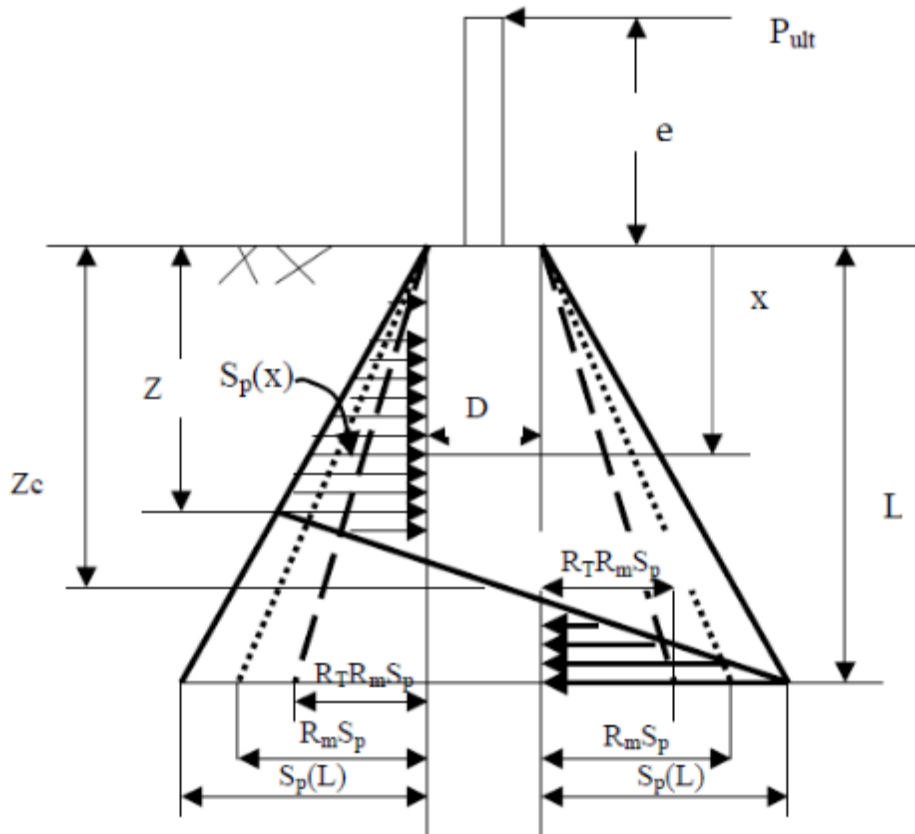
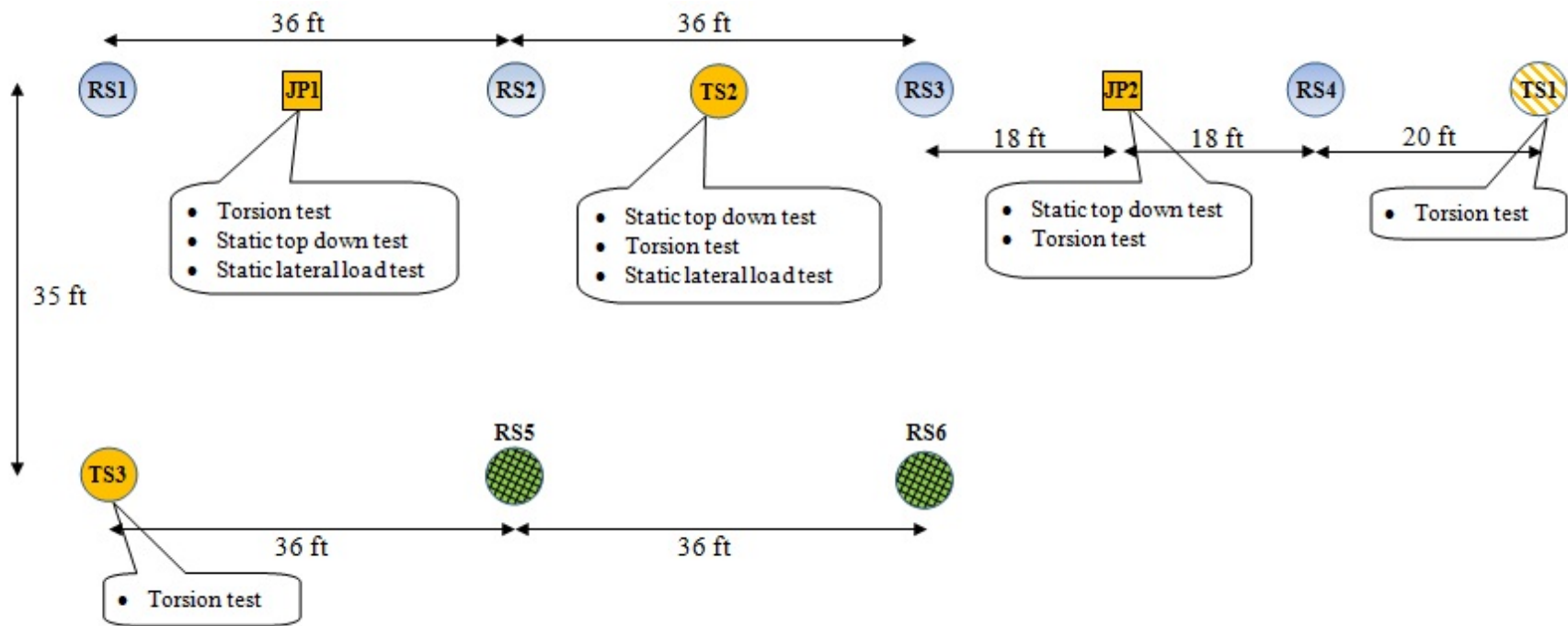


Figure 2-12. Soil pressure diagram proposed by McVay et al. (2003)

CHAPTER 3 SOIL EXPLORATION AT THE TEST SITE

The test site chosen for the research project was an FDOT borrow pit located in Keystone Heights, Florida. The test layout to accommodate the planned axial, torsion and lateral load tests is shown in Figure 3-1. There are four 4ft diameter x 40ft deep reaction drilled shafts (labeled RS1-4) to provide reaction for axial static top-down testing of jet-grouted piles (JP1 and 2) and drilled shaft (TS2). Note that the two 4ft diameter x 55ft deep drilled shafts (RS 5 and 6) in the second row (Figure 3-1) are for another FDOT research project (BDK-75-977-46: Bottom Side Grouting of Drilled Shafts Prior to Tip Grouting), but constructed along with other shafts to minimize the mobilization cost. Assisting with the shafts/piles locations/in situ testing at the site was the state materials office, SMO, at Gainesville. To align/position the shaft/piles for the axial top-down tests, a ‘Total station’ (Leica Geosystems) was used for the layout work. All shafts/pile locations were staked out in accordance with the field test layout shown in Figure 3-1. The accuracy of the work was cross-checked by setting instruments at the different stations.

After layout, a detailed subsurface exploration at the test site was undertaken by State Material Office personnel. Both in situ testing (SPT, CPT, PMT, and DMT) and laboratory soil testing (classification tests and direct shear tests) were conducted at the site and in the laboratory. Figure 3-2 depicts the location of various in situ tests along with the location of the shafts/piles. Also included are a description of the various laboratory tests performed, analysis and soil properties (e.g., angle of internal friction, un-drained strength, etc.) estimated.



- Two, 4ft diameter x 18ft deep **Test** drilled shaft
- Two, 4ft diameter x 12ft deep **Test** drilled shaft
- Two, 28in square x 18ft deep **Jet grouted piles**

- Four, 4ft diameter x 40ft deep **Reaction** drilled shaft
- Two, 4ft diameter x 55ft deep **Reaction** drilled shaft

Figure 3-1. Test layout

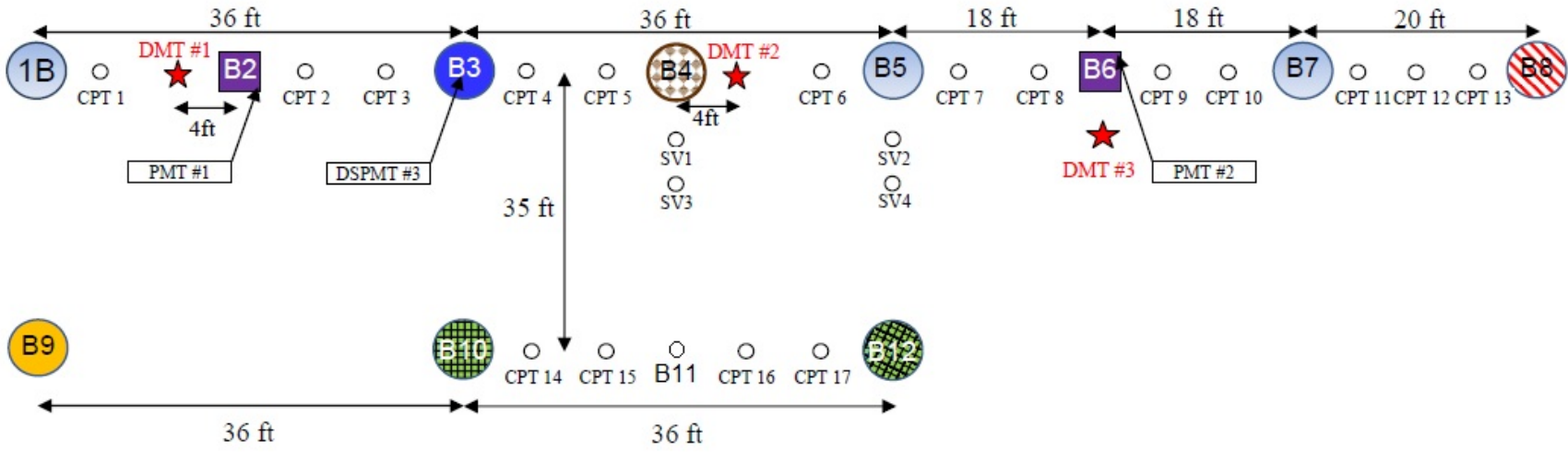


Figure 3-2. Location of various in situ tests along with the location of shafts and piles

3.1 In Situ Tests

3.1.1 Standard penetration test

Standard Penetration tests were performed within the footprint of all the shafts and piles to a depth of about 3 times diameter of pile/shaft to assist with the design/construction (e.g., skin friction and end bearing). Four additional SPT borings were made near shaft TS2 and RS3 (SV1 – SV4; Figure 3-2) for spatial variability studies. Figure 3-3 displays the SPT blow count (N) profile from all the borings performed at the site. Evident, all the borings indicate a similar spatial trend of N-values in the vertical direction. In addition, the borings revealed very high N value (exceeds 50) at a depth of 30 ft through 45 ft, representing the existence of a hard stratum. Figure 3-3 also exhibits the presence of some horizontal spatial variability at the test site. For instance, the SPT blow count (N) at 20ft depth varied from 10 to 20.

Soil samples at different depths were collected during SPT boring for laboratory classification tests, which will be discussed later. SMO, Gainesville, also drilled a 1.25 in diameter, 30 ft deep, well at the test site for monitoring water table during the various stages of the research project. Throughout the in situ soil testing, the water table at the test site was approximately 9.5 ft below ground surface, which appeared to be perched on the hard stratum located at 30 ft depth. The SPT N values obtained from the footprint of test shafts and piles were subsequently used to estimate the unit weight and angle of internal friction based on various empirical correlations available in the literature. The N values were also used to predict the axial and torsional resistance of the piles/shafts using the methods discussed in the previous Chapter (2).

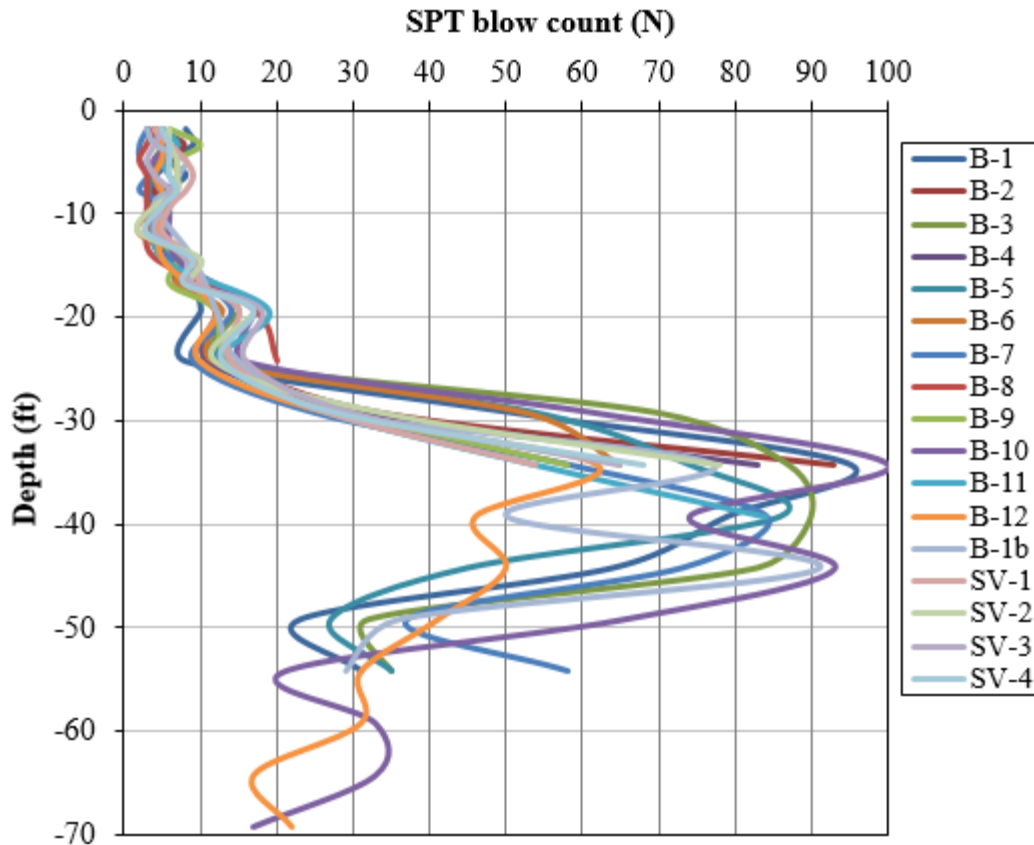


Figure 3-3. SPT blow count (N) profiles at the test site

3.1.2 Cone penetration test

Cone penetration tests were conducted at locations in between shafts/piles at an interval of approximately 6 ft to identify the spatial variability at the site. All the CPT soundings were performed to a depth range of 30-35 ft. Figure 3-4 shows the q_c profiles from all the CPT soundings at the site. Like the SPT blow count profiles, q_c profiles also indicate some spatial variability in the horizontal direction. All the q_c profiles show high tip resistance (about 350 tsf) near 30 ft depth, which confirm the presence of hard strata at that depth. The q_c profiles also show a more pronounced thin hard layer at 20 ft depth vs. SPT N profile (Figure 3-3, $10 < N < 15$ at 20 ft). Graphical presentation of the output (q_c , F_s , friction ratio) of the CPT soundings near some of the test shafts/piles are presented in Appendix A. The shear wave velocity profile

(m/sec) from geophysical site characterization (Figure 3-5) also indicates the presence of spatial variability at the test site, especially near the ground surface. It was later discovered that the top 6-10 ft had been excavated and later backfilled at the site.

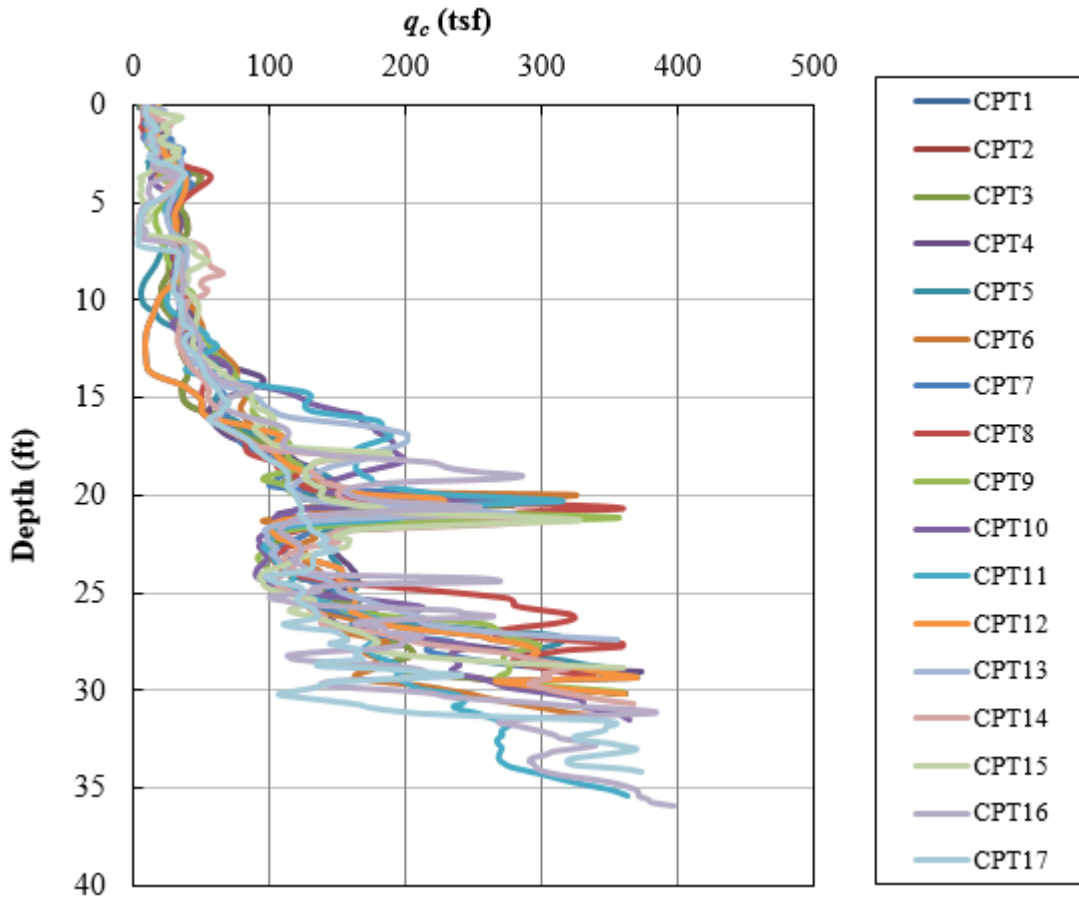


Figure 3-4. q_c profiles at the test site

The estimation of soil's unit weight, and angle of internal friction using various CPT based relationships are also presented later in this Chapter. The CPT results were also used in the axial and torsional resistance predictions (Chapters 6 and 7) for drilled shafts based upon different methods described in Chapter 2.

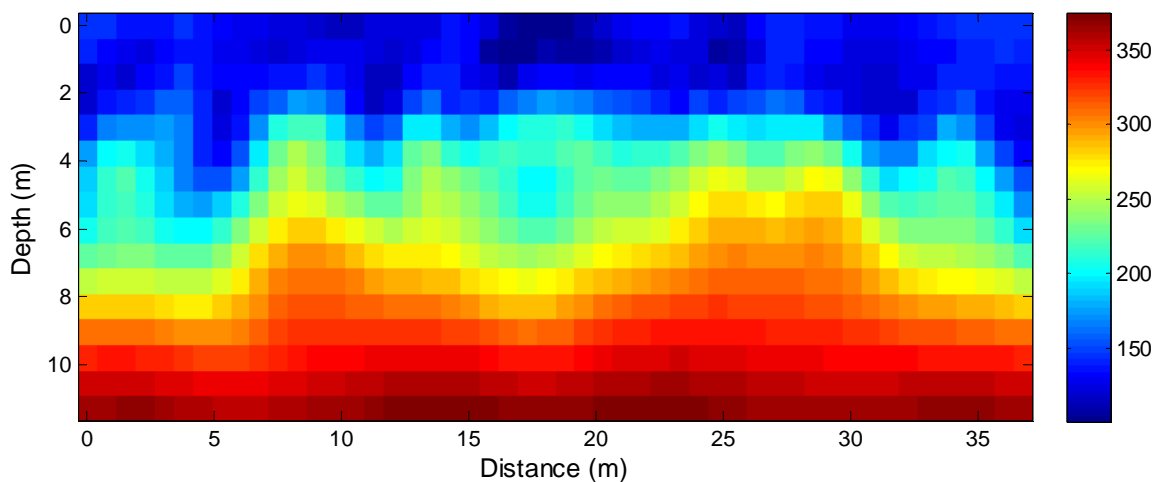


Figure 3-5. Shear wave velocity (m/s) profile at the test site

3.1.3 Pressuremeter test

Pressuremeter tests (PMT) were performed in the footprints of the two jet-grouted piles at depths of 8.5 ft and 16 ft, which is approximately at the center of each grout bag. In addition, one of the reaction drilled shafts, RS2, had tests performed at depths of 16 ft and 24.5 ft. Figures 3-6 and 3-7 show the pressure-volume curves from PMT at 8.5 ft and 16 ft depths, respectively, for the two jet-grouted piles. Similarly, Figure 3-8 depicts the pressure-volume curves for the reaction drilled shaft. The expected side grout pressure for each bag of jet-grouted piles will be nearly equal to the pressuremeter limit pressures at corresponding depth (McVay et al 2009; Thiyyakkandi et al. 2013). The limit pressure is the maximum pressure at which a steady-state cavity expansion occurs. It is evident from the Figures 3-6 through 3-8 that the limit pressure was not fully reached in any of the PMT; the expansion pressure was increasing with volume, and the loading (expansion) had to be stopped when the expansion limit of the pressuremeter probe or the capacity of the pressure gauge (e.g., in case of PMT_3b) was reached. However, the pressure-expansion curves at the location of jet-grouted piles (Figure 3-6 and 3-7) indicate that the maximum pressures were approaching the limit pressures (relatively flat slope), and hence

the measured maximum pressures given in Table 3-1 were considered to be representative of the limit pressures at the respective depths.

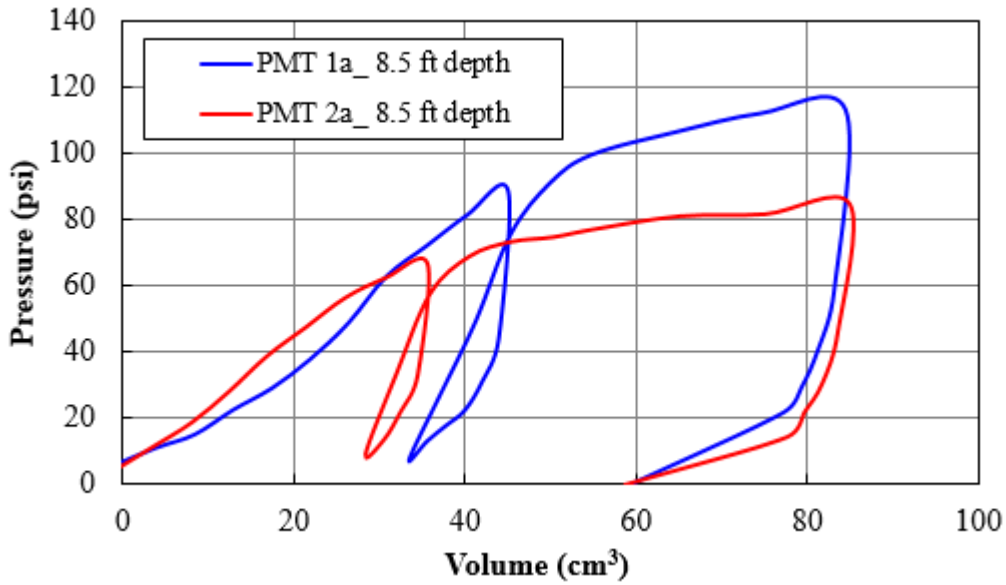


Figure 3-6. Pressure-volume curves from PMT at 8.5 ft for two jet-grouted piles

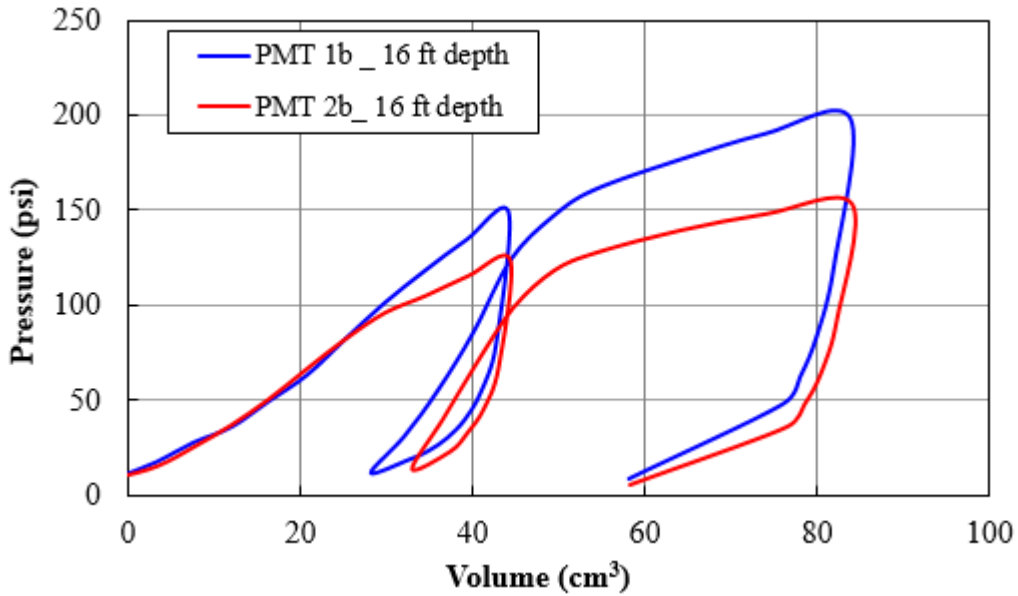


Figure 3-7. Pressure-volume curves from PMT at 16 ft for two jet-grouted piles

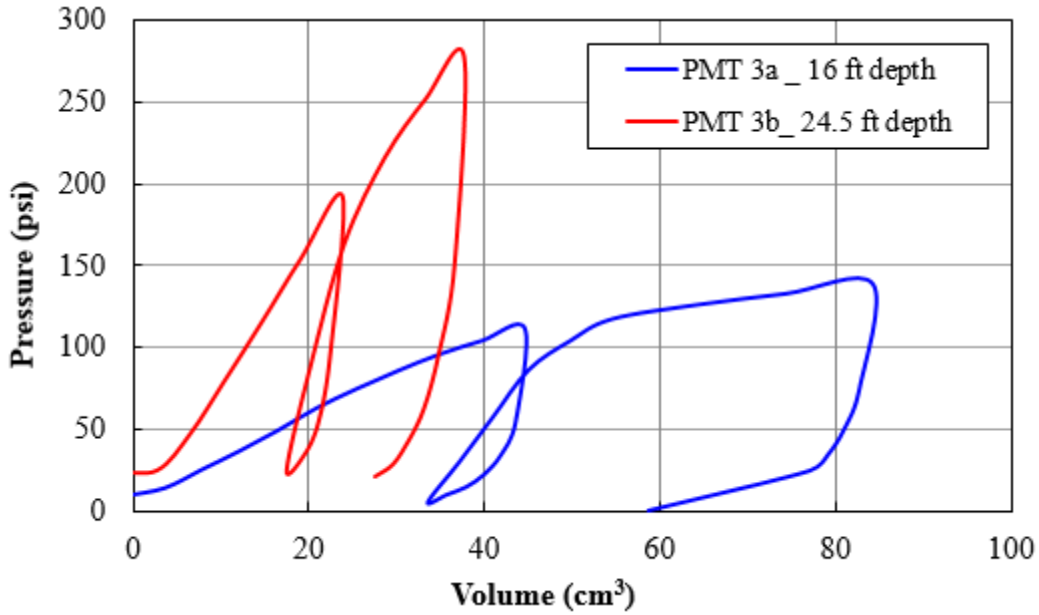


Figure 3-8. Pressure-volume curves from PMT at 16 ft and 24.5 ft for RS2

Table 3-1. Pressuremeter limit pressures for jet-grouted pile locations

Jet-grouted pile	Maximum pressure	
	8.5 ft depth	16 ft depth
JP1	113 psi	198 psi
JP2	85 psi	153 psi

3.1.4 Dilatometer test

Three separate dilatometer tests (DMT) were carried out, Figure 3-2, near the foot print of the jet-grouted piles and torque drilled shaft, TS2, to a depth of 18 ft. The location of each test was 4ft away from the center of foot print of respective pile/shaft. Figure 3-9 shows some of the DMT output. The Material Index (I_D) can be used as a rough guideline for classifying the soil type (Figure 3-9). Since the parameter, I_D only reflects the mechanical behavior of soil (not based on grain size analysis), it may sometimes misinterpret silt as clay and clay-sand mixture as silt. The Horizontal stress Index (K_D) is considered as an amplification of K_0 value (i.e., $K_0 \propto K_D$).

The parameter can be used to determine several soil parameters such as K_0 , OCR , undrained shear strength (s_u), and angle of internal friction (ϕ) of the soil.

3.2 Laboratory Tests and Soil Classification

SMO at Gainesville also performed laboratory classification tests such as, grain size analysis, liquid limit, plastic limit, and organic content determination, on the soil samples collected during the SPT boring. The test results generally showed that the soil to a depth of 3 to 8.5ft was a low compressible clay (CL) and/or clayey sand (SC). SPT N values in this layer ranged from 2 to 10. This layer was underlain by a poorly graded fine sand with silt (SP-SM) fraction down to depth of approximately 30 ft. SPT blow count in this sand-silt layer varied from 3 to 34. From depths of 30 to 50 ft, very dense sand stratum with N value ranged from 51-100 exists. The hard sand stratum was followed by medium dense fine sand (N value: 17 to 33), which extended to the end of boring (70 ft). Shown in Figure 3-10 are the typical grain size distributions for the different soils found at the site. Figure 3-11 presents the soil moisture content profile for all the borings at the test site. Moisture content of the soils above the water table (i.e., depth of 9.5 ft) varied from 1.5 to 20%, whereas the soils beneath the water table had reasonably uniform moisture content (25-30%) irrespective of the depth. The Unified Soil Classification (USC) and SPT blow count (N_{60} ; corrected for hammer efficiency) profile in the footprint of the jet-grouted piles and test drilled shafts including a schematic of installation are given in Figure 3-12 and 3-13 respectively. The USC classification and uncorrected SPT blow counts (N) for all reaction shafts locations are also included in Appendix A.

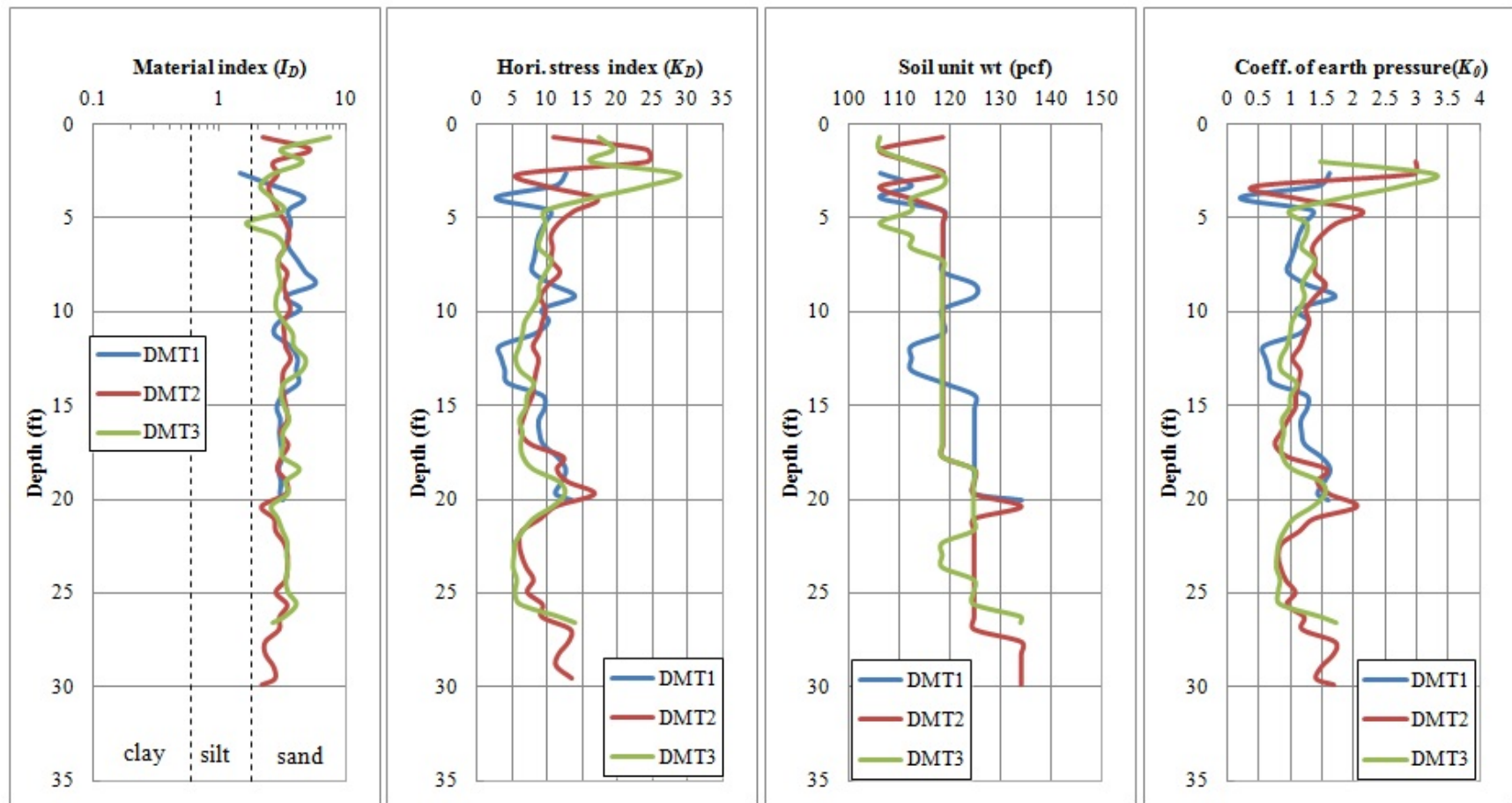


Figure 3-9: Graphical presentation of some of the DMT results

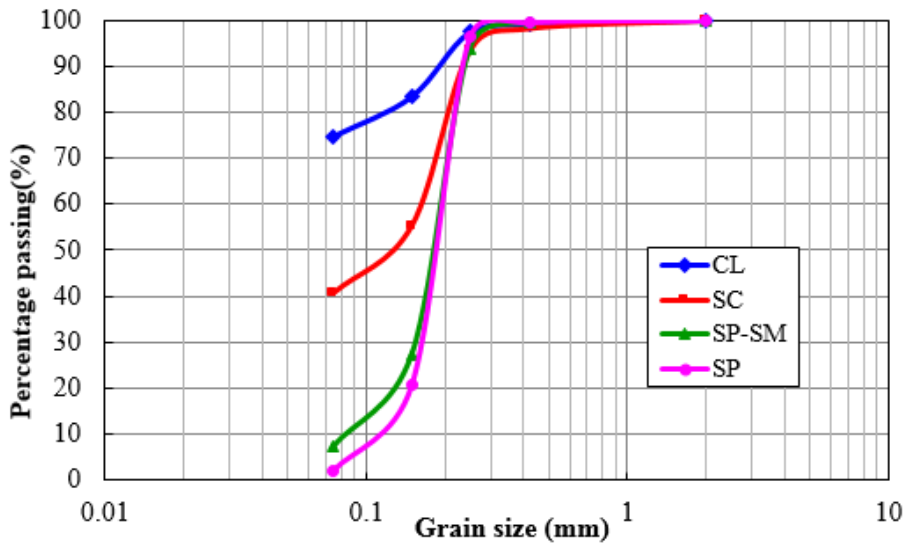


Figure 3-10. Typical grain size distributions for different soil at the site

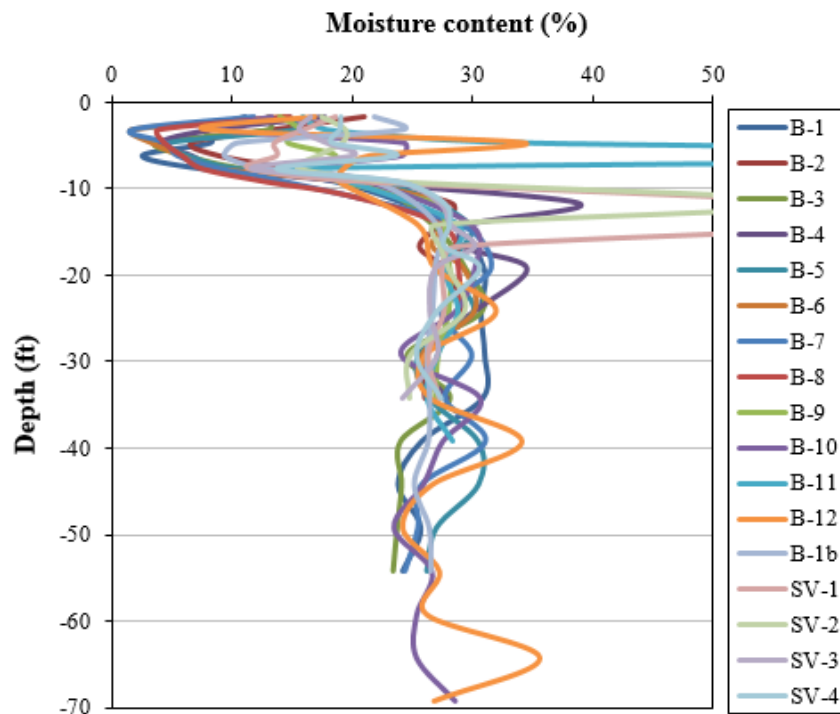


Figure 3-11. Soil moisture content profiles for all the borings

Undrained shear strength of the top clay layer (i.e., up to 3-8 ft depth) was determined by unconsolidated undrained triaxial compression tests (UU-test) on the undisturbed samples

obtained with Shelby tube sampling. The tests were conducted in accordance with AASHTO T 296. The undrained shear strength was found to be 620 psf.

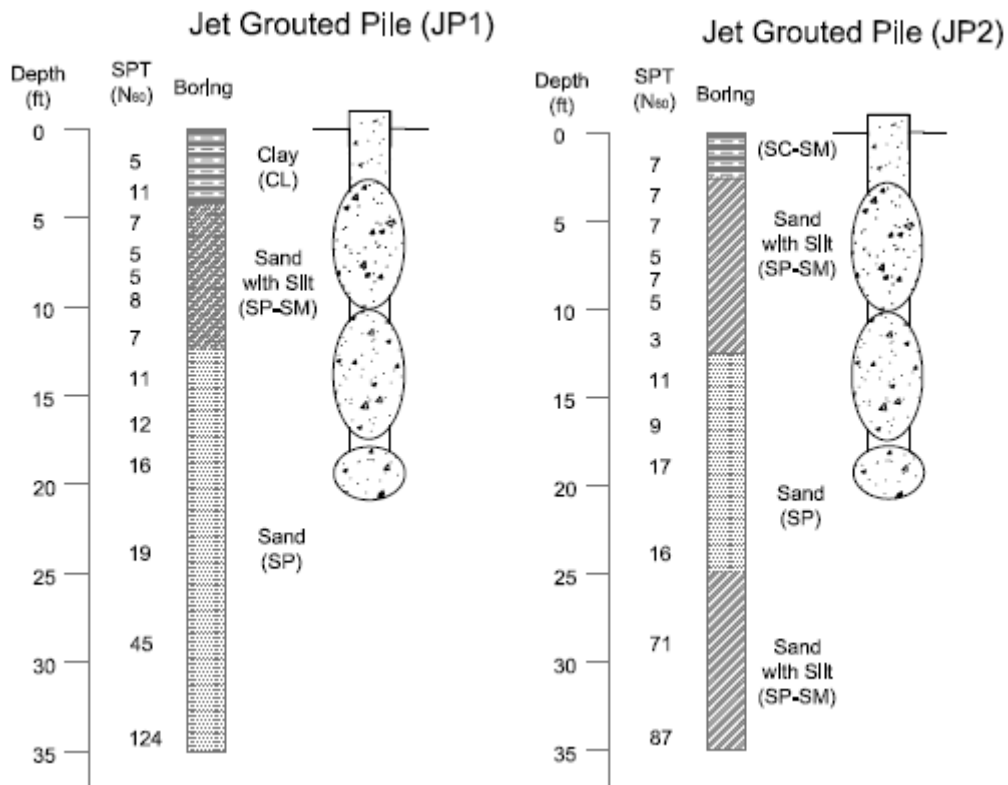


Figure 3-12. Soil classification (USC) and N_{60} at the location of jet-grouted piles

3.3 Estimation of Soil's Unit Weight

Accurate evaluation of total and effective overburden stresses is necessary for predicting the in situ soil stresses, as well as the axial and torsional resistance of the deep foundations, and the expected maximum grout pressures during the grouting of jet-grouted piles. The unit weight of each of the overlying soil layers is required for the estimation of the overburden stress at a particular depth. Undisturbed samples procured from soil boring are needed for laboratory assessment of unit weight, which is extremely difficult in the case of cohesionless soils. Therefore empirical methods (correlation, chart and empirical values) based on various in situ

tests were considered in this study to obtain the unit weight of the granular soils. The unit weight was predicted using CPT, SPT, and DMT results.

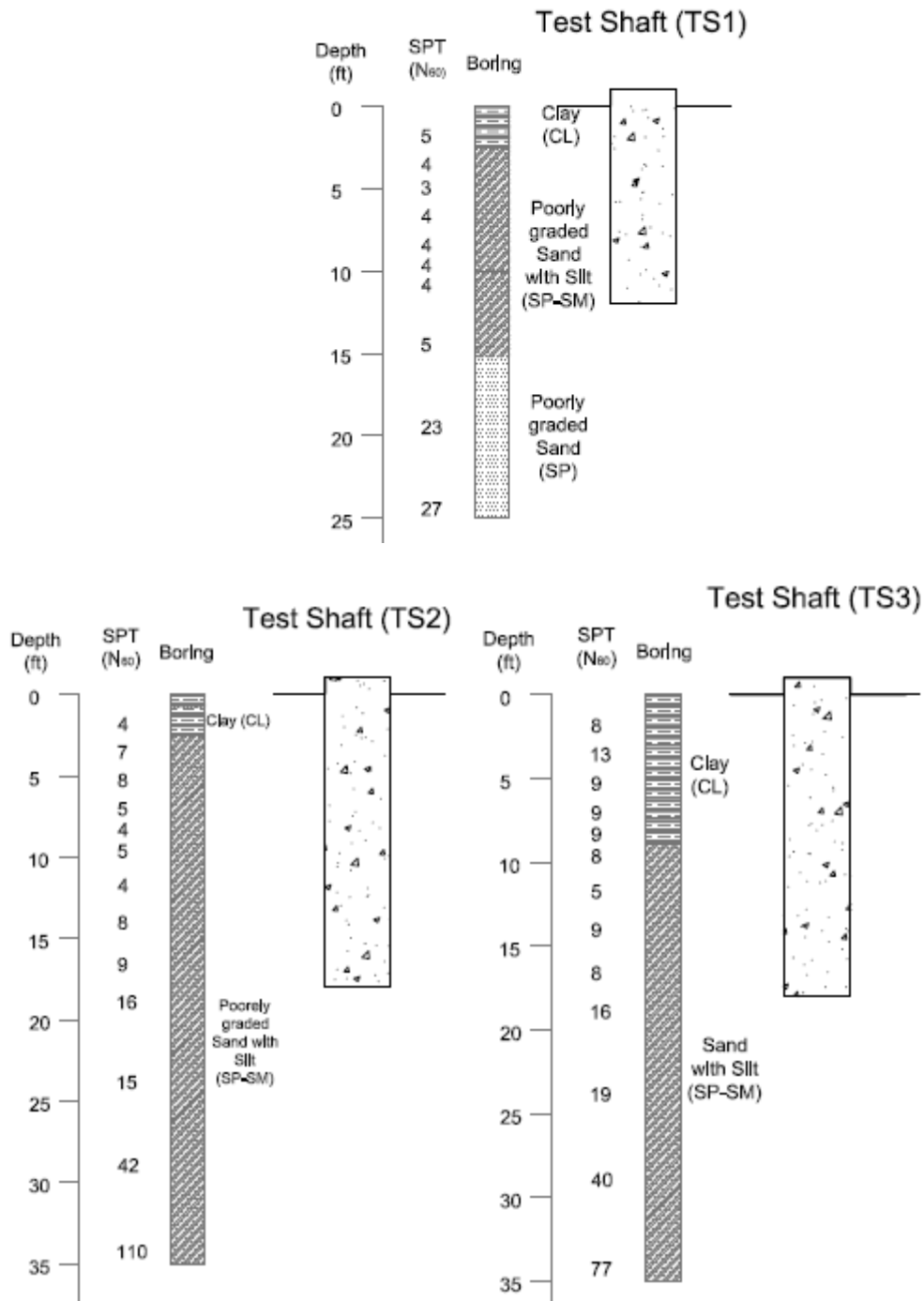


Figure 3-13. Soil classification (USC) and N₆₀ at the location test drilled shafts

CPT-based relationship [Equation (3-1)] proposed by Robertson and Cabal (2010) was used to estimate unit weight directly from CPT results, q_c and F_s (sleeve friction). The advantage of this method is that it is applicable for all types of soils.

$$\frac{\gamma}{\gamma_w} = 0.27[\log R_f] + 0.36 \left[\log \left(\frac{q_c}{P_a} \right) \right] + 1.236 \quad (3-1) \quad \text{Robertson and Cabal (2010)}$$

Where, γ is moist unit weight; γ_w is unit weight of water in the same units as γ ; R_f is friction ratio, which is equal to $(F_s/q_c) \times 100\%$; P_a – atmospheric pressure in the same units as q_c .

In the case of DMT data, the study used the chart suggested by Marchetti and Craps (1981). Finally, the empirical values based on the SPT N values (Bowles, 1996, adopted in FB-Multiplier) were considered for comparison with other predictions. Table 3-2 shows the unit weight values predicted for each soil layer at the location of test piles and shafts using the different approaches discussed above. It can be seen that the values predicted using CPT-based approach suggested by Robertson and Cabal (2010) were close to the average values predicted by all methods, including DMT and SPT approaches (JP1, JP2 and TS2). Consequently, the CPT-predicted unit weight was subsequently used for calculation of other soil properties (angle of internal friction, unit skin resistance, etc.).

3.4 Estimation of Angle of Internal Friction

Direct shear tests on the samples obtained from a depth of 6-8 ft near the footprint of jet-grouted pile 2 revealed a peak angle of internal friction (ϕ_p) of 34° and constant volume friction angle (ϕ_{cv}) of 30° (Table 4-4). At all other depths and locations, in situ soil test results were used to evaluate the peak friction angles using different correlations available in the literature. The most commonly used relationships for obtaining peak friction angle utilizing CPT, SPT, and DMT results are presented in Table 3-3.

Table 3-2. Unit weight estimation at the test piles and shafts locations using different approaches

Location	Soil layer	γ (pcf)				Soil Classification
		CPT based (Eq. (3-1))	DMT based	SPT based	Average	
JP1	0 - 4 ft	110.2	112.32	120	114.2	Clay (CL)
	4 - 12.5 ft	110.6	116.16	100	108.9	SP-SM
	12.5 - 17.5 ft	116.2	118.56	109	114.6	SP
	17.5 - 25 ft	122.6	123.24	113	119.6	SP
	25 - 30 ft	126.5	134.16	132.5	131.1	SP
JP2	0 - 2.5 ft	113.6	110.76	123.35	115.9	SC-SM
	2.5 - 12.5 ft	111.5	116.06	96.5	108.0	SP-SM
	12.5 - 17.5 ft	121.3	118.6	104.6	114.8	SP
	17.5 - 25 ft	123.9	123	112.5	119.8	SP
	25 - 30 ft	131.3	134.2	132.5	132.7	SP-SM
TS2	0-2.5 ft	113.6	113.88	120	115.8	Clay
	2.5-5.5 ft	114.9	114.816	102.5	110.8	SP-SM
	5.5-12.5 ft	109.8	118.56	94	107.5	SP-SM
	12.5-17.5 ft	120.7	118.56	109.6	116.3	SP-SM
	17.5-25 ft	125.7	125.06	115.3	122.0	SP-SM
TS1	0-2.5 ft	114.7	--	123.35	119.04	Clay
	2.5-12.5 ft	112.6	--	90	101.3	SP-SM
	12.5-15 ft	116.2	--	96	106.1	SP-SM
	15-25 ft	124.9	--	124.6	124.75	SP
TS3	0-8.5 ft	112.8	--	125.3	119.0	Clay
	8.5-17.5 ft	116.2	--	105.4	110.8	SP-SM
	17.5-25 ft	126.8	--	117.3	122.0	SP-SM
	25-30 ft	129.7	--	125	127.4	SP-SM

The peak friction angles for each of the soil layers at the test piles/shafts locations predicted using the different methods are listed in Table 3-4. As shown in the Table 3-4, both CPT and DMT based methods were predicting higher values compared to SPT based methods. It was found that the prediction using Schmertmann (1975) method was close to the measured value at the location of JP2 (Table 3-4). Therefore the peak friction angles obtained by Schmertmann (1975) equation were subsequently used for axial and torsional resistance (Chapters 5 & 6) of the piles/shafts.

Table 3-3. Correlations for peak friction angle prediction

In situ test	Source	Correlation for Peak angle of internal friction
CPT	Robertson and Campanella (1983)	$\phi' = \tan^{-1} \left\{ \frac{1}{2.68} \left[\log \left(\frac{q_c}{\sigma'_{v0}} \right) + 0.29 \right] \right\}$
	Kulhawy and Mayne (1990)	$\phi' = 17.6^\circ + 11 \log \left[\frac{q_c/P_a}{(\sigma'_{v0}/P_a)^{0.5}} \right]$
SPT	Schmertmann (1975)	$\phi' = \tan^{-1} \left[\frac{N_{60}}{12.2 + 20.3(\sigma'_{v0}/P_a)} \right]^{0.34}$
	Hatanaka and Uchida (1996)	$\phi' = [15.4(N_1)_{60}]^{0.5} + 20^\circ$ $(N_1)_{60} = \frac{N_{60}}{(\sigma'_{v0}/P_a)^{0.5}}$
DMT	Marchetti (1997)	$\phi'_{safe,DMT} = 28^\circ + 14.6^\circ \log K_D - 2.1^\circ \log^2 K_D$ $K_D - \text{Horizontal stress index from DMT}$

Table 3-4. Shear parameters at the test piles and shafts locations

Location	Soil layer	Peak angle of friction, ϕ' (degree)					Direct shear test	ϕ_{cv} (degree) (Direct shear test)	S_u (psf) (UU triaxial test)
		CPT		SPT		DMT			
		Robertson & Campanella (1983)	Kulhawy & Mayne (1990)	Schmertmann (1975)	Hatanaka & Uchida (1996)	Marchetti (1997)			
JP2	0 - 2.5 ft	--	--	--	--	--	--	--	620
	4 - 12.5 ft	38.6	35.8	33.0	31.6	40.5	34	30	--
	12.5 - 25 ft	41.7	39.7	36.1	33.8	42.4	--	--	--
	17.5 - 25 ft	42.4	40.9	39.5	36.7	39.3	--	--	--
JP1	0 - 4 ft	--	--	--	--	--	--	--	620
	4 - 12.5 ft	38.5	35.8	33.8	32.3	39.7	--	--	--
	12.5 - 17.5 ft	39.4	37.5	36.2	34.6	38.7	--	--	--
	17.5 - 25 ft	42.7	41.0	40	37.1	39.3	--	--	--
TS2	0-2.5 ft	--	--	--	--	--	--	--	620
	2.5-5.5 ft	41.2	36.6	36.7	35.2	41.9	--	--	--
	5.5-12.5 ft	36.1	34.1	31.2	30.6	40.5	--	--	--
	12.5-17.5 ft	40.0	38.4	34.2	32.5	39.3	--	--	--
	17.5-25 ft	42.6	41.3	38.3	35.7	40.3	--	--	--
TS1	0-2.5 ft	--	--	--	--	--	--	--	620
	2.5-12.5 ft	36.1	34.4	28.9	29.2	--	--	--	--
	12.5-15 ft	35.0	34.3	29.9	29.8	--	--	--	--
	15-25 ft	42.6	41.3	43.1	40.1	--	--	--	--
TS3	0-8.5 ft	--	--	--	--	--	--	--	620
	8.5-17.5 ft	38.4	36.6	32	32.3	--	--	--	--
	17.5-25 ft	43.7	41.9	40.7	37.7	--	--	--	--

CHAPTER 4 DESIGN AND CONSTRUCTION OF REACTION AND TEST DRILLED SHAFTS

This Chapter presents a detailed description of the structural design and construction of the reaction and test drilled shafts used in this study. FDOT's recently developed 'Embedded pipe and flange system' (BDK 75 977-04, Cook et al., 2010) for transferring torque, moment, etc. from Mast arm structure to supporting drilled shaft was used in the present study. The design and fabrication of the shafts, connecting pipe and flange system as well as construction of drilled shafts and Cross-Hole Sonic Logging (CSL) of the shafts are also presented.

4.1 Structural Design of Drilled Shafts

As discussed in Chapter 1, one of the longest FDOT Mast arm types, E7-T6 was considered in the present study; the recommended foundation for the structure is a 48-in diameter x 18 ft deep drilled shaft (FDOT Index No: 17743). According to the FDOT's revised design methodology for drilled shaft supporting Mast arm structures (FDOT Structures Manual, vol.9, January 2011 and MathCAD spread sheet: Drilled Shaft v2.0), a 48-in diameter x 18 ft deep drilled shaft will have a torsional resistance of 650 kip-ft. Recall that FDOT has re-revised the methodology (FDOT Structures Manual, vol.9, January 2013 and MathCAD spread sheet: Drilled Shaft v2.04), based on the results of the first torque test performed as a part of this study. As identified in the Chapter 2 (Literature survey: Figure 2-9), the torque to lateral load ratio for E7-T6 Mast arm assembly is 35 for wind speeds exceeding 60 mph (e.g., hurricane); in case of wind speed of 206 mph, a point lateral load of 18.57 kip at an eccentric distance of 35 ft will develop a torque of 650 kip-ft at the top of the foundation. Table 4-1 shows the forces and moments on the foundation top for E7-T6 Mast arm at a wind speed of 206 mph. Since the combined torsion and lateral load test is intended to cause soil-structure interaction failure

(torsion and/or lateral) the drilled shafts' reinforced section need to be designed to carry the forces and moments identified in Table 4-1.

Table 4-1: Moments and load on the foundation top for E7-T6 mast arm assembly at a wind speed of 206 mph

Forces and Moments	Magnitude
Torsion (M_y) kip-ft	650
Moment about axis parallel to axis of arm (M_x) kip-ft	374
Moment about axis normal to the axis of arm (M_z) kip-ft	121.6
Lateral load (V_x) kip	0.7
Lateral load (V_z) kip	18.6
Axial load (V_y) kip	5.6

The longitudinal and shear/torsion reinforcement for the test drilled shafts were calculated according to Building Code Requirements for Structural Concrete (ACI 318-08). The calculations are given in Appendix B. A concrete strength of 4000 psi was used in the design. The threshold torsional strength of the concrete shafts (without reinforcement) was estimated using ACI 318-08 11.6.1 (a) to be 114 kip-ft. Since the threshold strength is much less than the expected maximum torsion (650 kip-ft), torsional reinforcement is needed to provide the required strength. It is found that traverse reinforcement comprised of #5 bars spaced at 5-in, can provide a nominal torsional strength of 749.5 kip-ft (Appendix B). The longitudinal steel reinforcement consist of 15 #10 bars ($\rho = 1.05\%$ of C.S area) evenly spaced around a 39.48" c/c diameter. The reinforced concrete section with the above longitudinal and traverse reinforcement will have a flexural strength of 1542 kip-ft, an axial capacity of 5859 kip and a shear capacity of 363 kip (Appendix B). The ACI stress block method given in ACI 318-8, 10(5) was used to estimate flexural capacity of the section. This section is enough to carry the moments and forces generated in the foundation at its top (Table 4-1).

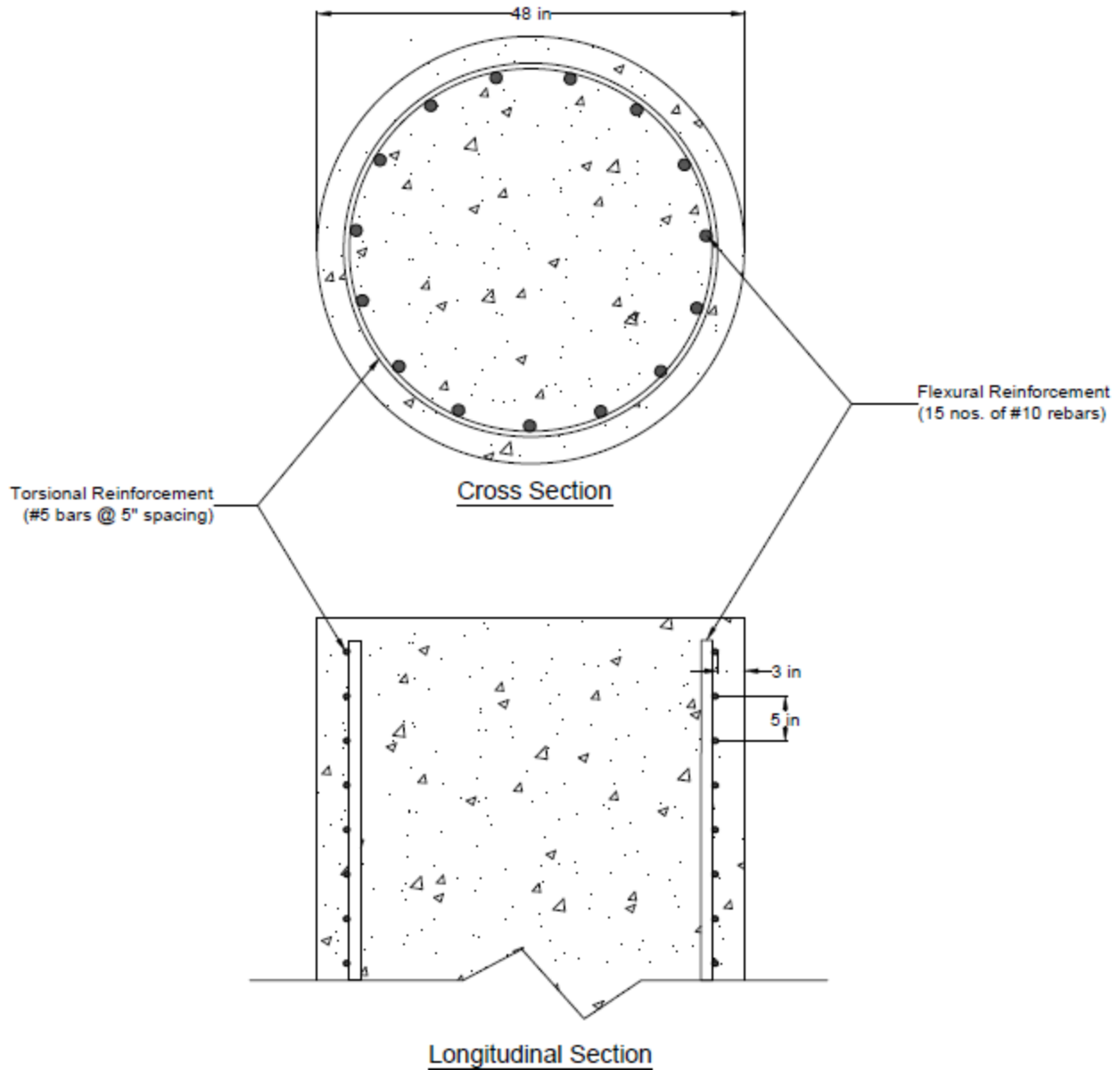


Figure 4-1. Longitudinal section and cross-section of test drilled shafts with reinforcement details

Figure 4-1 shows the longitudinal and cross-section of the test drilled shafts with reinforcement details. It was decided to use the same reinforcement for all reaction shafts except the RS2 which was planned to provide reaction for the lateral load testing of shaft and jet-grouted pile. For RS2, longitudinal reinforcement of 1.5 % of C.S area of shaft (18 # 11 bars)

was needed to prevent the formation of plastic hinge ($L/D = 10$, long shaft; FB-MultiPier Analysis) during the lateral load testing.

4.2 Design and Fabrication of Embedded Pipe and Flange Section

The failure of several Mast arm foundations in Florida during the 2004 hurricane event were caused by breakout failure of the anchor bolts in shear caused by torsional loading (wind). Since the present research focus is on the soil-foundation interaction during torsional loading, structural failure of foundation, Mast arm, or connections should not occur. FDOT recently developed an alternative support structure (BDK 75 977 -04, Cook et al., 2010) to transfer load from superstructure to foundation. The alternative system basically consists of an embedded pipe with annular flange and stiffeners (fins) welded to it. FDOT research (BDK 75 977 -04) revealed that the embedded pipe and plate section was able to transfer torsional and flexural loading to the foundation safely. The research also proved that ACI-318 code equations for concrete breakout from applied shear could be modified to accurately predict the concrete breakout strength of the new system. Figure 4-2 shows schematic of the alternative support system (Cook et al., 2010).

The new support structure (embedded pipe and plate section) was used for this study and designed according to the guidelines given in BDK 75 977-04 (Cook et al., 2010). The design was based up on the forces and moments on the foundation top, given in Table 4-1. The cross-section of embedded pipe (outer diameter = 24-in and thickness = 0.625-in) was chosen to be the same as the Mast arm pole (upright; discussed later) with yield strength = 42 ksi and ultimate strength = 60 ksi. The design calculations are given in Appendix B. The design capacity of 24-in diameter x 0.625-in thick HSS round pipe was determined using AISC 360-05 (Specification for structural steel building) and is presented in Table 4-2.

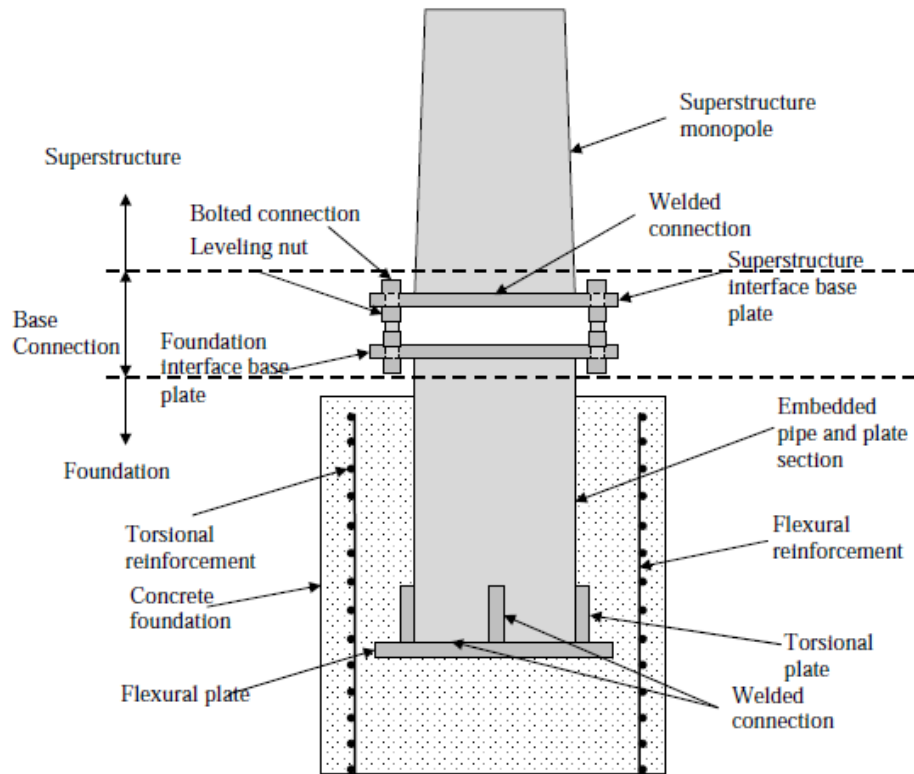


Figure 4-2. Alternative support structure (FDOT project BDK75-977-04, Cook et al., 2010)

Table 4-2. Design capacity of 24-in diameter x 0.625-in-thick HSS pipe

Capacity	Magnitude
Flexural capacity	1004 kip-ft
Shear capacity	484 kip
Torsional capacity	923 kip-ft
Axial capacity	2091 kip

The size (width and thickness) of the added torsional stiffener plates (Figures 4-2 and 4-4) was 1-in x1-in, which is approximately equivalent to an anchor bolt. Length of the plate was determined based on the required weld length for 3/8-in fillet weld (see Appendix B). It was found that 18-in long stiffener plate was adequate for the design. The torsional strength and side face rupture strength of the embedded pipe with 4 torsional stiffeners was calculated to be 1372 kip-ft and 1806 kip-ft respectively (see Appendix B). The annular flexural plate (Figure 4-4)

welded to the top of 24-in pipe was 1-in thick plate with inner diameter of 24-in and outside diameter of 29-in. The flexural breakout strength and side face blowout strength of the embedded pipe with the annular flexural plate were determined to be 988 kip-ft and 1045 kip-ft respectively (Appendix B). Since the torsion and moment will be acting concurrently on the foundation during the torsion test, there would be a possible interaction between torsional and flexural breakout due to the overlap in breakout surfaces (Cook et al. 2010). Figure 4-3 shows the assumed linear interaction diagram between torsion and flexure for concrete breakout along with the actual torque-moment combination acting on the foundation. Evident from the Figure 4-3, concrete breakout should not happen with the planned torsion and flexure testing of the foundation.

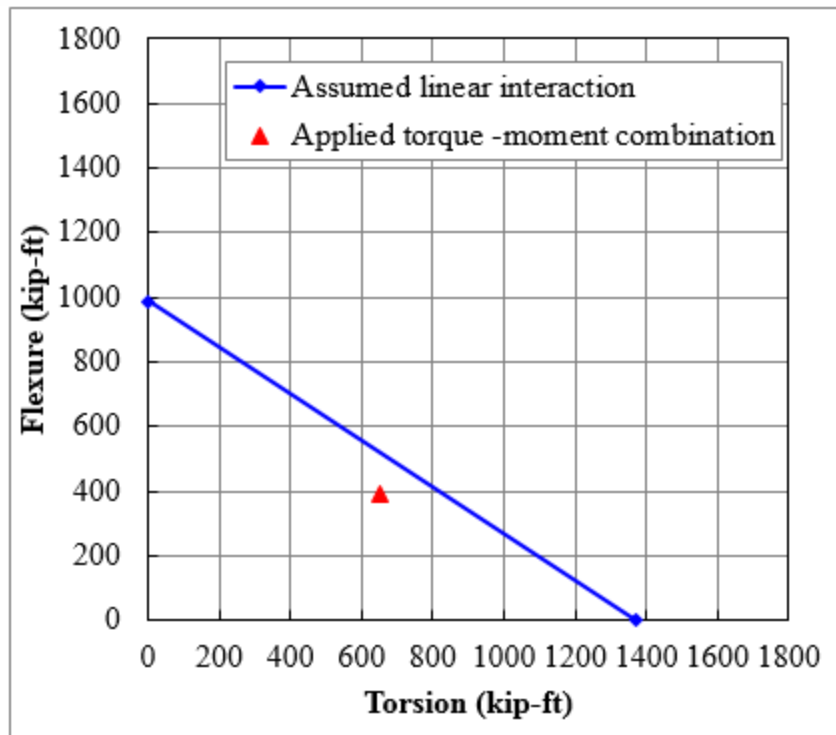


Figure 4-3. Assumed linear interaction between torsion and flexure for concrete breakout

Next, the required length of the embedded pipe was determined based on the development length for longitudinal reinforcement and concrete breakout length. The development length was determined to be 36 in using ACI 318-08 12.3.3. Concrete breakout length above the stiffener plate (18 in long) was estimated to be approximately 12.5-in. Therefore, the required length for embedded pipe to avoid the overlapping of reinforcement development length and concrete breakout was 66.5 in ($36 \text{ in} + 12.5 \text{ in} + 18 \text{ in} = 66.5 \text{ in} \approx 5.5 \text{ ft}$, see Appendix B).

Finally, the annular base plate (Figure 4-2 and 4-4) was designed to have a thickness of 1 in and outer diameter of 36 in with twenty-two 1.75-in diameter equally spaced bolt holes. The equivalent torsional bolt bearing strength and bolt shear were estimated to be 15,592 kip-ft and 3,499 kip-ft, respectively, which significantly exceeds the expected torsion. The weld size considered for the plate welding was 0.5-in fillet weld, which is expected to have a torsional and flexural capacity of about 1,104 kip-ft (Appendix B). In addition, the base plate stiffeners of 0.5-in thickness provided as shown in Figure 4-4 provide added strength to the annular base plate.

Figure 4-4 shows the longitudinal, cross-sectional and isometric views of the designed embedded pipe and plate section with all dimensions. The pipe and flange sections for three test shafts (TS1, 2, and 3) were fabricated in accordance with the dimensions of all the components (pipe, annular base flange, flexural base flange and torsional stiffeners) shown in Figure 4-4. The structures were fabricated at the University of Florida Coastal engineering laboratory, and then transported to the test site. First, the annular base flanges and flexural base flanges were made with dimensions as shown in Figure 4-4. Then, twenty-two 1.75-in diameter equally spaced bolt holes were drilled in each annular base flange. The annular base flange was subsequently welded to the 6-ft-long, 24-in HSS pipe. Then eleven, 0.5-in thick, base plate stiffeners (triangular

shaped) were welded to the pipe and annular base flange at equal spacing to provide added strength to the pipe-flange connection. Next, welding of the flexural base plate to the bottom end of HSS pipe was completed, followed by the welding of 4 torsional stiffeners (@ 90° apart) to the section. Figure 4-5 displays the fabricated embedded pipe and flange section ready for installation.

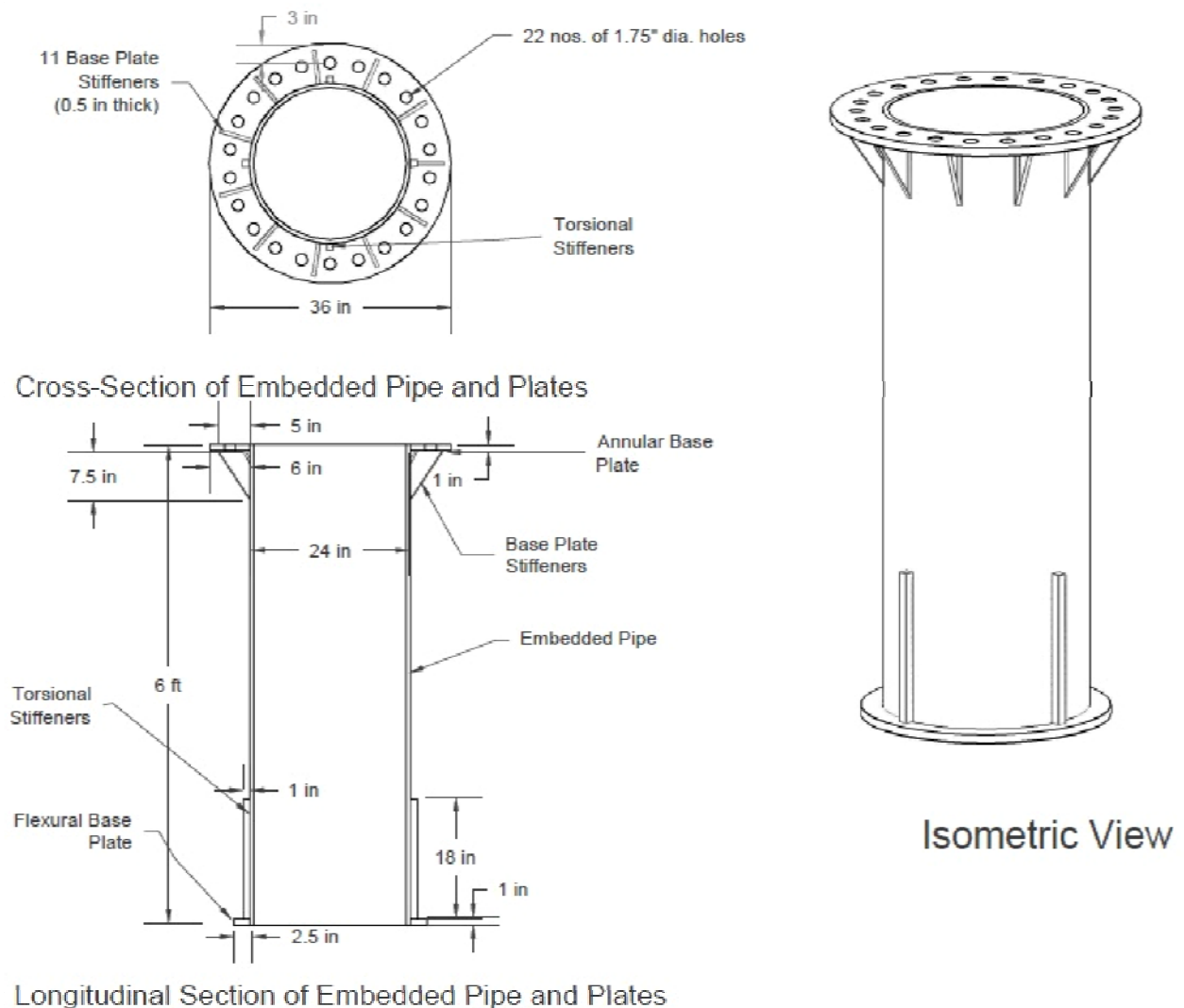


Figure 4-4. Longitudinal, cross-sectional, and isometric view of embedded pipe and flange section



Figure 4-5. Fabricated embedded pipe and flange section

4.3 Construction of Reaction Drilled Shafts

The construction of reaction and test drilled shafts were performed by third party vendor: Reliable Constructors Inc. Drilled shaft inspector from FDOT district 2 was present at the site throughout the construction period for monitoring all the construction activities, logging excavation & concrete placement, and quality control.

4.3.1 Construction of reinforcing cages, attachment of Dywidag bars, and instrumentation

The reinforcing cages for all the shafts were constructed on site in accordance with the design discussed in Section 4.1(Figure 4-6). Since FDOT beam girders (40 ft long) were planned for top-down axial load tests, 6 dywidag bars, spanning the full length (Figure 4-7) had to be installed within each reaction shaft during construction. Each Dywidag bar had a diameter of 1.25-in and a tensile strength of 150 kip. The Dywidag bars spanned the full length of the shaft by employing couplers between the 15 ft length sections. Researchers fabricated Dywidag bar cages (Figure 4-8) for top portion of shaft as no tolerance in the spacing between the Dywidag

bars was available for Acosta load frame system. For construction, the fabricated Dywidag bar cage was attached to the rebar cage (top) in accordance with the drawing (Figure 4-7), then the 14/15 ft Dywidag bars were coupled one by one to obtain in the full length of rebar cage; finally each bar was tied to rebar cage using short rebar pieces.



Figure 4-6. Construction of reinforcing cage

Reaction shaft RS2, which provide reaction during static top-down load testing of both test drilled shaft (TS3) and jet-grouted pile (JP1), was also instrumented with 8 sister bar strain gauges (2 gauges @ 180° apart in 4 levels) as shown in the Figure 4-9. The gauges used to monitor strain (axial and bending) were tied securely to the inside of reinforcement cage at 4 different levels after attaching the Dywidag bars.

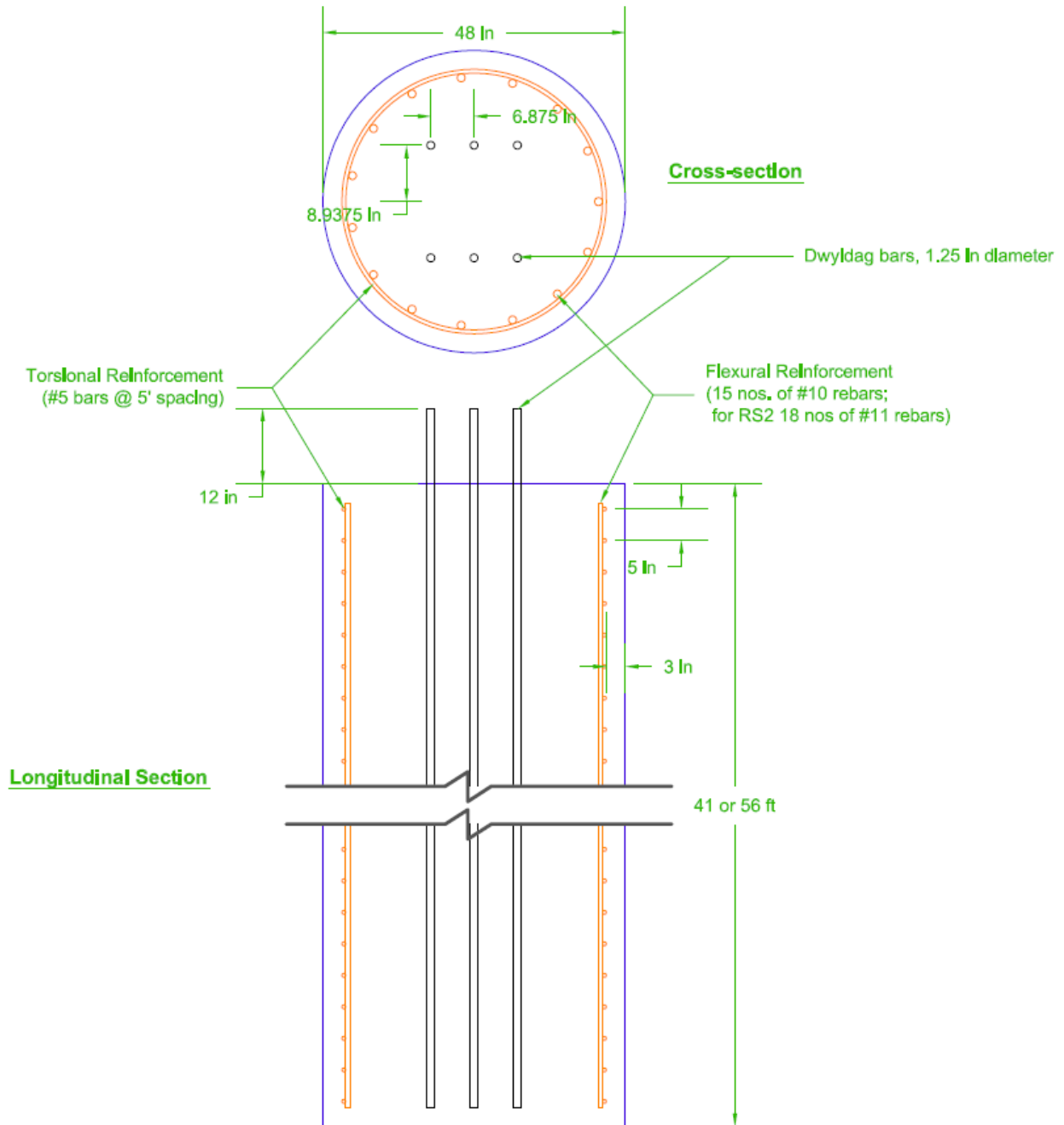


Figure 4-7. Schematic of reaction drilled shafts with reinforcement and Dywidag bars



Figure 4-8. Reinforcing cage with Dywidag bars

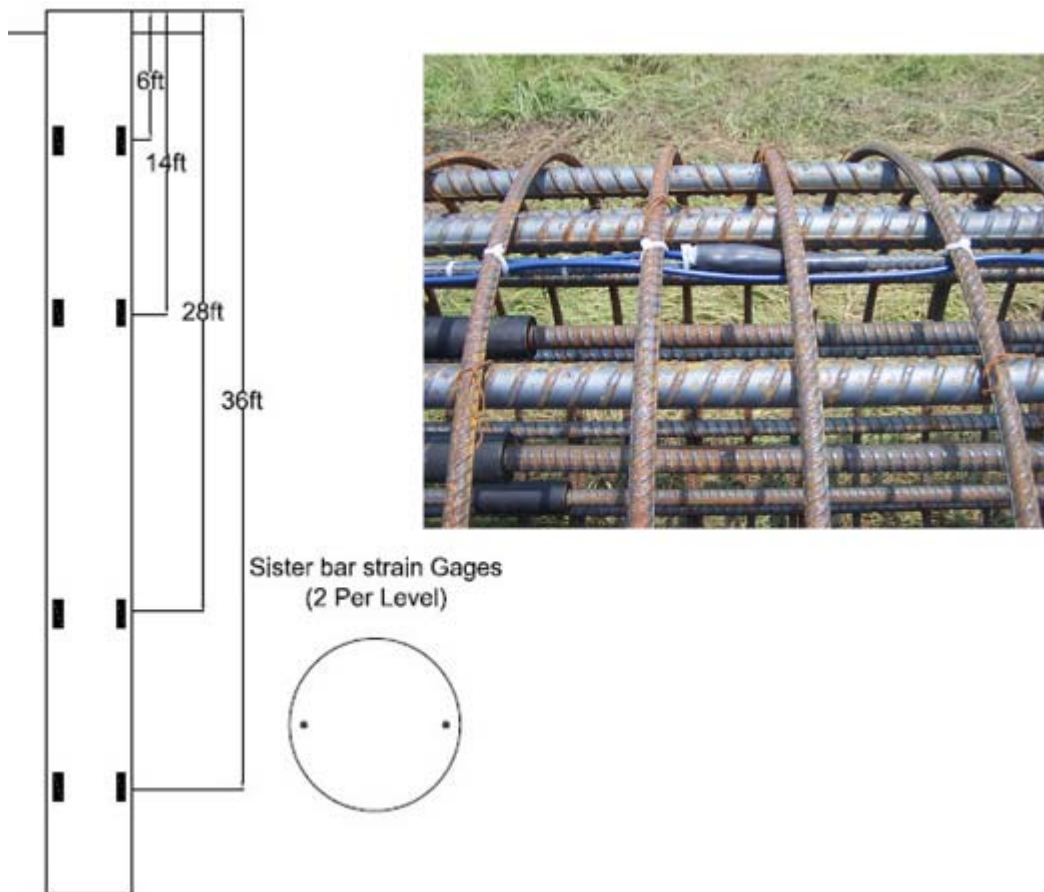


Figure 4-9: Instrumentation on RS2

4.3.2 Shaft excavation, reinforcing cage placement, and concreting

Wet shaft construction was employed for all the drilled shafts, as depth of water table was only 9 ft from the ground surface. Mineral slurry (bentonite clays) was used in all the excavations to provide hole stability. A truck mounted drill rig was used to excavate all the shafts (Figure 4-10). The contractors planned to use a 4.5 ft diameter x 6.3 ft long temporary surface casing (Figure 4-10) to support the top of the excavation. Since the diameter of casing was 6-in larger than the nominal diameter of shaft, the constructed shaft would have 4.5 ft diameter for the top 5.5 ft below ground surface. This was considered not acceptable for test shafts as this would increase the complexity of the load distribution during various load tests (e.g., end bearing due to larger diameter portion during top-down test). Hence, based upon the researchers' request, no casing was used for any of the test shafts.

No drilling concerns such as heaving, caving, slurry loss, etc., were observed during the excavation of any of the test/reaction shafts. Excavation of shaft hole and concrete placement were carried out in successive days for each reaction shaft. Before reinforcement cage placement in the excavation, desanding (Figure 4-11) and cleaning of the mineral slurry, as well as over reaming of the excavation wall with final cleaning of the excavation bottom by means of a bailing bucket (figure 4-12) were performed. The drilled shaft inspector (FDOT) performed all tests (Mud density balance, Marsh Cone Method- viscosity, pH indicator paper strips, FM 8-RP13B-3 - sand content) on mineral slurry used in the excavations to determine density, viscosity, pH and sand content. Table 4-3 presents the measured (range) properties of the bentonite slurry, which were within the range recommended by the FDOT specification 455.

Table 4-3. Measured range of properties of bentonite slurry

Properties	Measured	Range specified in FDOT specification: 455-15.8.1 (65 ⁰ F)
Density	64 - 65	64 - 73 lb/ft ³
Viscosity	30-34	30 - 40 seconds
pH	8 - 9	8 - 11
Sand content	0.1- 0.5%	≤4%



Figure 4-10. Excavating hole for drilled shaft construction



Figure 4-11. Desanding the bentonite slurry



Figure 4-12. Bailing bucket used for cleaning the excavation bottom

A truck mounted hydraulic crane was used to lift the reinforcing cages and position them within the hole as shown in Figure 4-13. After placing the cage into the excavation and setting at the proper elevation (3-in below shaft top), the cage with the Dywidag bars was turned and aligned for the axial top-down test with the aid of a “Total station”.



Figure 4-13. Setting rebar cage in the excavation

A 11-in diameter tremie and hopper was used for concrete placement of all shafts. A disposable plate was used at the bottom of each tremie placement to prevent inflow of slurry and segregation during initial placement of the concrete. Class IV drilled shaft concrete (4000 psi), recommended by FDOT specification 346 was used for all shafts. The specified minimum compressive strength of concrete after 28 day is 4000 psi. Table 4-4 shows the measured range of the properties (slump, air content) of the fresh concrete, which falls within the range specified by FDOT specification 346.

Table 4-4. Measured properties of fresh concrete

Properties	measured	Range specified in 346
Slump	8 – 10 in	7 - 10 in
Air content	1 - 1.5%	0 - 6%



Figure 4-14. Concrete placement



Figure 4-15. Forming the shaft top with the use of a template

During placement, the concrete trucks “tailgated” the concrete to the hopper with the tremie pipe gradually raised as concrete flowed into the shaft (Figure 4-14). After each truck load, depth of concrete to the top of casing was measured using a tape and actual volume of concrete placed was subsequently compared to the theoretical prismatic volume. Analysis showed that the actual placed volume was slightly more than the theoretical volume for all the shafts. After completely filling the hole with concrete, temporary surface casing was removed and a 4ft diameter x 1.5 ft long template (casing) and frame with adjustable legs were used to form the above ground section of the shaft (Figure 4-15). The alignment of Dywidag bars was rechecked and adjusted if necessary with the assistance of a “Total station”.

Concrete cylinders (4-in diameter x 8-in long) were taken from each concrete truck to measure compressive strength after 7th day and 28th day. Table 4-5 presents a summary of the cylinder tests results after 28 days.

Table 4-5. 28th day compressive strength

mean strength	5068 psi
coefficient of variation	0.133
minimum strength	4021 psi
maximum compressive strength	5914 psi

4.4 Construction of Test Drilled Shafts

Figures 4-16 (TS1, 12-ft deep shaft) and 4-17 (TS2 and TS3) show the plan and cross-sectional views of test shafts with steel reinforcement and connectors. The excavation and concrete placement for each test shaft were performed on the same day to avoid over-reaming the shaft bottom, which is required if the time of drilling to concreting exceeds 12 hours according to FDOT specification 455-15.11.5.

4.4.1 Instrumentation installed in test drilled shafts

Four CSL access tubes were installed full length in all the test drilled shafts to allow cross-hole sonic logging. The tubes were 2-in diameter schedule 40 black iron pipe. Tubes were equally spaced (90° apart) around the circumference of drilled shaft and aligned parallel to the vertical axis of the reinforcing cage. Tubes were then securely tied to the inside of the reinforcing cage (Figure 4-19). Bottom and top ends of the tubes were sealed with threaded caps.

The shafts, TS2 and TS3, were installed with inclinometer casing, which allowed the use of in-place inclinometers during the lateral load testing. The data was used to obtain the shaft's lateral displacement profile during lateral loading. Quick connect (QC) type inclinometer casing with an outer diameter of 3.34-in (85 mm) was used. Casing was placed along the central vertical axis of the reinforcing cages and attached to the cage by means of rebar pieces as shown in Figure 4-19 (blue pipe).

Test shaft, TS2 was instrumented with 8 sister-bar strain gauges (2 gauges diagonally opposite in 4 different levels) as shown in the Figure 4-18. The strain gauge data during axial top-down test was used to separate out skin resistance and tip resistance of shaft, as well as negate any bending of shaft recorded in the data. The gauges were tied securely to the inside of reinforcement cage at 4 different levels and aligned in direction of a pair of grooves in the inclinometer casing. All the strain gauge wiring was routed through two $\frac{3}{4}$ -in PVC pipes (i.e.,

strain relief, 4 strain gauge wiring in each pipe) to the top of shaft to avoid any damage during the torsional loading of the shaft (Figure 4-19).

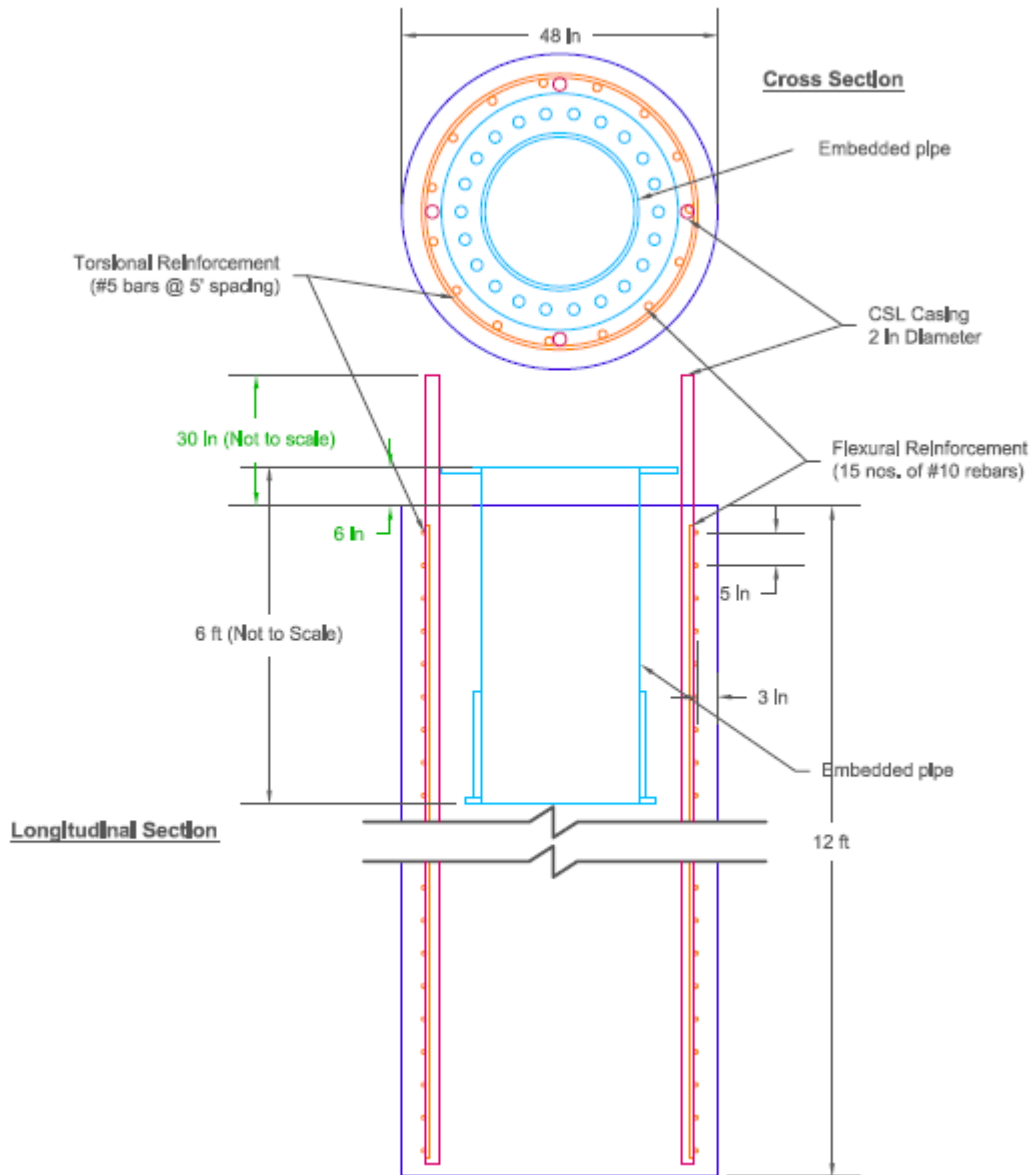


Figure 4-16. Schematic of test drilled shaft TS1

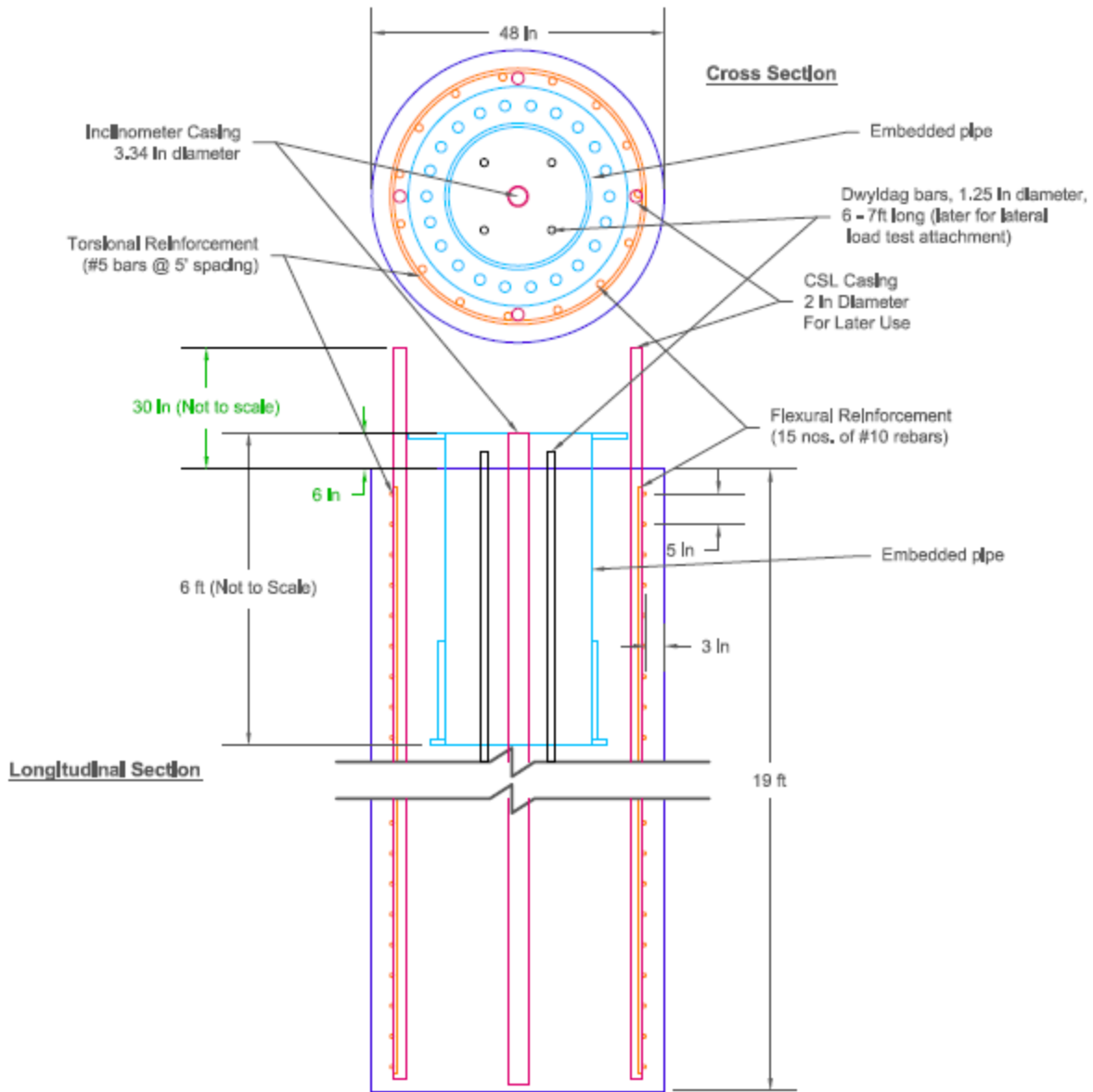


Figure 4-17. Schematic of test drilled shafts TS2 and TS3

Applied Foundation Testing Inc. (AFT) also instrumented the two 18-ft test shafts (TS2 and TS3) with EDC 601 and EDC 401 at no expense to FDOT for data acquisition in case of any dynamic load test will be planned on these shafts in future. Each EDC 601 consists of 3 sets of embedment strain gauge (Vishay Micro-Measurements) and accelerometer. EDC 401 comprised

of 2 sets of sister bar strain gauge and accelerometer. Figure 44 shows completely instrumented shafts TS2 and TS3.

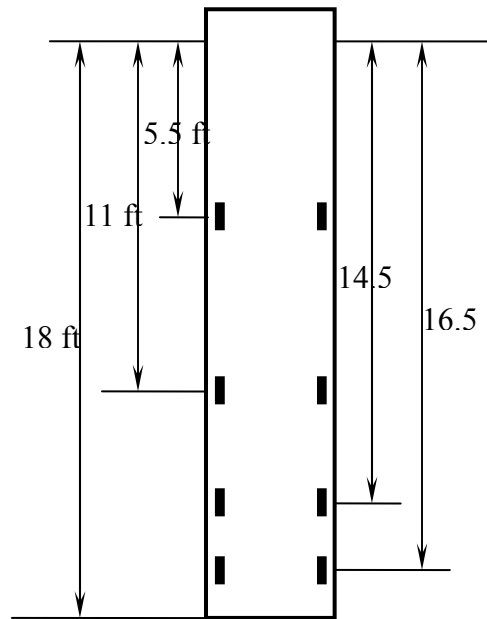


Figure 4-18. Location of sister-bar strain gauges in TS2

4.4.2 Shaft excavation

As mentioned earlier, no temporary surface casing was used in all test shaft excavations in order to construct shafts having uniform nominal diameter along their full lengths. The hole was drilled in dry condition up to a depth of about 6ft. Then, the bentonite slurry was pumped into the excavation to maintain hole stability and drilling continued to the required shaft depth. Like reaction drilled shaft construction, no drilling issues (heaving, caving, and slurry loss) were noticed during the excavation of any of the test shafts. For each test shaft, excavation was performed in the morning and the concrete placement was carried out in the afternoon. Before reinforcing cage placement in the excavation, the slurry was desanded, the hole was cleaned and the depth to the bottom of the excavation was rechecked. The FDOT drilled shaft inspectors measured the properties of bentonite slurry regularly; measured range of properties is presented in Table 4-6 along with the range specified in the FDOT specification 455. A 4-ft diameter x 1.5

ft long template (casing) and frame with adjustable legs were placed at the top of excavation to form the shaft above the ground surface (Figure 4-20).



(a) TS2



(b) TS3

Figure 4-19: Completely instrumented test shafts TS2 and TS3

Table 4-6. Measured range of properties of bentonite slurry (test shafts)

Properties	Measured	Range specified in FDOT specification: 455-15.8.1 (65 ⁰ F)
Density	64 - 65	64 - 73 lb/ft ³
Viscosity	32 - 33	30 - 40 seconds
pH	9	8 - 11
Sand content	< 0.5%	≤4%

4.4.3 Placement of reinforcement cage, concrete, embedded pipe and flange section, and Dywidag bars

After drilling and cleaning the hole, the reinforcing cage with CSL tubes and inclinometer casing (in case of TS2 and TS3) was lowered into the excavation using a truck mounted hydraulic crane (Figure 4-20). In the case of test shaft TS2, the cage was oriented with a “Total station” such that one pair of inclinometer casing grooves and strain gauges aligned with the direction of lateral load tests.



Figure 4-20. Lowering reinforcing cage to excavation

As shown in Figures 4-16 and 4-17, the minimum spacing between the embedded pipe & flange section and rebar cage with CSL tube was only 3.87-in. Use of #57 coarse aggregate (maximum size = 1 -1½-in, which is commonly used in class IV (drilled shaft) concrete) could possibly results in segregation of concrete or lifting of the reinforcing cage during concreting. In

order to avoid or reduce these issues, it was decided to use a smaller sized aggregate distribution. As per “FDOT standard specification, section 346: Portland Cement Concrete”, #89 aggregate (maximum size = ½”) may be used in concrete with Engineer’s approval. Accordingly a concrete mix with the properties as shown in Table 4-7 was used for all the test shafts. Table 4-8 shows the measured range of the properties of the fresh concrete, which was fully compliant with values recommended by FDOT specification 346. During the placement, concrete trucks tailgated the concrete to the hopper and the tremie was gradually raised as the concrete flowed into the shafts. The actual volume of concrete placed slightly exceeded the theoretical volume for all the test shafts (see Appendix B for drilled shaft logs). After completely filling the excavation and top template (casing resting on ground), the alignment of rebar cage and inclinometer casing (TS2) was verified using a “Total station”.

Table 4-7. Properties of new concrete mix

Mix number	HC62JD
Comp. Strength 28 days (psi)	4000
Slump (in)	8+/- 1”
Air Content (%)	1.5%
Plastic Unit Weight (lbs/cf)	143.4 +/- 1.5
Cement	70%
Slag	30%
Coarse aggregate	#89 aggregate

Table 4-8. Measured properties of fresh concrete

Properties	measured	Range specified in 346
Slump	8 – 10 in	7 - 10 in
Air content	1.4 - 1.5%	0 - 6%

Subsequent to the completion of concrete placement, the pipe and flange section was lowered into the concrete using a crane as shown in Figure 4-21. Since the top flange of the section needs to be 6-in above the shaft top, the required clearance was maintained using angle sections (bolted to flange) and steel clips resting on the top of the casing (Figure 4-21). The section was then aligned and leveled using digital level and the “Total station”. Next, for shafts TS2 and TS3, the Dywidag bar cage (4 bars) was placed within the embedded pipe as shown in Figure 4-22. The Dywidag bars are required for attaching the lateral load test frame to the test shafts. Figure 4-23 displays the test site after the construction of reaction and test drilled shafts.



Figure 4-21. Installation of embedded pipe and flange section



Figure 4-22. Installation of Dywidag cage within pipe and flange section

Concrete cylinders were collected for each truck to assess compressive strength (7th day and 28th day) and Young’s modulus. Table 4-9 presents the measured compressive strength for all test shafts after 28th day. As shown from the Table 4-9, the minimum 28th day compressive strength for the new mix was 6290 psi, which was much greater than the design 28th day compressive strength (4000 psi).

Table 4-9. Measured 28th day compressive strength (test shafts)

Shaft No.	Sample No.	28 th day comp. strength (psi)	Average (psi)
TS1	1d	6711	6718
TS2	1a	7195	
	2d	6761	
TS3	1b	6632	
	2b	6290	



Figure 4-23. Test site with reaction and test drilled shafts.

4.5 Cross-Hole Sonic Logging (CSL) Tests on Test Drilled Shafts

Cross-Hole Sonic Logging (CSL) Tests on the three test drilled shafts were performed by the State Material Office, Gainesville, to verify final integrity. Tests were conducted in accordance with ASTM D 6760 using Cross Hole Analyzer (CHA) manufactured by Pile Dynamics, Inc., after a curing period of 12-14 days. The later complies with FDOT specification 455-17.6.1.2, i.e., concrete compressive strength of test shafts must exceeded 3000 psi before testing. Figure 4-24 shows the CSL testing setup for one of the test shafts. The tests were carried out by lowering an ultrasonic source transmitter and a receiver/phone to the bottom of the shaft through separate CSL tubes and raising them simultaneously while the transmitter probe emits ultrasonic signals at 2.5-in depth intervals along the tubes with the receiver monitoring magnitude and arrival times. Considering all the possible tube pair combinations, a total of six log profiles were performed for each shaft.



Figure 4-24. CSL testing setup for test shaft

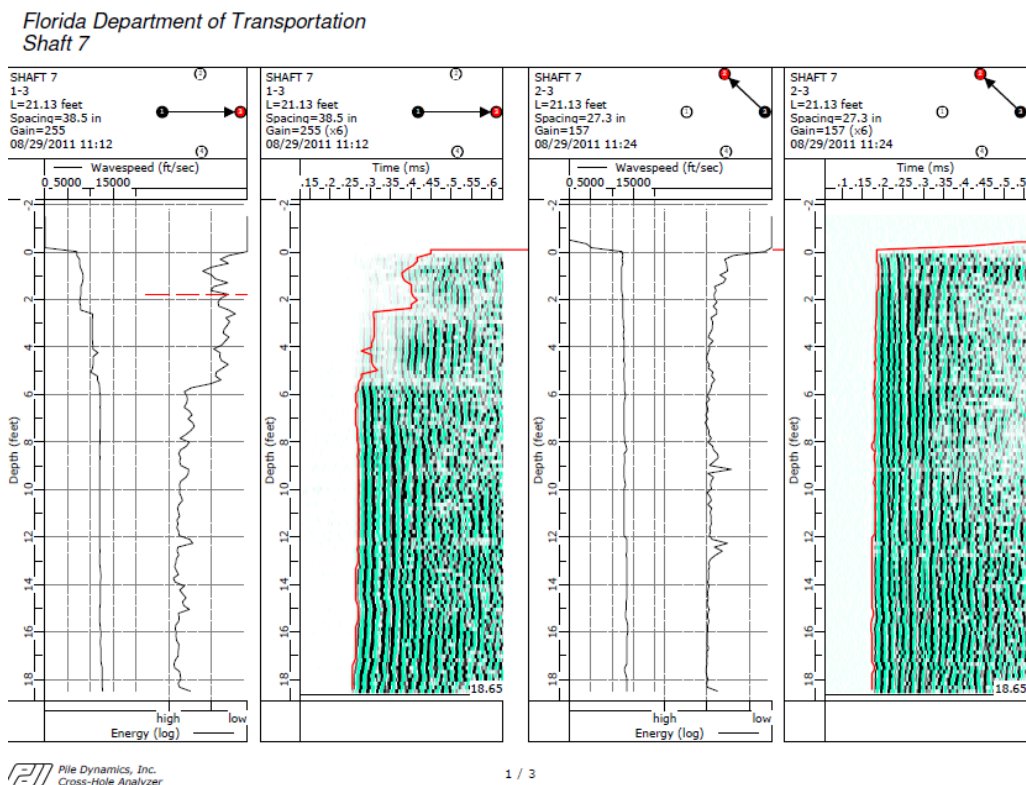


Figure 4-25. Typical CSL results for the test shafts (TS3)

Figure 4-25 presents typical CSL results for the test shafts. The results for each profile (each tube pair logging) include wave speed versus depth, pulse energy versus depth and sonic

map (or “water fall diagram”) along with first arrival time (FAT). The CSL results for all the shafts were nearly identical. As shown in the Figure 4-25, CSL results for all the adjacent tube pairs (perimeter tube pairs) indicated uniform first arrival time and energy throughout the depth. It is evident from the above observation that, all the shafts were of high quality and integrity. However, CSL results for the diagonal tube pairs for all the test shafts showed identical reduction in wave speed (increase in FAT) and energy/signal strength over the top 5.5 ft of shaft (Figure 4-25), which is the zone where the pipe and flange section for the combined torsion and lateral load test was embedded. The measured wave speed (or first arrival time) and energy were nearly constant for the shaft segment below 5.5 ft depth (Figure 4-25), which indicated that the shafts were of good quality, and hence the lower wave speed and energy for the top 5.5 ft was obviously due to the presence of embedded pipe and flange section. The actual mechanism behind this reduction is not clear. It is believed that the reduction may be due to the difference in impedance of steel and concrete. As the wave propagates through the embedded pipe and flange section during logging, it gets partially reflected and partially refracted at the interface of steel and concrete. The refracted component will be smaller because of the smaller impedance of concrete compared to steel. The smaller impedance will reduce the amplitude/energy of the transmitted wave and causing a shadowing effect as shown in the sonic map (Figure 4-25). The first arrival time (FAT) for all the testing was selected by setting absolute and relative thresholds in the cross-hole analyzer (CHA) system. The relative threshold is set based on the maximum signal received for the individual logging. Note that in determining FAT, the CHA system will only consider the received waves with energy exceeding the threshold values. Since the wave transmitted through the embedded pipe and flange section has greatly reduced amplitude/energy (may be less than threshold value), the CHA system filters it out while determining the FAT.

Consequently, the measured FAT may be greater than the true value, and hence the estimated wave speed (spacing between tubes/FAT) may be less than the actual value. Results of all the CSL testing performed are included in Appendix B.

CHAPTER 5 DESIGN AND CONSTRUCTION OF JET-GROUTED PILES

This Chapter discusses the design and construction of jet-grouted piles for axial lateral, and combined torsion with lateral load. To limit the influence of depth, diameter, etc., it was decided to compare the new pile with a current mast arm foundation (drilled shaft) of similar dimensions. Accordingly, the piles would be embedded 18 ft and have a diameter of 4 ft (i.e., after side grouting). To transfer the mast arm torque, moments, etc. to the pile, a reinforced concrete cap was designed. A detailed description of the design and construction of the concrete cap is included in this Chapter. Analysis of the noise and ground surface vibration data measured during the jetting and grouting of the piles is also presented.

5.1 Structural Design of the Precast Pile Section

The precast section for the jet-grouted pile should transfer the forces and moments acting on top of the foundation (torsion, axial and lateral) to the side and tip of the pile without structural failure. Moreover, the section should have enough cross-sectional area to accommodate both the reinforcement as well as the grout delivery system. Accordingly, a 28-in x 28-in reinforced concrete section was chosen for the precast pile element to carry the expected maximum loads. Steel reinforcement for the section was determined in accordance with ACI 318-08. Concrete compressive strength of 5000 psi was used in the design (Appendix C). The estimated threshold torsional strength for the section without reinforcement (32 kip-ft) was much less than the anticipated torsion (≈ 560 kip-ft), requiring the use of steel torsional reinforcement. Traverse steel reinforcements, #5 bars @ 2.5 -in spacing, was estimated to provide a nominal torsional resistance of 737 kip-ft (Appendix C). The pile section with 16 #9 bars (2.04% of C.S area) has a flexural strength of 783 kip-ft, an axial capacity of 3465 kip and a shear capacity of

403 kip as found in Appendix C. Shown in Figure 5-1 is the cross-section view of the precast pile with the rebar details.

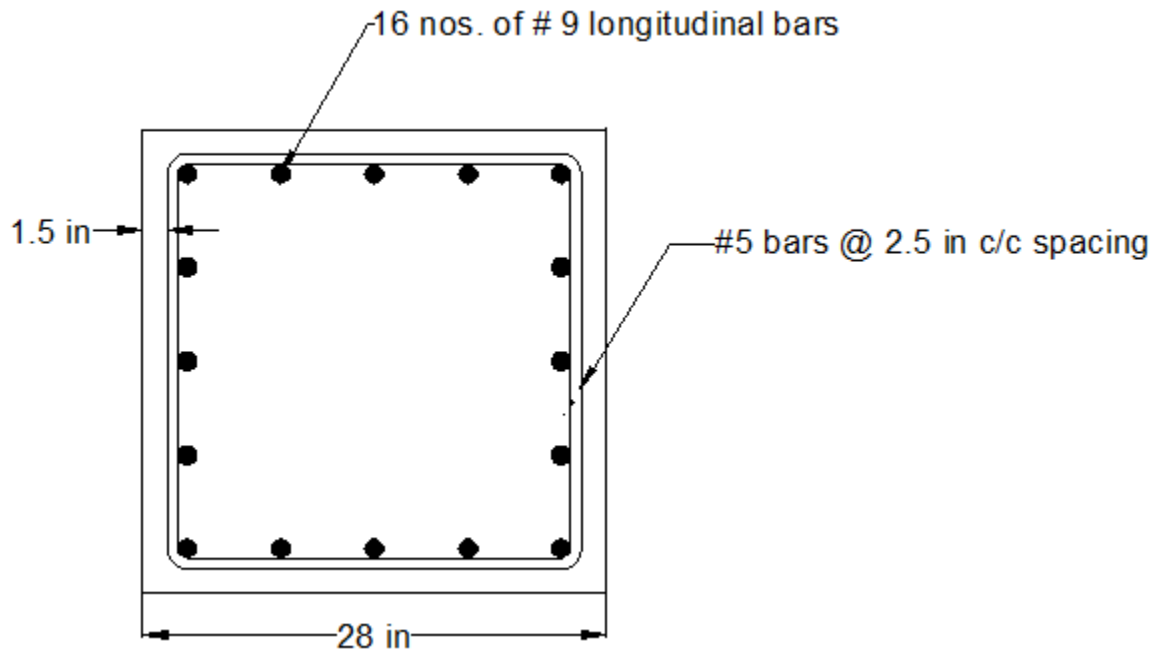


Figure 5-1. Cross-section of precast pile component with reinforcement details

5.2 Design and Fabrication of Grout Delivery and Jetting Systems

Figure 5-2 displays the schematic diagram of the jet-grouted pile with side grout membranes, instrumentation and concrete cap. External to the pile are two 7 ft long side grout bags with separate grout delivery systems. In conformity with the previous FDOT research projects (BD545, RPWO # 31 and BDK-75-977-07), 1-in PVC pipes were selected for the grout delivery systems. Figure 5-3 shows the fabrication of grout delivery systems. Each grout delivery system had its own grout entry and exit pipe. This facilitated the cleaning of grout system for potential of regrouting. Each of the grout pipes (entry & exit) had 7 pairs of holes with 3-in center to center spacing (Figure 5-3), evenly distributed (5-in intervals) along the bottom $\frac{2}{3}$ rd of each grout bag. For the bottom 4 pairs, the diameter of hole was $\frac{1}{2}$ -in and for the top 3 pairs, it

was $\frac{3}{8}$ -in. Each pair of holes was covered with 1-in diameter gum rubber (1/4-in thick) membranes (Figure 5-3). The gum rubber membrane allowed the grout to exit the grout pipe under high pressure, but prevented the exit of water when cleaning the pipes or re-entry of grout after placement.

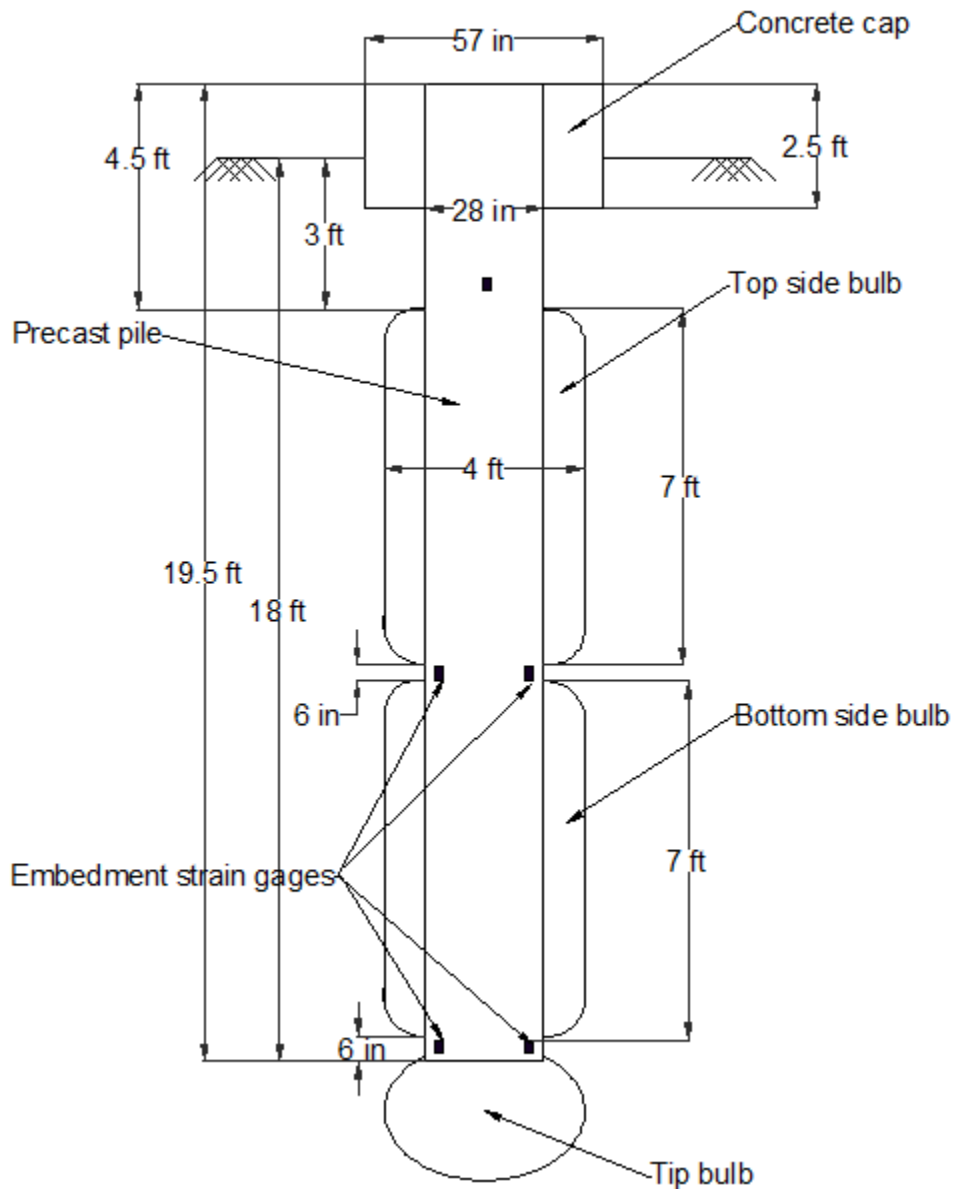


Figure 5-2. Schematic diagram of jet-grouted pile



Figure 5-3. Grout delivery systems for side grouting

Figure 5-4 shows the PVC piping which was used for jetting of precast pile into ground. The same jetting pipes were also used for tip grouting after side grouting of the pile. Diameter of the central jetting pipe was determined based on the guidelines recommended by Tsinker (1988) with the flow rate equation (Equation 2-1) for sandy soil suggested by Shestopal (1959).

Table 5-1. Estimation of required jet pipe diameter

D in (cm)	l ft (m)	d_{50} (mm)	Soil Type	k (m/day)	Q (m ³ /hr)	Velocity (m/s)	Jet pipe area $A = Q/V$ (mm ²)	Jet pipe diameter in (mm)
28 (71.1)	15 (4.57)	0.17 ^a	A3	11.23 ^b	82.3 ^c	5 ^d	4572	3 in (76.2 mm)

^a from grain size analysis

^b for A3 soil, Smith and Bloomquist (2010)

^c using Equation (2-1)

^d Tsinker (1988)



Figure 5-4. Jetting system for jet-grouted pile

Table 5-1 presents the estimation of diameter of the central (main) jetting pipe. Shestopal's Equation (2-1), suggests a flow rate of approximately 362 gallon/minute (82.3 m³/hr). Gabr et al. (2004) identified that pile insertion rate increases with increase in flow velocity for a given flow rate. Whereas, Tsinker (1988) recommended that velocity of flow

should not be greater than 16.4 ft/s (5 m/s). Hence an optimum velocity of 5 m/s was considered in the present case and required jet pipe diameter was estimated to be 3-in (Table 5-1). The central jet pipe branched off into five 2-in diameter pipes at bottom of pile for uniform distribution of water at tip. In order to maintain the uniform flow velocity, nozzles were attached at the exit of all the jet pipes after the curing of the precast piles (discussed later). It should be noted that the nozzles at the end of the jet pipes also prevent ingress of sand/fines into the jet/grout pipe after jetting, which can result in grout blockage during tip grouting.

5.3 Construction of Precast Piles

Formwork for casting the piles was assembled using plywood sheets reinforced with 2-in x 4-in wooden strips as shown in Figure 5-5. The bracings as shown were needed to provide adequate stability to the concrete when first placed.



Figure 5-5. Formwork for precast piles

The reinforcement cage was fabricated in accordance with the design (Section 5.1). Figure 5-6 shows the placement and attachment of PVC side and tip jetting/grouting pipes to the pile's reinforcing cage. Also shown in Figure 5-6 (Middle and Bottom) are 4 bolts/ side attached via 3/8-in thick x 2.5-in wide steel plates to reinforcing cage. These bolts will be used to attach the side grout membranes to the pile prior to jetting. One inch diameter threaded bolts were used for bottom membrane and 3/4-in diameter bolts were used for top membrane.



Figure 5-6. Reinforcement cage with grout delivery systems, jetting system, and instrumentation

The piles were instrumented with 5 concrete embedment strain gauges (Figure 5-2 and 5-6) for monitoring the load distribution along the piles during the top-down load test. One gauge was installed at the center of the pile, just above the top grout membrane (Figure 5-2), in order to assess load transferred to soil from the concrete cap during loading. The middle pair of gauges

was positioned between the top and bottom membranes for estimating load shedding between the top and bottom membranes. The final pair of gauges were installed at the bottom (i.e., below bottom membrane) of pile, in order to differentiate the tip resistance from the side resistance during axial top-down testing as well as mobilized tip resistance during tip grouting of the piles. All the strain gauge wiring was routed through ½-in PVC pipes to the top of pile to protect the wires during torsion testing of the piles. All gauges were tied securely to the inside of reinforcement cage using plastic tie wires.



Figure 5-7. Reinforcement cage within the formwork ready for concrete placement

Shown in Figure 5-7 is the rebar cage centered in the formwork ready for concrete placement. As shown from the Figure 5-7, the side grout delivery pipes were temporarily tied to formwork to keep them from moving during the concrete placement. Since the clear spacing of the shear steel, i.e., transverse reinforcement, was only 2-in, it was decided to use #89 aggregate (maximum size = ½-in) for the concrete mix. In conformity with the structural design

requirements (i.e., torsion), the required minimum 28th day compressive strength for the concrete was 5000 psi. The concrete was obtained from a nearby ready-mix yard (Florida Rock Industries, Inc.) and the properties of the mix are given in Table 5-2.

Table 5-2. Properties of the concrete mix

Mix number	C85JC
Comp. Strength 28 days (psi)	5000
w/c ratio	0.39
Slump (in)	5+/- 1"
Air Content (%)	3.0%
Plastic Unit Weight (pcf)	140.5 ± 1.5
Cement	C 150, type II
Fine aggregate	sand
Coarse aggregate	#89 stone
Admixture	C 494, W/reducer

Table 5-3. Measured properties of concrete

Properties	measured
Slump	5.25 in
Air content	3.3%
7 th day comp. strength	6848 psi
28 th day comp. strength	8069 psi

Table 5-3 shows the measured slump, air content of the placed concrete. During concreting, the truck “tailgated”, Figure 5-8, concrete was poured directly into the formwork and a concrete vibrator was used to consolidate the fresh concrete (release entrapped air and move large aggregate), ensuring bonding with the reinforcement. After completely filling the

formwork, the top surface was leveled using straight edge and trowel. The pile was then covered with plastic and was allowed to cure for 28 days.



Figure 5-8. Concrete placement

During the pour, concrete cylinders (4-in diameter x 8-in long) were collected to measure compressive strength and Young's modulus of the concrete. After 7 and 28 days, the concrete cylinders were tested under compression loading (Table 3). As shown in the table, even the 7th day compressive strength (6848 psi) of the poured material was greater than the design 28th day compressive strength (i.e., 5000 psi).

5.4 Preparation of Precast Piles for Jetting

After sufficient time for curing, the formwork was detached and excess concrete at the location of side grout exit ports (covered with gum rubber) was removed. Then the precast piles were prepared for jetting, which involved: (1) flushing of each grout delivery systems to ensure proper function, (2) testing the membrane, (3) attaching top and bottom side grout membranes, (4) attaching nozzles for jetting/tip grouting system, and (5) testing of nozzles to ensure uniform water distribution spread at the pile tip.

5.4.1 Flushing of each grout delivery systems to ensure proper function

Each grout delivery system (both top and bottom) was connected to the city water supply and flushed to ensure that the systems were working properly (Figure 5-9). A pressure of approximately 7 psi was needed for water to exit through the ports after expanding the gum rubber covers.



Figure 5-9. Flushing the grout delivery systems

5.4.2 Testing the membrane

The membrane used for side grout bags was 45-mil thick reinforced polypropylene geomembrane (RPP). This RRP membrane was slightly different from the one used in the ongoing FDOT research project: “Bottom side grouting of drilled shafts prior to tip grouting (BDK- 75-977-46). Therefore the membrane was first tested for interface friction angle (δ) and tensile strength. The friction angle for the membrane - soil interface (δ) was determined from direct shear testing at different normal stresses. The soil used for the tests was a typical Florida silty sand. Figure 5-10 presents the failure envelopes for the membrane-soil interface and the soil itself. The interface friction angle, δ , is found to be 22.5° versus $\phi = 33.5^\circ$ for soil ($\delta = 0.7 \phi$). To improve friction, small ($\approx 1/16$ -in) holes @ 6-in spacing (square pattern) were made in the membrane between the polymer reinforcements.

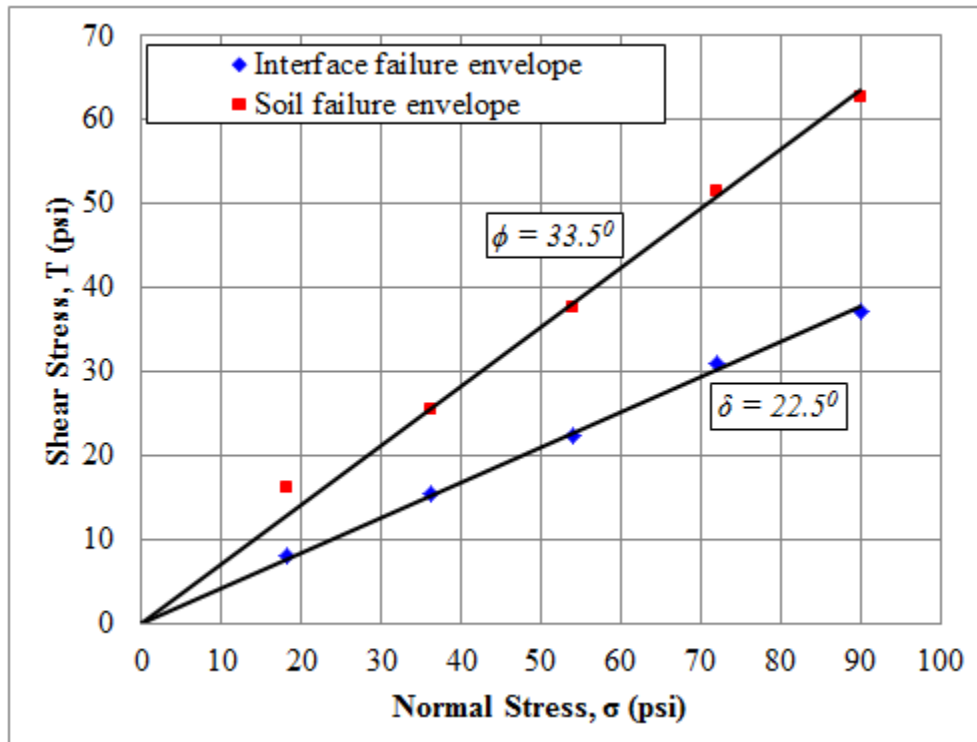


Figure 5-10. Failure envelope for direct shear tests on membrane-soil interface

Tensile strength of the membrane was estimated by conducting tension tests (Figure 5-11) on a number of 1.25-in wide continuous membrane loops formed by heat seaming the ends with an overlap of 6-in. Membranes with (1/16-in Ø, without cutting reinforcement) holes and without holes were tested. Using the universal testing machine (UTM), the specimens were loaded until failure. Average tensile strength of all membranes was 3210 psi. Both the strips with and without holes showed similar results, which indicated that drilling of holes without cutting the reinforcement does not cause any strength reduction.



Figure 5-11. Tension test of membrane strip

5.4.3 Attaching top and bottom side grout membranes

The width of the membrane roll purchased for the jet-grouted piles was 12 ft. As per the design, the final diameter of side grout bulbs for jet-grouted pile was 48-in, which equates to a perimeter of 150.8-in. Considering a vertical seam width (overlap) of 6-in, the total membrane width required to make a 48-in diameter cylinder was 156.8-in, which was rounded up to 160-in. Accordingly, the membrane roll was cut into four rectangular pieces of 160 -in width. Next, each

piece was rolled to form a cylinder (48-in diameter) and an overlap/pleat (i.e., heat seam) was created using two 6-in square hot plates at a temperature of about 130⁰C (5 minute holding time). The length of each side grout zone for the pile was 7 ft (84-in). For each grout zone, the total length of the required membrane was the sum of the length of side grout zone, additional length for expansion outward during grouting, and width of steel plates for attaching the membrane to pile at both ends (i.e., $84 + 20 + (2 \times 3) + 3$ in extra = 113 in). Each vertically seamed membrane was cut to a length of 113-in (Figure 5-12). A grid of small holes (1/16-in Ø) at 6-in spacing were drilled into the membrane, which was expected to allow the grout seepage through the membrane during grouting process and thus develop improved bonding between the grout bag and the surrounding soil.



Figure 5-12. Membrane seamed for side grout zone

In order to attach the membrane to the pile, both vertical and horizontal pleats had to be placed in the membrane. Note that the vertical pleats will reduce the circumference and one horizontal pleat will reduce the height of the membrane. For each pile, the horizontal pleat was placed first in the middle by folding the membrane roll. Then, the membrane was positioned at

the location of grout zone (Figure 5-13). Finally, the membrane was attached to the pile in such a way that a vertical pleat of about 4.5-in wide was made in the middle of each face. The membrane was secured to the pile by means of steel plates and threaded rods embedded in pile (Figure 5-13). Silicone gasket maker was used to seal the attachment (Figure 5-13). Figure 5-14 displays one of the piles after attaching the top and bottom grout membranes.



Figure 5-13. Attaching membrane to pile



Figure 5-14. Pile after attaching the grout membranes

5.4.4 Attaching nozzles for jetting/tip grouting system

At the bottom of pile, the central 3-in jet pipe branched off into five 2-in diameter pipes for tip jetting of the pile as discussed earlier. The nozzles were attached at the exit of all the 2-in jet pipes (Figure 5-15). The nozzle pattern for all the outer pipes was same; four – ½-in diameter holes, as shown in Figure 5-15. For the central pipe, the nozzle pattern consisted of four – ½-in diameter holes and one- 3/8-in diameter hole in the middle.



Figure 5-15. Pile after attaching nozzles

5.4.5 Testing of nozzles to ensure uniform water distribution at tip

After attaching the nozzles to the piles, they were tested to ensure uniform water distribution at the bottom (Figure 5-16). Test was performed by connecting the central jet pipe to

the city water supply. The maximum water pressure recorded by pressure gauge was less than 5 psi. As evident from the Figure 5-16, flow distribution was virtually uniform even under small pressure.



Figure 5-16. Nozzle testing

5.5 Jetting of Piles

After preparation, the piles were transported from Coastal Engineering Lab to the test site using a flatbed truck. Jetting of the piles was performed with the help of Reliable Constructors inc., Mount Dora, FL and SMO, Gainesville. In order to reduce water loss (e.g., percolation) and minimize water requirement during jetting, it was decided to collect the water flowing up around the pile during jetting. Accordingly, 3 ft deep holes were made at the location of both piles using a backhoe and 7 ft diameter x 5 ft long surface casings were installed to collect the water coming up during the jetting process (Figure 5-17). A 50 ton crane was used for positioning and holding the pile during the jetting process. After unloading the pile from flat bed, the jet hose was attached to the top of pile. Subsequently, the pile was positioned in the hole and aligned properly with reaction drilled shafts on either side using a surveying level.

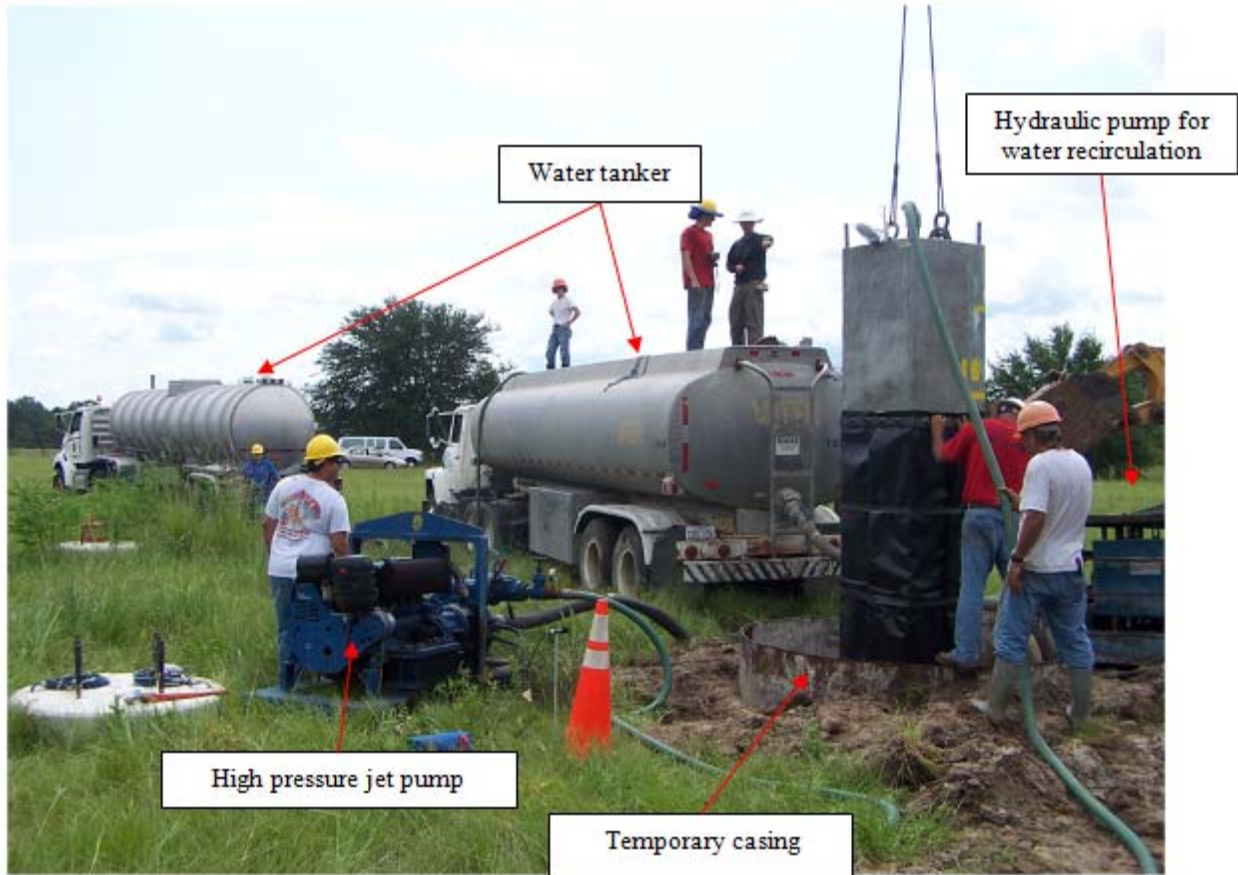


Figure 5-17. Pile jetting

Figure 5-17 shows the setup for pile jetting. As shown in the Figure 5-17 two water tankers were used; one tanker (Reliable Constructor's) provided water for jetting and the other (SMO's) as back up, i.e., water from the SMO's tanker was pumped to the Reliable's tanker when the water levels diminished. The pressurized water for jetting was provided to the test pile from the water tanker through a 6-in high pressure jet pump (max. flow rate = 1600 gallon/minute and max. pressure = 184 psi), Figure 5-17. The pump was equipped with flow meter and pressure gauge to monitor the flow rate and pressure respectively. Jetting initiated with flow of water from the water tank through the pump to the test pile with a flow rate of 400 gallon/minute and a pressure of about 130-135 psi. Subsequently the test pile was lowered with

the crane as penetration occurred. The pile was allowed to penetrate with its own self-weight by releasing the weight steadily from the crane. A hydraulic trash pump (maximum flow rate = 1300 gpm and pressure = 65 psi) was used to pump the water collected in the surface casing back to the tanker (Figure 5-17) at a flow rate of nearly equal to the jetting flow rate (400 gallon/minute). Total water loss (percolation) during the jetting of two piles was approximately 1000 gallons. After jetting of each pile, the casing was pulled out and soil was backfilled around the pile, Figure 5-18.

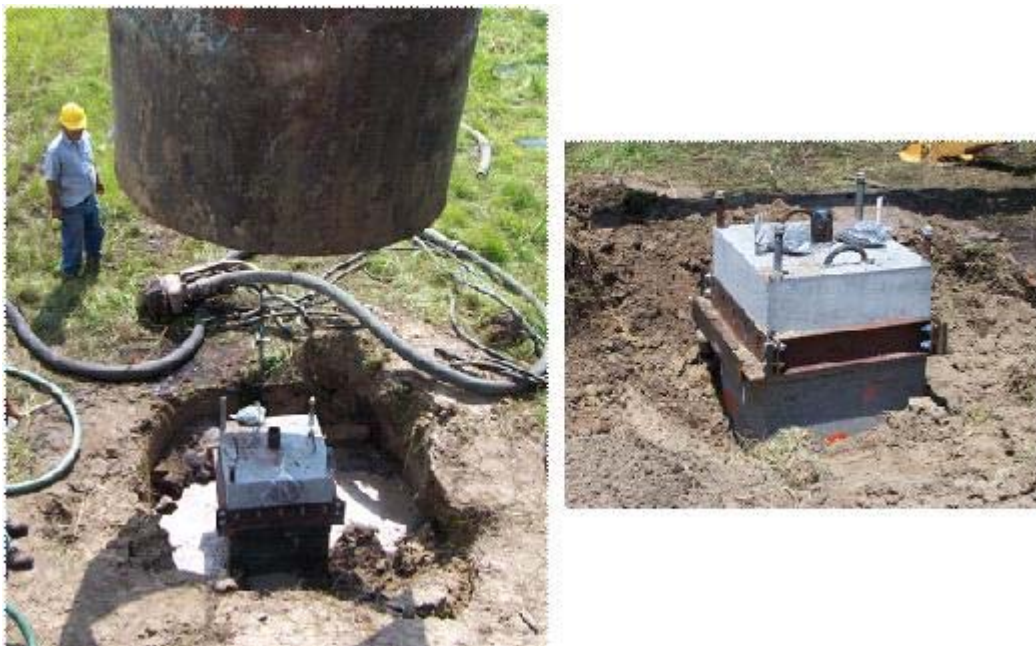


Figure 5-18. Pulling out the casing after jetting and soil backfilled

SMO, Gainesville, monitored the noise and ground surface vibration during the pile jetting operation. The equipment used for the measurement consisted of five sets of Vibration and Overpressure Monitor (Instantel® Minimate Plus™) with triaxial geophone (velocity transducer) and overpressure microphone. Analysis of the data collected using the instrumentation is presented later.

5.6 Design and Construction of Concrete Cap for Jet-Grouted Piles

A reinforced concrete cap was required for transferring the forces and moments from the loading assembly (Mast arm structure) to the pile during the combined torsion and lateral load testing. A precast concrete cap was chosen for one of the jet-grouted piles and a cast-in place cap for the other. Figure 5-19 depicts the schematic of precast concrete cap - pile connection.

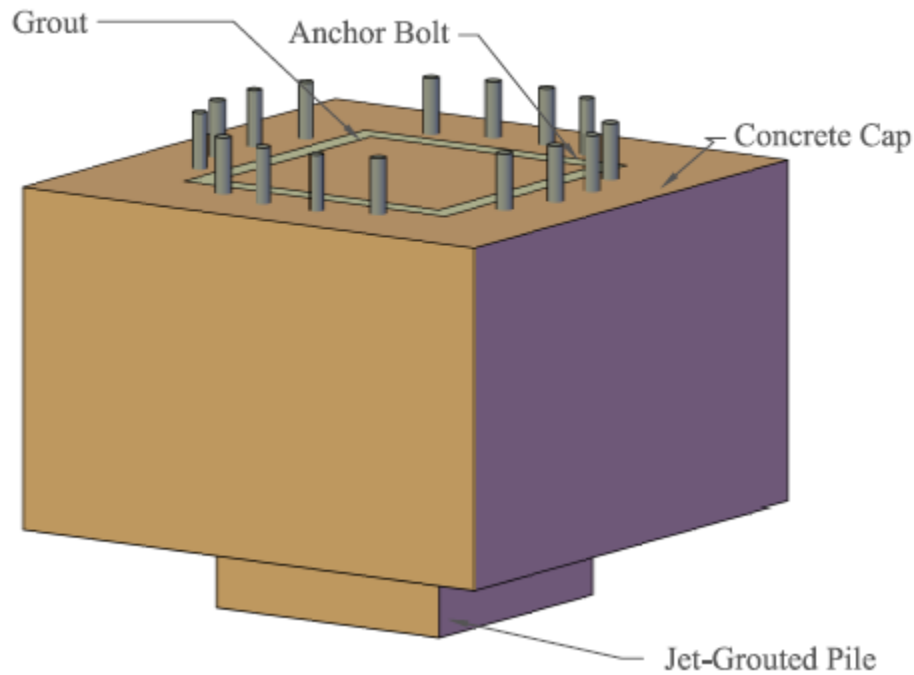


Figure 5-19. Schematic of precast concrete cap-pile connection

5.6.1 Design of concrete cap

The starting point for the design of concrete cap was the dimension of inner square hole required for the precast pile head. In case of the precast cap, a 2-in grout space/gap between the cap hole and pile was designed, which provided space for leveling as well as placement of the standard grout tube used in the industry. Next, the other dimensions (width, and depth), (anchor bolts, and reinforcement (flexural, torsional and shear) were designed to meet various standard code requirements (ACI 318 - 08, AASHTO LRFD, AISC 360-05, etc.). Detailed design

calculations for the cap are given in Appendix C. The diameter and the number of ASTM F1554 Grade 55 anchor bolts required to transfer the loads from Mast arm pole to foundation were determined by considering steel strength requirements of anchors in tension and shear (ACI 318 - 08, AASHTO LRFD, AISC 360-05). It was found that sixteen - 1.5-in diameter bolts were sufficient for transferring the anticipated forces and moments. Shown in Figure 5-20 are the longitudinal and cross-sectional views of concrete cap – pile connection.

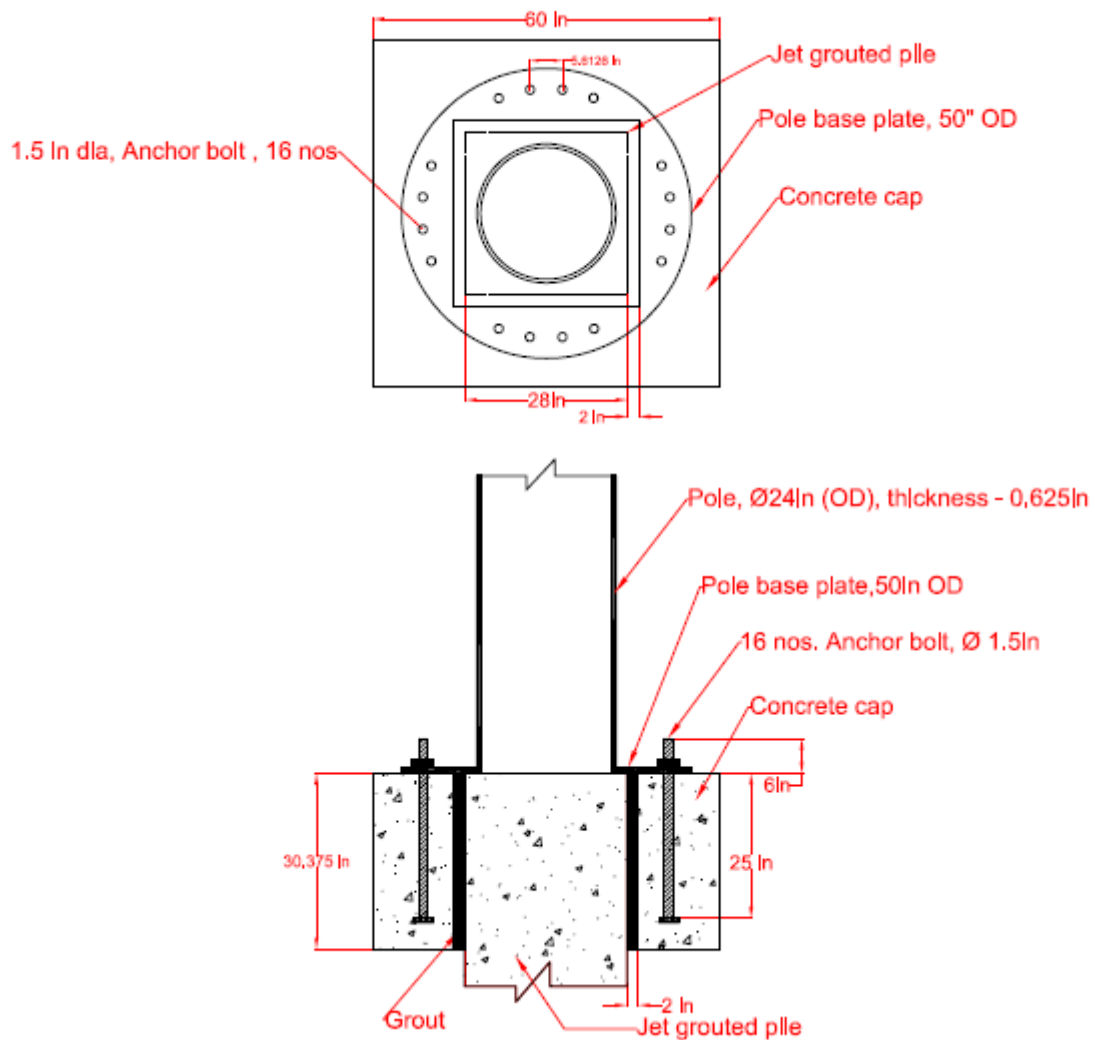


Figure 5-20. Longitudinal and cross-sectional views of concrete cap-pile connection

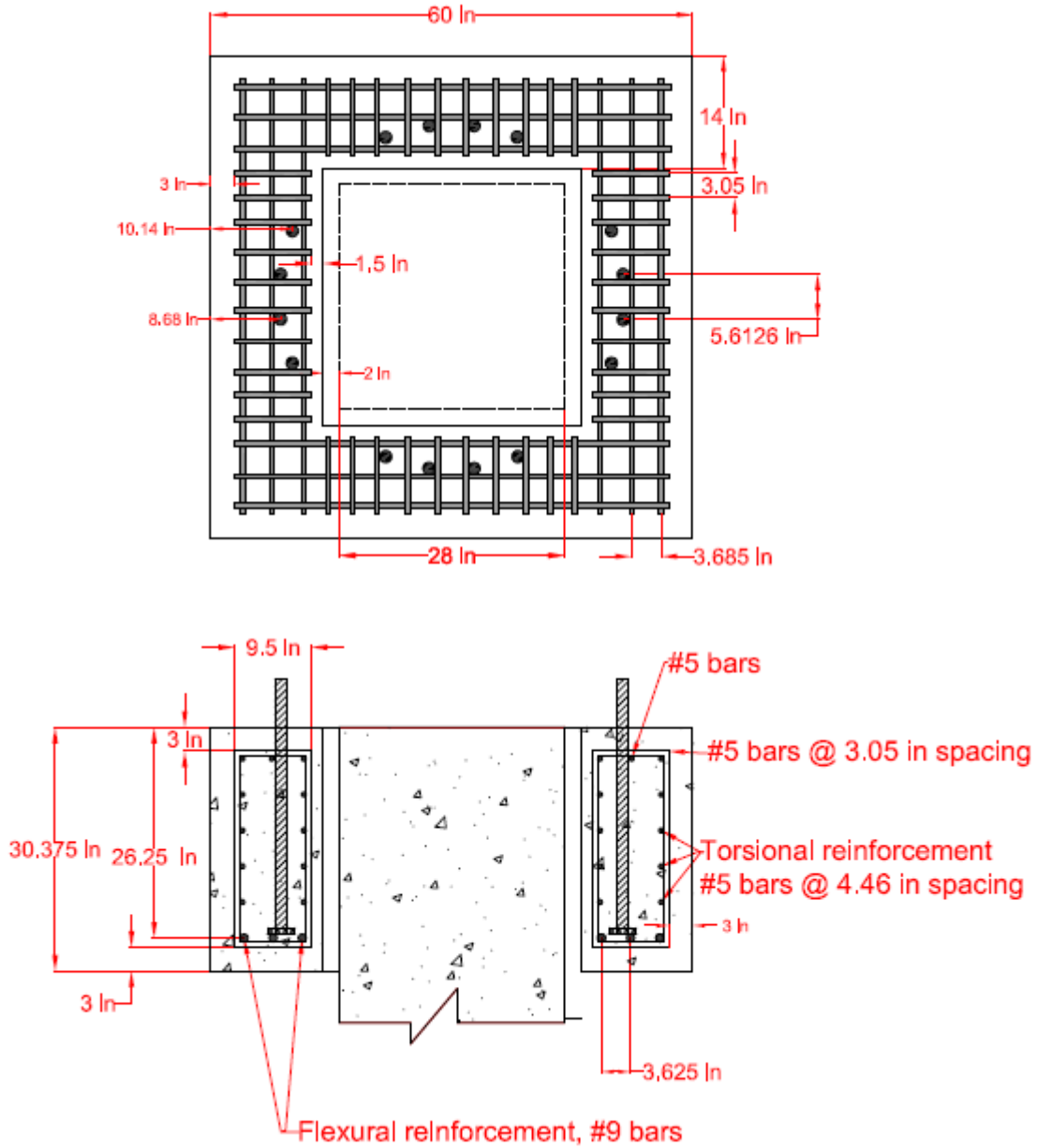


Figure 5-21. Longitudinal section and cross-section of concrete cap with reinforcement details

The optimum dimensions (outer width and depth) for the cap was selected considering the concrete breakout strength of anchor groups in shear, side face “blowout” failure of anchors in tension, concrete pry out strength in shear, anchor bolt embedment, FDOT’s clear cover requirement and cost. A square cap with 60-in outer width and 30.375-in depth was found to be adequate for transferring the forces and moments generated during load tests without concrete

breakout and side face blowout failure (Figure 5-20 and Appendix C). A minimum clear cover of 3-in was provided to all the reinforcements for all the exposed sides of cap in accordance with FDOT's "Structures Design Guidelines for LRFD" (2002), assuming that the site condition as "moderately aggressive". The required anchor bolt embedment depth was determined by considering the development length for longitudinal reinforcement and spacing between anchor bolts and longitudinal reinforcement in accordance with NCHRP (2003). The development length for # 5 rebars was determined to be 15.91in based on ACI 318-08 12.3.3. The minimum horizontal distance between the anchor bolts and the outer vertical reinforcement was 5.37 in. Consequently, the required embedded depth for anchors was estimated to be 24.28-in ($15.91+5.37+$ top clear cover (3) = $24.28 \approx 25$ -in, see Appendix C).

Steel reinforcement for concrete cap was calculated according to ACI 318-08. A concrete strength of 5000 psi was used in the design. The calculations are included in Appendix C. Figure 5-21 shows the longitudinal and cross-section of cap with reinforcement details. Flexural reinforcement comprised 6 - #9 bars in both directions (3 on each side as shown in Figure 5-21). Design flexural capacity (nominal x phi (Φ) factor) of the section with the above reinforcement was found to be 661 kip-ft. The torsional steel reinforcement consist of #5 bars at 4.46-in center to center spacing as shown in 5-21, which was shown to provide a design torsional strength of 2525 kip-ft (Appendix C). It was also verified that the design shear capacity (303 kip) of vertical section of cap is enough to resist the expected maximum shear force (279 kip) on the section during torsion test. Note that the dimensions and various reinforcements for both precast and cast-in place cap were the same. Only difference was the grout space/gap for the precast one. Estimation of grout tensile strength, shear strength and bond resistance at grout-concrete interface of the precast cap-pile connection using the strength properties of cementitious non-

shrink grout approved by FDOT (Qualified Products list) indicated that the interface could safely transfer the forces from cap to pile during different load tests (Appendix C).

5.6.2 Construction of concrete cap

Figure 5-22 displays the formwork assembled for casting the cap. The mold was assembled using plywood sheets (3/4-in thick) as facing with 2-in x 4-in wooden members as bracing. The bracing ensured minimal movement of the concrete during placement (hydrostatic pressure) as a result of the tight tolerance between pile and cap. The inner framework (only for precast cap) was the cutout of the pile with a 2-in grout gap.



Figure 5-22. Formwork for concrete cap

The reinforcing cage for the cap was fabricated in accordance with the design (Section 5.6.1) as shown in Figure 5-23. Figure 5-24 shows an anchor bolt welded to 3.5-in diameter x $\frac{3}{4}$ -in thick bearing plate. The anchor bolts were positioned within the reinforcement cage in

accordance with the design layout (Figure 5-20 and 21). Figure 5-25 depicts the reinforcement cages within the formwork ready for concrete placement. The template in the form of steel rings, Figure 5-25, aligns the anchor bolts both in circular pattern and elevation. The template was attached to the formwork/pile (Figure 5-25), which prevented the misplacement of anchor bolt group during the concrete placement operations (pouring, vibration, etc.).



Figure 5-23.: Reinforcement cage for concrete cap



Figure 5-24. Anchor bolt welded to 3.5-in diameter x $\frac{3}{4}$ -in-thick bearing plate



a) Precast cap



b) Cast-in place cap

Figure 5-25. Reinforcement cage for caps ready for concrete placement

The concrete mix used for the caps was the same as that for the piles. The ready mix truck “tailgated” concrete directly into the formwork and the concrete was then vibrated using a concrete vibrator to release entrapped air and move large size aggregates (Figure 5-26). After the concrete placement, the top surface was leveled by means of straight edge and trowel.



a) Precast cap



b) Cast-in place cap

Figure 5-26. Concrete placement for caps

Figure 5-27 displays the placement of precast concrete cap. It was ensured that the gap between the pile and cap was uniform (i.e., 2-in) all around the pile. The gap was then grouted using the FDOT approved cementitious non-shrink non-metallic grout: Vibropruf#11 (Reference: FDOT Quality Product List- section 934). The grout was mixed to a fluid consistency (4.5 quarts water per 50 lb bag of grout) using a revolving concrete mixer as per the manufacturer's recommendation (Figure 5-27). The grout was filled from bottom to top (free

flow) using a funnel and a hose. Any air entrapped in the filled region was removed by tamping with a steel rod. About 32 gallon of grout was required to completely fill the gap.



Figure 5-27. Precast cap placement and grouting

5.7 Side Grouting of Jetted Piles

Side grouting of the jetted precast piles was performed with the help of Applied Foundation testing, Inc. (AFT) of Jacksonville, FL. The side membranes were grouted only after allowing sufficient time for the hydration of concrete cap installed at the top of piles. Theoretical grout volume required to fill a prismatic cylindrical side membrane was estimated to be about 350 gal. Since the membrane had vertical pleats on both ends to attach to the pile faces (reduced

perimeter at both ends), the actual volume needed to fill the membrane will be less than the theoretical volume. A grout volume of about 300 gal may be sufficient for each membrane. The mixing and pumping of grout was carried out using AFT's grout pump, Figure 5-28. The grout volume and sustained grout pressure were recorded throughout the grouting process for each membrane. The grout pressure was recorded at the pump and the top of the pile (both inlet and outlet pressures, Figure 5-29). Pile head and soil displacement were also monitored (Figure 5-29) throughout the grouting process. SMO, Gainesville, monitored noise and ground surface vibration during the side grouting of top membrane of both piles, which is discussed later.



Figure 5-28. Grout mixing



Figure 5-29. Grout pressure and displacement measurement

Figures 5-30 present the grout pressure (inlet pressure at pile head) versus the accumulated grout volume pumped in each top and bottom membranes of the piles. In grouting the top membranes, grouting terminated when surface cracks (expansion cracks; Figure 5-31) were observed on all sides of the pile cap and theoretical volumes were reached. In the case of bottom membrane, grouting ceased when the theoretical volume 300 gallons was exceeded. Grout test cylinders were obtained during the grouting of each membrane to determine 28th day compressive strength of the injected grout.

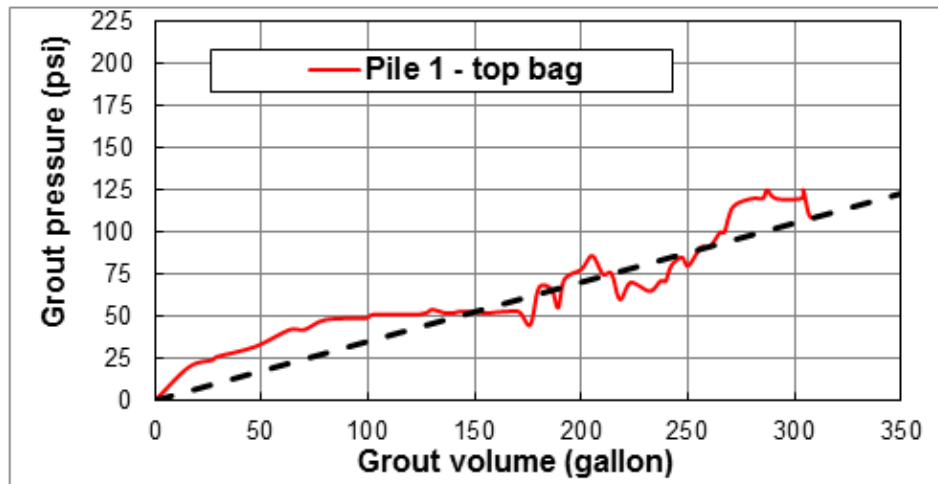


Figure 5-30a. Pile 1, top membrane, measured side grout pressure vs. grout volume

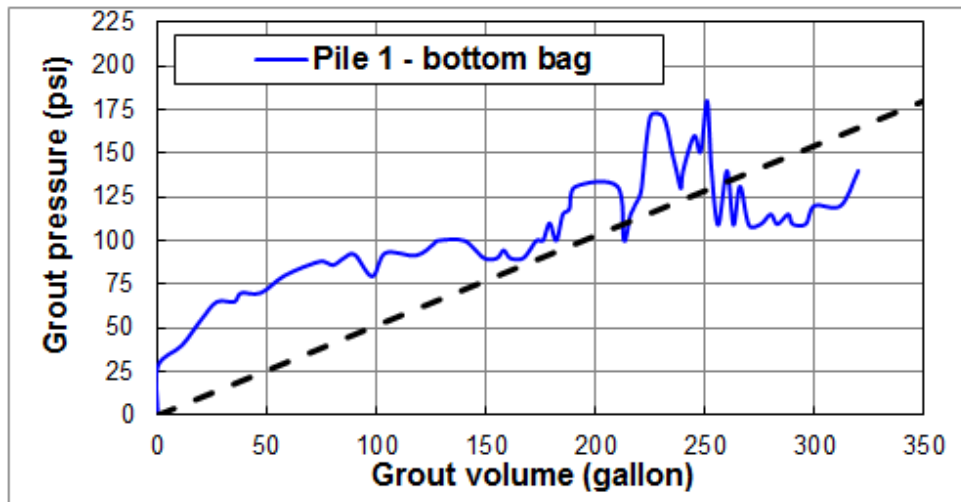


Figure 5-30b. Pile 1, bottom membrane, measured side grout pressure vs. grout volume

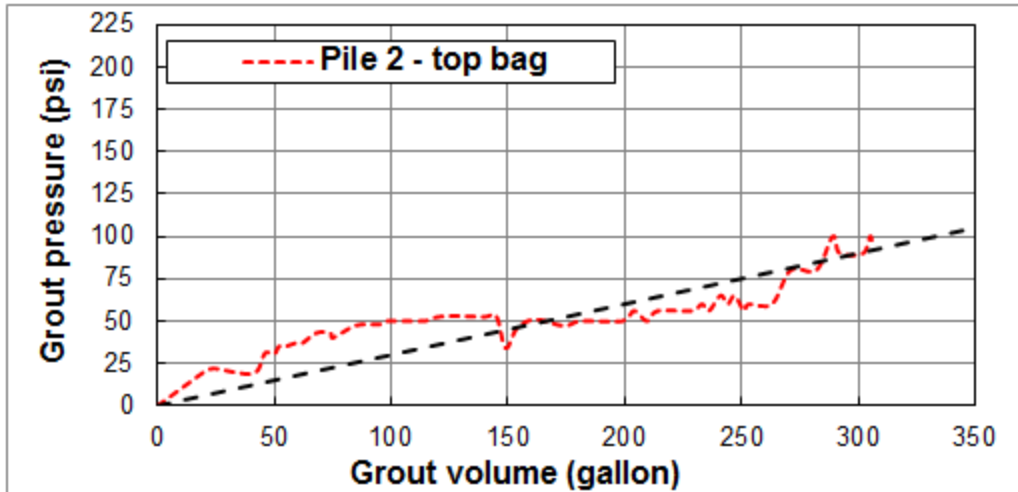


Figure 5-30c. Pile 2, Top membrane, measured side grout pressure vs. grout volume

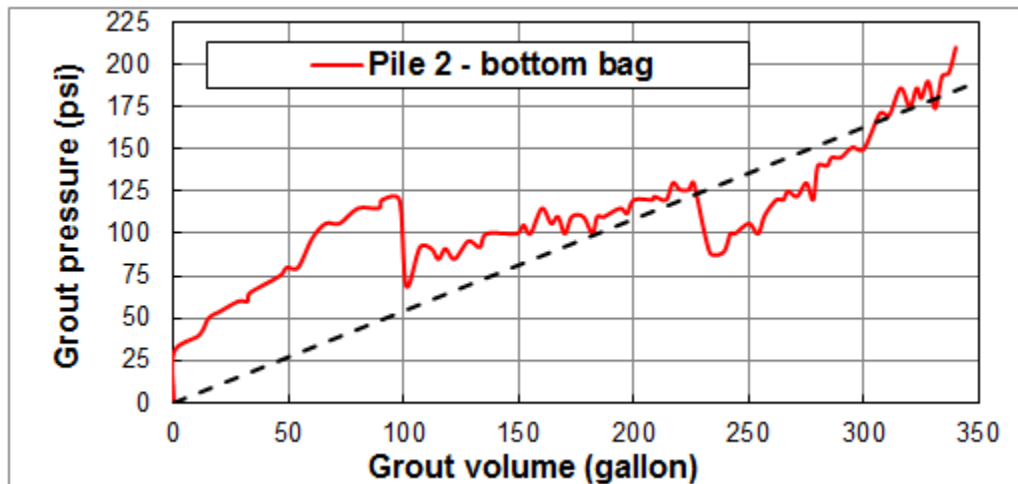


Figure 5-30d. Pile 2, Bottom membrane, measured side grout pressure vs. grout volume



Figure 5-31. Ground surface crack (pile 2: top bag)

As side grouting involves increase in lateral stress alongside the pile, cylindrical cavity expansion theory may be used to predict the expected maximum lateral stresses during the side grouting phase. Table 2 shows the comparison of measured grout pressures with predicted grout pressures from multiple approaches. For the predictions, field limit pressures (Pressuremeter test data), elastic-perfectly plastic closed-form solutions, Yu and Houlsby (1991), and charts provided by Salgado and Randolph (2001) were used. It is evident from the table that the measured side grout pressures are in the range of predicted grout pressures.

Table 5-4. Comparison of measured and predicted grout pressures

	Top membrane		Bottom membrane	
	JP1 ^a	JP2 ^a	JP1 ^b	JP2 ^b
Measured Maximum Pressures (psi)	100-120	90-100	140-160	180-200
Yu and Houlsby's solution (psi) [*]	110	110	224	224
Salgado and Randolph's chart (psi) [*]	116	116	210	210
PMT (psi)	113 ^d	85 ^d	198 ^e	153 ^e

^{*} Corresponds to the middle of top and bottom membrane: 6.5ft and 14ft

^a Poisson's ratio (ν) = 0.3, & Relative density (Dr) = 45%, Critical state friction angle (ϕ_c) = 29°, Linear equivalent friction angle (ϕ) = 33°, Linear equivalent dilation angle (ψ) = 5°

^b ν = 0.3, & Dr = 55%, ϕ_c = 30°, ϕ = 35°, ψ = 7.5°

(Where, ϕ and ψ estimated from ϕ_c based on Salgado & Prezzi 2007),

^d At a depth of 8.5ft

^e At a depth of 16ft

5.8 Tip Grouting of the Piles

After allowing sufficient time for the curing of side grout zones, tip grouting of the piles were undertaken with the help of Applied Foundation testing, Inc. (AFT) of Jacksonville, FL (Figure 5-32). The sustained grout pressure, grout volume, and vertical displacement of pile and surrounding soil were recorded throughout the grouting process (Figure 5-33). The tip grouting was controlled by the upward displacement of pile head. Specifically, the grouting stopped when

the average upward pile head displacement exceeded $\frac{3}{8}$ -in in combination with a steady or dropping tip grout pressure. Generally, $\frac{3}{8}$ to $\frac{1}{2}$ -in of displacement is considered sufficient to fully mobilize skin resistance on a pile in the literature.



Figure 5-32. Grout mixing and pumping



Figure 5-33. Grout pressure and displacement monitoring

Shown in Figure 5-34 is the measured grout pressure versus grout volume pumped during the tip grouting of piles. Figure 5-35 presents the pile head displacement versus grout pressure versus plots. In the case of Pile 2, Figure 5-34, there was an approximate linear increase of grout pressure with volume until pile began to move upward (390 psi), and grout pressure dropped off (280-300 psi) with further vertical movement (i.e., full mobilization of skin friction). In case of pile 1, the grout pressure and volume increased until 210 psi, whereupon pressure dropped, and grout volume still increased below the tip, Figure 5-34. However, the increase in upward movement of the pile was insignificant unlike the pile 2 (Figure 5-35). The latter suggests that the soil beneath pile 1 was being compacted (i.e., SPT N values went from 5-10 range at 15ft to over 20 at 20-25 ft depth). Interestingly, at grout volume of 85 gallons (Figure 5-34), the grout pressure started to increase again and at grout volume of 140 gallons, upward movement had reached 3/8" and grout pressure dropped again, suggesting full mobilization of skin friction had occurred.

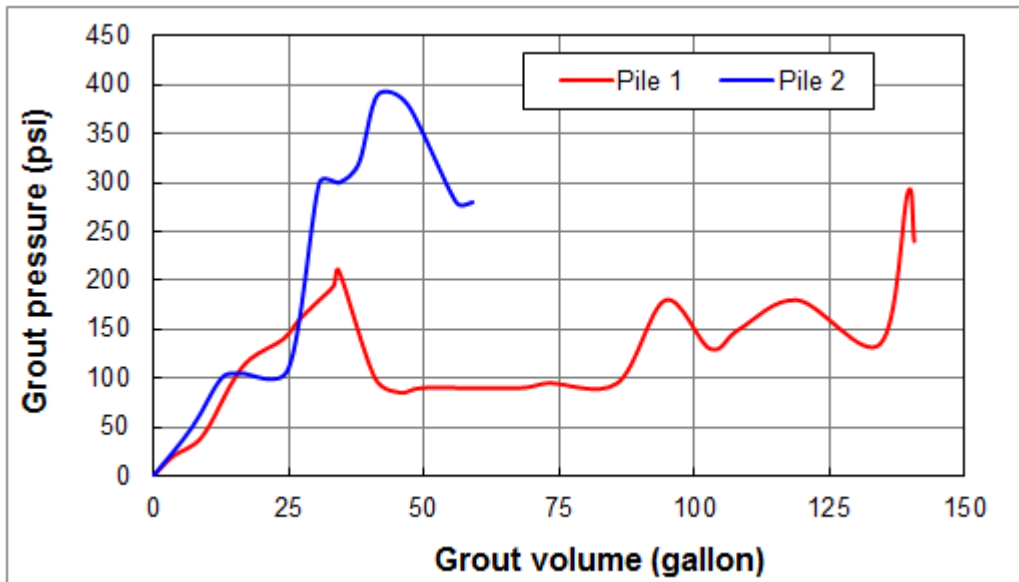


Figure 5-34. Tip grout pressure versus grout volume pumped

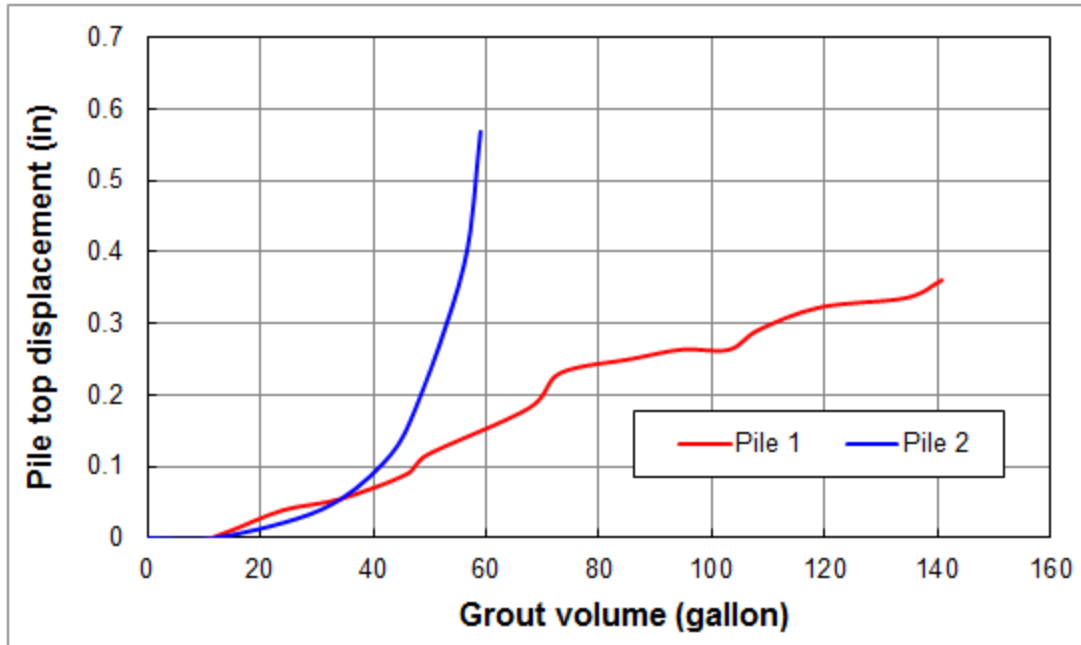


Figure 5-35. Pile head displacement versus grout volume pumped

Table 5-5 Comparison of the measured and predicted tip grout pressures

	JP1	JP2
Measured tip grout pressure (psi)	290	280-300
Yu and Houlsby's solution (psi) ^a	509	509
Salgado and Randolph's chart (psi) ^a	522	522

^a $\phi_c = 29^\circ$, $\phi = 35^\circ$, $\psi = 7.5^\circ$ (Salgado & Prezzi 2007), $\nu = 0.3$, & $Dr = 55\%$

Table 5-2 presents a comparison of the sustained tip grout pressures versus the spherical cavity expansion limit pressures at the pile tips predicted using Yu and Houlsby's (1991) closed form solutions, and Salgado and Randolph's (2001) charts. It is evident from the table that the sustained grout pressure was about 60% of the spherical cavity limit pressures at that depth. In general, the maximum possible tip grout pressure will be the minimum of the spherical cavity expansion pressure and the pressure required to mobilize the full side resistance of the pile. In the present case, the maximum sustained tip grout pressure was governed by the available skin

resistance. However, it should be noted that the side grouting of the piles had significantly improved the side resistance, (i.e., increased lateral stresses) upon which tip grouting developed very high grout pressures. In case of tip grouting without a prior side grouting, the tip grout pressure will be significantly less than the present values (e.g., tip grouted drilled shafts; McVay et al. 2010).

5.9 Analysis of Noise and Vibration Data

As mentioned earlier, SMO, Gainesville, measured the noise and ground surface vibration during the pile jetting and grouting operation. Vibration and Overpressure Monitor (InstanTel® Minimate Plus™) with triaxial geophone (velocity transducer) and overpressure microphone were used for the measurement (Figure 5-36). The monitors were located at different radial distances from the pile location.

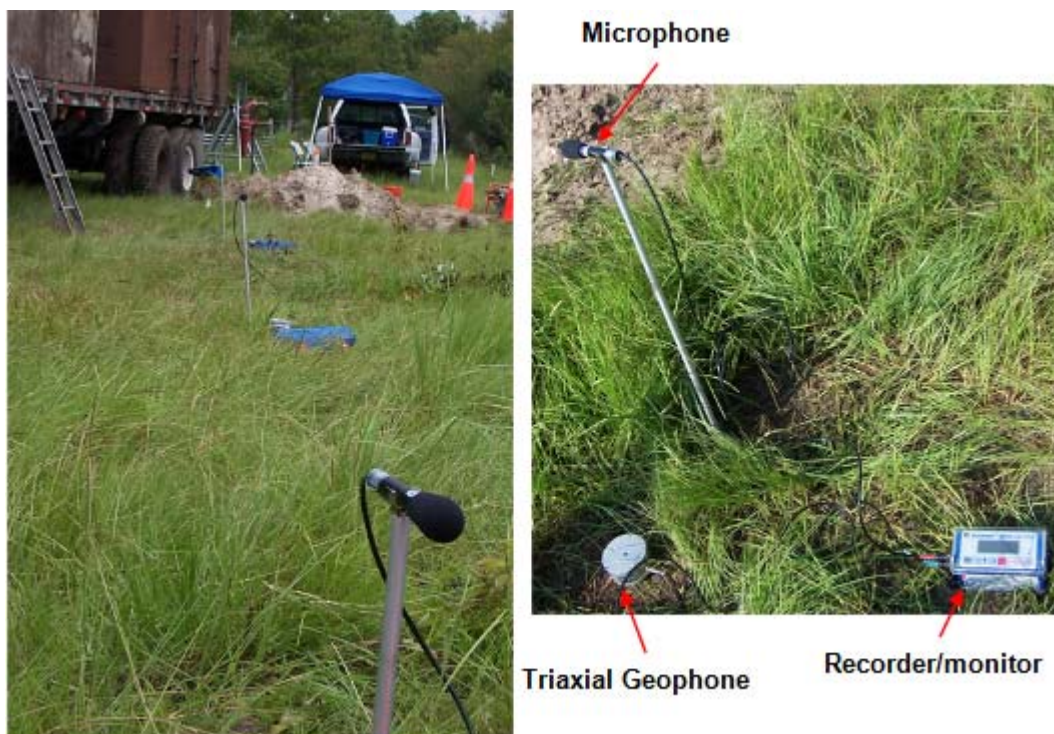
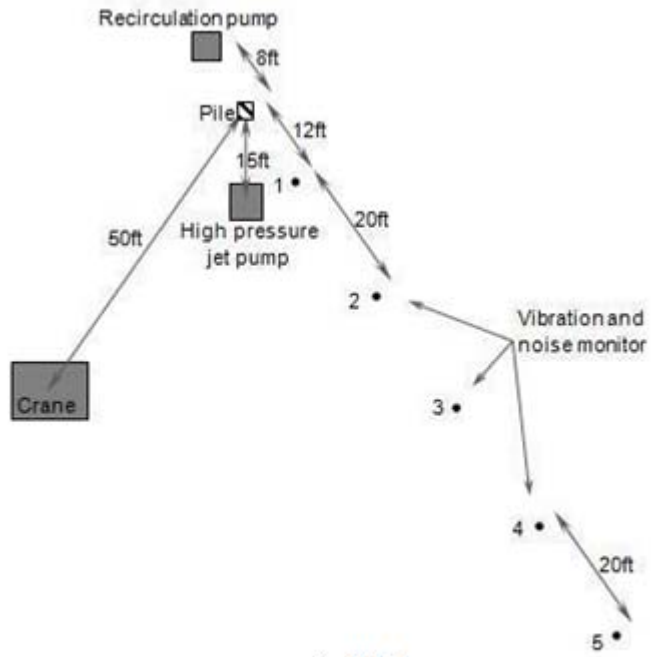


Figure 5-36. Instrumentation for noise and vibration measurement

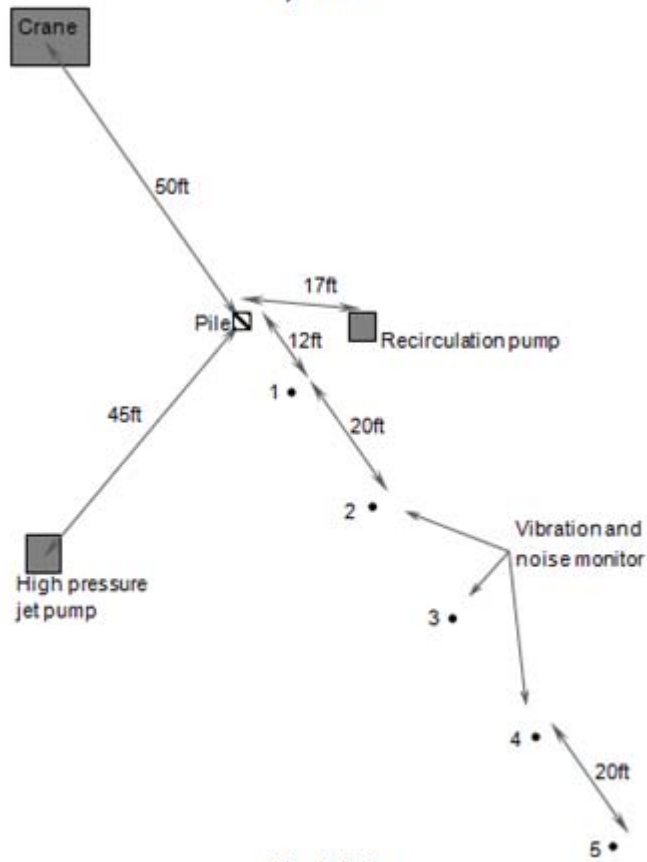
5.9.1 Measured noise

Figure 5-37 shows the location of construction equipment and vibration and noise monitors with respect to the pile location during the jetting process. Note that the layout of noise and vibration monitors was same for both piles, but the locations of the construction equipment were different. The construction equipment used for jetting of the piles were: 1) high pressure jet pump, 2) crane, and 3) water recirculation pump, as identified earlier. Therefore the major sources of noise in the jetting operation were the sound/noise emitted from the motors of these equipment, and not from the jetting process itself.

According to FHWA's Noise Abatement Criteria (NAC), hourly equivalent steady-state sound level (L_{eq}) should be limited to 67dBA in residential, hospital, school, picnic, and recreational areas and 72dBA in developed lands (commercial and industrial areas). Figure 5-38 shows the noise measured at different locations during the operation of crane alone, crane and recirculation pump, and pile jetting process (i.e., operation of jet pump, crane, and recirculation pump) for pile 2. Noise is reported in "A-weighted" decibels (dBA), which is the sound level measurement in decibel (dB) adjusted/weighted to match the sensitivity of human ear. Noise measured during the operation of crane alone was less than 70dBA at all locations, as the crane was located 50ft away from the pile in the opposite direction of measurement points (Figure 5-37). It can be seen from the Figure 5-38 that the noise in the vicinity of pile location was in the range of 85-92 dBA, which is attributed to the operating noise of water recirculation pump and high pressure jet pump.



a) Pile 1



b) Pile 2

Figure 5-37. Location of construction equipment and vibration and noise monitors

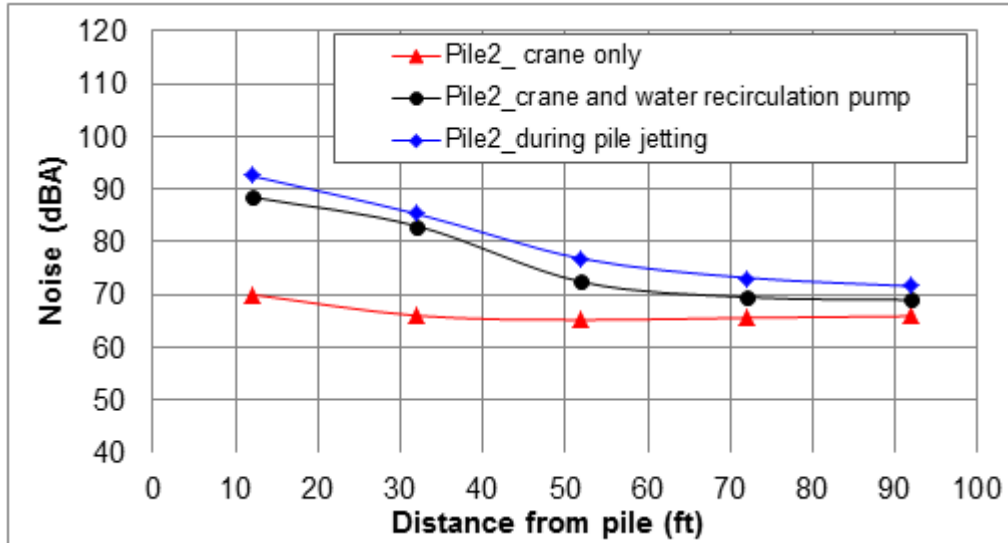


Figure 5-38. Noise measurement for Pile-2

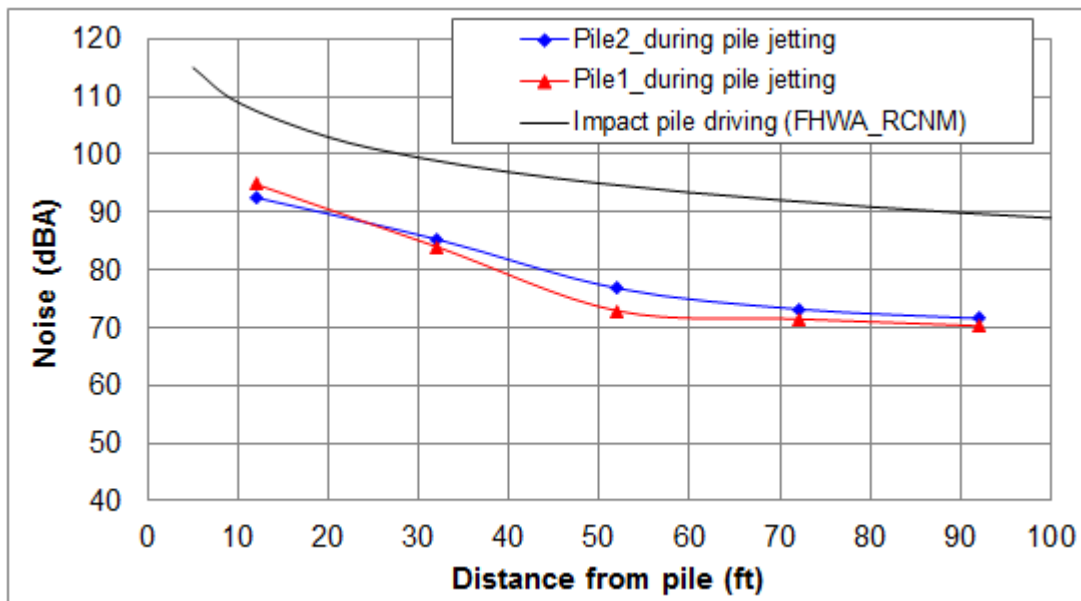


Figure 5-39. Noise measurement during pile jetting process

Shown in Figure 5-39 is the noise measurements during the jetting of both piles. It is evident from the figure that noise levels at different points were nearly the same for both cases, even though the locations of equipment were different. This is due to the fact that resultant noise level at a location due to multiple noise sources is dominated by the highest individual noise level (as sound level, dB or dBA is logarithmic). It can also be seen from the Figure 5-39 that for

the distance beyond 70 ft (21.3 m), the noise level is less than 72 dBA (FHWA-NAC criterion). The noise can be further reduced by shielding the equipment (jet pump and water recirculation pump) and locating the pumps away from any sensitive building/structure under consideration.

FHWA's Road Construction Noise Model (RCNM) database suggests an A-weighted maximum sound level (L_{max}) of 95dBA at a distance of 50 ft for any impact pile driving operation. Since the noise levels decrease with the logarithm of distance from the source, the corresponding hourly equivalent sound level (L_{eq}) at various distances can be obtained using Eq. 5-1 (FHWA: RCNM). Figure 5-39 also displays the estimated variation of noise levels with distance for an impact pile driving operation (using Eq.5-1, $L_{max} = 95$ dBA and U.F (%) = 100). In the case of impact/dynamic pile driving, it can be found using Eq.5-1 and an L_{max} value of 95 dBA that the noise level is less than 72 dBA (FHWA 2006) at a radial distance beyond 700 ft (213 m). Therefore it can be concluded based on limited data that the noise generated during a pile jetting operation is much less than a dynamic pile driving as expected.

$$L_{eq} = L_{max} - 20\log(D/50) + 10\log\left(\frac{U.F(\%)}{100}\right) \quad (1)$$

Where, D - distance from source, U.F (%) - time-averaging equipment usage factor

Noise and ground surface vibration were also measured during the side grouting (top membrane) and tip grouting of both piles. The grout pump/diesel generator was the only construction equipment and hence the only source of noise during the grouting process. Figure 5-40 shows the schematic of grout pump and the monitors' locations for pile 1 and pile 2 during side grouting. In both cases, the grout pump was about 50 ft away from the pile and in the opposite side of noise and vibration monitor's locations. During tip grouting the grout pump was located at a distance of 28-34 ft away from the piles.

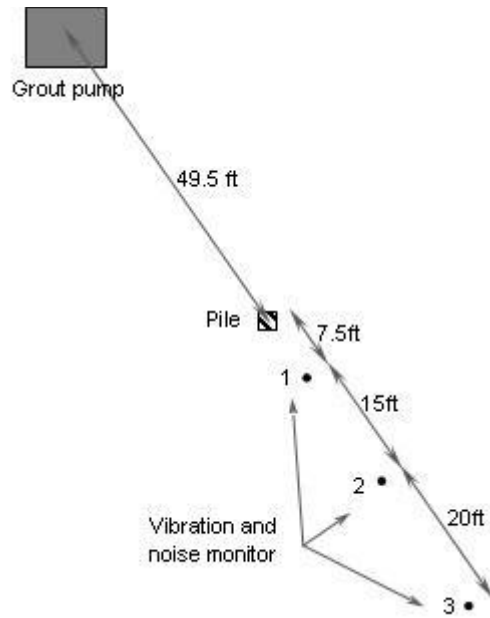


Figure 5-40. Location of grout pump and vibration and noise monitors for side grouting

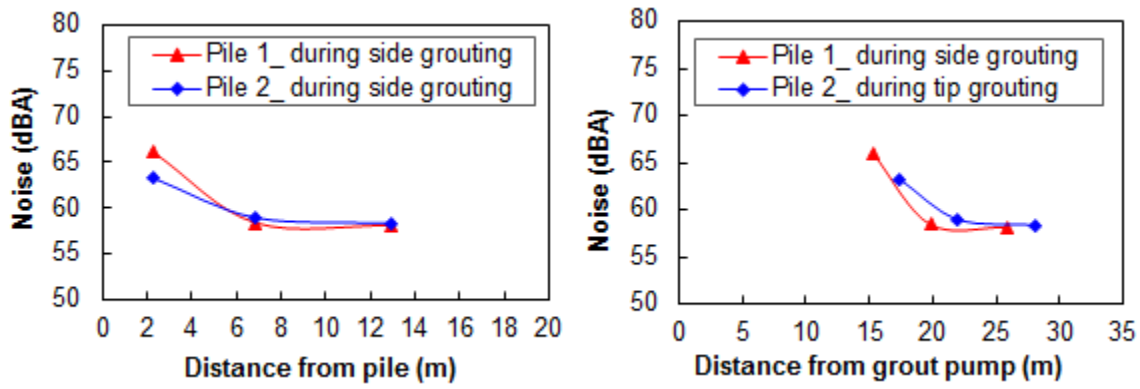


Figure 5-41 Noise measurement during side grouting

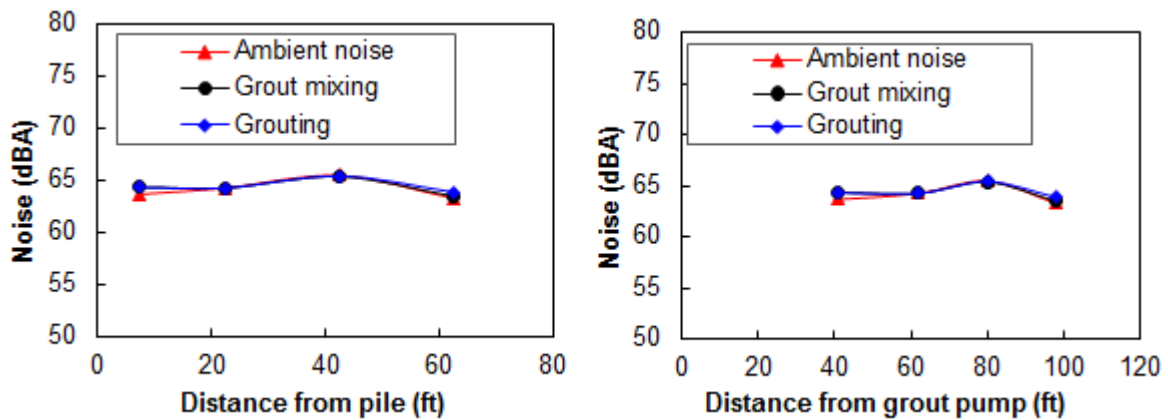


Figure 5-42 Noise measurement during tip grouting

Figures 5-41 and 5-42 show the noise measured at different locations during the top membrane grouting and tip grouting respectively. It is evident from the figures that the noise measured at all locations was less than 67dBA (FHWA's Noise Abatement Criteria for residential area) and hence the noise during the grouting process is not critical as long as the source (grout pump) is at least 55 ft (16.75 m) away from the location under consideration.

5.9.2 Measured ground surface vibration

Also of significance is the induced ground vibration during the construction. Ground motion may cause structural and architectural damage to nearby structures. Triaxial geophones (velocity transducers) were used to measure the three orthogonal components (transverse, vertical, and longitudinal) of particle motion at different radial distance during the pile jetting and grouting operation. The resultant particle motion was determined as the vector sum of three orthogonal components. Figure 5-43 presents the peak (maximum) particle velocity measured during the operation of crane alone, crane and recirculation pump, and pile jetting process (i.e., operation of jet pump, crane, and recirculation pump) for pile 2. It is evident from the figure that vibration during the operation of crane alone, and crane & water recirculation pump were negligible. Ground vibration during the jetting process (although small) was due to the high pressure jet pump operation.

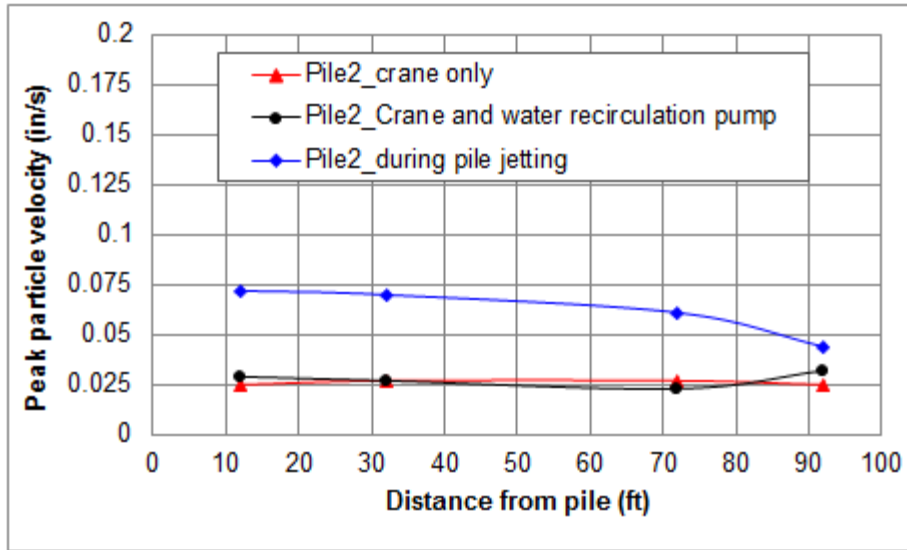


Figure 5-43. Peak particle velocity measurement for pile 2

Shown in Figure 5-44 are the peak particle velocity profiles for pile 1 and 2. The peak particle velocity was higher (0.19 in/s) for pile 1 and it was attributed to the proximity of jet pump to the pile as shown in Figure 5-37a. However, beyond 30ft, the particle velocity was negligible. For pile 2, the peak particle velocities were similar (0.07 in/s) at 12ft and 32ft due to the distance from jet pump to the pile (similar, see Figure 5-37b). At larger distances, peak particle velocity was higher in the case of pile 2 than pile 1, which is attributed to the difference in location of the jet pump as identified from Figure 5-37a & b.

Table 5-6. Limiting velocity suggested by AASHTO Designation R8-81

Type of situation	Limiting velocity (in/s)
Historical sites or other critical locations	0.1
Residential buildings, plastered walls	0.2-0.3
Residential building in good repair with gypsum board walls	0.4-0.5
Engineered structures, without plaster	1.0-1.5

Source: AASHTO Designation R8-81

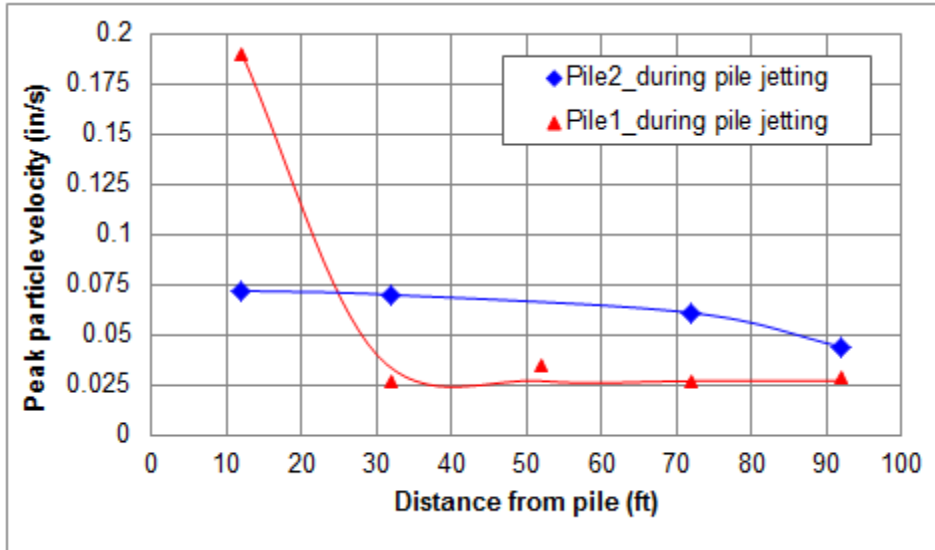
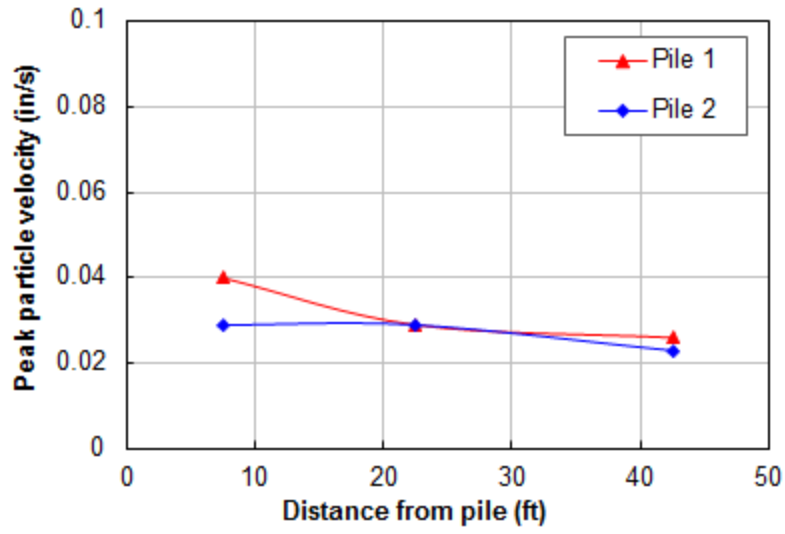


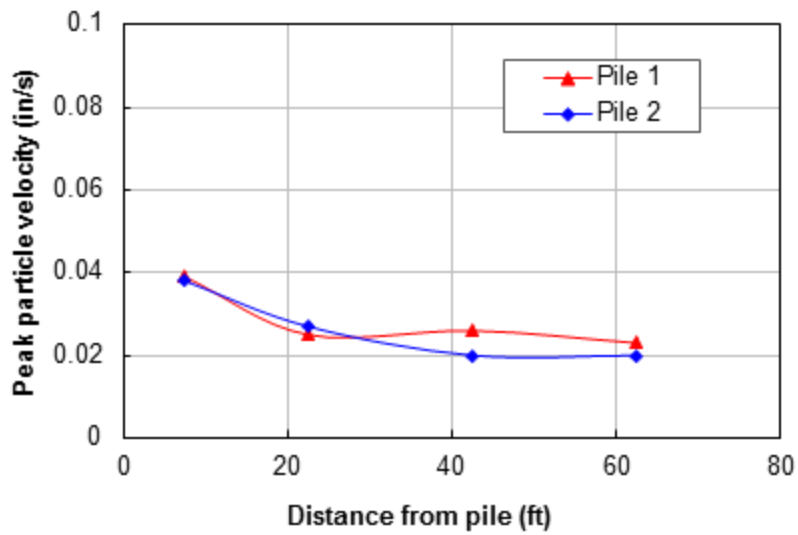
Figure 5-44. Peak particle velocity during jetting process

Table 5-3 presents the maximum vibration level recommended by AASHTO Designation R8-81 to avoid structural damage. It is evident from Figure 5-44 that for distance greater than 22 ft (6.7 m), peak particle velocities were less than the minimum limiting velocity (0.1 in/s) suggested by AASHTO Designation R8-81 for historical or critical structures.

Figure 5-45 presents the peak (maximum) particle velocity measured during the side and tip grouting of the piles. It is clear from the Figure 5-45 that vibrations during the process were negligible; much less than minimum limiting velocity suggested by AASHTO Designation R8-81 (Table 5-3) for even historical sites or other critical locations.



a) Side grouting



b) Tip grouting

Figure 5-45. Peak particle velocity measurement during side and tip grouting

CHAPTER 6 AXIAL TOP-DOWN LOAD TESTS ON A DRILLED SHAFT AND JET-GROUTED PILES

Axial top-down load tests were performed on the two jet-grouted piles and a similar sized drilled shaft to compare axial resistance (i.e., skin and tip) as well as validate the capacity and design estimates for typical Florida conditions. This chapter presents detailed description of the test setup, instrumentation, data acquisition, and the analysis of the results from all top-down load tests. Measured skin resistances for both types of foundations were compared with values predicted from methods reported in the literature.

6.1 Top-Down Static Load Testing of Drilled Shaft

Static top-down load test on one of the 4 ft diameter x 18 ft long drilled shafts (TS2) was performed in accordance with ASTM Designation: D 1143/D 1143M – 07. Figure 6-1 shows the setting up of the reaction system for the load test. The reaction was provided by two 4ft diameter x 40 ft long reaction drilled shafts (RS2 and RS3). Reaction support stands used in previous FDOT project: BDK-75-977-07, were modified for this project. The support stand is principally a three-dimensional frame fabricated using different steel sections (tube, channel, pipe, etc.). Diagonal bracings were added to the frame to provide sufficient lateral stiffness against wind loading. The stand provides enough clearance (7.5 ft.) between the shaft/pile top and the bottom of the reaction beam for placing the hydraulic jack, load cell, and displacement instrumentation (Figure 6-1). FDOT's 40ft long reaction beam girders and load distribution systems (Acosta load test frame) were used for the test. The girders and load distribution systems were transported from SMO, Gainesville to the test site using a 50 ton crane and flat beds. On site, the beam girders were placed on top of reaction stands and then the Dywidag support and transfer assemblies were positioned across the top of the beams (Figure 6-1). The assembly was then bolted using Dywidag plates and nuts. Finally, the load test shear transfer plate (transfer load

from jack/load cell to beam girders) was placed under the beams directly above the test shaft using the crane, and attached to the beam girders by means of fabricated HSS tube and Dywidag bars system (Figure 6-1).



Figure 6-1. Setting reaction beam girders on the top of reaction support stands

Figure 6-2 shows the load test setup. SMO's 2000 kip hydraulic jack was used for applying the load (Figure 6-3). The applied load was measured using the 600 kip load cell, which was connected to a visual digital readout box for load control. Vertical shaft displacement monitoring included digital dial gauges and a mirrored scale with wire line reference. The digital dial gauges were attached to a wooden reference beam as shown in Figure 6-3. The end supports

for the reference beam and wire lines reference were 20 ft (5x shaft \emptyset ; ASTM D 1143) away from the test drilled shaft. The sister-bar strain gauges installed at the different elevations of the test drilled shaft were also monitored throughout the test to estimate the load distribution along the shaft and separate out the side and tip resistance (Figure 6-3). In addition, the vertical displacements of both reaction drilled shafts and sister-bar strain gauges embedded in one of the reaction shafts (RS2) were monitored during the test.



Figure 6-2. Load test setup for the 4-ft diameter x18-ft-long drilled shaft (TS2)

The load was applied in 20 kip increments with a time interval of 10 minutes. Since the test drilled shaft had to undergo a combined torsion and lateral load test later, the loading was stopped when the shaft underwent a vertical displacement of approximately 0.5-in (i.e., after ensuring skin resistance is fully developed). Then the load was removed in four approximately equal decrements. The water table during the load test was 10 ft below the ground surface.



Figure 6-3. Hydraulic jack, load cell, digital dial gauges, mirrored scale with wire line reference, and data acquisition using National Instruments device

Figure 6-4 presents the measured strains at different elevations during the load test. The loads at the different elevations were determined from the measured strains using modulus (laboratory testing) and estimated cross-sectional area. Shown in Figure 6-5 is the load distribution along the shaft during the application of each load increments. It is clearly evident from the figure that the side resistance of the shaft was fully mobilized (240 kip – lines become parallel) prior to peak test load (320 kip). Table 6-1 lists the estimated ultimate unit skin frictions for each segment. Figure 6-6 displays the total load vs. top displacement of the shaft along with

separated skin and tip contributions. The ultimate skin resistance of the drilled shaft was found to be 141 kip. The maximum upward displacement observed at the top of the reaction drilled shafts RS2 and RS3 were 0.0964 and 0.0937-in respectively.

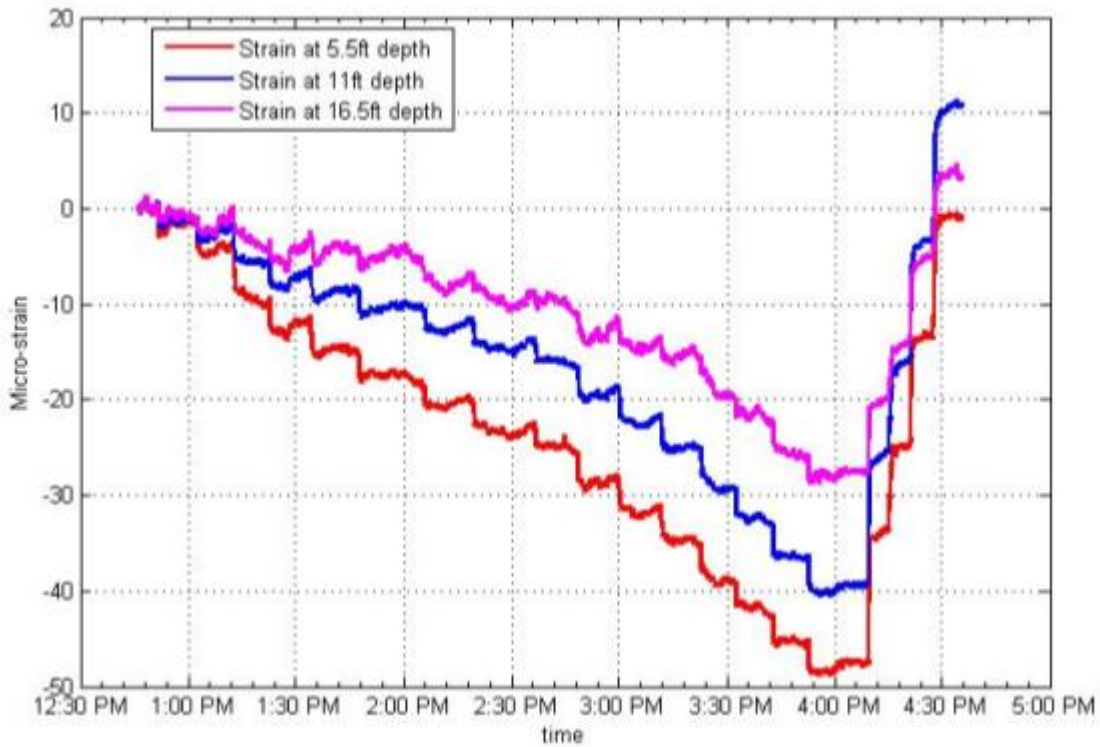


Figure 6-4. Measured strain at various levels within the drilled shaft

Table 6-1: Unit skin frictions for each segment

Segment	Unit skin (ksf)
0 - 5.5 ft	0.275
5.5 – 11 ft	0.767
11- 16.5 ft	0.998

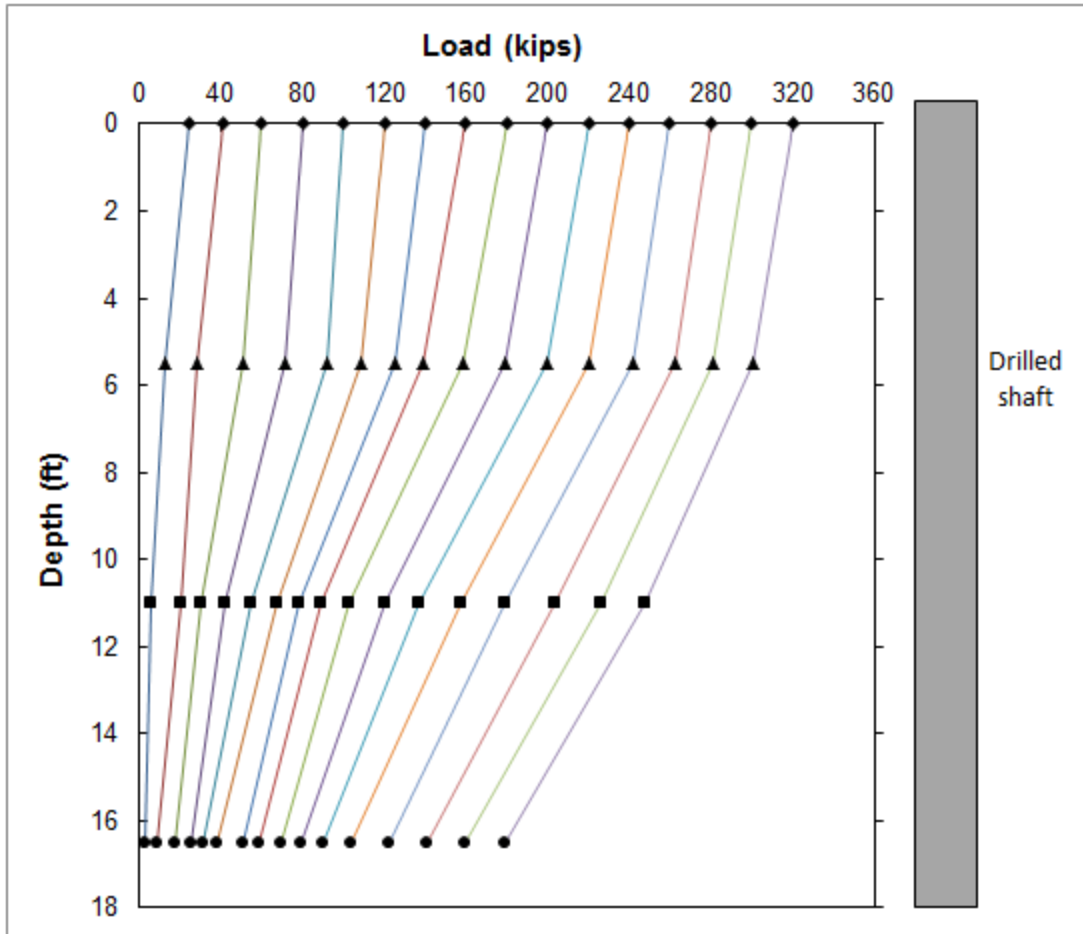


Figure 6-5. Load distribution along the shaft

The measured skin resistance was then compared with the values predicted using different SPT and CPT based methods discussed in Chapter 2. Table 6-2 gives a comparison of the measured vs. the predicted values. Detailed calculations for each method are given in Appendix D.. It is evident that the prediction using Rational method (FHWA 2010) was very close to the measured value. SPT based O'Neill and Hassan (1994) method under-predicted the measured resistance by 22%. But the predictions based on all the CPT methods (Aoki and Velloso's method, LCPC method and UIUC method) were significantly different from the measured value ($\pm 50\%$ difference).

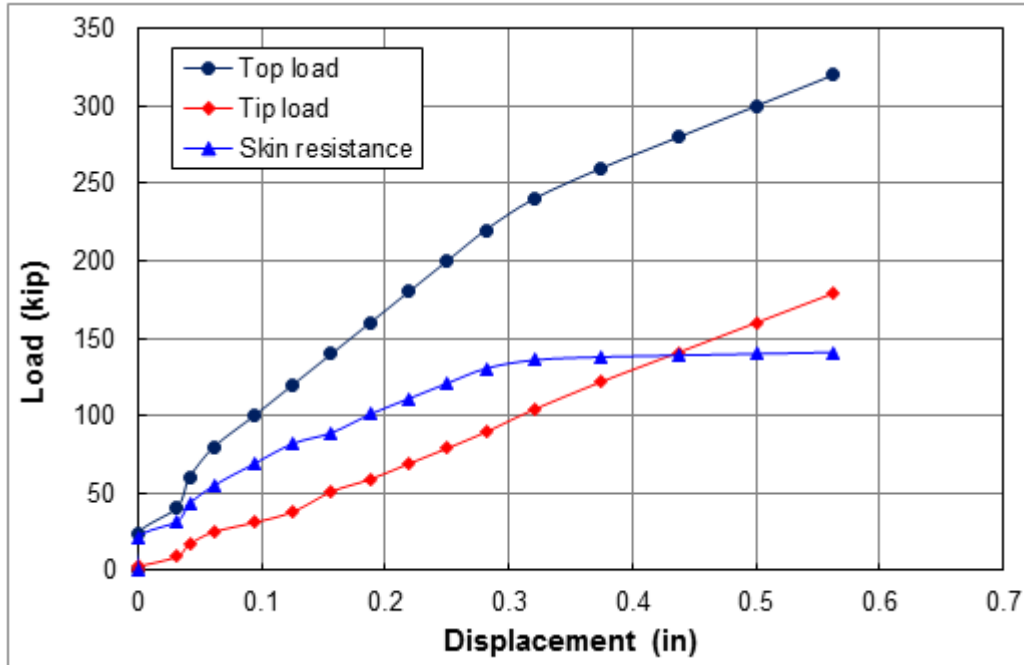


Figure 6-6. Load vs. displacement response of the drilled shaft

Table 6-2. Comparison of the measured vs. the predicted values

In situ test	Method	Skin resistance (kip)	% of difference
SPT	O'Neill and Hassan (1994) method	110	-22%
	Rational method (FHWA 2010)	136	-3.5%
CPT	Aoki and Velloso's method	61	-57%
	LCPC method	210	+49%
	UIUC method (Alsamman 1995)	219	+55%
Measured Value		141	--

6.2 Top-Down Static Load Testing of Jet-grouted Piles

In order to study the influence of test sequence on axial results, the load tests on jet-grouted piles were performed in two different orders. Jet-grouted pile-1 (JP1) was first subjected to top-down load test and then to a combined torsion and lateral load test. Whereas, jet-grouted pile-2 (JP2) first underwent combined torsion and lateral load test and then a top-down load test.

6.2.1 Axial load test on jet-grouted pile 1

After waiting approximately four weeks following the tip grouting of the piles, a static top-down axial load test was performed on jet-grouted pile 1 (JP1). The pervious load frame for the test drilled shaft (TS2) was dismantled and re-assembled at the location of the test pile with the help of a 50 ton crane. The two reaction drilled shafts used for the load test were RS1 and RS2. Note that RS2 was used in the previous top-down load test (TS2) also. The measured depth of water table on the day of testing was 8.6ft.



Figure 6-7. Load test setup with all instrumentation

Figure 6-7 shows the load test setup with all the instrumentation. SMO's 2000 kip load cell was used to measure the applied load. The vertical displacement of the pile was monitored using digital levels, digital dial gauges, and a mirrored scale (Figure 6-8). The digital levels were borrowed from LOADTEST, Gainesville, Florida. The upward displacement of the reaction drilled shafts was also monitored throughout the test. The data from the strain gauges embedded within the test pile and reaction shaft (RS2) was acquired using the National Instruments data

acquisition system. The data was later used to identify the load distribution along the pile and used to separate the skin and tip components.



Figure 6-8. Pile displacement monitoring instrumentations

The load was applied in 25 kip increments and each increment was kept for a constant time interval of 10 minutes in conformity with ASTM D 1143. The loading could not be continued beyond 350 kip due to failure (upward movement, i.e., pullout – 180 kip) of one of the reaction drilled shafts (RS2). Before the application of the last load increment, the total upward displacement of the reaction shaft (RS2) was only 0.079 in. When the last load increment (total load = 350 kip on test pile) was applied, the RS2 subjected to an additional movement of 0.78-in and additional loading of the pile was not possible. At this point, the total upward displacement of the other reaction drilled shaft (RS1) was only 0.047-in. Note that RS2 had been previously subjected an uplift load of approximately 160 kip during the top-down load testing of drilled shaft. The maximum displacement observed on the top of the test pile was only 0.15-in. The applied load was then removed in five decrements.

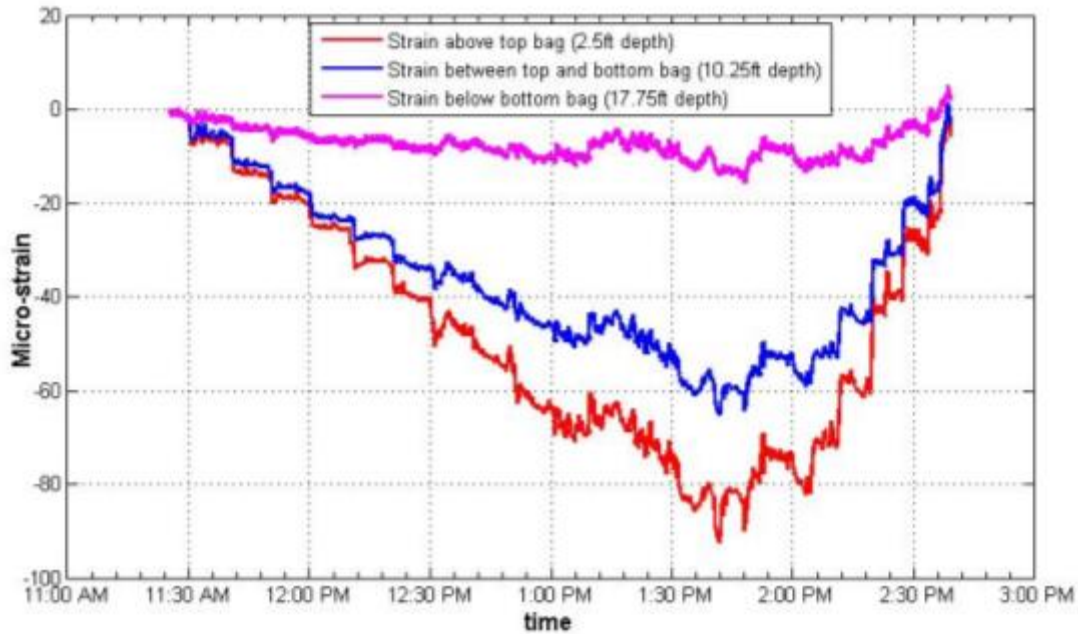


Figure 6-9. Measured strain at different depths

Shown in Figure 6-9 is the strain measured at different locations: above the top membrane, between membranes, and below the bottom membrane; during the load test. The load distribution along the pile, and skin and tip contributions were estimated using the measured strains and applied top load. Figure 6-10 depicts the load distribution along the pile during the incremental loading and Figure 6-11 presents the total load, mobilized tip load, and mobilized skin resistance versus top displacements during the load test. It can be seen from the Figures 6-10 and 6-11 that that the side resistance of the pile was not fully mobilized during the load test. Also it should be noted that approximately 10 kip was transferred to the soil from the concrete cap due to vertical movement of the cap, i.e., 0.15”.

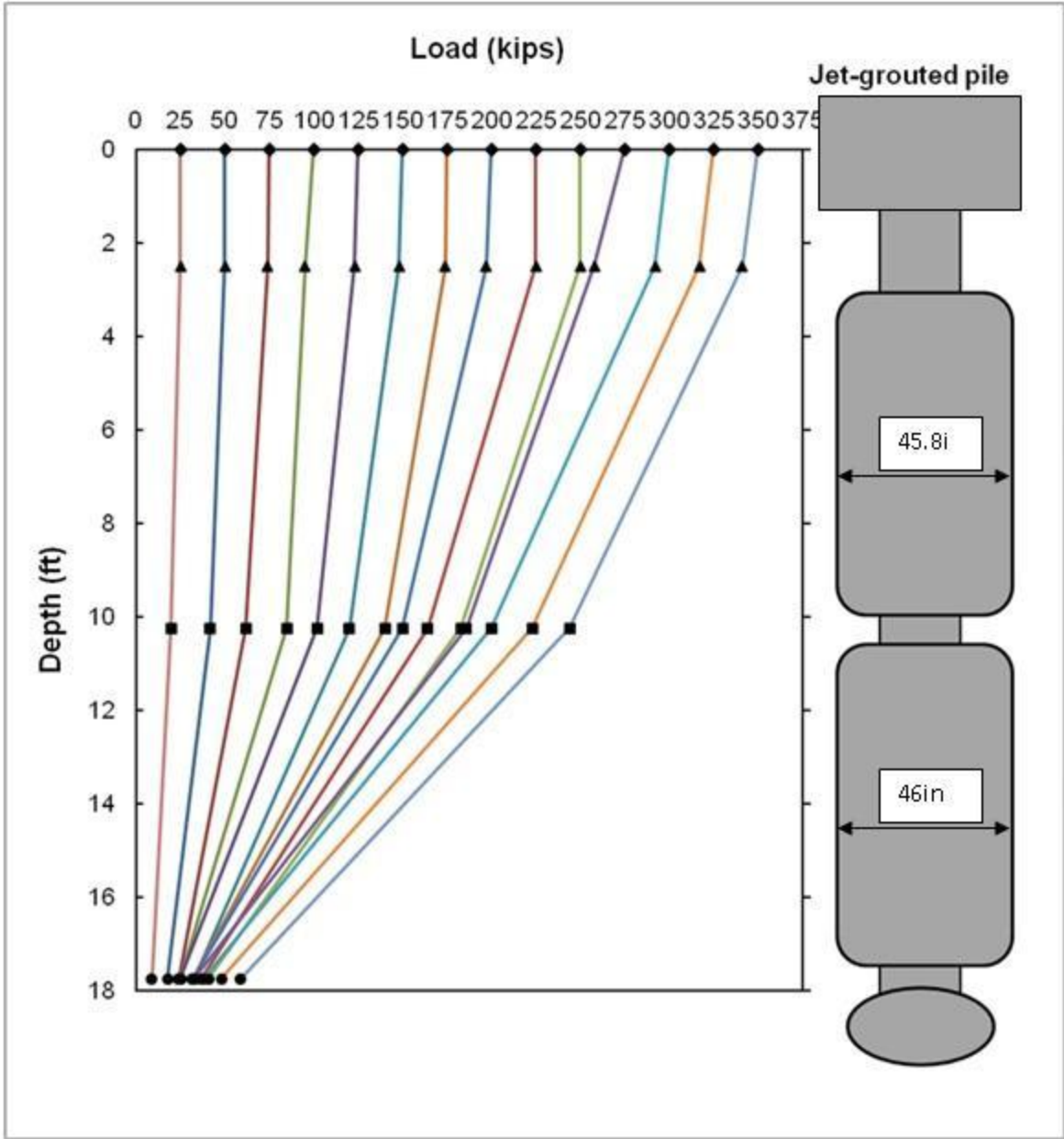


Figure 6-10. Load distribution along the jet-grouted pile 1

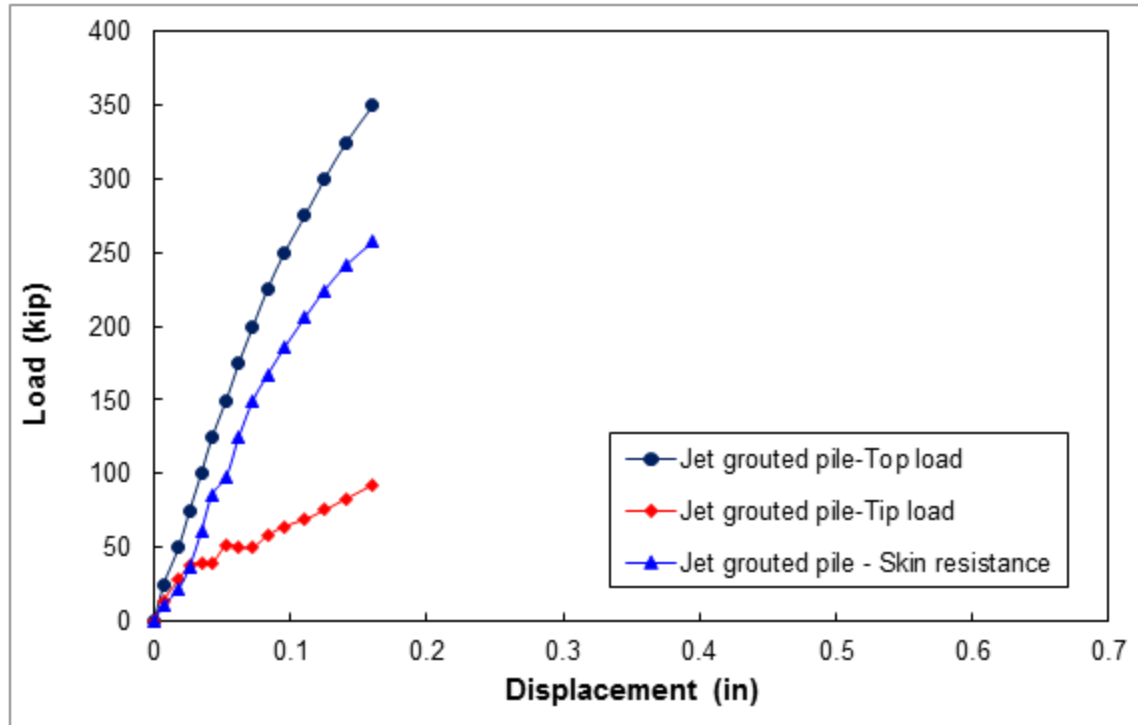


Figure 6-11. Load-displacement response for the jet-grouted pile

6.2.2 Load test on jet-grouted pile 2

After the completion of the combined torsion and lateral load test (discussed in Chapter 7), a static top-down load test was performed on jet-grouted pile 2. The test set-up was the same as the previous top-down load tests. The reaction for the load test was provided by RS3 and RS4. Figure 6-12 shows the reaction girder, jack, and monitoring system. The load was applied in 25 kip load increments. Each load increment was kept constant for a time interval of 10 minutes in accordance with ASTM D 1143. The vertical pile displacement was monitored using digital levels with invar staffs, digital dial gauges and mirrored scale with wire line reference. The vertical displacement of the wooden reference beam supporting the digital dial gauges was also monitored using a digital level (Figure 6-12). The resistance strain gauges embedded in the pile at the different elevations were monitored throughout the test at 20 sec intervals using National Instruments data acquisition system. The vertical displacements of both reaction drilled shafts

were also measured during the test. The measured depth of water table on the day of testing was 8.6-ft.



Figure 6-12. Test setup for top-down testing of jet-grouted pile 2

The loading was stopped at a total load of 375 kip due to pullout failure of one of the reaction drilled shafts (RS4). When the last load increment was applied (i.e., from 350 to 375 kip), the reaction shaft, RS4, underwent 0.265-in of incremental displacement, for a total upward displacement of 0.362-in. From statics, reaction shaft, RS4, had a pullout resistance (skin resistance) of 187.5 kip and hence further loading was not viable with the current reaction system.

It should be noted that similar reaction shaft failure (RS2) was observed during the top-down testing of jet-grouted pile 1. In that test, top-down loading could not be continued beyond 350 kip. It was thought that failure of reaction shaft, RS2, may have been due to repeated use of the reaction shaft. Specifically, the reaction shaft, RS2 was first used for the testing of TS2, which may have resulted in residual stresses in shaft-soil system due to permanent upward

deformation. However, reaction shaft RS4 was only used for top-down testing of jet-grouted pile 2 and hence no residual stresses due to prior load testing was possible. This suggests that the lower skin friction which caused failure in both tests is mainly attributed to either spatial variability at the test site or different construction practices. It should also be noted in the present test, the maximum upward displacement of the other reaction drilled shaft (RS3) was 0.092-in. Comparing this with the upward displacement of RS4 (0.097-in) during the previous load increment, it may be concluded that RS3 might be in the verge of failure; i.e., another load increment may cause the failure of the shaft. The downward displacement of the test pile was only 0.198-in at the maximum load. Subsequently the applied load was removed in eight decrements.

The strain measured at three different elevations within the pile was used to calculate load distribution along the pile as shown in Figure 6-13. About 15 kip of the total applied load was transferred through the pile cap to the underlying soil (i.e., a bearing stress of 0.76 ksi). Note that the total settlement of the pile was only 0.198-in, which is not sufficient to fully mobilize the cap's bearing capacity. Skin and tip contribution along the pile were then separated out from the strain data. Figure 6-14 displays the total load, mobilized tip load, and mobilized skin resistance versus top displacement. It is evident from the Figures 6-13 and 6-14 that the side resistance of the pile (bottom zone) was not fully mobilized during the load test, similar to the JP1 load test.

Figure 6-15 presents a comparison of the total load – displacement response of the jet-grouted piles 1 and 2. It can be seen from the figure that the stiffness response (loading and unloading) of the piles are nearly the same, which indicates that the axial response of JP2 was not influenced by the prior combined torsion and lateral load test. The difference is attributed to the difference in the side grout and tip grout volumes.

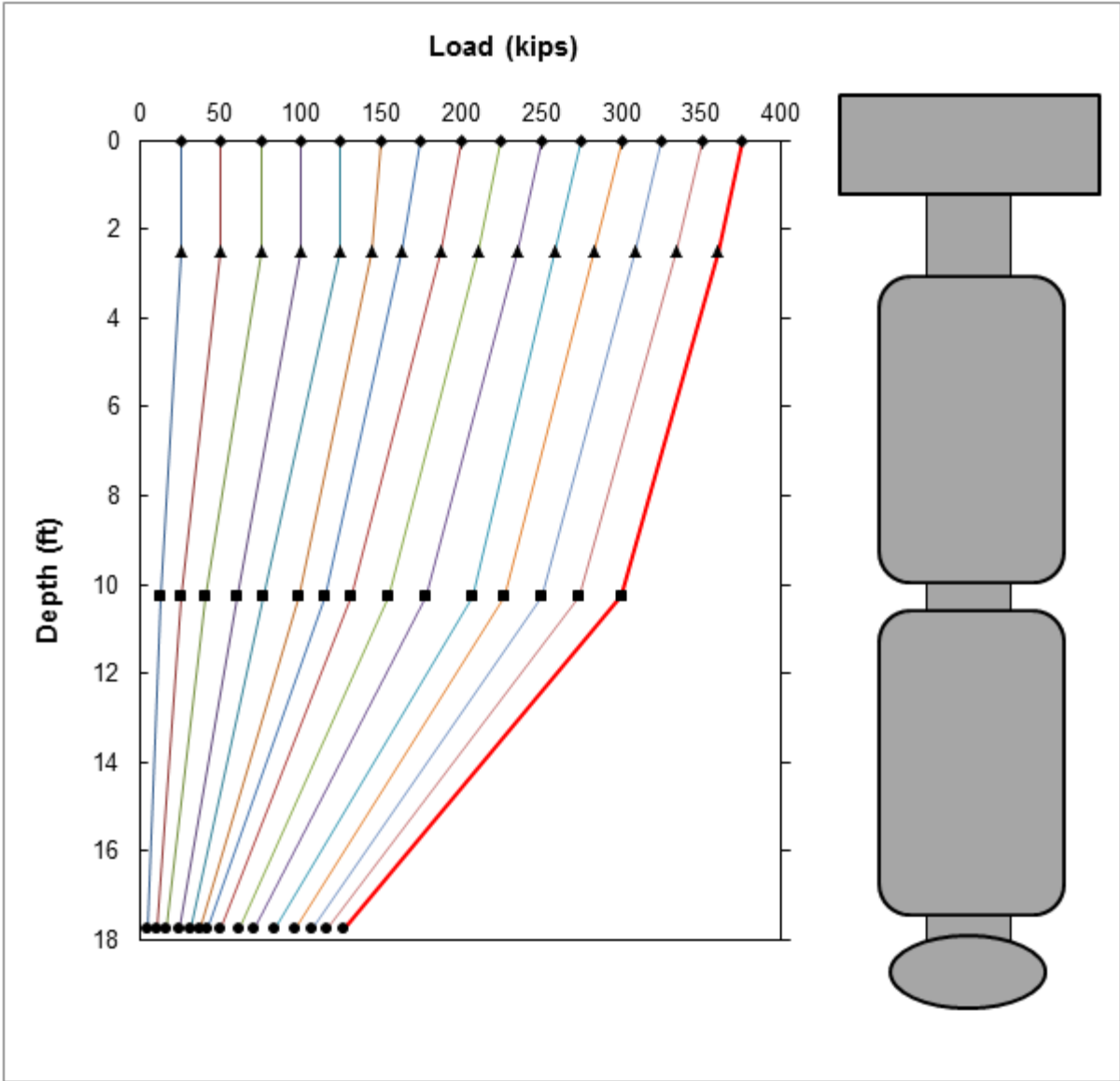


Figure 6-13. Load distribution along the jet-grouted pile 2

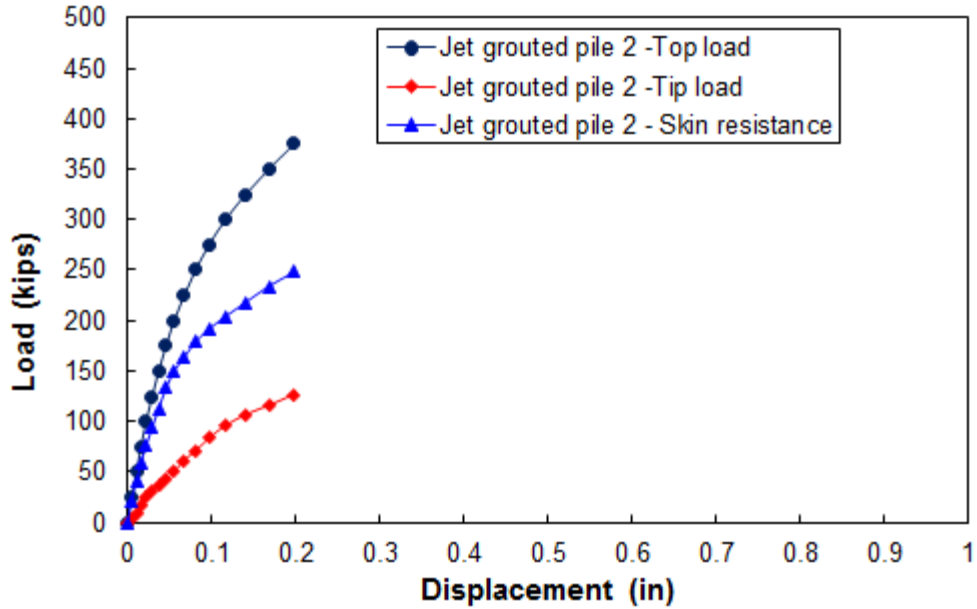


Figure 6-14. Load-displacement response of JP2

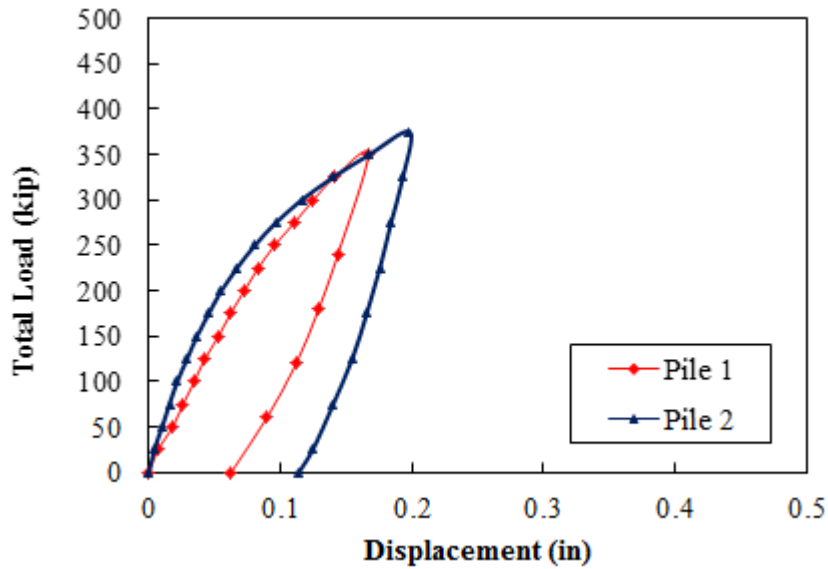


Figure 6-15. Comparison of load-displacement response of pile 1 and 2

Also evident from Figure 6-15, the ultimate capacity or even the Davisson capacity of both jet-grouted piles could not be obtained from the static load tests due to the pullout failure of reaction drilled shafts. Therefore a Statnamic load test was undertaken on one of the jet-grouted piles (JP1) using a 500 ton Statnamic device to obtain the ultimate axial capacity of the jet-grouted pile.

6.3 Statnamic Load Testing of Jet-grouted Pile 1

On Nov 13, 2013 Applied Foundation Testing performed a 500 ton Statnamic Load Test on jet-grouted pile 1 (JP1), Figure 6-16. The same foil strain gauge instrumentation used to measure static resistance was used to measure the dynamic forces along the pile, Figure 6-17. Note, the top of the jet-grouted pile had four dynamic load cells and accelerometers to measure forces, and accelerations applied to the top of the shaft. The average top applied dynamic force (1400 kip) is presented in Figure 6-17 (dynamic applied), along with inertia (mass x measured acceleration), and damping force (viscous damping x velocity). The peak dynamic force within the pile was just beneath the cap (dynamic-top5), followed by middle (dynamic-mid3) and the tip



Figure 6-16. 500-ton Statnamic testing on jet-grouted pile 1

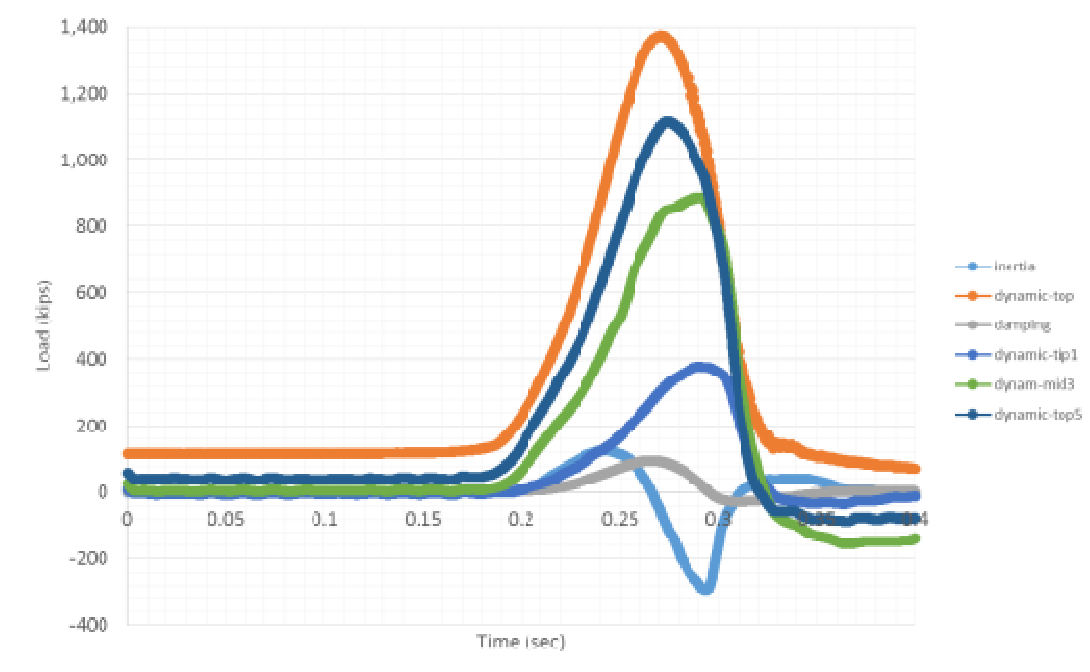


Figure 6-17. Dynamic forces in the jet-grouted pile

(dynamic-tip1). Based on the strain gauge data, Figure 6-17, 300 kip of dynamic resistance was transferred to the soil through the cap, 400 kip through the shaft tip, and 600 kip through side friction. Next, using Midendorf's unloading point method, the static resistance was estimated, Figure 6-18. That is, the estimated inertia and damping (Figure 6-17) was subtracted from the measured dynamic force applied to the top of the jet-grouted pile. The measured ultimate static capacity of the pile is approximately 1400 kip of which 450 kip is skin friction.

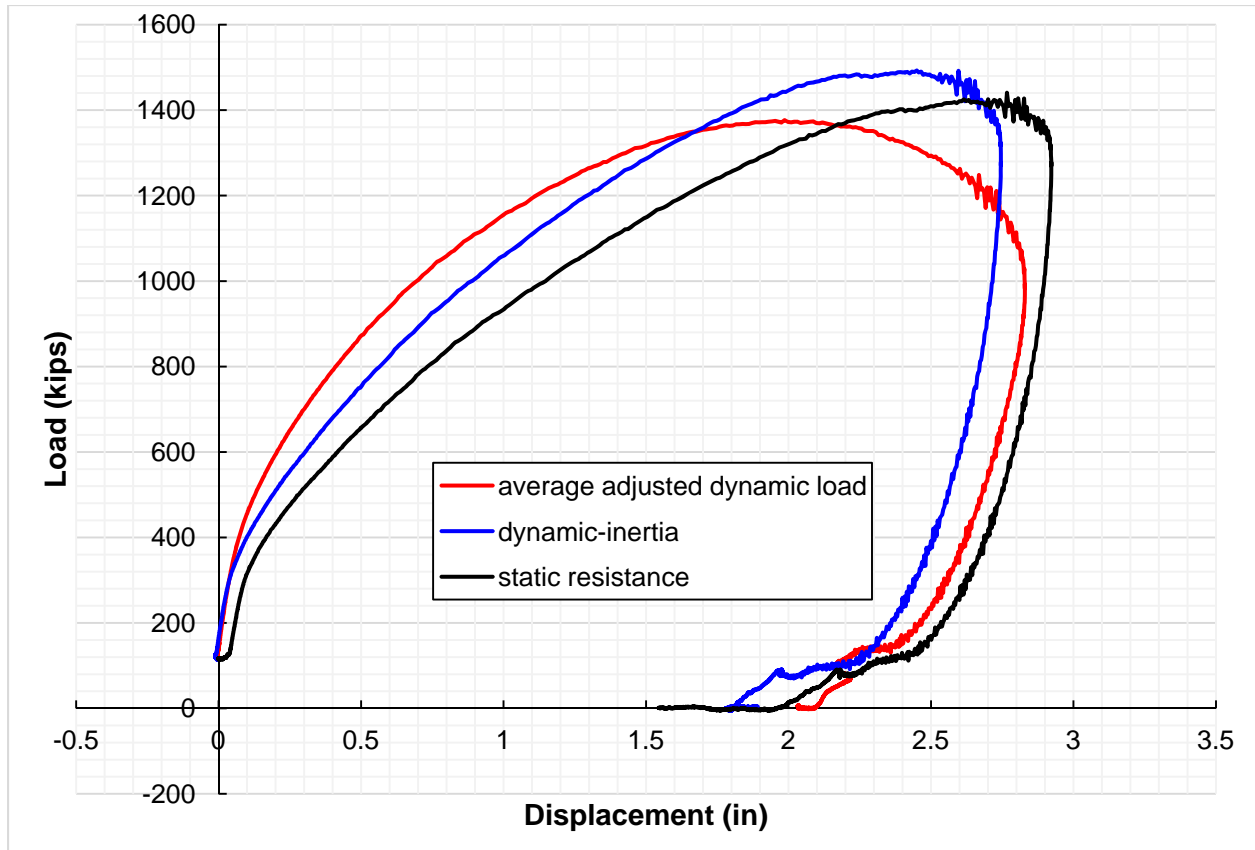


Figure 6-18. Dynamic and static resistance of jet-grouted pile 1.

6.4 Prediction of Unit Skin Resistance of Jet-grouted Pile

The unit skin and ultimate side resistance of the jet-grouted piles was estimated using three different approaches (K_g , pressuremeter, and tip grout pressure). A discussion of each prediction method follows:

6.4.1 K_g method

The first approach used was the K_g method suggested by previous FDOT projects: BD545-031 and BDK-75-977-07 (McVay et al. 2009; Thiyyakkandi et al. 2013). The average unit skin friction for each membrane was determined at the average depth using the K_g plot (Figure 2-6) and unit skin friction equation (Eq. 2-2). It should be noted that previous test chamber studies (BD545-031 and BDK-75-977-07) were conducted at loose to medium dense

soil state and the peak friction angle (ϕ_p) was very close to the constant volume or critical state friction angle (ϕ_c). In addition, a semi-rigid canvas membrane was used to confine the side grout zones, which had interface friction angle (δ) nearly equal to the soil's friction angle.

Consequently, Kg plot (Figure 2-6) and unit skin friction equation (Eq. 2-2) are in terms of critical state friction angle (ϕ_c). But, in the present case, the peak friction angle (ϕ_p) was greater than the critical state friction angle (i.e., dilation angle, $\psi \neq 0$) and the interface friction angle (δ) was about 0.7 times the soil's friction angle. Since the expansion ratio (i.e., final radius to initial radius) of side grout zone is very small (1.64), the reduction in frictional angle due to cavity expansion process will be negligible (i.e., $\phi = \phi_p$). Recall that during cavity expansion process, the friction angle near cavity wall diminish from ϕ_p initially to ϕ_c at the steady state cavity expansion (i.e., once limit pressure is reached), which requires large expansion ratio (>10). Therefore, the peak friction angle (ϕ_p) was used to estimate Kg value from Figure 2-6.

Previous finite element analysis of jet-grouted piles (McVay et al. 2010; Thiyyakkandi et al. 2013) showed that under axial top-down loading, the shearing of the pile is not purely along the pile-soil interface, but partially through the soil itself as shown in Figure 6-19, due to the non-prismatic shape of the grout zones. Consequently, the use of interface friction angle (δ) for skin resistance prediction (Eq. 2-2) may underestimate, and a prediction based on soil's friction angle (ϕ) may overestimate the actual skin resistance of the pile. The actual skin resistance will fall within these two predictions. However for design purposes it is safer to use the prediction based on interface frictional angle.

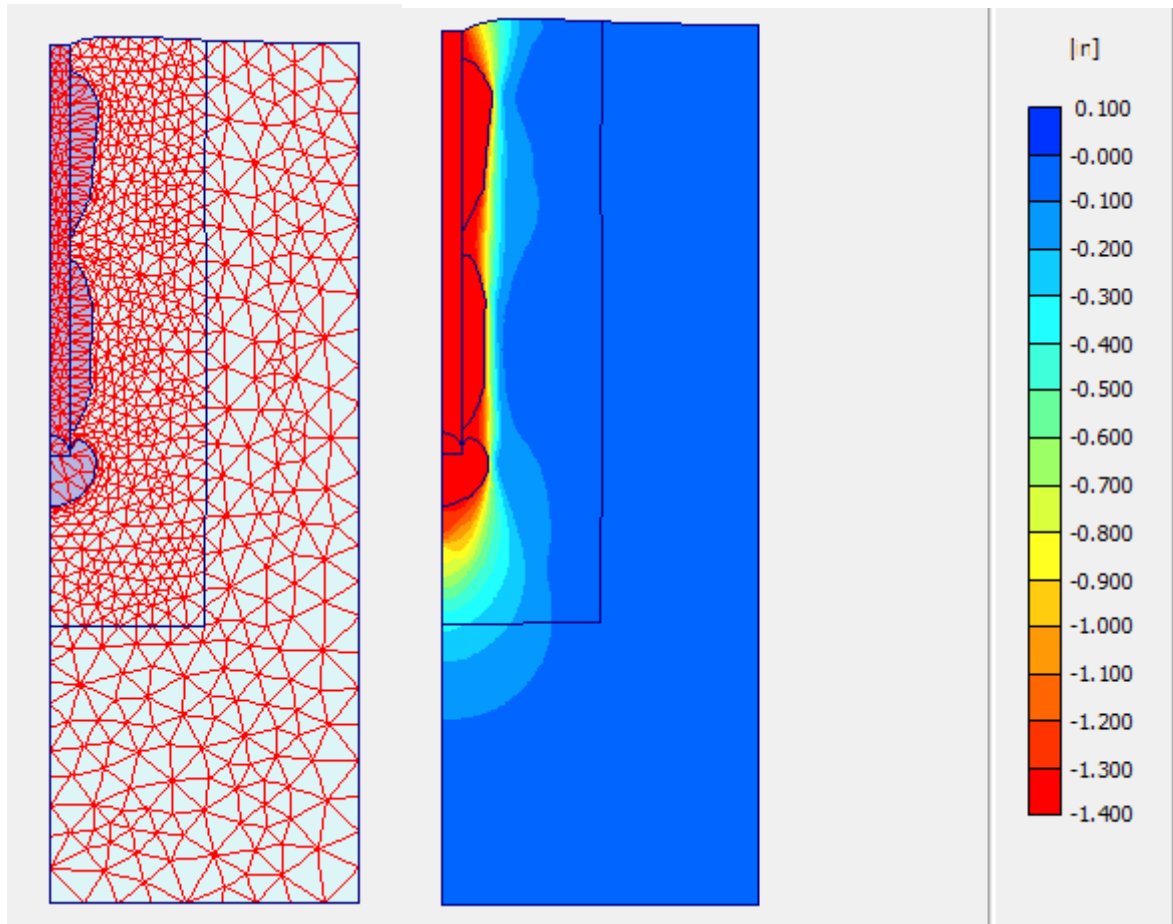


Figure 6-19. Deformed mesh after grouting and displacement profile during top-down loading of jet-grouted pile

Table 6-3 presents the prediction of the average ultimate unit skin friction (f_s) and side resistance (Q_s) of jet-grouted piles using both δ and ϕ . The side resistance was obtained by multiplying the average unit skin friction with the pile surface area. Note that the diameter of the bulb was estimated by assuming a purely cylindrical shape with volume equal to the volume of grout pumped.

6.4.2 Using in situ pressuremeter test data

The second approach uses the recorded in situ Pressuremeter test data. As evident from the previous FDOT research projects, the horizontal stress around side grouted pile diminishes immediately after grouting due the elastic unloading and incompressible nature of the grout. It is

well known that side grouting is analogous to Pressuremeter test. In case of Pressuremeter test, during the unloading phase, large decrease in pressure occurs under a very small decrease in volume as can be seen from the Figure 6-20. The unloading response is initially linear (elastic unloading) and further decrease in volume causes reverse yielding of the cavity wall. For the current prediction, it is assumed that the residual stress around a side grouted pile are approximately equal to the pressure just before reverse yielding (i.e., 22 & 50 psi for JP1 and 16 & 39 for JP2). Note that reversing yielding around a side grout bulb is not likely due to the incompressible nature of grout. Using the residual stresses (22 & 50 psi for JP1 and 16 & 39 psi for JP2) from the Pressuremeter test, the unit skin friction along the piles was estimated (Table 6-4). For the prediction, the conservative interface friction angle (δ) was used, as the soil's friction angle (ϕ) in the prediction would be significantly higher (e.g., 600 kip vs. 400 kip for JP1). Further research on interface friction angle (δ), and Pressuremeter modeling of side grouted piles/shafts are warranted.

Table 6-3. Side resistance using Kg method

Pile	Grout zone	Zone length $H(ft)$	Depth to middle of zone (ft)	Initial vertical eff. stress at middle σ'_{vo} (psf)	K_g at middle Fig.2-6	Grouted vertical eff. stress $\sigma'_{vg}=K_g \sigma'_{vo}$ (psf)	$\delta - \phi$	f_s (psf) (Eq. 2-2) ($\delta - \phi$)	A_s Surface area (ft ²)	Q_s Side resistance (kip) ($\delta - \phi$)	Total (kip) ($\delta - \phi$)
JP1	Top	7	6.5	717.3	2.33 ^a	1671.3	23.8° - 34°	1035-1758	83.84	87-147	235-401
	Bottom	7	14	1305.6	2 ^b	2611.2	25.2° - 36°	1752-3012	84.29	148-254	
JP2	Top	7	6.5	730.0	2.33 ^a	1700.9	23.8° - 34°	1053-1789	83.39	88-150	239-409
	Bottom	7	14	1331.4	2 ^b	2662.8	25.2° - 36°	1787-3072	85.77	151-259	

^a From Figure 2-6 for $\phi = 34^\circ$

^b Extrapolated from Figure 2-6 for $\phi = 36^\circ$

Table 6-4. Estimation of side resistance using the pressuremeter test data

Pile	Grout zone	Zone length $H(ft)$	δ	Horizontal stress after grouting, σ_h (psi) Fig. 6-16	$f_s = \sigma_h \tan(\delta)$ (psf)	A_s Surface area (ft ²)	Q_s Side resistance (kip)	Total (kip)
JP1	Top	7	23.8°	22	1397	83.84	117	403
	Bottom	7	25.2°	50	3388	84.29	286	
JP2	Top	7	23.8°	16	1016	83.39	85	311
	Bottom	7	25.2°	39	2643	85.77	227	

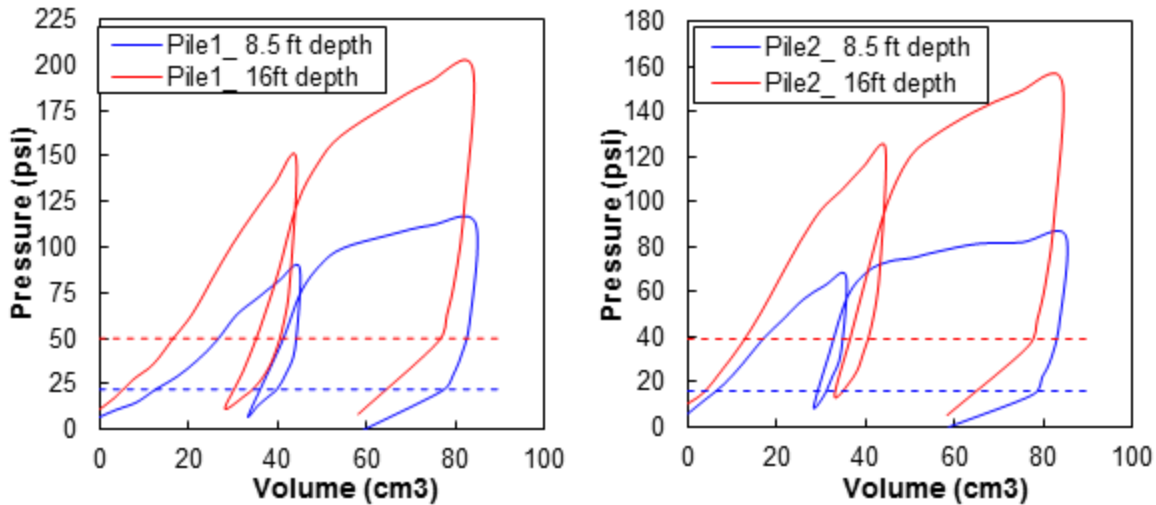


Figure 6-20. Estimation of residual stress from pressuremeter expansion curves

6.4.3 Using the measured tip grout pressure

The last approach used to estimate skin frictions were based on the field reported tip grout pressures (i.e., construction approach). The ultimate axial skin friction of a pile should be equal to the maximum tip grout pressure times the effective tip area (Table 6-5). The effective area is assumed as the area of circle with diameter equal to the diagonal distance of precast pile ($\pi \times (28\sqrt{2})^2/4 = 1231 \text{ in}^2$). The skin resistance based on the tip grout pressure is found to be 357 kip (Table 6-5). Evident sufficient top-down load was not been applied during the static testing of both piles to mobilize full skin friction or tip resistance. In the case of JP1, the Statnamic tests reports a skin friction of approximately 450 kip which is greater than Table 6-5 value. However, the upward movement of 0.35-in (Figure 5-35) may have been insufficient to mobilize the full skin friction on JP1.

Table 6-5. Side resistance using sustained tip grout pressures

Pile	Tip grout pressure (psi)	Effective tip area (in ²)	Side resistance (kip)
JP1	290	1231	357
JP2	280-300	1231	345-369

Table 6-6 provides a comparison of the measured skin resistances with the predicted skin resistance using the different approaches. It is evident from the measured skin resistances, that the predicted values are generally conservative and in reasonable agreement with the measured values. Since the estimated static ultimate resistance from the Statnamic load test requires some estimation (e.g., damping), the estimated ultimate skin resistance from the different methods are reasonable.

Table 6-6. Comparison of measured and predicted skin resistance

Pile	Method	Top membrane	Bottom membrane	Total
JP1	Measured (kip)	97	151*	248 (450)
	<i>Kg</i> method (kip)	87-147	148-254	235-401
	Pressuremeter data (kip)	117	286	403
	Tip grout data (kip)	--	--	357
JP2	Measured* (kip)	60	173*	233
	<i>Kg</i> method (kip)	88-150	151-259	239-409
	Pressuremeter data (kip)	85	227	311
	Tip grout data (kip)	--	--	345-369

*not fully mobilized
value in bracket from Statnamic load test

6.5 Comparison of the Axial Response of Jet-grouted Piles and Drilled Shafts

Figure 6-21 shows the total load-displacement response of jet-grouted piles and drilled shaft. It is evident from Figure 6-21 that the axial resistance of the jet-grouted pile is much greater than that of the similar sized drilled shaft. Table 6-6 presents the mobilized unit skin frictions for each zones and a comparison with the maximum unit skin obtained during the drilled shaft test. It is evident from the table that unit skin friction for the jet-grouted pile is much greater than that for drilled shaft, especially in the bottom zone (2.6 times).

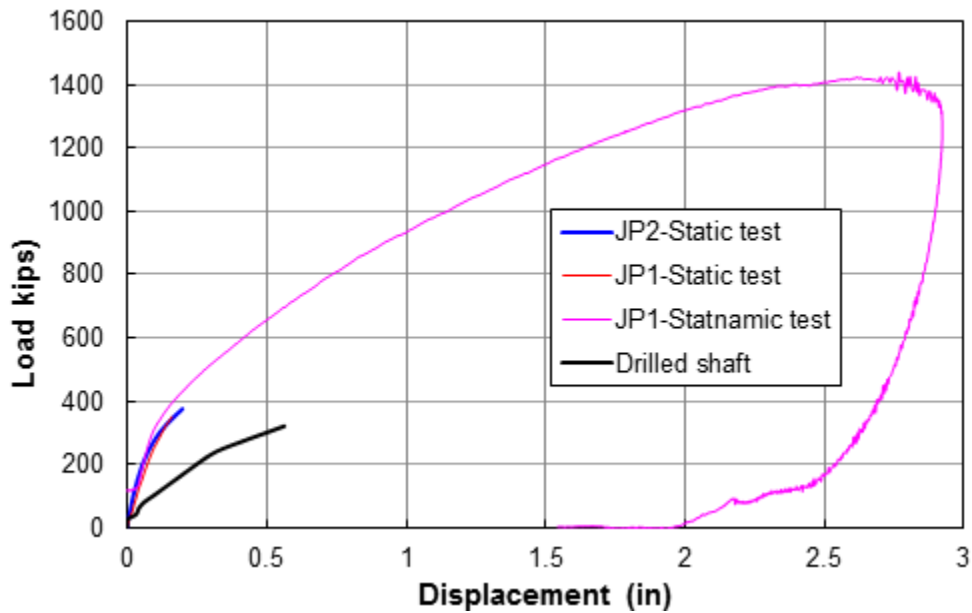


Figure 6-21. Total load-displacement response of jet-grouted piles and drilled shaft

Table 6-7: Comparison of unit skin frictions for jet-grouted pile vs. drilled shafts

Segment	Unit skin (ksf)		
	JP1	JP2	Drilled shaft
Top membrane (3 – 10 ft)	1.16	0.72	0.591
Bottom membrane (10.5- 17.5 ft)	1.79*	2.02*	0.852

*not fully mobilized

CHAPTER 7 COMBINED TORSION AND LATERAL LOAD TESTS ON DRILLED SHAFTS AND JET- GROUTED PILES

This Chapter presents the combined torsion and lateral load test program on the jet-grouted piles and drilled shafts as well as a comparison of their torsional response. For the testing, a full-scale mast arm assembly was designed and fabricated. The test procedure, field instrumentation, analysis of results and the comparison of resistance are discussed in detail.

7.1 Design and Fabrication of Mast Arm – Pole System and Connections

In the case of a foundation supporting a standard FDOT mast arm assembly, the eccentric dead load of the structure develops (see Figure 2-8) axial load, V_y and moment, M_z (about the axis perpendicular to arm) on the foundation. Similarly wind loading along the length of the Mast arm generates torsion (T or M_y), lateral load, V_z , and bending moment about the arm axis, M_x (function of pole height). Consequently to simulate the actual loading scenario, a full scale Mast arm structure needs to be used in the testing. Accordingly, one of FDOT's longest Mast arm type (E7-T6: 78-ft long) was considered for the study. As discussed in Chapter 4, the recommended foundation for the E7-T6 type structure is a 48-in diameter x 18 ft deep drilled shaft (FDOT Index No: 17743). Of interest is the ultimate torsional resistance of drilled shafts and jet-grouted piles. Therefore, the mast arm structure should be sufficient to carry the forces and moments (torque >500 kip-ft) developed by the applied lateral loading until failure of the foundation. Unfortunately, the standard E7-T6 Mast Arm assembly is not capable of generating/carrying torque exceeding 305 kip-ft at the foundation. Consequently, a new Mast arm assembly (arm, pole and connection bracket) was designed using the FDOT's MathCAD spread sheet: Mastarm v4.3. The spread sheet was slightly modified to incorporate a point lateral load instead of wind load acting on the arm. The dimensions of arm and pole are given in Table

7-1. Figure 7-1 shows the designed arm-pole connection with the dimensions of all the components. Triangular stiffeners of 1/2" thickness were provided at the connection between arm and pole base plate as shown in Figure 7-1 for additional strength. Figure 7-2 shows the fabricated arm and pole with connection bracket. There are 10 - 1.5" diameter bolt holes (5 on each side) for 1.25" Ø bolts on the connection bracket.

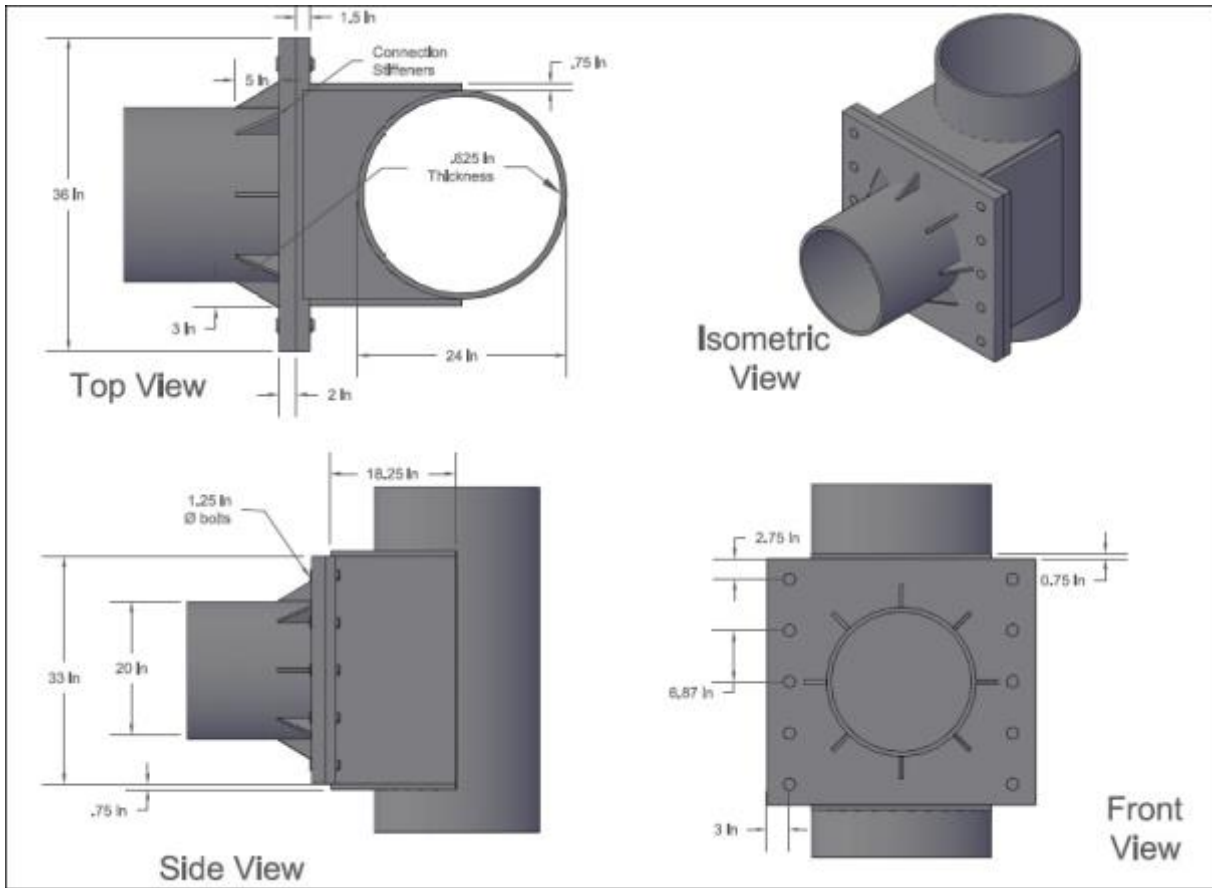


Figure 7-1. Arm-pole connection with dimensions

Table 7-1. Dimensions of arm and pole

	Length (ft)	Diameter (in)	Thickness (in)	Taper angle (deg)
Arm	40	20	0.625	0
Pole	22	24	0.625	0



Figure 7-2. New mast arm assembly

7.2 Combined Torsion and Lateral Load Testing of Drilled Shafts

Combined torsion and lateral load tests were performed on three test drilled shafts to verify FDOT's revised design approach for drilled shafts supporting Mast arm structures. It should be noted that TS1 (4-ft diameter x 12-ft long) and TS3 (4-ft diameter x 18-ft long) was only subjected to combined torsion and lateral load test (i.e., no prior loading). Foundation TS2 (4-ft diameter x 18-ft long) underwent a static top-down loading prior to the combined torsion and lateral load test to investigate the influence of axial loading on the torsional resistance of a shaft. A description of each test and analysis of the results is presented followed by comparison with multiple prediction methods.

7.2.1 Combined torsion and lateral load test on TS1

Combined torsion and lateral load test on the 4-ft diameter x 12-ft long shaft (TS2) was carried out in two phases: (1) Setting Mast arm – pole assembly on the top of foundation, and (2) Applying lateral load on Mast arm at a standoff distance of 35 ft. Setting of Mast arm assembly itself develops axial load, $V_y = 10.7$ kip and bending moment, $M_z = 118$ kip-ft (about axis perpendicular to arm) at the top of the foundation due to the eccentric dead load of the assembly. Of interest was the tilt/overturning response of this short shaft (12-ft) as a result of dead weight of pole (axial) and mast arm (axial and moment). In the Second phase, lateral load was applied to

the Mast arm, (simulate wind loading; e.g., hurricane) which generates torsion (T or M_y), bending moment (M_x , about axis of arm), and lateral load, V_z at the top of the shaft. In the second phase, the foundation is under a combination of loads and moments (V_x, V_y, M_z, M_x, T). Discussion of each test phase is as follows,

7.2.1.1 Setting of mast arm – pole assembly on top of shaft

The fabricated Mast arm and pole were transported separately from the Coastal engineering lab to the test site; whereupon they were bolted together on ground with the aid of a forklift (total estimated weight 8.5 kip). Next, a crane with an axial capacity of 75 ton was used to lift and set the assembly on shaft (Figure 7-3). Still under crane support, the bottom flange of the pole was bolted to the pipe and flange system embedded in shaft (Figure 7-3). The load cell on crane indicated that the crane was carrying approximately 8.1 kip (note weight of cable and ball: 2.2 kip), which means, 2.6 kip ($10.7 - 8.1 = 2.6$ kip) was transferred to shaft in the bolting phase. Next, 2 sets of string pots (4 pots in each set) for monitoring rotation, translation and tilt/overturning of the shaft were attached to pole. Figure 7-4 shows the schematic of string pots arrangement and Figure 7-5 displays the placement of the pots at the test site. The first set of string pots (bottom) were at an elevation of 0.5 ft above the bottom flange and the second set (top) were 5ft above the bottom set. The string pots with supporting frame were kept outside the influence zone of shaft [i.e., 20-ft (5D) away from shaft]. A National Instruments data acquisition system was used to record string pot data. Digital levels were also used to monitor the vertical displacement of shafts at three different locations (120° apart) as shown in Figure 7-6. Invar staffs were attached to the top of flange by means of an angle sections. After setting all the instrumentation, the dead load of the assembly was gradually released to shaft at an increment of about 0.5 kip (i.e., unloading from crane).



Figure 7-3. Setting mast arm assembly on the top of shaft using a crane

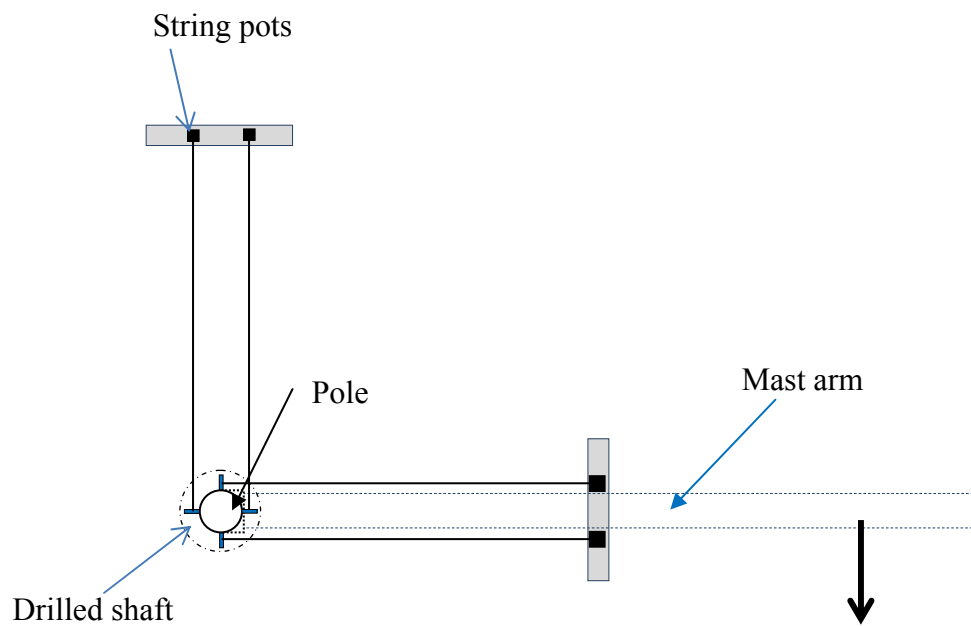


Figure 7-4. Schematic of string pot arrangement



Figure 7-5. String pot arrangement at the site



Figure 7-6. Digital level and invar staffs for vertical deformation monitoring

Shown in Figure 7-7 is the vertical load vs. lateral displacement (along mast arm x-axis) measured at the top of foundation during the release of load from crane. Maximum lateral displacement observed was 0.12-in under the axial load of 10.7 kip and moment, M_z of 118 kip-ft. Note that lateral displacement was negligible up to an axial load of about 4.5 kip, which is approximately equal to the self-weight of pole alone (4.8 kip). Note, it may be assumed that moment, M_z on shaft head is zero up to this load. However, the additional load, i.e., the dead weight of the mast arm is eccentric and generates a moment, M_z , causing lateral translation and overturning of shaft. Table 7-2 depicts the maximum vertical displacement measured at three different locations at the end of the first phase of testing. It is evident from the table that the vertical displacement was non-uniform at shaft top, supporting the shaft tilting, i.e., overturning as results of load and moment.

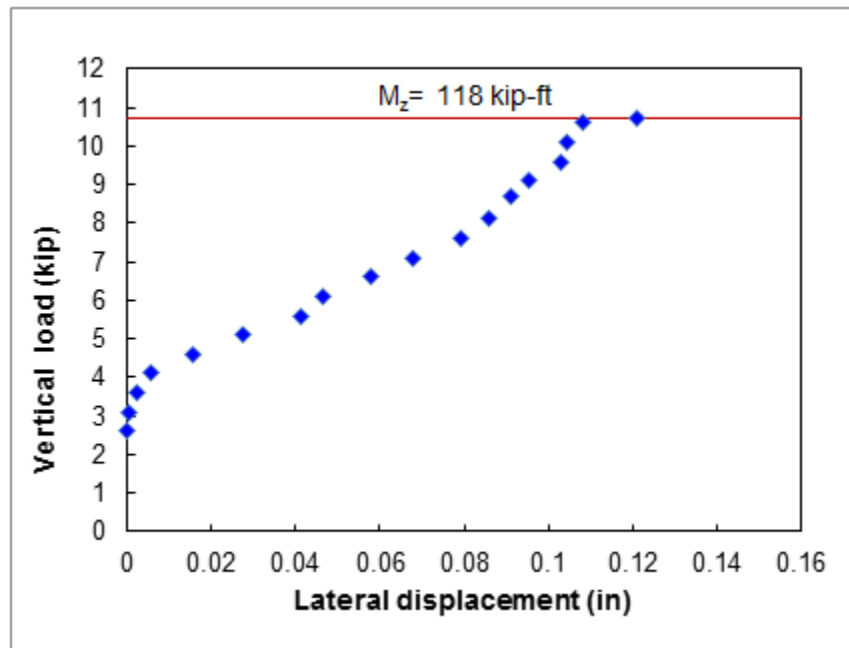
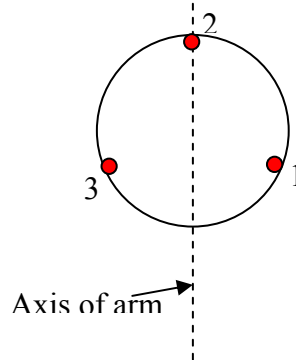


Figure 7-7. Axial load vs lateral displacement during the application of dead wt. of mast arm assembly

Table 7-2. Maximum vertical displacement at the top of shaft

Level No.	Displacement (in)
1	-0.06
2	0.05
3	-0.118

Note: -ve represent downward movement



7.2.1.2 Application of lateral load on mast arm at an eccentric distance of 35 ft

The combined torsion and lateral loading of shaft was performed after the completion of phase 1. The lateral load on the mast arm was applied with the crane’s winch cable at an eccentric distance of 35-ft along the mast arm, Figure 7-8. After setting the Mast arm assembly on shaft (i.e., unloading from crane; phase 1), the crane was re-positioned at a distance of about 130 ft away from the arm. Next, the boom of the crane was adjusted to a height of 21.5 ft for horizontal pulling. The crane’s winch cable was then attached to the Mast arm. A ‘Total station’ was used to ensure that the cable was horizontal (i.e., the arm and boom is at the same elevation). The crane applied the lateral load incrementally by pulling on the arm (Figure 7-8). The applied lateral load was measured using a load cell installed at the load transfer point of the Mast arm and the crane’s winch cable. It was found that the application of a small load (less than 1 kip) resulted in rotation of the shaft. When the load increased beyond 2 kip, it immediately dropped to 2 kip as the shaft rotated. The maximum observed load was 4 kip (i.e., spike – strain controlled

with 0.1 sec duration) but it dropped to 2 kip (> 1 sec duration) and hence sustained load (> 1 sec) were used when plotting the ultimate torsional resistance of shaft. The test stopped when a considerable rotation (about 12°) of shaft was observed. The water table was 10 ft below the ground surface during the load test.



Figure 7-8. Applying lateral load to mast arm

Figure 7-9 displays the torque vs. rotation response measured during the combined torsion and lateral load testing. Even though the test continued up to a rotation of 11.6° , it is evident from the figure that torsional resistance of the shaft was fully mobilized under a rotation of about 8° . In addition, the shaft had a lateral translation of about 4-in (at ground level) and an overturning rotation of 1.4° . The latter suggests that the shaft was approaching a limiting lateral resistance under a combined lateral load of 2-kip in combination with torque of 70 kip-ft.

Figure 7-10 displays photographs of the shaft after all load testing. Evident from the photographs, large torsional cracks as well as a gap between the soil and shaft (due to lateral movement) formed on the back side of shaft (Figure 7-10).

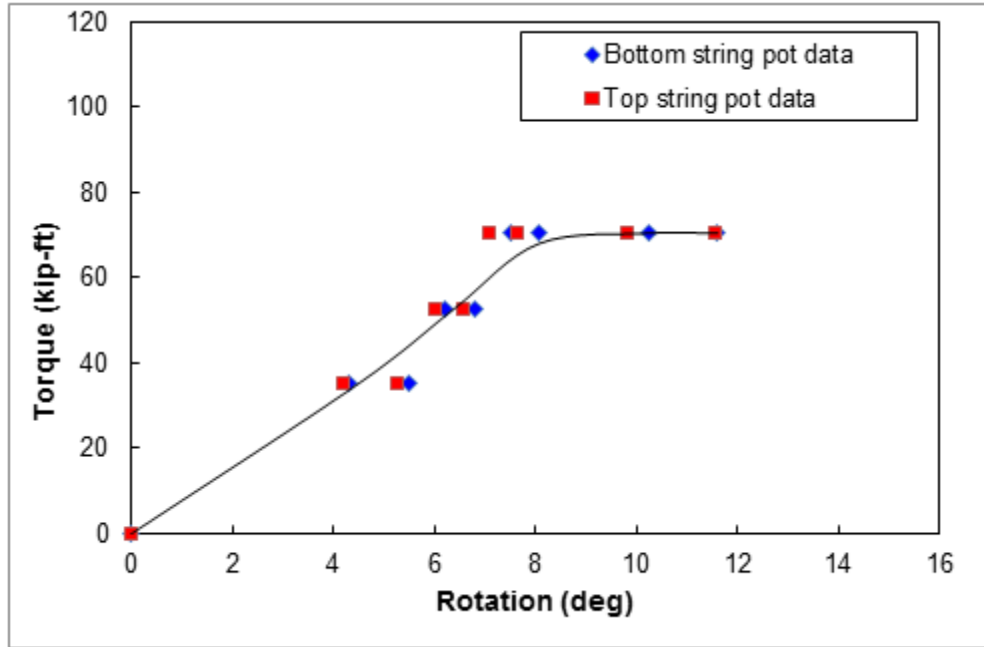


Figure 7-9. Torque vs. rotation during combined torsion and lateral load test

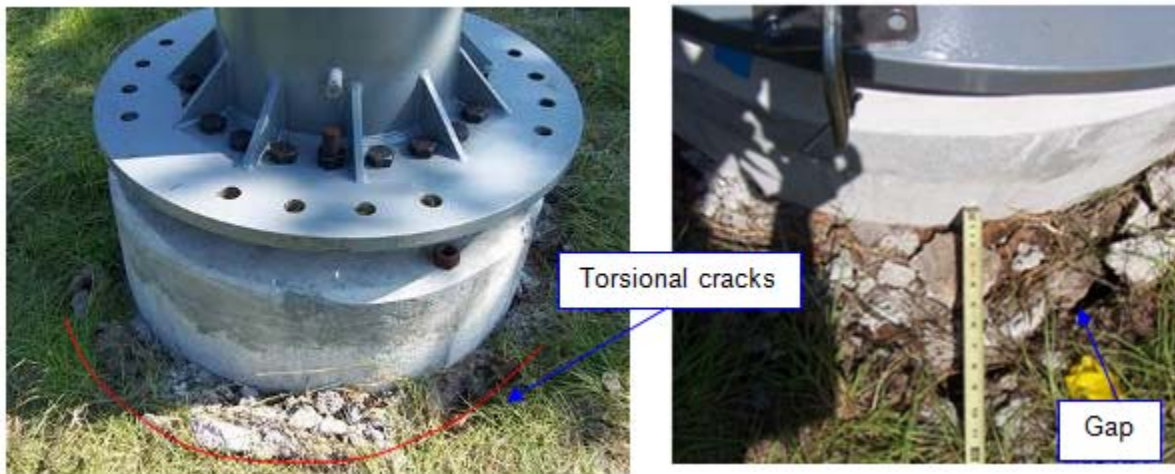


Figure 7-10. Test shaft after load test

7.2.2 Combined torsion and lateral load test on TS2 (4-ft diameter x 18 ft long)

A crane with an axial capacity of 75 ton was used to set the Mast arm assembly on the top of drilled shaft, TS2. After setting and orienting the Mast arm assembly properly, the bottom

flange of the pole was bolted to the embedded pipe and flange system, while the crane supported a major portion of the dead load of the structure. It was found from the previous test (TS1) that string pots data were adequate to determine the rotation, but translation could not be obtained accurately. Therefore three different types of instrumentations: (1) 2- Total Stations, (2) 2-sets of string pots (4 pots in each set as in the previous test), and (3) a set of four digital dial gauges, were used in the subsequent tests for rotation and translation monitoring. Note, model tests in the laboratory had revealed that two “Total Stations” could measure both rotation and translation accurately. Figure 7-11 shows the locations of Total Stations and the targets on the pole. As can be seen from the Figure 7-11, the reflective tapes were used as the targets, which were attached to eye bolts at the end of 1.5-in diameter steel pipes projecting outward from the pole. The targets were at the two different levels (4 at each levels; Figure 7-11); the first set (bottom) was 0.5-ft above the bottom flange and the second set (top) was 5-ft above the bottom set. The arrangement of the string pots was the same as the previous test (TS1). The string pots sets (4 in each set) were nearly at the same elevation of the reflective tape targets (Figure 7-12). The digital dial gauges are placed at the elevation of bottom reflective targets and string pot set (Figure 7-13). The gauges were supported by a wooden reference beam as shown in Figure 7-13. Depth of water table during the test was 6-ft.

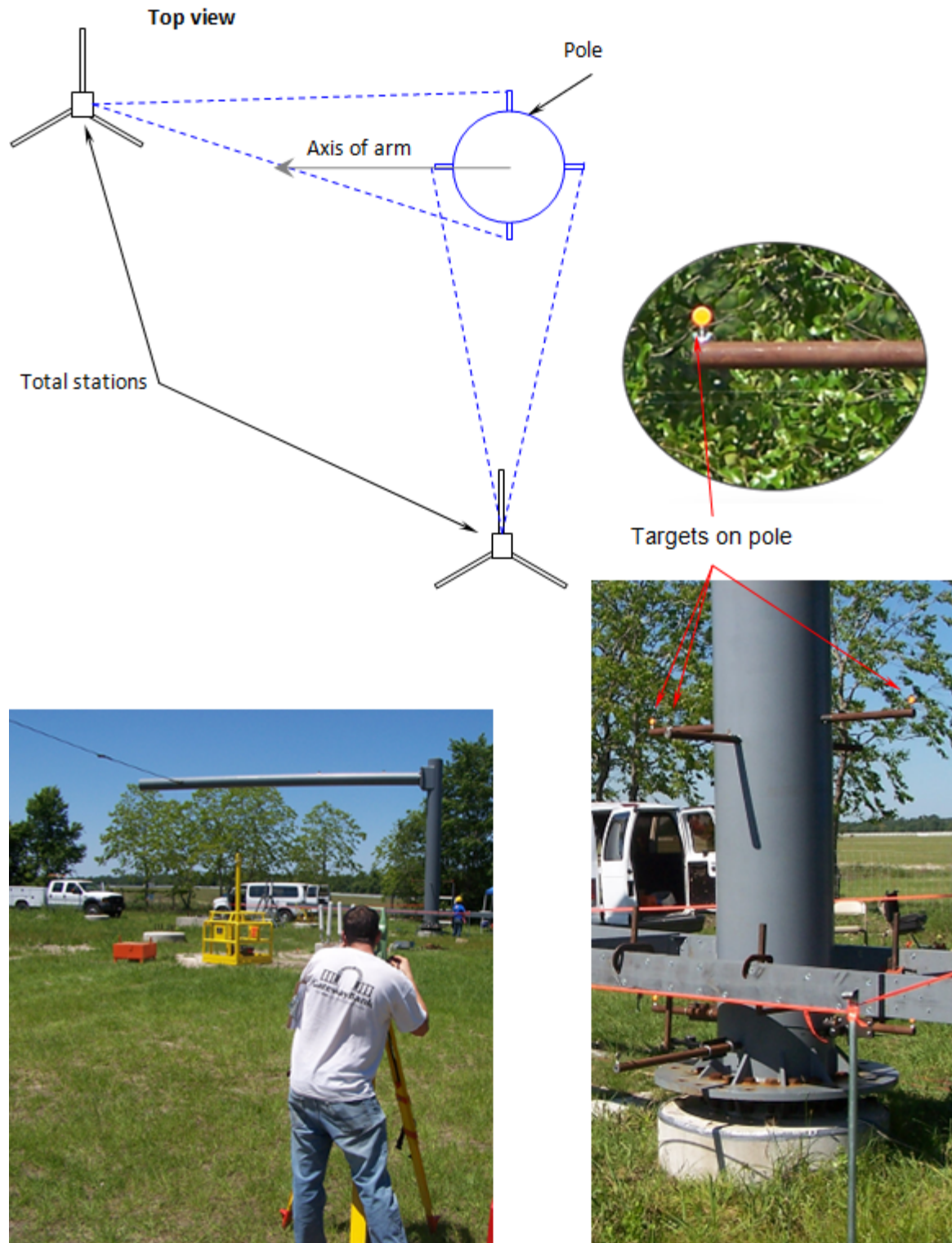


Figure 7-11. Total station for rotation and translation measurement

As in the previous test, the loading was performed by pulling on the Mast arm at an offset (35-ft) from the center of the pole with a crane (Figure 7-14). A surveying level was used to ensure that the cable was horizontal during the loading (crane boom orientation was lowered after each load increment). The applied load was measured using a 20 kip capacity tension load cell attached to the winch cable (Figure 7-15). Each load increment was kept for a time interval of 5 minutes. The loading was continued until a rotation of approximately 5° was observed at the top of the shaft. Note, loading was applied until the torsional resistance of the shaft was fully mobilized. Then unloading was performed in six approximately equal load decrements with 5 minute hold times. The maximum lateral load applied on the mast arm was 6 kip when the full torsional capacity was developed.



Figure 7-12. String pot layout and support system

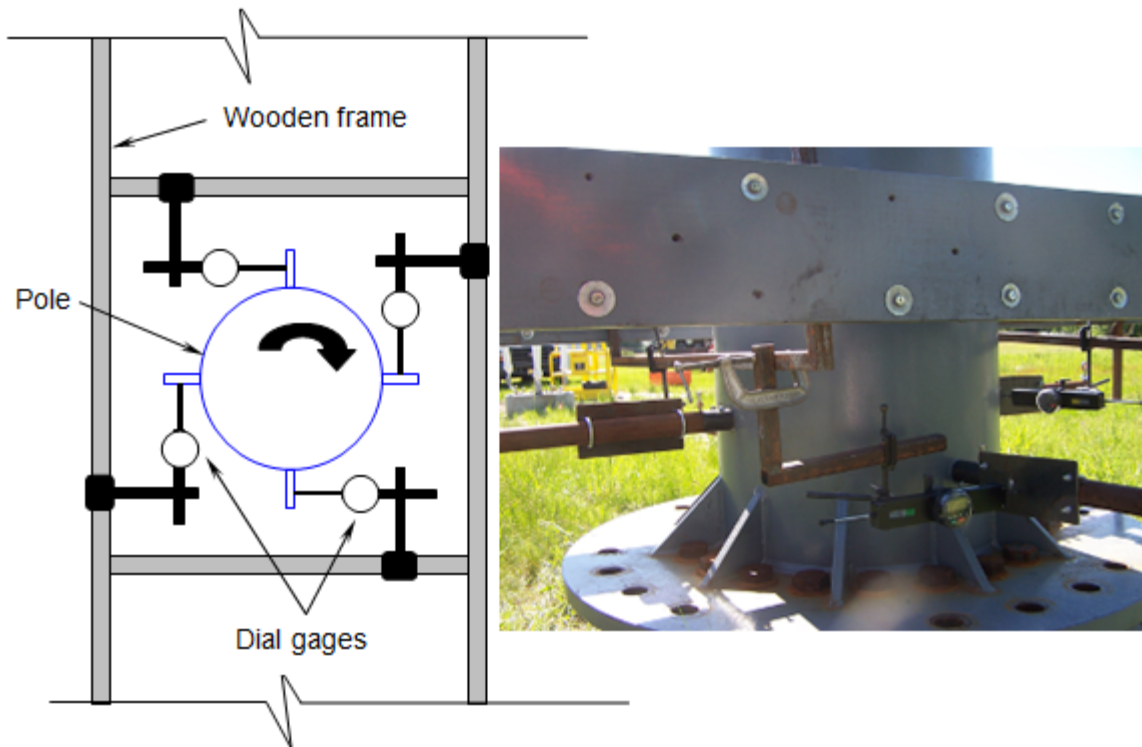


Figure 7-13. Placement of digital dial gauges



Figure 7-14. Combined torsion and lateral loading on the 18-ft-long drilled shaft (TS2)



Figure 7-15. 20-kip capacity load cell used for the test

Figure 7-16 displays the torque vs. rotation response for the drilled shaft. As can be seen from the figure, the rotation measured using the three sets of instrumentation (total station, string pot, and dial gauges) were the same. Figure 7-16 indicates that the torsional resistance of the shaft was fully mobilized at a torque of 210 kip-ft. The lateral load vs. resultant lateral displacement of the top of the shaft is given in Figure 7-17. Similarly, Figure 7-18 presents lateral load vs. angular rotation of the top of the shaft. Evident, from the figures (7-16 to 7-18) torsion resistance controlled the failure of the longer shaft. However, even though the maximum translation was only 0.364in, its behavior (Figure 7-17) had become highly nonlinear with lateral resistance influenced by the torsion component. Note, the failure mode for TS1 (4-ft \varnothing x 12-ft shaft) was combined torsion - lateral failure. Figure 7-19 presents the photograph of the torsional crack and gap formed around the shaft during the load test.

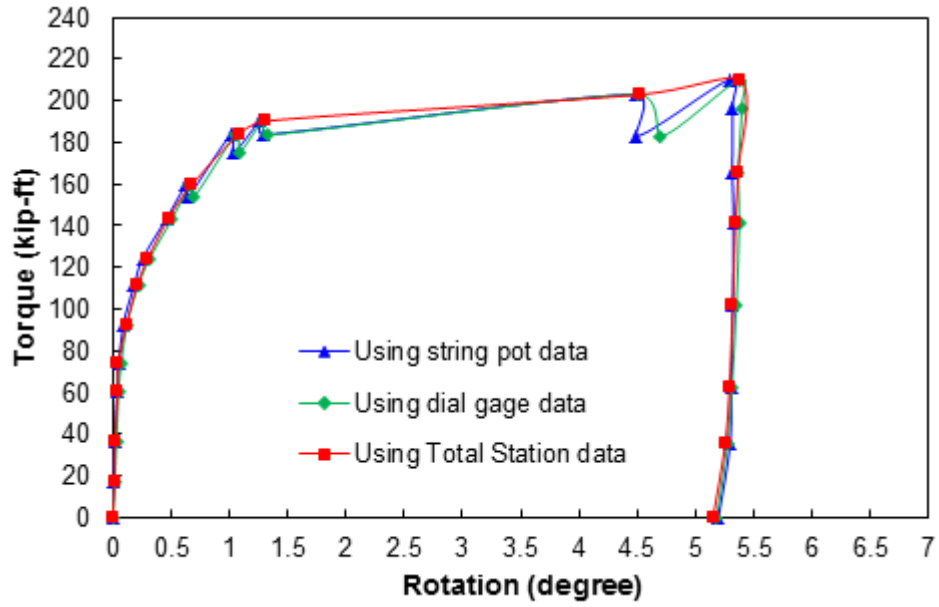


Figure 7-16. Torque vs. rotation response of TS2

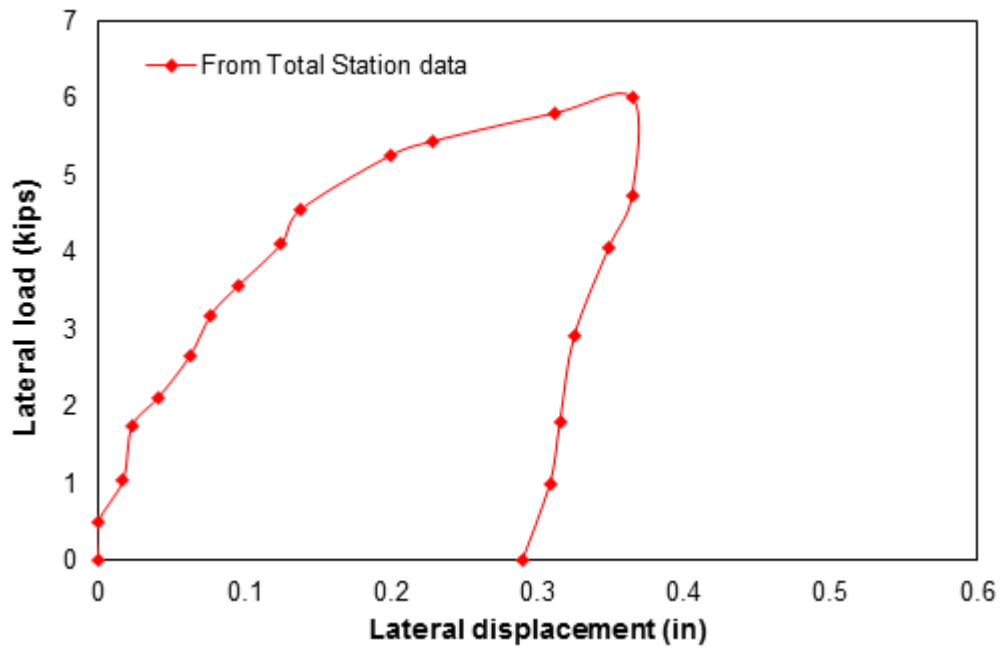


Figure 7-17. Lateral load vs. resultant lateral displacement response of TS2

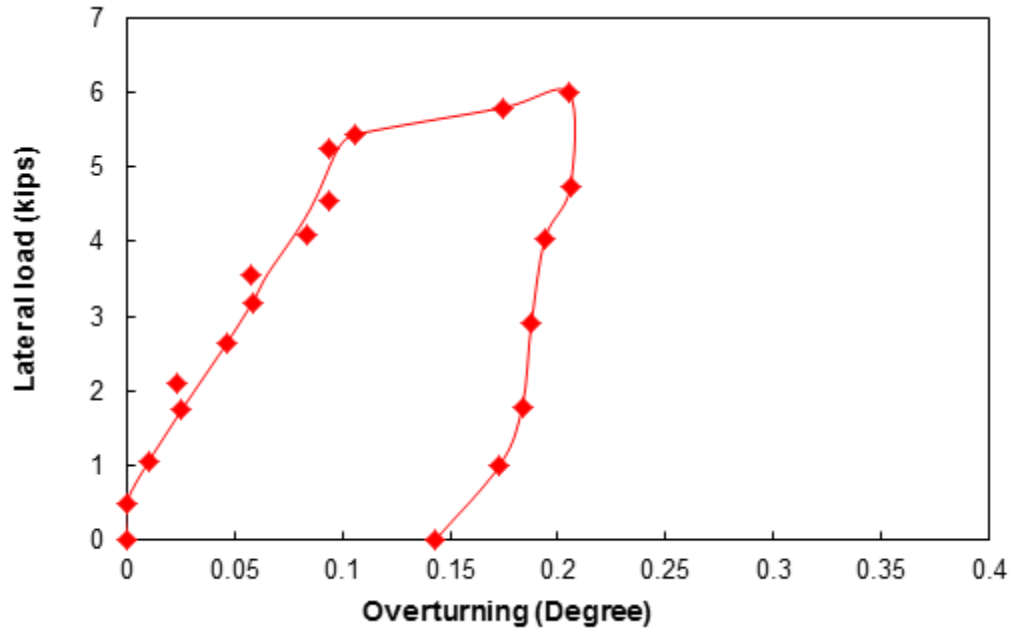


Figure 7-18. Lateral load vs. overturning response of TS2



Figure 7-19. Torsional crack and gap after loading

7.2.3 Combined torsion and lateral load test on TS3 (4-ft diameter x 18 ft long)

The load test set-up and instrumentation layout was the same as the TS2 shaft (4-ft \O x 18-ft long). However, strain gauge data could not be obtained due to malfunctioning of data acquisition system. Just prior to the test, the water table was measured 6-ft below the ground surface. The lateral load was applied in 0.5 kip increments with a constant hold time of 5

minutes. The loading was continued until failure, which was sustained rotation of the shaft. The maximum continuous lateral load on the mast arm was just 4.88 kip. After peak load, the load was removed in three load decrements with 5 minute wait intervals in between.

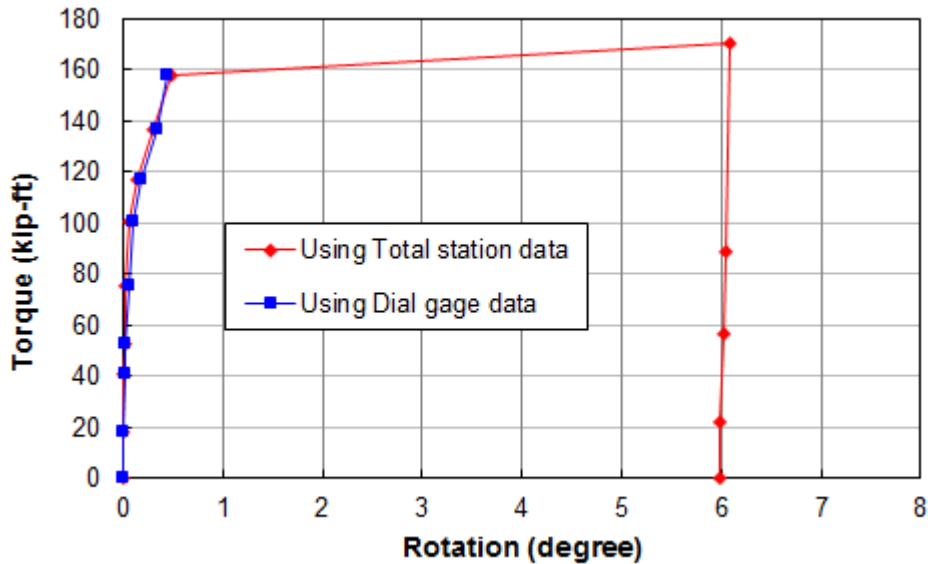


Figure 7-20. Torque vs. rotation response of drilled shaft

Figure 7-20 shows the torque vs. rotation response for the drilled shaft. It is evident from the figure that the torsional resistance of the shaft was fully mobilized during the test (171 kip-ft). Figure 7-21 presents the lateral load vs. lateral displacement of the top of the drilled shaft. Evident from the small value of maximum translation (0.151-in; Figure 7-21), full nonlinear lateral resistance vs. displacement did not occur. Note, however the applied lateral load and torque for TS3 was only 80% of TS2. A comparison of the measured torsional response of the two 18-ft deep drilled shafts (TS2 and TS3) is shown in Figure 7-22. TS3 had lower torsional resistance compared to TS2, which was attributed to the difference in soil profile at two locations. Specifically, at the location of TS2, the top clay layer is 8.5 ft thick, whereas, it is only

2.5 ft deep at the TS3's location (Figure 3-13). This soft clay layer offered lower lateral and torsional shear resistance in the case of TS3.

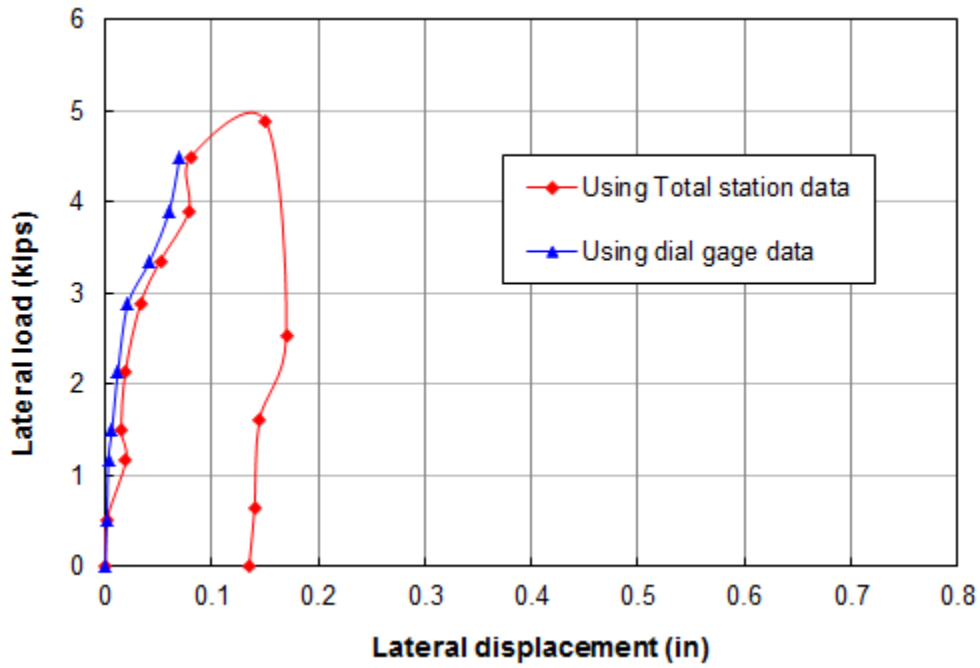


Figure 7-21. Lateral load vs. resultant lateral displacement response for drilled shaft

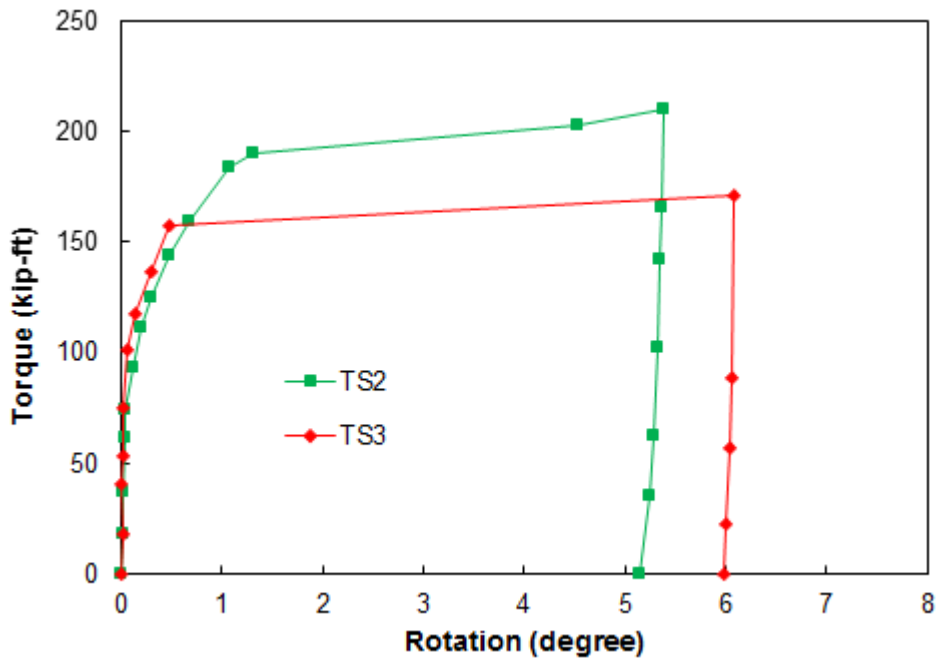


Figure 7-22. Torque vs. rotation responses for TS2 and TS3

7.2.4 Comparison of measured and predicted torsional resistance of the test shafts

The measured torsional resistance of the test shafts was compared with the predicted values using the different methods discussed in Chapter 2 (Section 2.4). Table 7-3 summarizes the methods and the predicted values. Detailed calculations for each method are given in Appendix E. It is evident from the table that depth dependent beta (β) method (O'Neill and Hassan 1994) predicted the torsional resistance quite well ($\pm 10-14\%$). If the side contribution is only considered, FDOT's re-revised prediction method over-predicted the measured torsional capacity by 25-45%. Whereas, the predictions using FHWA's rational method were 20-70 % more than the measured values.

Also shown in the Table 7-3 is the torsional resistance of TS2 estimated using the skin resistance measured during the prior top-down load test (Chapter 6). Since the depth of water table during the top-down load test was 10 ft vs. 6 ft during the combined torque and lateral load response had to be normalized. Using O'Neill' and Hassan (1994) beta method, it was found that raising the water table by 4 ft (i.e., from 10 ft to 6 ft) caused a decrease in torsional resistance of 31 kip-ft (see Appendix E). If this decrease is taken into account, the predicted value using the axial load test would be 251 kip-ft (i.e., 282-31 kip-ft). The difference, 41 kip-ft, (i.e., 251 kip-ft axial vs. 210 kip-ft combined, Table 7-3) indicates that the reduction may be due to combined loading (Hu et al., 2006) or due to prior loading (i.e., residual stresses).

Table 7-3. Comparison of measured and predicted torsional resistance

Method	TS1			TS2			TS3		
	Skin (kip-ft)	Tip (kip-ft)	Total (kip-ft)	Skin (kip-ft)	Tip (kip-ft)	Total (kip-ft)	Skin (kip-ft)	Tip (kip-ft)	Total (kip-ft)
Measured	--	--	70	--	--	210	--	--	171
FDOT's Re-Revised ω method	99	25	124	264	30	294	249	28	277
O'Neill and Hassan (1994)*	80	--	80	189	--	189	191	--	191
Rational method) FHWA 2010*	119	--	119	253	--	253	236	--	236
Based on axial load test*	--	--	--	(282) 251**	--	(282) 251**	--	--	--

*No tip contribution is considered (Hu et al. 2006)

**Corrected for Water Table

Hu et al. (2006) reported that the lateral overturning resistance is significantly reduced by the combined torsion and lateral load. Plots for estimating the reduction factors (R_T = lateral capacity with torque/lateral capacity without torque) based on torque/lateral load ratio (i.e., standoff distance) were developed. In the case of the present test series, only TS1 (shortest shaft, i.e., $L/D = 3$, $D=4$ ft and $L=12$ ft), underwent combined torsion and lateral translation failure. In case of the longer shafts, TS2 ($L/D = 4.5$) exhibited rotational failure and significant nonlinear displacement, but not failure. However, TS2 did exhibit 20% less torque resistance (210 kip-ft) due to combined loading than estimated from just axial (i.e., Chapter 6 – 251 kip-ft).

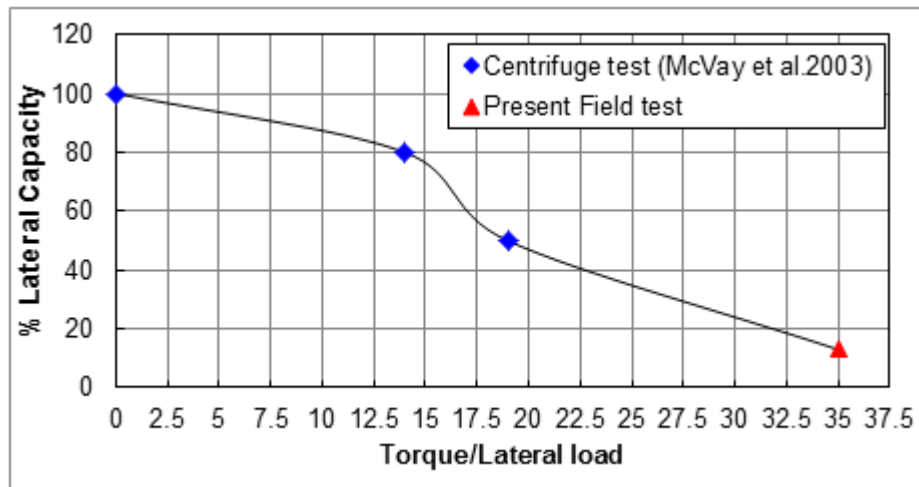


Figure 7-23. Lateral resistance reduction factor due to torsion for L/D ratio = 3

Of interest is where the field TS1 results compared to Hu et al. (2006) centrifuge results. Using soil properties of the site, an ultimate lateral resistance, 15.7 kip, for TS1 ($L/D = 3$) due to lateral loading (i.e., load on pole) was predicted using the force and moment equilibrium approach suggested by Hu et al. (2006). Since, the reduction factor (R_T) plot, Figure 7-23, for shafts with L/D ratio = 3 were developed to a maximum eccentric distance of 20 ft (Centrifuge tests; McVay et al. 2003; Hu et al. 2006) the curve was extrapolated. That is, with a standoff distance of 35 ft and the measured lateral load (i.e., 2 kip), the R_T factor was estimated, 13 %

(i.e., $R_T = 2 \text{ kip}/15.7 \text{ kip}$) and plotted in Figure 7-23 for a torque to lateral load ratio of 35. Evident from the Figure, the lateral load reduction (i.e., R_T) follows the centrifuge results; suggesting the lateral capacity decreases almost linearly with R_T .

7.3 Combined Torsion and Lateral Load Testing of Jet-Grouted Piles

As explained earlier, past FDOT research in large test chamber environment (BD545, RPWO # 31; McVay et al. 2009) found that the jet-grouted pile possess very high torsional resistance and suggested that such a pile could be used as the foundation for Mast arm structures supporting highway signs and signals (large combined torque & lateral resistance). To verify this in the typical field condition (i.e., no boundary effect), combined torsion and lateral load tests were performed on the installed jet-grouted piles using the higher capacity mast arm. The tests were performed in two different sequences to identify the influence of prior top-down loading on the torsional resistance of the pile; for Jet-grouted pile-2 (JP2) combined torsion and lateral load test was performed initially, whereas combined torsion and lateral load test on JP1 was conducted after the static top-down test. Details of each test, analysis of results, and the comparison of measured vs. predicted resistances are presented below:

7.3.1 Combined torsion and lateral load test on JP2

A crane with an axial capacity of 75 ton was used to move the mast arm assembly from the top test drilled shaft TS3 to the top of the jet-grouted test pile -2. After setting and orienting the mast arm assembly properly, the bottom flange of the pole was bolted to the anchor rods embedded in the concrete cap, while the crane supported a major portion of the dead load of the structure. The instrumentation for rotation and translation measurement was the same as TS2 and TS3 shafts, except that the strain gauge layout was slightly changed (Figure 7-24) in order to

obtain increased translation accuracy. As mentioned earlier, translation could not be obtained accurately using the strain gauge data with the previous layout.

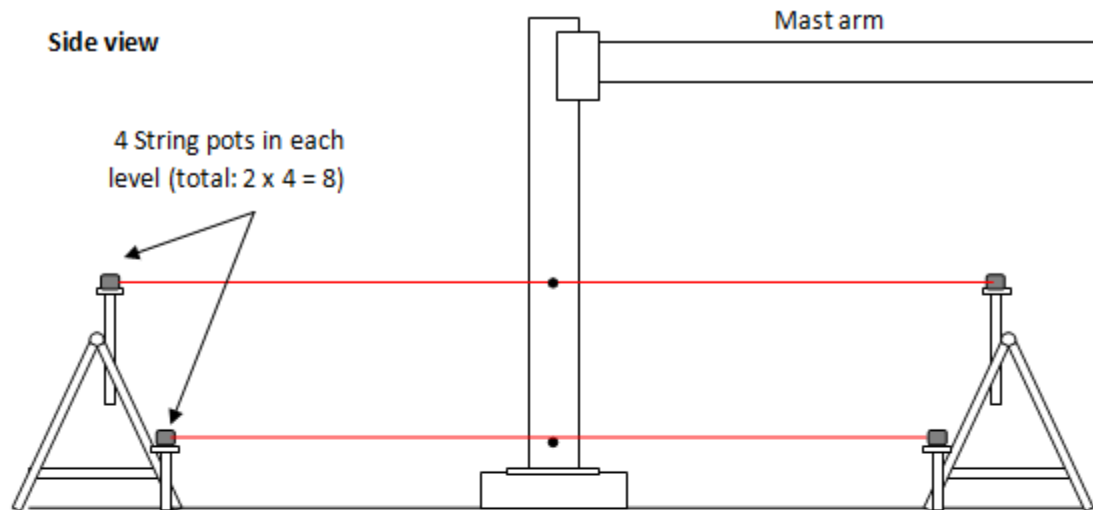


Figure 7-24. String pot layout and support system

The lateral load was applied in increment of 0.5 kip. The crane was located approximately 100-ft away from the arm, Figure 7-25. Each increment was kept for a uniform time interval of 5 minutes as in the previous tests. The loading continued up to 12.17 kip; further

loading was not possible due to the pull capacity of the crane's winch cable (tag line).

Subsequently, the load was removed in seven decrements with a time interval of 5 minutes. The depth of water table during the test was 8.6 ft.

Figure 7-26 shows the torque vs. rotation response measured using different types of instrumentation (total station, string pots and dial gauges). It is evident that the rotations measured using different instrumentations were quite similar. The maximum observed rotation was 1.45° corresponding to a mobilized torsional resistance of 426 kip-ft (Figure 7-26). The small permanent rotation, 0.7° , suggests that half of the maximum rotation was due to elastic behavior and the ultimate torsional resistance of the pile was not developed in the test.



Figure 7-25. Application of lateral load on the arm by pulling with a crane

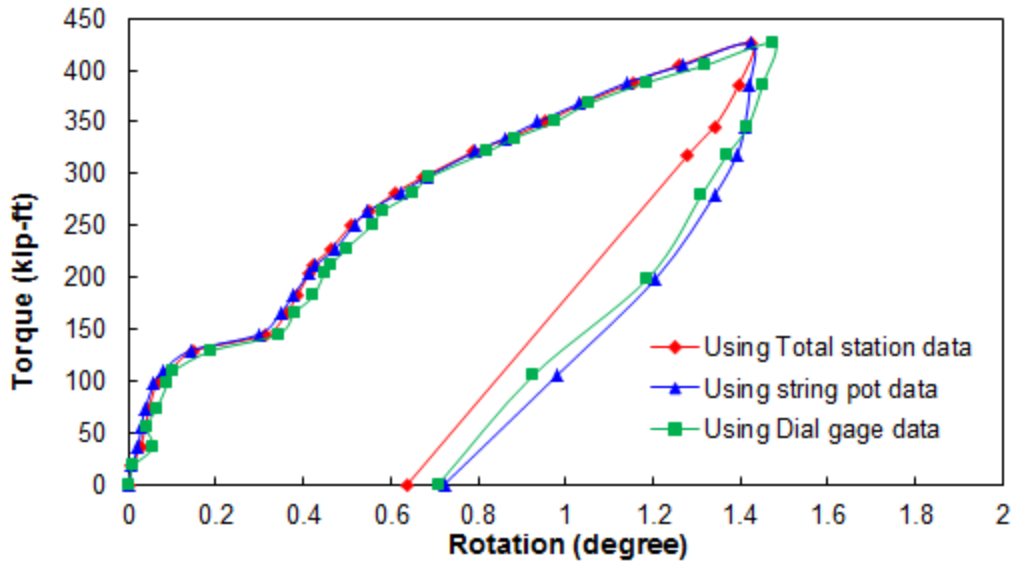


Figure 7-26. Torque vs. displacement response for JP2

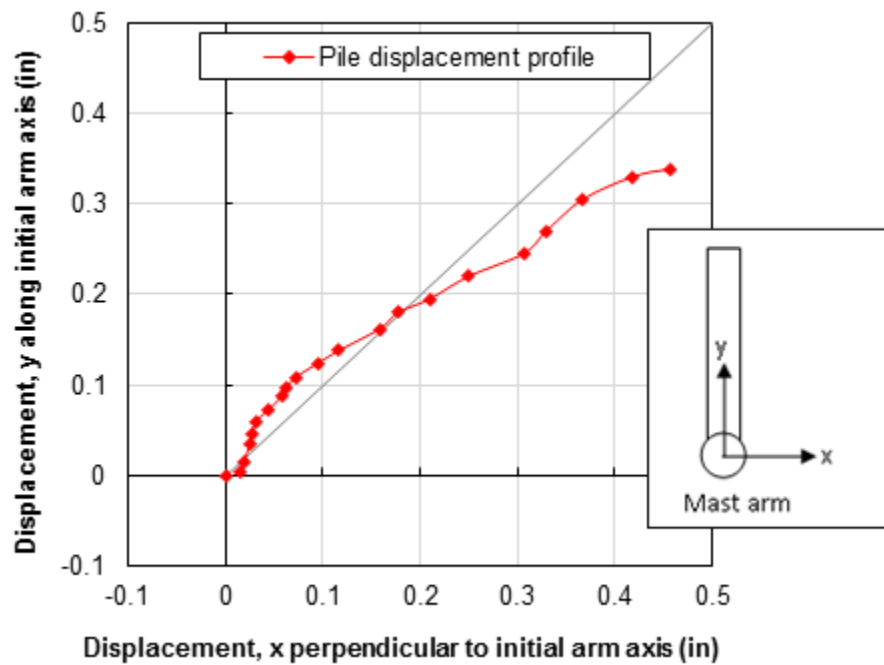


Figure 7-27. Lateral displacement components during the load test

Shown in Figure 7-27 are the components of lateral displacement along the direction of lateral load (X-axis) and axis of arm (Y-axis), 1.5 ft above the ground surface. It can be seen from the figure that the displacement components (x & y) were similar up to 8 kip (0.2") and afterward the component along the pull direction, x, became larger. Figure 7-28 displays the

lateral load vs. resultant lateral displacement response. The maximum lateral displacement observed was only 0.57-in. Note that lateral displacement could not be obtained accurately from the strain gauge data even though a new layout was attempted. It is interesting to note in Figure 7-7-28 that there was significant elastic translation, i.e., rebound during the unloading phase of the test. The latter agrees with the rotation (Figure 7-26), i.e., more than 50% of the rotation and translation was elastic in nature (i.e., recovered during unloading). Figure 7-29 shows the torsional cracks and gaps due to combined rotation and translation after maximum loading and after unloading. Note that the gaps formed during the loading phase were almost recovered during the unloading phase.

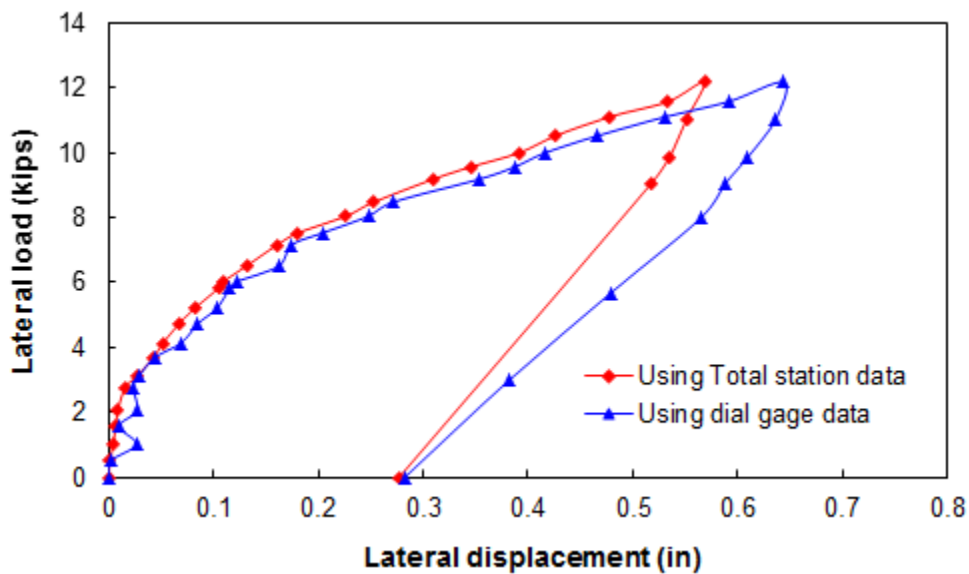


Figure 7-28. Lateral load vs. resultant lateral displacement

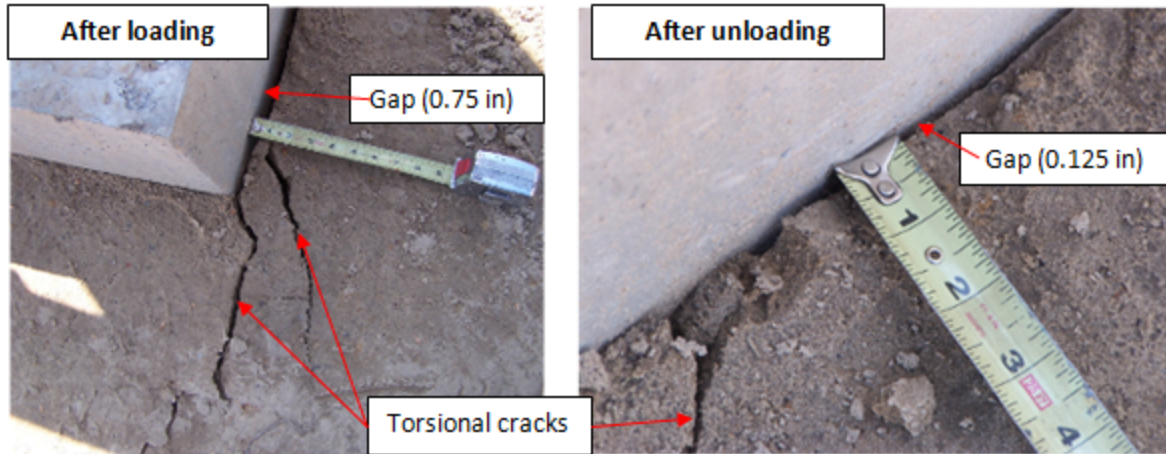


Figure 7-29. Torsional cracks and gaps after loading and unloading

7.3.2 Combined torsion and lateral load test on JP1

Combined torsion and lateral load test was performed on JP1 with a larger crane, Figure 7-30, subsequent to a static top-down load test (Chapter 6). The instrumentation set-up for the test was the same as that for the TS2 and TS3 drilled shafts load test. For the test, the measured depth of water table was 7-ft.



Figure 7-30. Torsion test on JP 1

The lateral load was applied in increment of 0.750 kip and each increment was kept for a time interval of 5 minutes. The loading was stopped at a maximum load of 13.9 kip (~14 kip), which was close to the design force and moment capacity of the Mast arm structure. The load was subsequently removed in eight decrements at 5 minute time intervals.

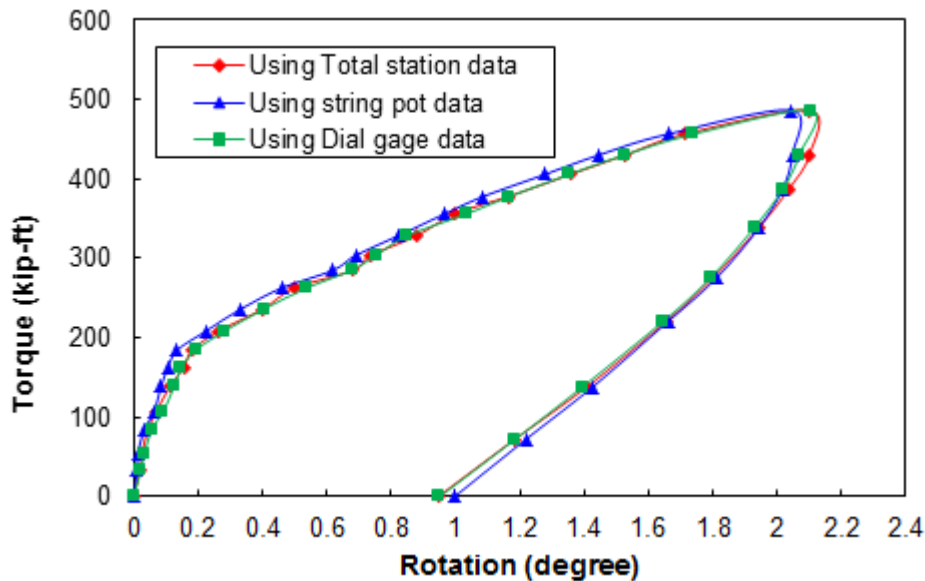


Figure 7-31. Torque vs. rotation response for jet-grouted pile 1

Shown in Figure 7-31 is the measured torque vs. rotation of JP1. As evident from the figure, the rotations measured using the different instrumentations were nearly identical. The rotation of pile (measured at 1.5ft above ground) corresponding to the maximum applied torque (487 kip-ft) was only 2.1°. Again upon unloading, more than 50% of rotation was recovered, i.e., elastic in nature (i.e., small permanent rotation). It is evident from this small permanent rotation that the test did not mobilize the ultimate torsional resistance of the pile. Figure 7-32 shows the measured lateral load vs. lateral displacement response of the pile. The maximum lateral displacement (1.5ft above ground) was only 0.76-in. As in the case of rotation, more than 50% of the lateral displacement was recovered during the unloading stage as well.

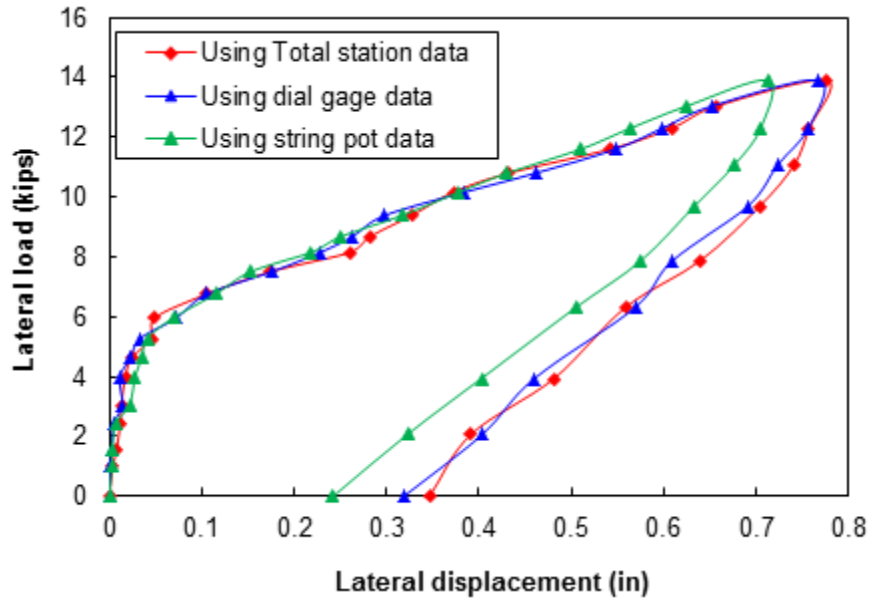


Figure 7-32. Lateral load vs. lateral displacement

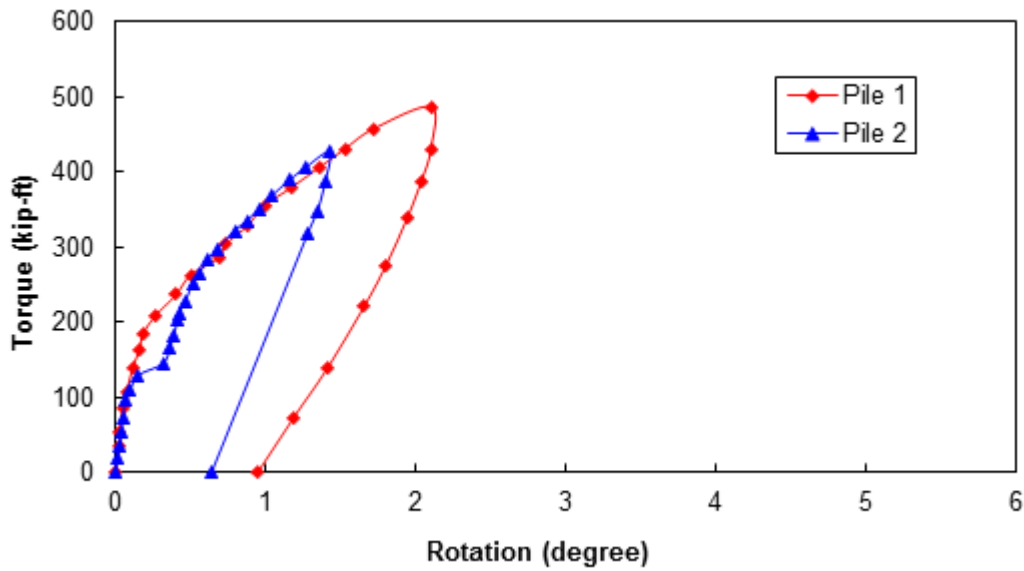


Figure 7-33. Torque vs. rotation responses for piles 1 and 2

Figure 7-33 compares the torque vs. rotation response of jet-grouted piles 1 and 2. Similarly, Figure 7-34 shows the comparison of lateral load vs. displacement response of the two piles. Evident from the figures, the stiffness behavior of the piles are quite similar even though

the loading sequence were different. Specifically, the torsional resistance of the jet-grouted pile 1 seems to be little if any influenced by the prior static top-down load test. This behavior may be influenced by the fact that the skin resistance of the pile was not fully mobilized during the top-down load test.

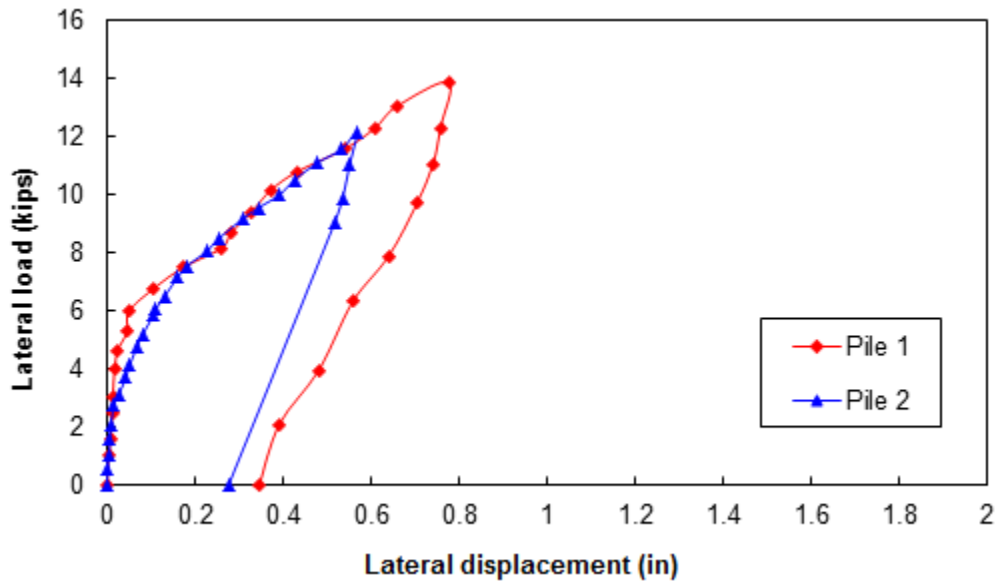


Figure 7-34. Lateral load vs. lateral displacement responses JP1 and JP2

7.3.3 Comparison of measured and predicted torsional resistance of jet-grouted pile

The torsional resistance mobilized during the test was subsequently compared with the predicted values (Table 7-4). The K_g method (McVay et al. 2009; Thiyyakkandi et al. 2012), the Pressuremeter test data, and tip grout pressure data were used for the prediction. A discussion of prediction methods was presented in previous Chapter (Section 6.4). The surface area and radius of the pile was estimated by assuming that purely cylindrical shaped bulbs with volume equal to the volume of grout pumped alongside the pile. Detailed calculations are given in Appendix E. Note that the torsional resistance contribution due to the pile tip is not considered in the prediction. In case of K_g method, the predictions were made using both interface friction angle

(δ) and soil's friction angle (ϕ). It is evident from the Table 7-4 that the measured torsional resistance was in reasonable agreement with the predicted values. Because the torsional resistance was not fully developed during the load tests, it is expected that the ultimate torsional resistance of the pile may be between the Kg method and the Pressuremeter results, i.e., the tip grout pressure approach (~ 680 kip-ft; i.e., shearing resistance was measured during tip grouting).

Table 7-4. Comparison of measured and predicted torsional resistance

Pile	Method	Torsional resistance (kip-ft)
JP1	Measured (kip)	487*
	Kg method (kip)	450 ^a -768 ^b
	Pressuremeter data (kip)	772
	Tip grout data (kip)	684
JP2	Measured* (kip)	426*
	Kg method (kip)	456 ^a -783 ^b
	Pressuremeter data (kip)	598
	Tip grout data (kip)	661-707

*not fully mobilized

^a using interface friction angle (δ) – see Appendix E

^b using soil's friction angle (ϕ)

7.4 Comparison of the Axial Response of Jet-grouted Piles and Drilled Shafts

Figure 7-35 presents a comparison of torque vs. rotation response of jet-grouted piles and drilled shafts. It is clearly evident from the figure that the torsional resistance of the piles are much larger than the ultimate torsional capacity of drilled shafts (>2.5 times) even though both have identical lengths.

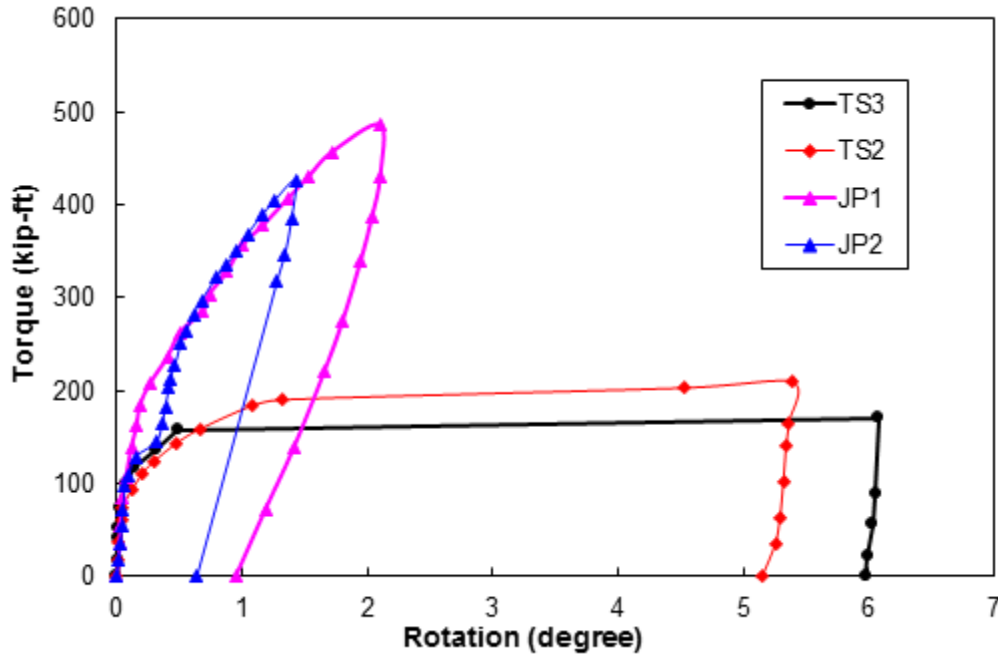


Figure 7-35. Torque-rotation response of jet-grouted piles and drilled shafts

Table 7-5 presents the estimated forces and moments developed on the top of drilled shafts and jet-grouted piles under the maximum applied lateral load in each case. Also presented in the Table 7-5 (column 6) are the expected forces and moments on a foundation supporting an E7-T6 Mast arm assembly under a design wind speed of 130 mph. Note, as specified in FDOT Index No. 17743, a 4-ft diameter x 18-ft long drilled shaft is sufficient to support an E7-T6 Mast arm assembly under a design wind speed of 130 mph in typical Florida soil conditions. However, the present field tests indicate that the ultimate torsional resistance of the drilled shafts (TS3=171 & TS2=210 kip-ft measured vs. 259 kip-ft required) is less than the required un-factored torsional resistance (i.e., without factor of safety). Consequently, a 4-ft diameter x 18-ft long drilled shaft may not be adequate to support an E7-T6 Mast arm assembly during a severe wind loading (e.g., hurricane). However, the torsional resistance of jet-grouted piles (JP2=426 & JP1=487 kip-ft measured) even under very small rotation is significantly greater than the design

torque (259 kip-ft) for an E7-T6 pole/mast arm assembly. It is even greater than the structural capacity of E7-T6 Mast arm assembly (300 kip-ft – wind speed 140 mph, FDOT Mastarm v4.3). The tests suggest that the new jet-grouted pile system is well-suited for all FDOT pole/Mast arm structures beneath highway signals and signs in Florida soils, i.e., silts and sands.

Table 7-5. Comparison of forces and moments on the foundation during the load tests

Forces and Moments	TS2	TS3	JP1	JP2	E7-T6*
Torsion, M_y (kip-ft)	210	171	487	426	258.8
Moment about axis of arm, M_x (kip-ft)	120	97.6	278	243	149
Moment about axis normal to arm, M_z (kip-ft)	118	118	118	118	116.6
Lateral load, V_x (kip)	0	0	0	0	0.3
Lateral load, V_z (kip)	6	4.88	13.9	12.17	7.4
Axial load, V_y (kip)	10.7	10.7	10.7	10.7	5.6

* E7-T6 Mast Arm assembly at design wind speed = 130 mph

CHAPTER 8
LATERAL LOAD TEST ON DRILLED SHAFT AND JET-GROUTED PILE

A novel lateral load testing of a jet-grouted pile and a similar sized drilled shaft (TS2) was performed by loading against one another. Test setup, instrumentation, procedure, and results are presented.

8.1 Test Setup, Instrumentation, and Loading

Static lateral load testing of jet-grouted pile-2 (JP2) and test shaft TS2 was undertaken using a novel three dywidag bars (75 kip capacity each) setup shown in Figure 8-1. The load was applied on one end (jet-grouted pile) using a 300-kip capacity hydraulic jack and the applied load was measured using a 600-kip load cell positioned at the other end (drilled shaft). The three Dywidag bars transferred the load to each end of the assembly. For the loading configuration, Figure 8-1, the lateral displacement of each foundation will be toward one another. Since, the distance between the foundations was 36ft center to center, no overlapping of passive zones was expected.

In-place inclinometers (Figure 8-2) were used to obtain the displacement profile of drilled shaft at each load increment. Note, inclinometers were installed at different elevations within the casing cast within the shaft. The inclinometer readings were collected using a Micro-measurement datalogger. The lateral load was applied in approximately 23 kip increments and each increment was kept for a time interval of 10 minutes. The loading was stopped, when the drilled shaft failed under lateral load (displacement = 3.5 in). Subsequently the load was removed in equal decrements.

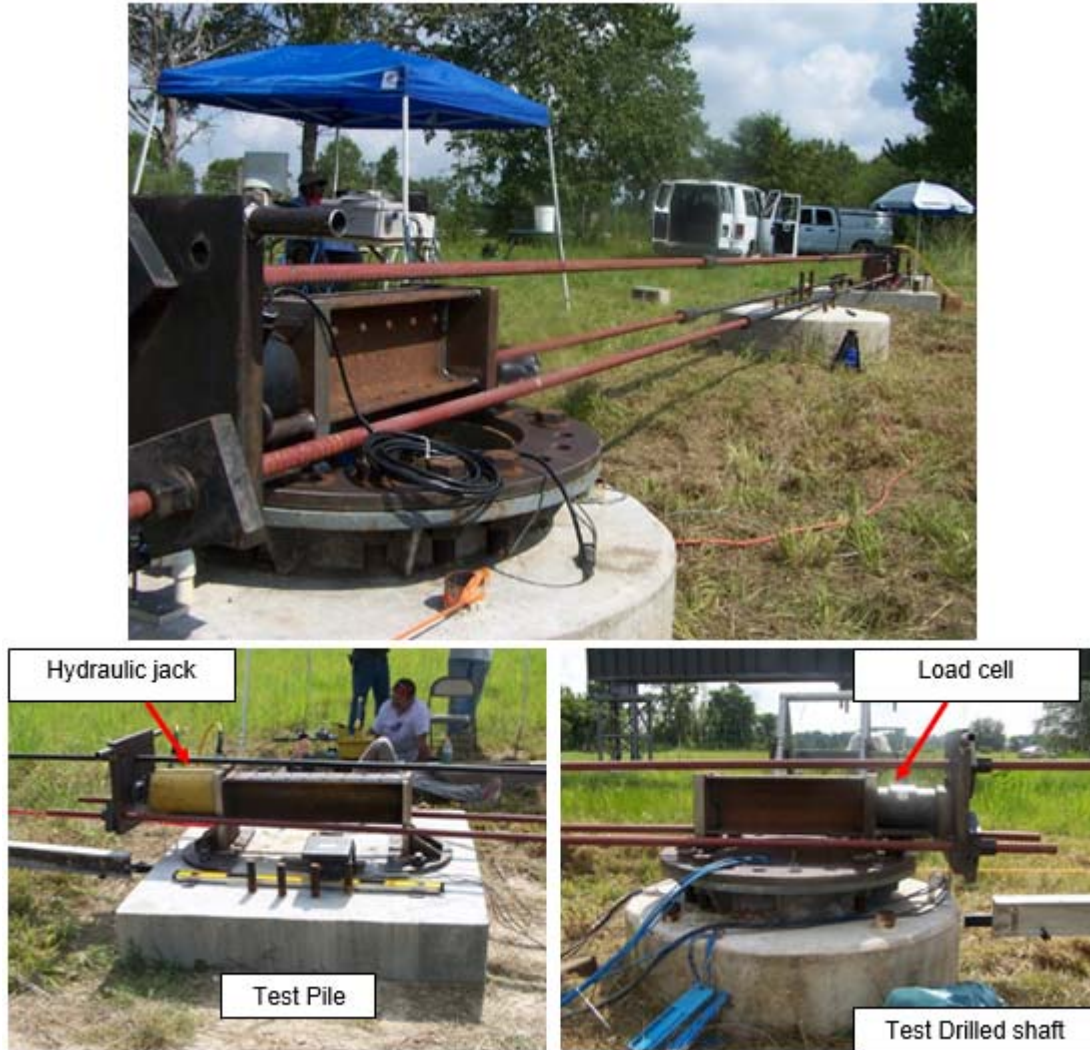


Figure 8-1. Lateral load test setup

8.2 Analysis of Results

Figure 8-3 shows the displacement profiles for drilled shaft at different load increments obtained from the inclinometer data. As evident and expected, the shaft underwent rigid body rotation ($L/D = 4.5$) under the lateral loading.



Figure 8-2. In-place inclinometer installation in the test shaft

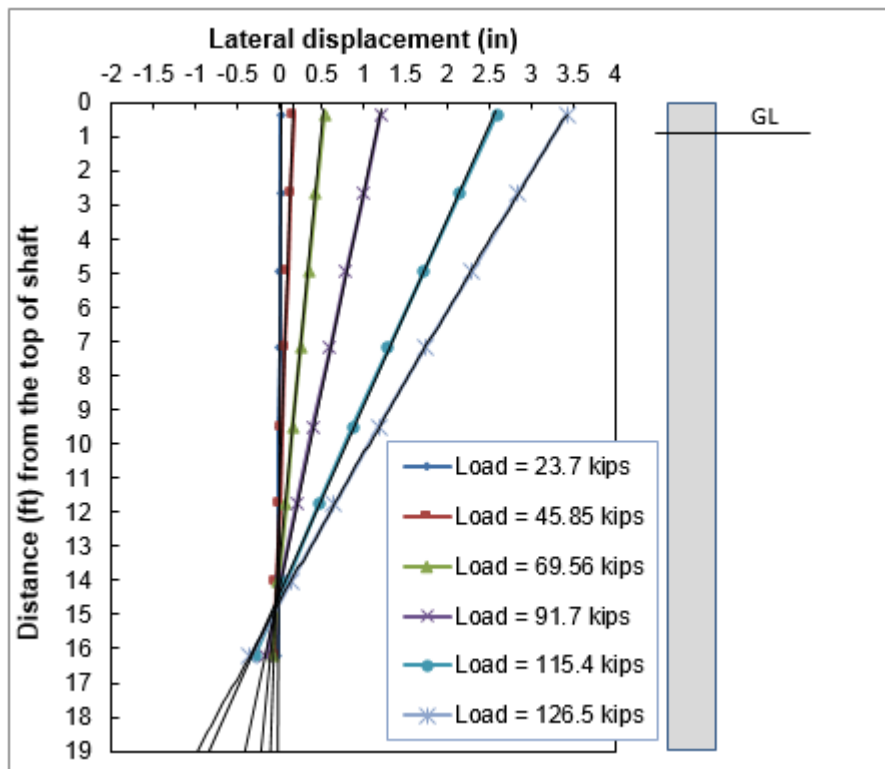


Figure 8-3. Displacement profile for drilled shaft

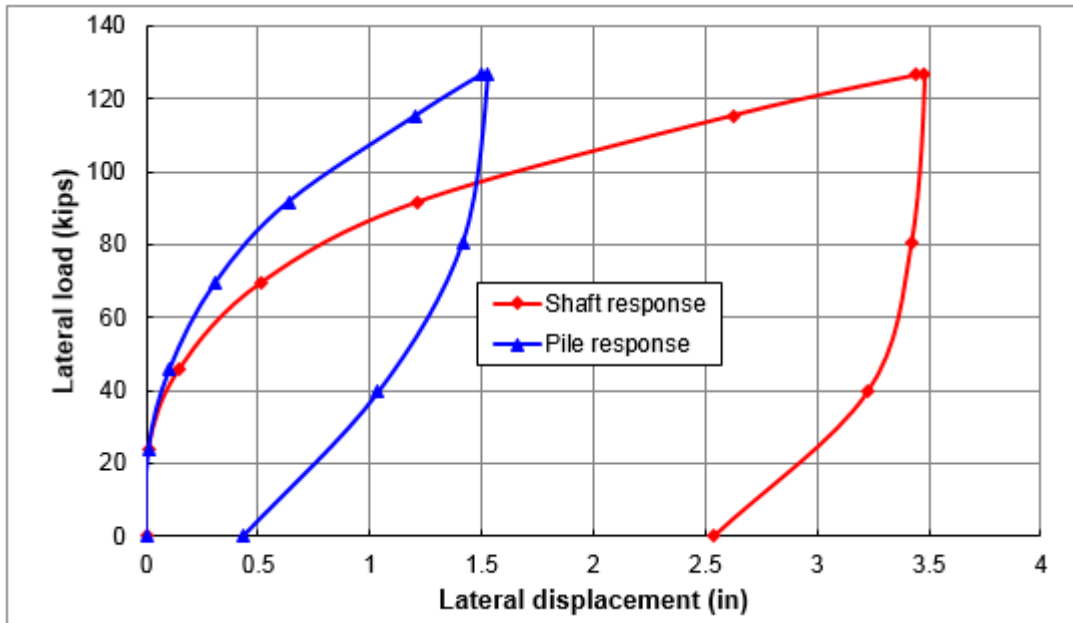


Figure 8-4. Lateral load vs. lateral displacement responses

Shown in Figure 8-4 is the lateral load vs. lateral displacement responses of drilled shaft vs. jet-grouted pile, JP2. The maximum lateral displacement measured for the drilled shaft was 3.5 in, whereas the displacement of jet-grouted pile was only 1.5 in. It was thought that the drilled shaft and jet-grouted pile would undergo similar displacement since the diameter of drilled shaft (48-in) and jet-grouted pile (46-in after grouting based on volume of grout pumped) were nearly the same. However, the increased lateral stiffness may be due to an increased stiffness of the soil around JP2 due to grouting, as well as the increased rotational stiffness provided by the cap. It is also interesting that the lateral unloading stiffness of the shaft and JP2 are quite similar; suggesting excellent bond between the grout and the pile, similar to the shaft concrete.

CHAPTER 9 COST COMPARISON OF JET-GROUTED PILES VS. DRILLED SHAFTS

A cost comparison of the construction of jet-grouted piles vs. drilled shafts was performed to assist with the implementation of the new pile. Both direct (labor and materials), and indirect costs (rental, size of equipment, mobilization, demobilization, and cleanup) were considered for the comparison.

9.1 Jet-grouted Pile Construction Costs

The construction cost for jet-grouted pile was estimated using the actual cost of construction for the two jet-grouted piles (28 in square x 18 ft deep and 48-in diameter side grout zones) installed for this research. The cost of single pile was then taken as the half of the total cost. It should be noted that the individual construction cost still could be significantly reduced with increasing the number of piles as the mobilization cost is distributed among the piles and the purchase of materials in bulk quantity could result in significant savings.

Table 9.1 presents the material cost for all items purchased for the construction of the two jet-grouted piles. Tables 9.2 through 9.4 summarize the labor cost, pile jetting service cost, and pile grouting service costs, respectively. Adding all the identified costs, a total cost for the construction of the two 28 in square x 18 ft deep jet-grouted piles is \$19,881; therefore the construction cost of a single 28 in square x 18 ft deep jet-grouted pile is \$9940.5.

The jet-grouted pile had an axial capacity (settlement equal to 5% diameter) greater than 1000 kip and a torsional capacity of 750 kip-ft. But the axial and torsional capacity of a similar sized drilled shaft (48 -in x 18 ft) was approximately 400 kip (settlement equal to 5% diameter) and 210 kip-ft, respectively. Since the jet-grouted pile has significantly greater resistance compared to a similar sized drilled shaft, the cost of jet-grouted pile needs to be compared with an equivalent capacity drilled shaft (i.e., axial and torsional resistance).

Table 9.1. Material cost for the construction of two jet-grouted piles

I	Materials Cost			
	Item	Rate	Quantity	Amount*
a	<i>Reinforcing steel</i>			
	Longitudinal reinforcing steel (#9 rebars, 20-ft long)	\$32.56	32	\$1,165.57
	Shear/torsional reinforcing steel (#5 rebars)	\$6.93	190	\$1,316.70
	Rebar wire ties (12-in long, 500 /bundle)	\$17.82	4 bundles	\$79.15
b	<i>Jetting system</i>			
	Jet pipes (3-in diameter × 20-ft long PVC pipe)	\$25.02	3	\$75.06
	PVC Bushings, caps, elbows, adaptors			\$41.95
	Double PVC wyes (3-in diameter; schedule 40)	\$25.76	4	\$103.04
	Black steel threaded nipples (3-in diameter × 12-in long)	\$29.40	2	\$58.80
	Steel for nozzle			\$54.03
	Rubber sheet for nozzles (0.1875-in thick × 48-in wide)			\$147.94
	Anchors for nozzle (20 /pack)	\$9.86	2 packs	\$19.76
c	<i>Grout delivery systems</i>			
	Gum rubber tubes (0.25 in thick, 1.25-in ID)	\$8.97	30 ft	\$276.60
	Grout delivery pipes (1-in,schedule 40, 20 ft long)	\$7.44	7	\$52.08
	Black steel threaded nipples (1-in diameter × 2-ft long)	\$12.53	8	\$100.24
c	<i>Concrete</i> (4 cub. yard/pile)	\$100.25	8 cub. yards	\$802.00
d	<i>Grout membrane and attachment</i>			
	Steel Plates for holding membranes			\$258.61
	Studs for attaching membranes to pile			\$421.12
	Nuts for attaching membranes to pile			\$133.07
	Grout membranes			\$610.22
	Silicon gasket maker for sealing the attachment	\$15.66	6	\$99.46
e	<i>Side and tip Grouting (1480 gallon)</i>			
	Cement	\$10.42	148 bags	\$1,542.16
	Fly-ash (Micron3; 1700 lbs)			\$615.43
	Total Material cost			\$7,972.99

Table 9.2. Labor cost for the construction of two jet-grouted piles

II	Labor cost			
	Item	Rate	Quantity	Amount*
a	Reinforcing cage fabrication	\$17/hr	20 hrs	\$340.00
b	Jetting system fabrication and installation	\$17/hr	8 hrs	\$136.00
c	Grout delivery system fabrication and installation	\$17/hr	16 hrs	\$272.00
d	Fabrication & installation of grout bag retention system	\$20/hr	12hrs	\$240.00
e	Concrete Placement	\$17/hr	8 hrs	\$136.00
f	Preparation and attachment of grout membranes	\$17/hr	28 hrs	\$476.00
g	Fabrication and installation of nozzles	\$17/hr	6 hrs	\$102.00
	Total labor cost			\$1,702.00

Table 9.3. Pile jetting service cost for two jet-grouted piles

III	Pile Jetting cost (Based on quote)			
a	<i>Equipment rental</i>			
	Crane	\$1200/day	1 day	\$1,200.00
	Backhoe			\$750.00
	High pressure water pump	\$750/LS		\$750.00
	Hydraulic pump	\$150/LS		\$150.00
	Provide 8000 gallon water tanker	\$850/LS		\$850.00
b	Labor	\$1500/day	1 day	\$1,500.00
	Total Jetting cost			\$5,200.00

Table 9.4. Grouting service cost for two jet-grouted piles

IV	Grouting service cost (Based on quote)			
	Equipment rental (Grout pipe, hoses, generator, etc.)	\$2700/week	3 days	\$1,157.00
	Personnel (labor cost)	\$1283/day	3 days	\$3,849.00
	Total Grouting cost			\$5,006.00

9.2 Drilled Shaft Construction Costs

According to FDOT's Bridge Development Report (BDR) Cost Estimating (Effective 7/01/2013), the cost for a 4 ft diameter x 18 ft deep drilled shaft is \$7,740. A quote for the construction of two similar sized drilled shafts (4 ft diameter x 18 ft deep) at the same test site (Keystone Heights) was obtained from Reliable Constructors Inc., Table 9-5. As shown from the table, the contract amount for one drilled shaft is \$8,700, which is about 12% more than the BDR estimation. It can be seen that the cost of construction (based on quote) for drilled shaft was only 12 % less than the cost of a similar sized jet-grouted pile (\$9940). However, the 4 ft diameter x 18 ft deep drilled shafts were not equivalent to the jet-grouted piles in terms of axial and torsional resistance. It was found that 4 ft diameter x 30 ft deep and 5 ft diameter x 25 ft deep drilled shafts are equivalent to jet-grouted pile in terms of torsional capacity (750 kip-ft; no tip contribution considered). Similarly, for axial capacity, a 4 ft diameter x 45 ft deep and 5 ft diameter x 35 ft deep drilled shafts are equivalent to the 28-in square (48-in side grout zone) x 18-ft deep jet-grouted pile. Table 9-6 shows the estimated construction cost for the identified drilled shafts according to FDOT's BDR cost estimate. As evident from Table 9-6, the torsion equivalent drilled shaft was 28%, and the axial equivalent drilled shaft was 80% more than the jet-grouted piles. This cost comparison suggests that the jet-grouted pile is an economically viable foundation system for the future. In addition the foundation provides its own proof test (i.e., tip grouting), to assess skin and tip resistance, allowing for higher LRFD Φ values.

Table 9-5. Construction cost for two 4-ft diameter x 18-ft-deep drilled shaft

Shaft size	Quantity	Unit price	Total	Dirt Haul
48-in Ø x 18 ft	2	\$8,500.00	\$17,000	\$400.00
Total contract amount: \$17400				
Contract amount per shaft: \$8,700				

Table 9-6. BDR cost estimate for equivalent drilled shaft

	Shaft size	Cost	% cost > jet-grouted pile cost
Torsional equivalent	4 ft diameter x 30 ft deep	\$12,900	29.8%
	5 ft diameter x 25 ft deep	\$12,750	28.3%
Axial equivalent	4 ft diameter x 45 ft deep	\$19,350	94.7%
	5 ft diameter x 35 ft deep	\$17,850	79.6%

CHAPTER 10 SUMMARY AND CONCLUSIONS

A significant number of FDOT structures (bridges, signage, lighting, noise wall, etc.) are supported on deep foundations. Current deep foundations (driven pile, CFA piles, and drilled shafts) suffer a number of drawbacks for urban use. For instance, pile driving generally creates significant noise and vibration issues; drilled shafts and CFA piles suffer quality control issues and lower skin resistance due to the installation process. Recently, FDOT developed a new foundation system, “jet-grouted pile”, which overcomes the limitations of both driven piles and drilled shafts. The structural component of the new pile is basically a precast pile (with grout delivery and jetting systems), which is first jetted into ground and then side grouted to improve skin resistance and finally tip grouted to improve tip resistance. Previous FDOT research in the large test chamber environment showed that the new pile possess significantly higher axial and torsional resistance; making the new pile as an excellent replacement foundation for mast arm structures supporting signs, signals, lightings, etc., in Florida. Even though the pile’s capacity was verified in a large test chamber environment, the constructability and the resistance of the pile had to be validated and compared with similar sized drilled shafts in typical field condition. Similarly, the FDOT recently revised the design method for foundation of Mast arms structures. Of interest was the field capacity of a drilled shaft using this new design.

Consequently, the primary focus of this research was to validate through field testing, axial and torsional capacity of jet-grouted piles, as well as standard drilled shaft foundations. Since construction/installation was also an issue, the jet-grouted piles were to be installed with a general contractor. Finally, for implementation of the new pile, a cost comparison was made between jet-grouted piles and equivalent capacity drilled shafts. The research was successfully completed in 11 tasks as indicated in Chapter 1.

The test site used for the study was FDOT's borrow pit at Keystone heights, Florida. Three test drilled shafts (two 4-ft \O x 18 ft deep and one 4 ft \O x 12 ft deep) and four reaction drilled shafts (4 ft \O x 40 ft deep) were installed for the load test program. All the shafts were constructed with the wet-hole approach employing mineral slurry.

The constructability of the jet-grouted piles in typical Florida field conditions was verified by performing full-scale field installation of two piles. The piles considered for the study were 28-in square x 19.5 ft precast pile (embedment depth = 18 ft) with two 48-in \O side grout zones. The grout distribution and jetting systems were fabricated in conformity with previous FDOT research. After the hydration of concrete, the side grout membranes and nozzles were attached to the pile. The piles were subsequently installed at the test site by pressurized water jetting (Figure 10-1) by a contractor. Water was recirculated during the jetting process to minimize the water loss. Water for jetting was provided from a water tanker through a high pressure pump to the test pile with a flow rate of 400 gallon/minute and a pressure of 130-135 psi. The test pile was positioned using a crane and allowed to penetrate with its self-weight by steadily releasing the weight from the crane. A hydraulic trash pump (maximum flow rate = 1300 gpm and pressure = 65 psi) was used to pump the water collected in the surface casing back to the tanker for recirculation. Total water loss (percolation) during the jetting of two piles was approximately 1000 gallons. It was found that water should be continuously provided with a uniform flow rate and pressure until the required penetration is reached. Also, the total quantity of water required for jetting was significantly reduced by recirculation.



Figure 10-1. Pile jetting

After jetting, reinforced concrete caps were installed on top of the piles for combined torsion and lateral load testing. Next, side grouting of top and bottom membranes were completed. After hydration of the side grout zones, the piles were tip grouted. Analysis of the noise and ground surface vibration measurements during the jetting and grouting operations suggested that the pile is well-suited for urban environment where the noise and vibrations during the construction operations are of critical concern.

Static top-down tests were subsequently conducted on the two jet-grouted piles to verify their axial capacity vs. the design estimates. A similar sized drilled shaft was also tested for comparison. FDOT's beam girders, 2000 kip hydraulic jack and load cell were used for the top-down axial tests. In order to study the influence of prior loading, one of the piles underwent top-down loading only after the combined torsion and lateral load test. For both jet-grouted piles,

ultimate axial capacity could not be mobilized in the top-down tests because of uplift failure of the reaction drilled shafts. Consequently, a Statnamic load test was performed on one of the jet-grouted piles (JP1) to estimate ultimate capacity. The top-down load test program revealed that the axial capacity of jet-grouted pile was approximately 3 times greater than a similar sized drilled shaft (Figure 10-2). Comparison of the total load – displacement response of the jet-grouted piles 1 and 2 showed that the stiffness response (loading and unloading) of the piles were nearly the same irrespective of the loading sequence, (Figure10-3). Specifically, the axial response of JP2 was not influenced by the prior torsion test.

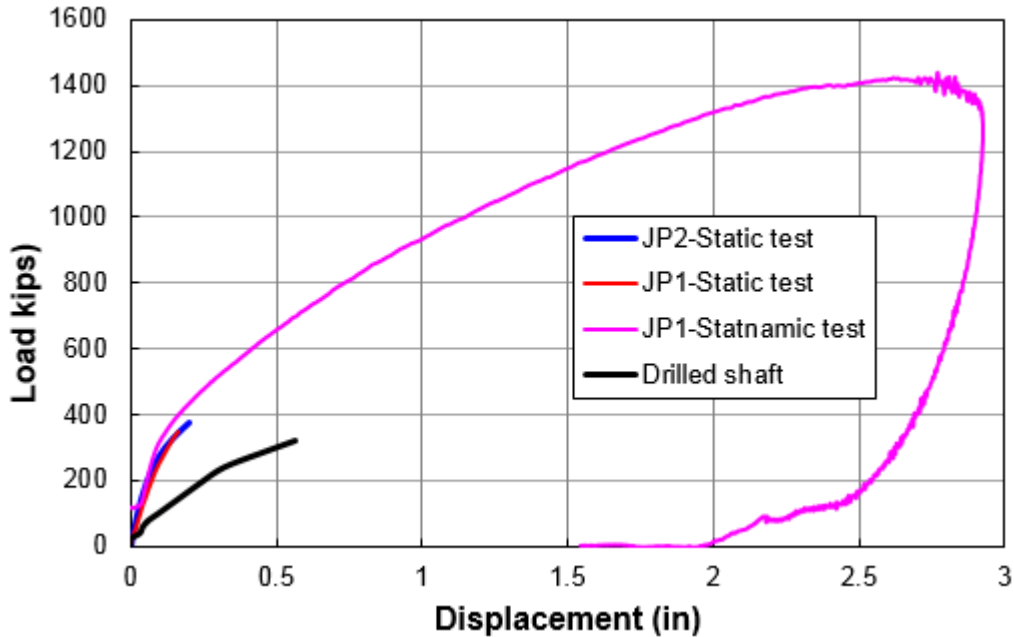


Figure 10-2. Total load-displacement response of jet-grouted piles and drilled shaft

A comparison of the measured skin resistance of the piles with the predicted skin resistance using the different approaches revealed that the predicted values were generally conservative and in reasonable agreement with the measured values. In case of drilled shaft, the measured skin resistance was very close to the prediction based on FHWA’s Rational method. SPT based O’Neill and Hassan (1994) method under-predicted the resistance by 22%. However

all the CPT based methods (Aoki and Velloso's method, LCPC method, and Alsamman 1995) under or over-predicted the skin resistance by about 50%.

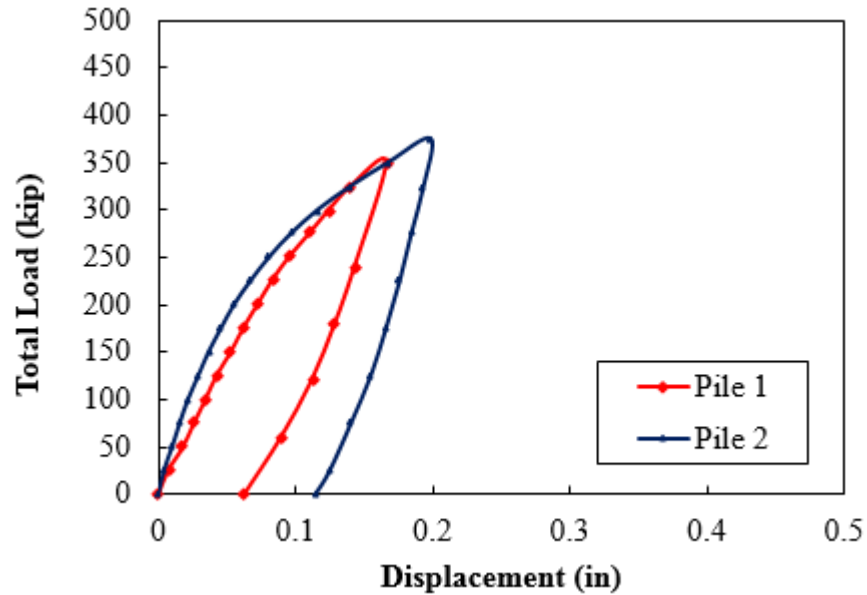


Figure 10-3. Comparison of load-displacement response of JP1 and JP2

Combined torsion and lateral load testing of three drilled shafts (two 4 ft Ø x18 ft deep and one 4 ft Ø x 12 ft deep, two jet-grouted piles) were also conducted. A heavy duty full-scale mast arm assembly was used for the combined loading. The test was performed by applying lateral load on the mast arm at an eccentric distance of 35 ft from the pole using a crane. For all the shafts, the test was continued until the failure. The shorter shaft (12-ft deep) had a combined torsion – lateral mode of failure, whilst the 18 ft deep shafts were failed by torsion. A comparison of measured torsional resistance of test shafts with the predicted values using different methods was undertaken. O'Neill and Hassan's (1994) beta (β) method predicted the torsional resistance quite well; the difference was only $\pm 10-14\%$. FDOT's re-revised prediction method over-predicted the torsional capacity by 25-45%, if skin contribution is only considered. But there was 20-70 % over-prediction in the case of FHWA's rational method.

Testing of both jet-grouted piles had to be stopped before mobilizing the ultimate torsional resistance due to the pull capacity of the crane’s winch cable and/or the design capacity of mast arm structure. It was also found that the stiffness response of the jet-grouted piles were very similar even though JP1 had been subject to a prior static top-down load test (Figure 10-4). There was a reasonable agreement between the measured torsional resistance and the prediction based on the different design approaches (Kg, tip grout pressure measurements, and Pressuremeter). Comparison of torque vs. rotation response of jet-grouted piles and drilled shafts showed that torsional resistance of the piles were more than 2.5 times of the ultimate torsional capacity of drilled shafts (Figure10-4).

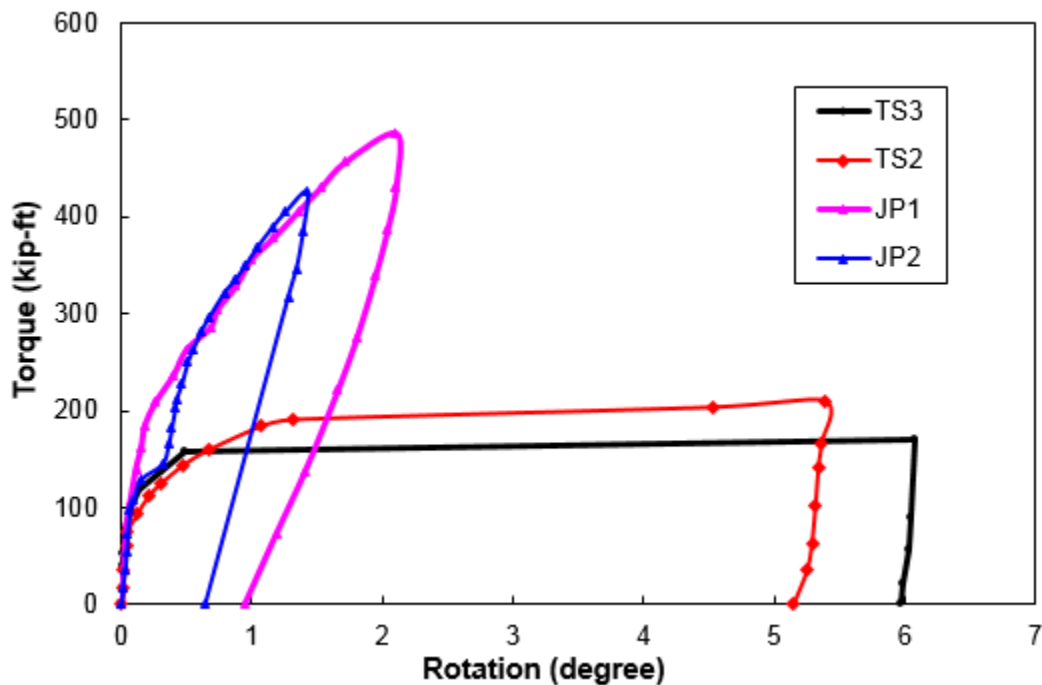


Figure 10-4. Torque-rotation response of jet-grouted piles and drilled shafts

According to FDOT Index No. 17743, a 4-ft diameter x 18-ft long drilled shaft is adequate for an E7-T6 mast arm assembly under a design wind speed of 130 mph. However, it was identified from the present study that the ultimate torsional resistance of the drilled shafts

was less than the required un-factored torsional resistance (Table 10-1). Therefore, a 4-ft diameter x 18-ft long drilled shaft might not be sufficient to support an E7-T6 Mast arm assembly during an extreme event (hurricane). However, jet-grouted piles show significantly higher torsional resistance even under very small rotation, even greater than the structural capacity of E7-T6 mast arm assembly.

Table 10-1. Comparison of forces and moments on the foundation during the load tests

Forces and Moments	TS21	TS3	JP1	JP2	E7-T6*
Torsion, M_y (kip-ft)	210	171	487	426	258.8
Moment about axis of arm, M_x (kip-ft)	120	97.6	278	243	149
Moment about axis normal to arm, M_z (kip-ft)	118	118	118	118	116.6
Lateral load, V_x (kip)	0	0	0	0	0.3
Lateral load, V_z (kip)	6	4.88	13.9	12.17	7.4
Axial load, V_y (kip)	10.7	10.7	10.7	10.7	5.6

* E7-T6 mast arm assembly at design wind speed = 130 mph

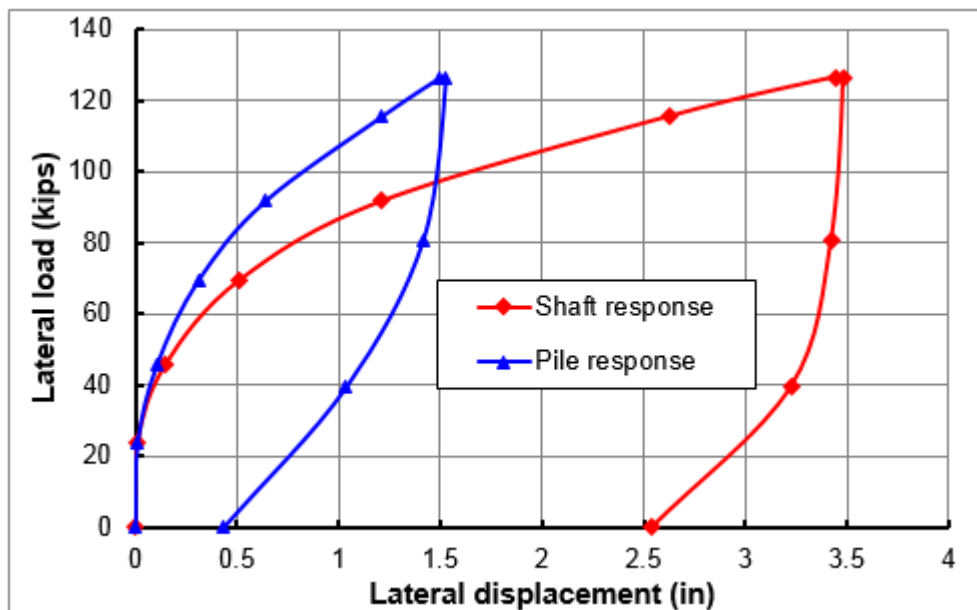


Figure 10-5. Lateral load vs. lateral displacement of jet-grouted pile vs. drilled shaft

In the case of simple lateral load testing, a novel dywidag bar setup was constructed to test one of the jet-grouted piles against a similar sized drilled shaft. The lateral resistance of jet-grouted pile was found to be greater than that of similar sized drilled shaft as shown in Figure 10-5. The larger lateral stiffness of the pile was believed to be the result of increased soil stiffness around pile after grouting, as well as the increased rotational stiffness of the cap.

Finally, the cost of construction and installation of a jet-grouted pile was compared with equivalent capacity drilled shaft. It was found that the cost of the jet-grouted pile is 22% less than that of a drilled shaft comparing equivalent torsional resistance; in the case of axial resistance, the jet-grouted pile is 44% cheaper than a similar capacity drilled shaft. Consequently, the research validates as well as suggests that jet-grouted pile are a viable foundation alternative for FDOT pole/mast arm structures supporting highway signals and signs in Florida silts or sands.

REFERENCES

- AASHTO (1982). *Standard recommended practice for evaluation of transportation related earth-borne vibrations (AASHTO R8-81)*. AASHTO, Washington, D. C.
- AASHTO (2010). *LRFD bridge design specifications*. 5th Edition, AASHTO, Washington, D. C.
- ACI Standard ACI 318-08. (2008). *Building code requirements for structural concrete*. American Concrete Institute, Farmington Hills, Michigan.
- Alsamman, O. M. (1995). *The use of CPT for calculating axial capacity of drilled shafts*. PhD thesis, UIUC, IL, 299 pages.
- Aoki, N., & Velloso, D. A. (1975). An approximate method to Estimate Bearing Capacity of Piles. *Proceedings of 5th Pan-American Conference of Soil Mechanics and Foundation Engineering*, Bueno Aires, Vol.1, 367-376.
- ASTM D 1143/D 1143M (2007). *Standard test methods for deep foundations under static axial compression load*. ASTM International, West Conshohocken, Pennsylvania.
- Bolognesi, A. J. L., & Moretto, O. (1973). Stage grouting preloading of large piles on sand. *Proceedings of 8th ICSME*, Moscow, 20.
- Bowles, J.W., (1996), *Foundation Analysis and Design*. 5th Edition, McGraw-Hill, New York.
- Briaud, J. L. & Tucker, L. M. (1988). Measured and predicted axial response of 98 piles. *Journal of Geotechnical Engineering*, 114(8), 984-1001.
- Briaud, J. L., Moore, B. H., & Mitchell, G. B. (1989). Analysis of pile load tests at lock and dam 26. *Proceedings of the Congress, Foundation Engineering: Current Principles and Practices, ASCE*, 1, 925-942.
- Brown, D.A., Turner, J.P., & Castelli, R.J. (2010). *Drilled shafts: Construction Procedures and LRFD design methods (FHWA NHI-10-016)*. FHWA, Washington, D. C.
- Bruce, D.A. (1986). Enhancing the performance of large diameter piles by grouting, Parts 1 and 2. *Ground Engineering*, 19(4), 9-15 and 19(5), 1121-1126.
- Bruce, D.A. (2005). Glossary of grouting terminology. *Journal of Geotechnical and Geoenvironmental Engineering*, 131(12), 1534-1542.
- Bustamante, M., & Gianceselli, L. (1982). Pile bearing capacity prediction by means of static penetration CPT. *Proceedings of 2nd European Symposium on Penetration Testing*, Amsterdam, Vol.2, 493-500.
- Bustamante, M., & Frank, R. (1997). Design of axially loaded piles-French practice. *In: Design of Axially Loaded Piles-European Practice, Proceedings of the ERTC3 Seminar*, Brussels, Belgium, Balkema, Rotterdam, The Netherlands, 161-175.

- Carter, J. P., Booker, J. R., & Yeung, S. K. (1986). Cavity expansion in cohesive frictional soils. *Geotechnique*, 36(3), 349-358.
- Cook, R. A., & Jenner, K. L. (2010). *Alternative support systems for cantilever signal/sign structures (BDK75 977-04)*. Final report submitted Florida Department of Transportation, Tallahassee, FL.
- Dai, G., Gong, W., Zhao, X., & Zhou, X. (2010). Static testing of pile-base post-grouting piles of the Suramadu bridge. *Geotechnical Testing Journal*, 34(1), Paper ID GTJ102926.
- Dapp, S., & Brown, D. (2010). Evaluation of base grouted drilled shafts at the Audubon bridge. *Proceedings of GeoFlorida 2010: advances in analysis, modeling & design*, ASCE, 1553-1562.
- Dapp, S. D., Muchard, M., & Brown, D. A. (2006). Experience with base grouted drilled shafts in the southeastern United State. *Proceedings of 10th international conference on piling and deep foundations*, Deep foundations institute, Amsterdam, article #1385, publication #77 (IC-2006).
- Duan, X., & Kulhawy, F. H. (2009). Tip post-grouting of slurry-drilled shafts in soil: Chinese experiences. *Proceedings of International Foundation Congress and Equipment Expo*, Contemporary Topics in Deep Foundations (GSP 185), Orlando, FL, ASCE; 47-54.
- FDOT (2002a). *Section 455- Structures Foundations*. Florida Department of Transportation Standard, FDOT, Tallahassee, FL.
- FDOT (2002b). *Structures design guidelines for load and resistance factor design*. Florida Department of Transportation Standard, FDOT, Tallahassee, FL.
- FDOT (2011). *Structures Manual, 9*. Florida Department of Transportation Standard, FDOT, Tallahassee, FL.
- FHWA (2006). *Roadway Construction Noise Model User's Guide (FHWA-HEP-05-054)*. FHWA, Washington, D. C.
- Gabr, M. A., Borden, R. H., Denton, R. L., & Smith, A. W. (2004). *Characterization of jetting-induced disturbance zone and associated ecological impacts (Report No. FHWA/NC/2006-09)*. North Carolina State University in Corporation with North Carolina Department of Transportation and Institute for Transportation Research and Education, NC.
- Gouvenot, D., & Gabiax, F. D. (1975). A new foundation technique using piles sealed by concrete under high pressure. *Proceedings, Seventh Annual Offshore Technical Conference*. Houston, Texas, Vol. 2, Paper No. OTC 2310, 641-656.
- Gunaratne, M., Hameed, R. A., Kuo, C., & Reddy, D. V. (1999). *Investigation of the effect of pile jetting and performing (Research Report No. 772)*. Florida Department of

Transportation, in Corporation with US Department of Transportation and Federal Highway Administration, Tallahassee, FL.

- Hatanaka, M., & Uchida, A. (1996). Empirical correlation between penetration resistance and effective friction of sandy soil. *Soils and Foundations*, 36(4), 1-9.
- Hu, Z., McVay, M., Bloomquist, D., Herrera, R., & Lai, P. (2006). Influence of torque on lateral capacity of drilled shafts in sands. *Journal of Geotechnical and Geoenvironmental engineering*, 132(4), 454-464.
- Jamiolkowski, M., LoPresti, D.C.F., & Manassero, M. (2001). Evaluation of relative density and shear strength of sands from Cone penetration test and Flat dilatometer test. *Soil Behavior and Soft Ground Construction (GSP 119), Proceedings of the Symposium*, Reston, VA, ASCE, 201-238.
- Joer, H. A., Randolph, M. F., & Gunasena, U. (1998). Experimental modeling of the shaft capacity of grouted driven piles. *Geotechnical Testing Journal, ASTM*, 21(3), 159-168.
- Kulhawy, F.H., & Mayne, P.H. (1990). *Manual on estimating soil properties for foundation design (Report EL-6800)*. Electric Power Research institute, EPRI, August 1990.
- Kulhawy, F. H., & Chen, J. R. (2007). Discussion of 'drilled shaft side resistance in gravelly soils' by Kyle M. Rollins, Robert J. Clayton, Rodney C. Mikesell, and Bradford C. Blaise. *Journal of Geotechnical and Geoenvironmental Engineering*, 133(10), 1325-1328.
- Lai, P., McVay, M., Bloomquist, D., & Forbes, M. (2010). An innovative prefabricated pile installation method utilizing jetting and pressure grouting. *Proceedings of the GeoFlorida 2010: Advances in Analysis, Modeling & Design (GSP 199)* © 2010, ASCE. 1592-1601.
- Lee, J. H., & Salgado, R. (1999). Determination of pile base resistance in sands. *Journal of Geotechnical and Geoenvironmental Engineering*, 125(8), 673-683.
- Marchetti, S., & Craps, D. (1981). *Flat dilatometer manual*. Internal report of G.P.E. Inc., Gainesville, FL.
- Marchetti, S. (1997). *The flat dilatometer: design applications. Proc. Third International Geotechnical Engineering Conference*, Keynote lecture, Cairo University, Jan., 421-448.
- Matlock, H., & Reese, L.C. (1960). Generalized solutions for laterally loaded piles. *Journal of Soil Mechanics and Foundation Division*, ASCE, 86, 63-91.
- Mayne, P.W., & Kulhawy, F.H. (1982). K_0 -OCR relationships in soil. *Journal of Geotechnical Engineering*, Vol. 108 (GT6), 851-872.
- Mayne, P.W. (2007). *NCHRP Synthesis 368: Cone Penetration Testing*. Transportation Research Board, National Research Council, Washington, D.C., 117 pages.

- McVay, M. C., O'Brien, M., Townsend, F. C., Bloomquist, D. G., & Caliendo, J. A. (1989). Numerical analysis of vertically loaded pile groups. *Proceedings of Foundation Engineering Congress*, ASCE, Northwestern University, Illinois, 675-690.
- McVay, M.C., Herrera, R., & Hu, Z. (2003). *Determine Optimum Depths of Drilled shafts subject to combined torsion and lateral loads using centrifuge testing (BC-354, RPWO #9)*. Final report to Florida Department of Transportation, Tallahassee, FL.
- McVay, M., Bloomquist, D., Forbes, H., & Johnson, J. (2009). *Prestressed concrete pile installation – utilizing jetting and pressure grouting*. Final Report submitted Florida Department of Transportation, Tallahassee, FL.
- McVay, M., Thiyyakkandi, S., Joiner, J. & Adams, V. (2011). *Group efficiencies of grout-tipped drilled shafts and jet-grouted piles (BDK-75-977-07)*. Final report submitted Florida Department of Transportation, Tallahassee, FL.
- Menard, L. (1957). *An apparatus for measuring the strength of soils in place*. MSc Thesis, University of Illinois, Illinois, USA.
- Milovic, D. M., & Milovic, S. D. (1993). Predicted and observed behavior of piles. *Proceedings of the 1st International Geotechnical Seminar on Deep Foundations on Bored and Augur Piles, Balkema*, Rotterdam, 381-384.
- Mullins, G., Dapp, S., Frederic, E., & Wagner, R. (2001). *Pressure grouting drilled shaft tips – phase I*. Final report submitted Florida Department of Transportation, Tallahassee, FL.
- Mullins, G., & O'Neill, M. (2003). *Pressure grouting drilled shaft tip - a full-scale load test program*. Research Report, Univ. of South Florida, Tampa, Florida.
- Mullins, G., & Winters, D. (2004). *Pressure grouting drilled shaft tips – phase II*. Final report submitted to Florida Department of Transportation, Tallahassee, FL.
- Mullins, G., Winters, D., & Dapp, S. (2006). Predicting end bearing capacity of post-grouted drilled shaft in cohesionless soils. *Journal of Geotechnical and Geoenvironmental Engineering*, 132(4), 478–87.
- NCHRP (2003). *Structural supports for Highway signs, Luminaires and Traffic signals (NCHRP report 494)*. National Cooperative Highway Research Program, TRB, Washington, D. C.
- O'Neill, M. W., & Hassan, K. M. (1994). Drilled shafts: effects of construction on performance and design criteria. *Proceedings, International Conference on Design and Construction of Deep Foundations*, FHWA, 137-187.
- O'Neil, M. W., & Reese, L. C. (1999). *Drilled shafts: Construction procedures and design methods (FHWA-IF-95-025)*. FHWA, Washington, D. C.
- Plumbridge, G. D., & Hill, S. J. (2001). Performance of shaft grouted piles and barrettes. *Geotechnical Engineering: Meeting Society's needs, proceedings of 14th Southeast Asian Geotechnical Conference*, Hong Kong, Vol.1, ISBN 90 5809 250 X, 407-412.

- Randolph, M. F., & Wroth, C. P. (1978). Analysis of deformation of vertically loaded piles. *Journal of Geotechnical Engineering Division, ASCE, 104(12)*, 1465-1488.
- Randolph, M. H., Dolwin, J., & Beck, R. (1994). Design of driven piles in sand, *Geotechnique, 44(3)*, 427-448.
- Reese, L.C., & Matlock, H. (1956). Non-dimensional solutions for laterally loaded piles with soil modulus assumed proportional to depth. *Proceedings of the 8th Texas Conference on Soil Mechanics and Foundation Engineering*, Austin, Texas, 1-41.
- Reese, L. C., Cox, W. R., & Koop, F. D. (1974). Analysis of laterally loaded piles in sand. *Proceedings, Sixth Annual Offshore Technology Conference, 2*, Houston, Texas, 246-258.
- Robertson, P.K., & Campanella, R.G. (1983). Interpretation of cone penetration tests - part I (sand). *Canadian geotechnical Journal, 20(4)*, 718-733.
- Robertson, P.K., & Cabal, K.L. (2010). Estimating soil unit weight from CPT. *Second International Symposium on Cone Penetration Testing (CPT 10)*, Huntington Beach, CA.
- Ruiz, M. E. (2005). *Study of axially loaded post grouted drilled shafts using CPT based load transfer curves*. M.S. Thesis, Department of Civil Engineering, University of Puerto Rico.
- Salgado, R., Mitchell, J. K., & Jamiolkowski, M. (1997). Cavity expansion and penetration resistance in sand. *Journal of Geotechnical and Geoenvironmental Engineering, 123(4)*, 344-354.
- Salgado, R., & Prezzi, A.M. (2007). Computation of cavity expansion pressure and penetration resistance in sands. *International Journal of Geomechanics, 7(4)*, 251-265.
- Salgado, R., & Randolph, M. F. (2001). Analysis of Cavity Expansion in Sand. *International Journal of Geomechanics, ASCE, 1(2)*, 175-192.
- Schmertmann, J.H. (1975). Measurement of in situ shear strength. Keynote lecture, *Proceedings of the conference on in situ measurement of soil properties*, June 1-4, 1975, vol. II, ASCE.
- Selby, A. R. (1991). Ground vibrations caused by pile installation. *Proceedings of the 4th International Conference on Piling and Deep Foundations*, Stresa, Italy, 497-502.
- Sharp, M. R., McVay, M., Townsend, F. C., & Basnett, C. R. (1988). *Evaluation of pile capacity from in situ tests. Soil Properties Evaluation from Centrifuge Models and Field Performance at ASCE National Conference*, Nashville, Tennessee, 134-156.
- Shestopal, A. O. (1959). *Jetting of pipes, piles, and sheet piles*. Hydro project Institute, Moscow, USSR.

- Smith, C. B., & Bloomquist, D. (2010). Horizontal Permeameter: the design, development and testing of a horizontal permeability laboratory test. *Magna Cum Laude Honors Research Project*, University of Florida.
- Stocker, M. (1983). Influence of post-grouting on the load-bearing capacity of bored piles. *Proceedings of the European conference on soil mechanics and foundation engineering*, A. A. Balkema, Helsinki: Rotterdam, Finland, 167–70.
- Svinkin, M. R. (2006). Mitigation of soil movements from pile driving. *Practice Periodical on Structural Design and Construction, ASCE, 11(2)*, 80-85.
- Tand, K. E., & Funegard, E. G. (1989). Pile capacity in stiff clays- CPT method. *Proceedings of the 12th International Conference on Soil Mechanics and Foundation Engineering, ICSMFE-12, Rio De Janeiro, 1*, 349-352.
- Tawfiq, K. (2000). *Drilled shafts under torsional loading conditions (B-9191)*. Final report to Florida Department of Transportation, Tallahassee, FL.
- Teng, W. C. (1962). *Foundation Design*, Prentice-Hall Inc., Englewood Cliffs, NJ.
- Thiyyakkandi, S., McVay, M., Bloomquist, D., & Lai, P. (2013a). Measured and predicted response of a new jetted and grouted precast pile with membranes in cohesionless soils. *Journal of Geotechnical and Geoenvironmental Engineering, 139 (8)*, 1334-1345.
- Thiyyakkandi, S., McVay, M., Bloomquist, D., & Lai, P. (2013b). Experimental study, numerical modeling of and axial prediction approach to base grouted drilled shafts in cohesionless soils. *Acta Geotechnica*, Springer. DOI: 10.1007/s11440-013-0246-3.
- Tsinker, G. P. (1988). Pile Jetting. *Journal of Geotechnical Engineering, ASCE, 114(3)*, 326-336.
- White, D. J., Finlay, T. C. R., Bolton, M. D., & Bearss, G. (2002). Press-in piling: ground vibration and noise during pile installation. *Proceedings of the International Deep Foundations Congress*, Orlando, USA, ASCE Special Publication 116, 363-371.
- White, D. J., Sidhu, H. K., Finlay, T. C. R., Bolton, M. D., & Nagayama, T. (2000). Press-in piling: the influence of plugging on drivability. *Proceedings of the 8th International Conference of the Deep Foundations Institute*, New York, 299-310.
- Woods, R. D. (1997). *Dynamic effects of pile installations on adjacent structures (NCHRP Synthesis 253)*. Transportation Research Board, National Research Council, Washington D.C.
- Youn, H., & Tonon, F. (2010). Numerical analysis on post-grouted drilled shafts: a case study at the Brazo River Bridge, TX. *Computers and Geotechnics, 37*, 456–465.

Yu, H. S. (2000). *Cavity expansion methods in geomechanics*, Kluwer Academic Publishers, London.

Yu, H. S., & Houlsby, G.T. (1991). Finite cavity expansion in dilatant soils – loading analysis. *Geotechnique*, 41(2), 173-183.

APPENDIX A: SOIL EXPLORATION DATA

Operator: TSB
 Sounding: CPT#2
 Cone Used: DSA0481

CPT Date/Time: 6/30/2011 10:22:52 AM
 Location: Kingsley #2
 Job Number: Kingsley

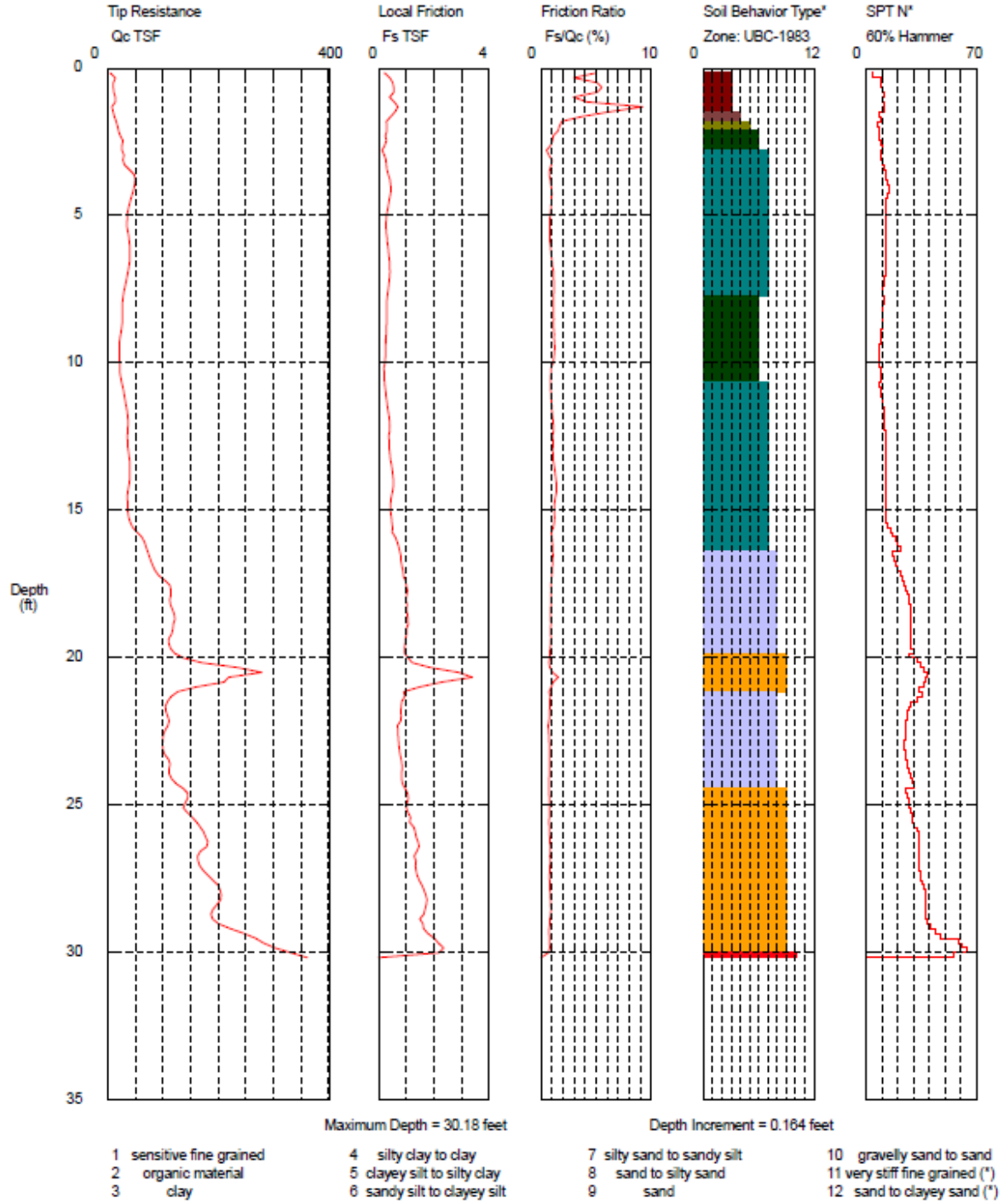


Figure A-1. CPT boring data near JP1

Florida DOT

Operator: TSB
 Sounding: CPT#5
 Cone Used: DSA0272

CPT Date/Time: 6/30/2011 12:19:34 PM
 Location: Kingsley #5
 Job Number: Kingsley

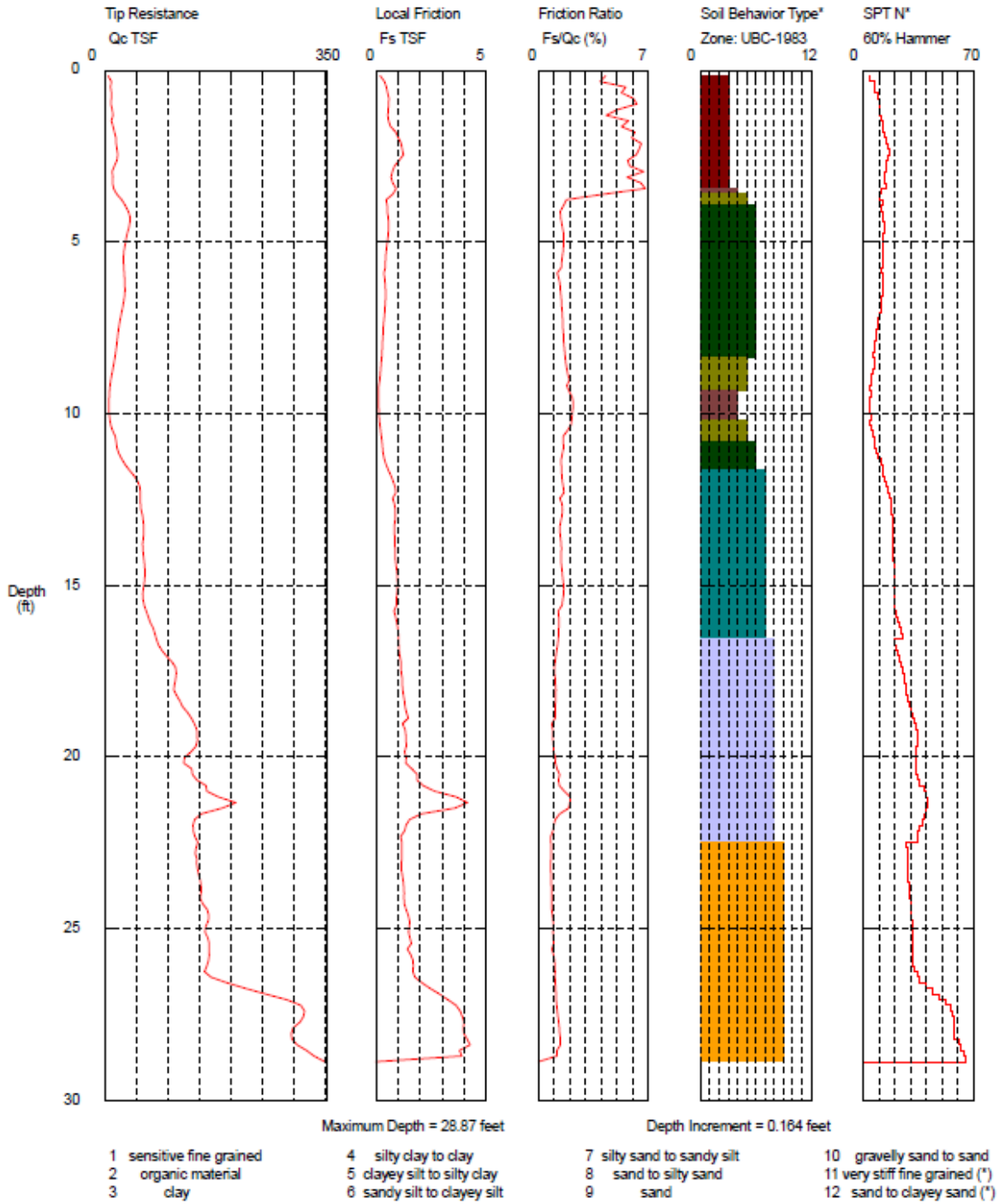


Figure A-2. CPT boring data near TS2

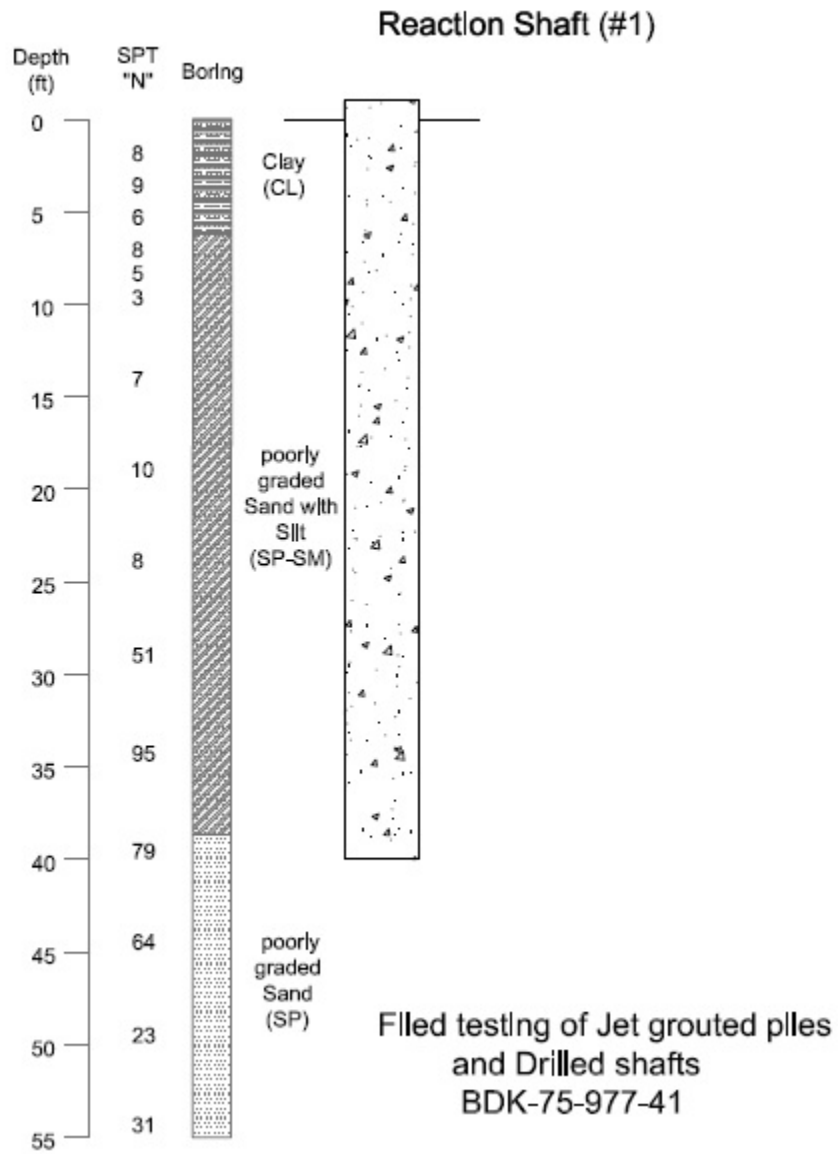


Figure A-3. Soil classification and uncorrected SPT blow counts at the location of RS1

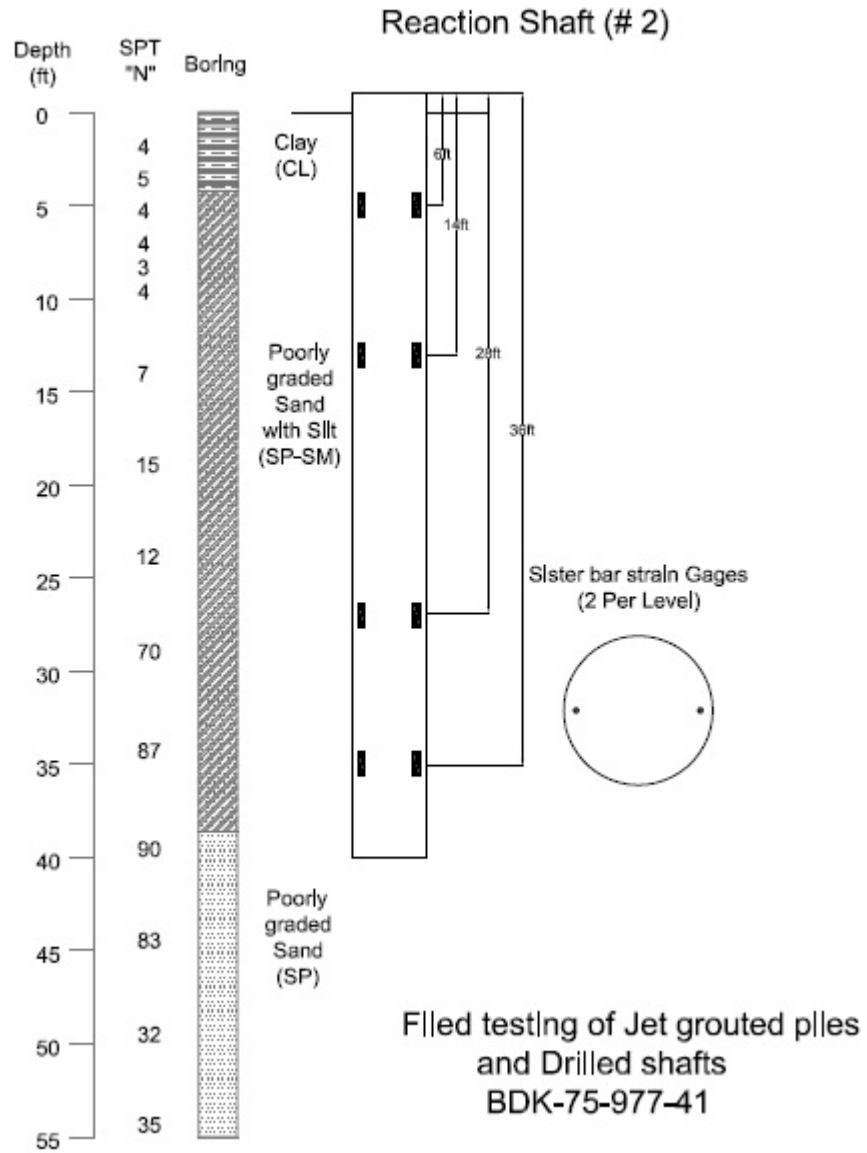


Figure A-4. Soil classification and uncorrected SPT blow counts at the location of RS2

Reaction shaft # 3

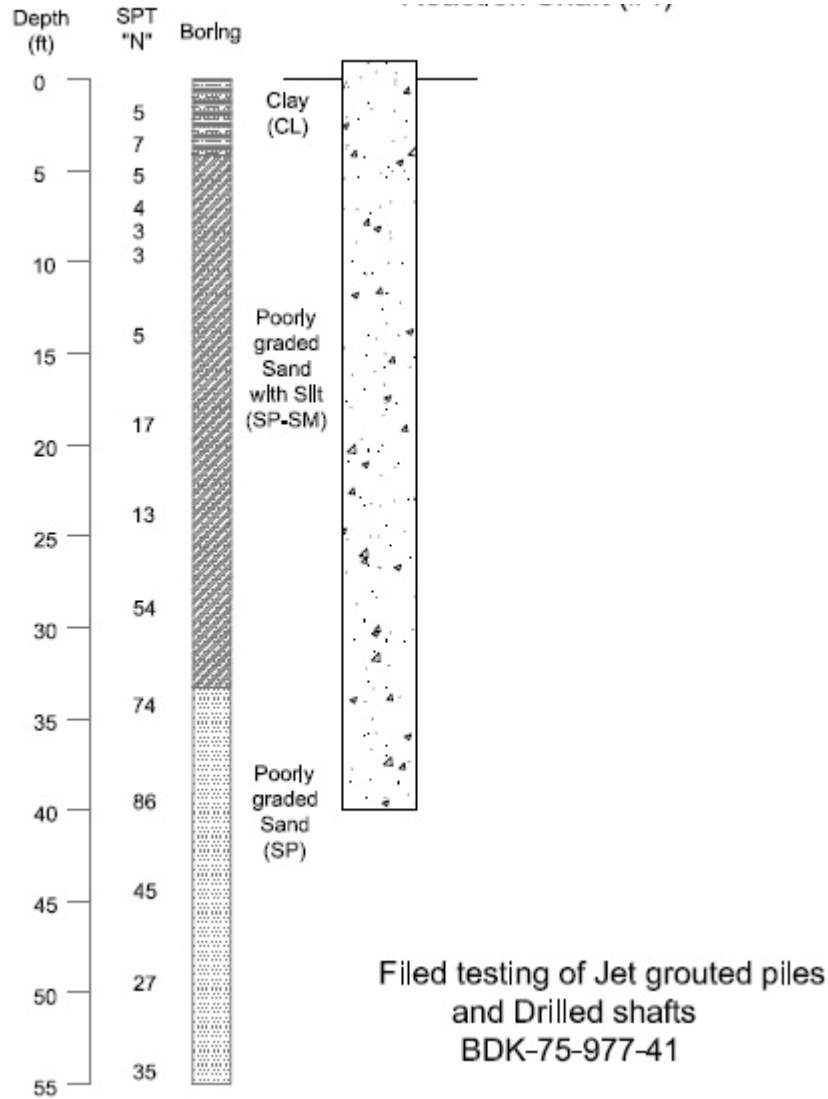


Figure A-5. Soil classification and uncorrected SPT blow counts at the location of RS3

Reaction shaft # 4

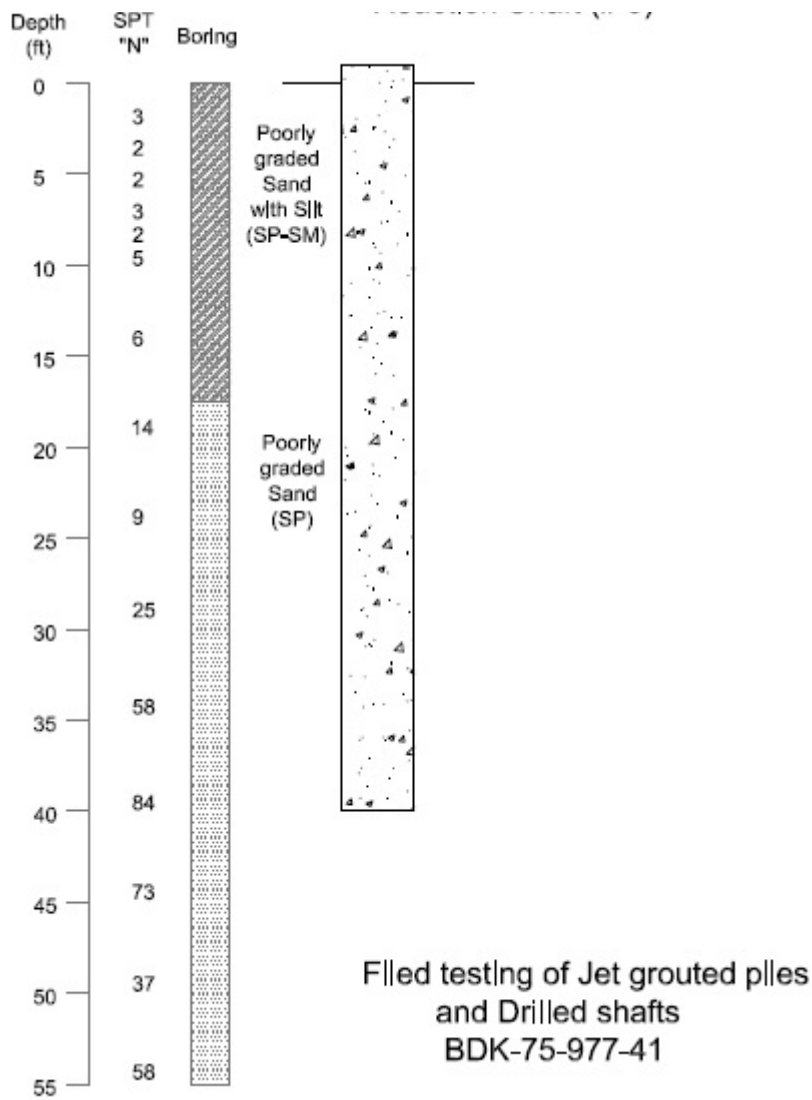


Figure A-6. Soil classification and uncorrected SPT blow counts at the location of RS4

APPENDIX B: STRUCTURAL DESIGN OF DRILLED SHAFTS, EMBEDDED PIPE AND FLANGE SECTION, AND CSL RESULTS

Structural design of test drilled shafts

Forces and Moments on foundation top (from Mast Arm analysis)

$T_u := 650 \text{kip}\cdot\text{ft}$

$P_n := 10.7 \text{kip}$

$M_x := 118 \text{kip}\cdot\text{ft}$

$V_x := 0.6 \text{kip}$

$M_z := 371.4 \text{kip}\cdot\text{ft}$

$V_z := 18.57 \text{kip}$

$M_u := \sqrt{M_x^2 + M_z^2}$

$M_u = 389.695 \text{kip}\cdot\text{ft}$

$V_u := \sqrt{V_x^2 + V_z^2}$

$V_u = 18.58 \text{kip}$

Shaft Design - Flexural Capacity

Input **Check Flexural Capacity of Shaft**

Diameter of shaft

$d_s := 48 \text{in}$

Radius of Shaft

$R_{\text{shaft}} := \frac{d_s}{2} = 0.61 \text{m}$

Area of shaft

$A_s := \pi \cdot \left(\frac{d_s}{2}\right)^2$

Longitudinal Reinforcement

Number of Longitudinal Bars

$n_{\text{long}} := 15$

Yield Strength of Longitudinal Reinforcement

$f_{y_long_steel} := 60 \text{ksi}$

Longitudinal Steel Area

$A_{\text{long_steel}} := 1.27 \text{in}^2$

Number of Bars Yielded (Assumption)

$n_{\text{long_yield}} := 9$

Concrete strength

$f_c := 4000 \text{psi}$

$\phi_{\text{flexure}} := 0.9$

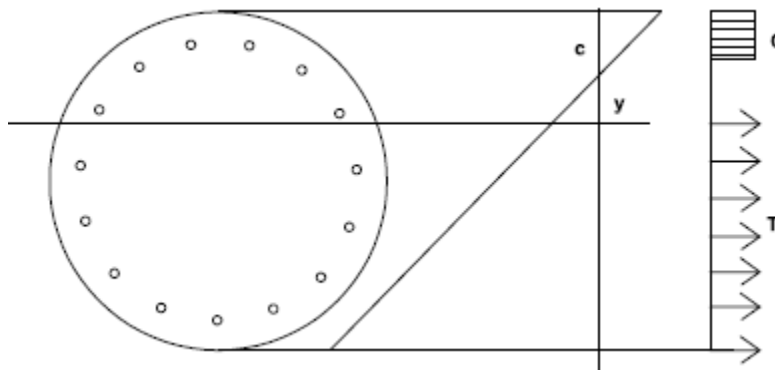


Figure B-1. ACI stress block diagram for 48-in diameter drilled shaft

Calculations Using ACI Stress Block

$$\beta_1(f_c) := \begin{cases} .85 & \text{if } f_c < 4000\text{psi} \\ .65 & \text{if } f_c > 8000\text{psi} \\ \left[.85 - .05 \cdot \left[\frac{(f_c - 4000\text{psi})}{1000\text{psi}} \right] \right] & \text{if } 4000\text{psi} \leq f_c \leq 8000\text{psi} \end{cases} \quad \beta_1(f_c) = 0.85$$

ACI 10.2.7.3

$$A_{\text{comp}} := \frac{(n_{\text{long_yield}} \cdot A_{\text{long_steel}} \cdot f_{y_long_steel})}{.85 \cdot f_c} \quad A_{\text{comp}} = 1.401 \cdot \text{ft}^2$$

Initial guess: $a := 5\text{in}$

$$\text{Given} \quad \left[R^2 \cdot \text{acos} \left[\frac{(R - a)}{R} \right] - (R - a) \cdot \sqrt{2 \cdot R \cdot a - a^2} \right] - A_{\text{comp}} = 0$$

$$a := \text{Find}(a) \quad a = 8.097 \cdot \text{in}$$

$$c := \frac{a}{\beta_1(f_c)} \quad c = 9.525 \cdot \text{in}$$

$$y := .002 \cdot \frac{c}{.003} \quad y = 6.35 \cdot \text{in}$$

$$d_{\text{bar}} := \begin{pmatrix} 21.936 \\ 30.1 \\ 37.21 \\ 42.03 \end{pmatrix} \text{in} \quad d_{\text{bar}_0} = 21.936 \cdot \text{in} \quad A_{\text{long_steel}} = 1.27 \cdot \text{in}^2$$

$$d_{\text{bars}} := \frac{\left[\sum_{i=0}^3 (d_{\text{bar}_i} \cdot A_{\text{long_steel}} \cdot 2) \right] + 43.74 \text{in} \cdot A_{\text{long_steel}}}{n_{\text{long_yield}} \cdot A_{\text{long_steel}}} \quad d_{\text{bars}} = 34.032 \cdot \text{in}$$

$$M_{n_shaft} := \phi_{\text{flexure}} \cdot n_{\text{long_yield}} \cdot A_{\text{long_steel}} \cdot f_{y_long_steel} \cdot \left(d_{\text{bars}} - \frac{a}{2} \right) \quad M_{n_shaft} = 1542.233 \cdot \text{kip} \cdot \text{ft}$$

$$\text{Flexure_Check} := \begin{cases} \text{"Insufficient"} & \text{if } M_{n_shaft} \leq M_u \\ \text{"Sufficient"} & \text{otherwise} \end{cases} \quad \text{Flexure_Check} = \text{"Sufficient"}$$

Check Shear Capacity of Shaft

Input

Gross cross-sectional area

$$A_g := \pi \cdot R^2 = 1.81 \times 10^3 \cdot \text{in}^2$$

Axial load

$$N_u := 0$$

Effective depth of the section

$$d := d_s = 48 \cdot \text{in}$$

Area in compression

$$A_{\text{comp}} = 201.706 \cdot \text{in}^2$$

Hoop Steel Area

$$A_{\text{hoop_steel}} := 0.306 \cdot \text{in}^2$$

Hoop Steel Diameter

$$d_{\text{hoop_steel}} := 0.625 \cdot \text{in}$$

Spacing of Hoop Steel

$$s_{\text{hoop_steel}} := 5 \cdot \text{in}$$

Yield Strength of Hoop Steel

$$f_{y_hoop_steel} := 60 \cdot \text{ksi}$$

Centerline of Hoop Steel Diameter

$$d_h := 41.625 \cdot \text{in}$$

$$\phi_{\text{shear}} := 0.9$$

Shear Capacity of the Concrete

$$V_c := 2 \sqrt{\frac{f_c}{\text{psi}}} \cdot \text{psi} \cdot 41.375 \cdot \text{in} \cdot d$$

$$V_c = 251.211 \cdot \text{kip}$$

Shear Capacity of the Steel

$$V_s := \frac{(A_{\text{hoop_steel}} \cdot f_{y_hoop_steel} \cdot 41.375 \cdot \text{in})}{s_{\text{hoop_steel}}}$$

$$V_s = 151.929 \cdot \text{kip}$$

Shear Capacity of the Shaft

$$V_{n_shaft} := \phi_{\text{shear}} \cdot (V_c + V_s)$$

$$V_{n_shaft} = 362.826 \cdot \text{kip}$$

$$\text{Check_Shear_Strength} := \begin{cases} \text{"Insufficient"} & \text{if } V_{n_shaft} \leq V_u \\ \text{"Sufficient"} & \text{otherwise} \end{cases}$$

$$\text{Check_Shear_Strength} = \text{"Sufficient"}$$

Check Axial Capacity of the Shaft

Input

Radius of Shaft

$$R = 24\text{-in}$$

Area of shaft

$$A_s = 1.81 \times 10^3 \cdot \text{in}^2$$

Longitudinal Reinforcement

Number of Longitudinal Bars

$$n_{\text{long}} = 15$$

Yield Strength of Longitudinal Reinforcement

$$f_{y_long_steel} = 60\text{-ksi}$$

Longitudinal Steel Area

$$A_{\text{long_steel}} = 1.27 \cdot \text{in}^2$$

Number of Bars Yielded (Assumption)

Hoop Steel

Hoop Steel Area

$$A_{\text{hoop_steel}} = 0.306 \cdot \text{in}^2$$

Hoop Steel Diameter

$$d_{\text{hoop_steel}} = 0.625\text{-in}$$

Spacing of Hoop Steel

$$s_{\text{hoop_steel}} = 5\text{-in}$$

Yield Strength of Hoop Steel

$$f_{y_hoop_steel} = 60\text{-ksi}$$

Centerline of Hoop Steel Diameter

$$d_h = 41.625\text{-in}$$

$$\phi_{\text{comp}} := 0.9$$

Axial Capacity of the Shaft

Area of the tied core

$$A_c := \pi \cdot \left(\frac{d_h}{2} \right)^2$$

$$P_{\text{shaft}} := f_c \cdot (A_c - n_{\text{long}} \cdot A_{\text{long_steel}}) + f_{y_long_steel} \cdot n_{\text{long}} \cdot A_{\text{long_steel}}$$

$$P_{\text{shaft}} = 6.51 \times 10^3 \cdot \text{kip}$$

$$P_{n_shaft} := \phi_{\text{comp}} P_{\text{shaft}}$$

$$P_{n_shaft} = 5859.046\text{-kip}$$

$$\text{Check_Axial_Strength} := \begin{cases} \text{"Insufficient"} & \text{if } P_{n_shaft} \leq P_n \\ \text{"Sufficient"} & \text{otherwise} \end{cases}$$

$$\text{Check_Axial_Strength} = \text{"Sufficient"}$$

Check Torsional Capacity of the Shaft

Input

Radius of Shaft

$$R = 24\text{-in}$$

Area of shaft

$$A_{cp} := A_s = 1.81 \times 10^3 \cdot \text{in}^2$$

Perimeter of the shaft

$$P_{cp} := \pi \cdot d_s = 150.796\text{-in}$$

Longitudinal Reinforcement

Number of Longitudinal Bars

$$n_{long} = 15$$

Yield Strength of Longitudinal Reinforcement

$$f_{y_long_steel} = 60\text{-ksi}$$

Longitudinal Steel Area

$$A_{long_steel} = 1.27 \cdot \text{in}^2$$

Hoop Steel

Hoop Steel Area

$$A_{hoop_steel} = 0.306 \cdot \text{in}^2$$

Hoop Steel Diameter

$$d_{hoop_steel} = 0.625\text{-in}$$

Spacing of Hoop Steel

$$s_{hoop_steel} = 5\text{-in}$$

Yield Strength of Hoop Steel

$$f_{y_hoop_steel} = 60\text{-ksi}$$

Centerline of Hoop Steel Diameter

$$d_h = 41.625\text{-in}$$

$$\phi_{torsion} := 0.9$$

Threshold Torsion

$$T_{\text{threshold}} := \sqrt{\frac{f_c}{\text{psi}}} \cdot \text{psi} \cdot \frac{(A_{\text{cp}})^2}{P_{\text{cp}}}$$

$$T_{\text{threshold}} = 114.446 \text{ kip-ft}$$

ACI 11.6.1a

$$\text{Neglect_Torsion} := \begin{cases} \text{"Yes"} & \text{if } \phi_{\text{torsion}} \cdot T_{\text{threshold}} \geq T_u \\ \text{"No"} & \text{otherwise} \end{cases}$$

$$\text{Neglect_Torsion} = \text{"No"}$$

Cracking Torsion

$$T_{\text{cr}} := 4 \cdot \sqrt{\frac{f_c}{\text{psi}}} \cdot \text{psi} \cdot \left(\frac{A_{\text{cp}}^2}{P_{\text{cp}}} \right)$$

$$T_{\text{cr}} = 457.786 \text{ kip-ft}$$

ACI R11.6.1

Nominal Torsional Strength

$$A_o := \pi \cdot \left(\frac{d_h}{2} \right)^2$$

$$A_t := A_{\text{hoop_steel}}$$

$$A_o = 0.878 \text{ m}^2$$

$$A_t = 1.974 \times 10^{-4} \text{ m}^2$$

$$\theta := 45 \text{ deg}$$

$$\theta = 0.785$$

$$T_{\text{torsion}} := \frac{2 \cdot A_o \cdot A_t \cdot f_{y_hoop_steel}}{s_{\text{hoop_steel}}} \cdot \cot(\theta)$$

$$T_{\text{torsion}} = 832.817 \text{ kip-ft}$$

$$T_{\text{n_shaft}} := \phi_{\text{torsion}} \cdot T_{\text{torsion}}$$

$$T_{\text{n_shaft}} = 749.536 \text{ kip-ft}$$

$$\text{Check_Torsion_Shaft} := \begin{cases} \text{"Insufficient"} & \text{if } T_{\text{n_shaft}} \leq T_u \\ \text{"Sufficient"} & \text{otherwise} \end{cases}$$

$$\text{Check_Torsion_Shaft} = \text{"Sufficient"}$$

Shaft Design - Torsional Capacity

Design of Embedded pipe and plate section

Input and Properties

Input and properties

Shaft

Diameter of the Shaft

$$d_s := 48\text{in}$$

Concrete Strength

$$f_c := 4000\text{psi}$$

Hoop Steel

Hoop Steel Area

$$A_{\text{hoop}} := .306\text{in}^2$$

Hoop Steel Diameter

$$d_{\text{hoop}} := .625\text{in}$$

Spacing of Hoop Steel

$$s_{\text{hoop}} := 5\text{in}$$

Yield Strength of Hoop Steel

$$f_{y_hoop} := 60\text{ksi}$$

Centerline of Hoop Steel Diameter

$$d_h := 41.625\text{in}$$

Longitudinal Steel

Longitudinal Steel Area

$$A_{\text{long}} := 1.27\text{in}^2$$

Longitudinal Steel Diameter

$$d_{\text{long}} := 1.27\text{in}$$

Yield Strength of Longitudinal Steel

$$f_{y_long} := 60\text{ksi}$$

Number of Long Steel Bars

$$n_{\text{long}} := 15$$

Torsional Stiffener Plates

Thickness of the plate

$$t := 1\text{in}$$

Width of the plate

$$b := 1\text{in}$$

Length of plate

$$L_{\text{st}} := 18\text{in}$$

Yield strength of the plate

$$f_{y_plate} := 50\text{ksi}$$

Flexural Stiffener (base) Plates

Width of the stiffener plates

$$b_{\text{flex_plate}} := 2\text{in}$$

Thickness of the stiffener plates

$$t_{\text{flex_plate}} := 1\text{in}$$

Embedded Pipe

Thickness of the pipe

$$t_{\text{pipe}} := .581\text{in}$$

Diameter of the pipe

$$d_{\text{pipe}} := 24\text{in}$$

$$F_{y_pipe} := 42\text{ksi}$$

$$F_{u_pipe} := 58\text{ksi}$$

Input and Properties

STIFFENER DESIGN

☑ Torsional Capacity Using Breakout Capacity

Input

Width of the stiffener plates

$$b = 1 \text{ in}$$

Thickness of the stiffener plates

$$t = 1 \text{ in}$$

Length of the stiffener plates

$$L = 18 \text{ in}$$

Diameter of upright/embedded pipe

$$d_{\text{pipe}} = 24 \text{ in}$$

Diameter of stiffeners

$$d_{\text{st}} := d_{\text{pipe}}$$

Number of stiffeners

$$\text{No_Stiff} := 4$$

$$\psi_{\text{ecV}} := 1$$

$$\psi_{\text{edV}} := 1$$

$$\psi_{\text{cV}} := 1.4$$

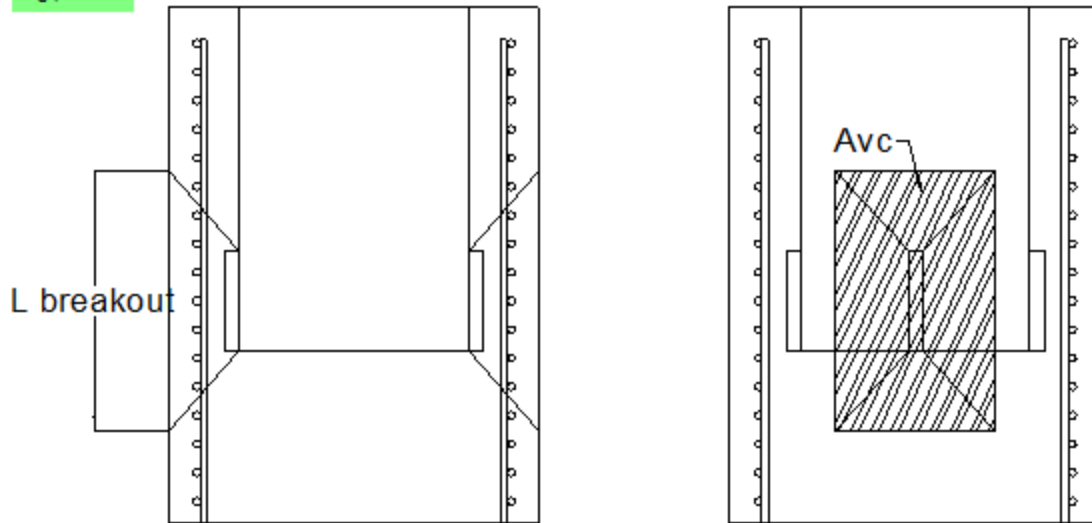


Figure B-2. Concrete breakout failure for embedded pile and flange section in torsion

Concrete Breakout Equivalent Torsional Strength

Based on ACI 318 Appendix D - Design requirements for shear loading

$$\text{cover} := \frac{(d_s - d_{\text{st}})}{2}$$

$$\text{cover} = 12 \text{ in}$$

$$c_{a1} := \frac{\left[\sqrt{\left(\frac{d_{st}}{2}\right)^2 + 3.25 \cdot \left[\left(\frac{d_s}{2}\right)^2 - \left(\frac{d_{st}}{2}\right)^2\right]} - \left(\frac{d_{st}}{2}\right) \right]}{3.25} \quad c_{a1} = 8.41 \text{ in}$$

$$A := \frac{360 \text{ deg}}{\text{No_Stiff}} \quad A = 90 \text{ deg}$$

$$\text{chord_group} := 2 \cdot \frac{d_s}{2} \cdot \sin\left(\frac{A}{2}\right) \quad \text{chord_group} = 33.94 \text{ in}$$

$$A_{\text{min_group}} := 2 \cdot \text{asin}\left(\frac{3.0 \cdot c_{a1}}{d_s}\right) \quad A_{\text{min_group}} = 63.45 \text{ deg}$$

$$+ \text{Check_Group_Effect} := \begin{cases} \text{"Group Effect"} & \text{if } A \leq A_{\text{min_group}} \\ \text{"No Group Effect"} & \text{otherwise} \end{cases} \quad \text{Check_Group_Effect} = \text{"No Group Effect"}$$

$$l_{\text{breakout}} := L + 2 \cdot 1.5 \cdot c_{a1} \quad l_{\text{breakout}} = 43.24 \text{ in}$$

$$A_{Vc} := l_{\text{breakout}}^3 \cdot c_{a1} \quad A_{Vc} = 1.09 \times 10^3 \text{ in}^2$$

$$A_{Vco} := 4.5 \cdot c_{a1}^2 \quad A_{Vco} = 318.56 \text{ in}^2$$

$$l_e := L \quad l_e = 18 \text{ in}$$

$$V_b := 13 \cdot \left(\frac{l_e}{b}\right)^2 \cdot \sqrt{\frac{b}{\text{in}}} \cdot \sqrt{\frac{f_c}{\text{psi}}} \cdot \left(\frac{c_{a1}}{\text{in}}\right)^{1.5} \cdot \text{lbf} \quad V_b = 35.77 \text{ kip}$$

$$V_{\text{cbg}} := \left(\frac{A_{Vc}}{A_{Vco}}\right) \cdot \psi_{ec} V_e \cdot \psi_{ed} V_e \cdot \psi_{cV} \cdot V_b \quad V_{\text{cbg}} = 171.58 \text{ kip}$$

$$V_{\text{cbg_parallel}} := 2 \cdot V_{\text{cbg}} \quad V_{\text{cbg_parallel}} = 343.15 \text{ kip}$$

$$V_c := V_{\text{cbg_parallel}} \cdot \text{No_Stiff} \quad V_c = 1.37 \times 10^3 \text{ kip}$$

$$T_{n_breakout_plate} := V_c \cdot \left(\frac{d_{st}}{2}\right) \quad T_{n_breakout_plate} = 1372.61 \text{ ft} \cdot \text{kip}$$

▢ Torsional Capacity Using Breakout Capacity

☑ Torsional Capacity Using Side-Face Blowout Capacity

Input

Width of the stiffener plates

$$b = 1 \text{ in}$$

Thickness of the stiffener plates

$$t = 1 \text{ in}$$

Length of the stiffener plates

$$L = 18 \text{ in}$$

Diameter of upright/embedded pipe

$$d_{\text{pipe}} = 24 \text{ in}$$

Diameter of stiffeners

$$d_{\text{st}} := d_{\text{pipe}}$$

Number of stiffeners

$$N_{\text{Stiff}} := 4$$

Concrete Breakout Equivalent Torsional Strength

Based on ACI 318 Appendix D

$$c_{a1} := \frac{\left[\sqrt{\left(\frac{d_{\text{st}}}{2}\right)^2 + 3.25 \cdot \left[\left(\frac{d_s}{2}\right)^2 - \left(\frac{d_{\text{st}}}{2}\right)^2\right]} - \left(\frac{d_{\text{st}}}{2}\right) \right]}{3.25}$$

$$c_{a1} = 8.41 \text{ in}$$

$$A_{\text{brg}} := L \cdot b = 18 \text{ in}^2$$

$$N_{\text{sb}} := 200 \cdot c_{a1} \cdot \sqrt{A_{\text{brg}}} \cdot f_c^{.5} \cdot \text{psi}^{.5}$$

$$N_{\text{sb}} = 451.53 \text{ kip}$$

$$T_{\text{n_blowout}} := N_{\text{Stiff}} \cdot N_{\text{sb}} \cdot \frac{d_{\text{st}}}{2}$$

$$T_{\text{n_blowout}} = 1806.11 \text{ ft-kip}$$

☑ Torsional Capacity Using Side-Face Blowout Capacity

☑ Welding for Stiffener Plates

Weld Design

$$V_{\text{weld}} := \frac{T_{\text{n_blowout}}}{4(.5d_s)}$$

$$V_{\text{weld}} = 225.76 \text{ kip}$$

$$t = 1 \text{ in}$$

$$t_{\text{pipe}} = 0.58 \text{ in}$$

$$\text{Weld_Size} := \frac{3}{8} \text{ in}$$

AISC Spec. J2
Table J2.4

$$F_{\text{electrode}} := 70 \text{ ksi}$$

$$F_{\text{W}} := .6 \cdot F_{\text{electrode}}$$

AISC Spec. J2
Table J2.5

$$\text{Throat} := .707 \cdot \text{Weld_Size}$$

$$R_{n_weld} := \text{Throat} \cdot F_W$$

$$R_{n_weld} = 11.14 \cdot \frac{\text{kip}}{\text{in}}$$

$$R_{n_yield} := .6 \cdot F_{y_pipe} \cdot \frac{t}{2}$$

$$R_{n_yield} = 12.6 \cdot \frac{\text{kip}}{\text{in}}$$

$$R_{n_rupture} := .45 \cdot F_{u_pipe} \cdot \frac{t}{2}$$

$$R_{n_rupture} = 13.05 \cdot \frac{\text{kip}}{\text{in}}$$

$$R_n := \min(R_{n_weld}, R_{n_yield}, R_{n_rupture})$$

$$R_n = 11.14 \cdot \frac{\text{kip}}{\text{in}}$$

$$\text{Required_Length_Each_Side} := \frac{V_{weld}}{2 \cdot R_n}$$

$$\text{Required_Length_Each_Side} = 10.14 \text{ in}$$

$$\text{ceil}\left(\frac{\text{Required_Length_Each_Side}}{\text{in}}\right) \cdot \text{in} = 11 \text{ in}$$

Welding for Stiffener Plates

CAPACITY OF PIPE

Flexural and shear Capacity of Pipe

Embedded Pipe

Design Wall Thickness

$$t_{\text{pipe}} = .581 \text{ in}$$

Diameter of the Pipe

$$D_{\text{pipe}} = 24 \text{ in}$$

$$D_o = D_{\text{pipe}}$$

$$D_i = D_o - 2t_{\text{pipe}}$$

Cross Sectional Area of Pipe

$$A_{\text{pipe}} := \pi \frac{(D_o^2 - D_i^2)}{4}$$

$$A_{\text{pipe}} = 42.75 \text{ in}^2$$

Diameter to Wall Thickness Ratio

$$D_t := \frac{D_{\text{pipe}}}{t_{\text{pipe}}}$$

$$D_t = 41.31$$

Nominal Weight

$$W_{\text{pipe}} = 156 \frac{\text{lb}}{\text{ft}}$$

Moment of Inertia

$$I_{\text{pipe}} := \pi \frac{(D_o^4 - D_i^4)}{64}$$

$$I_{\text{pipe}} = 2932.299 \text{ in}^4$$

Elastic Section Modulus

$$S_{\text{pipe}} := \pi \frac{(D_o^4 - D_i^4)}{32 \cdot D_o}$$

$$S_{\text{pipe}} = 244.36 \text{ in}^3$$

Radius of Gyration

$$r_{\text{pipe}} := \left(\frac{I_{\text{pipe}}}{A_{\text{pipe}}} \right)^{0.5}$$

$$r_{\text{pipe}} = 8.28 \text{ in}$$

Plastic Section Modulus

$$Z_{\text{pipe}} := \frac{(D_o^3 - D_i^3)}{6}$$

$$Z_{\text{pipe}} = 318.71 \text{ in}^3$$

Torsional Constant

$$J_{\text{pipe}} := \pi \frac{\left[\left(\frac{D_o}{2} \right)^4 - \left(\frac{D_i}{2} \right)^4 \right]}{2}$$

$$J_{\text{pipe}} = 5864.598 \text{ in}^4$$

HSS Torsional Constant

$$C_{\text{pipe}} := \pi \frac{(D_o^4 - D_i^4)}{32 \cdot \frac{D_o}{2}}$$

$$C_{\text{pipe}} = 488.72 \text{ in}^3$$

Yield Strength

$$F_{y_{\text{pipe}}} := 42 \text{ ksi}$$

Ultimate Strength

$$F_{u_{\text{pipe}}} := 58 \text{ ksi}$$

Modulus of Elasticity

$$E := 29000 \text{ ksi}$$

$$L_{\text{pipe}} := 6 \text{ ft} \quad +$$

Determine design Shear Strength of Round HSS

$$L_v := \frac{L_{\text{pipe}}}{2} \quad \phi_{\text{shear}} := .9 \quad \text{AISC Spec. G1}$$

$$F_{\text{cr}_1} := \max \left[\left[\frac{(1.6 \cdot E)}{\sqrt{\frac{L_v}{d_{\text{pipe}}} \cdot (D_t) \left(\frac{5}{4}\right)}} \right], \left[\frac{(.78 \cdot E)}{(D_t) \left(\frac{3}{2}\right)} \right] \right] \quad F_{\text{cr}_1} = 361.77 \text{ ksi}$$

$$F_{\text{cr}} := \min(F_{\text{cr}_1}, .6 \cdot F_{y_{\text{pipe}}}) \quad F_{\text{cr}} = 25.2 \text{ ksi}$$

$$V_{n_{\text{pipe}}} := \frac{\phi_{\text{shear}} \cdot F_{\text{cr}} \cdot A_{\text{pipe}}}{2} \quad V_{n_{\text{pipe}}} = 484.74 \text{ kip}$$

Determine design Flexural Capacity of Round HSS

$$\text{Check_Applicable} := \text{if} \left[D_t < \left(\frac{.45 \cdot E}{F_{y_{\text{pipe}}}} \right), \text{"Applicable"}, \text{"N/A"} \right] \quad \text{AISC Spec. F2.1}$$

Check_Applicable = "Applicable"

$$\lambda_p := .07 \cdot \frac{E}{F_{y_{\text{pipe}}}}$$

$$\lambda_r := .31 \cdot \frac{E}{F_{y_{\text{pipe}}}}$$

$$\text{Check_Compact} := \begin{cases} \text{"Compact"} & \text{if } D_t \leq \lambda_p \\ \text{"Noncompact"} & \text{if } \lambda_p < D_t \leq \lambda_r \\ \text{"Slender"} & \text{if } D_t > \lambda_r \end{cases} \quad \text{Check_Compact} = \text{"Compact"}$$

$$M_p := F_{y_{\text{pipe}}} \cdot Z_{\text{pipe}} \quad \phi_{\text{flexure}} := 0.9 \quad \text{AISC Spec. F1}$$

$$M_{n_{\text{pipe}}} := \phi_{\text{flexure}} \cdot M_p \quad M_{n_{\text{pipe}}} = 1003.95 \text{ ft} \cdot \text{kip}$$

Flexural and shear Capacity of Pipe

Design Torsional Strength

$$\phi_{\text{torsion}} := 0.9$$

AISC Spec. H3.1

$$F_{cr} := \begin{cases} \left[\frac{(1.23 \cdot E)}{\sqrt{\frac{L_{\text{pipe}}}{D_{\text{pipe}}} \cdot (D_t)^{1.25}}} \right] & \text{if } \left[\frac{(1.23 \cdot E)}{\sqrt{\frac{L_{\text{pipe}}}{D_{\text{pipe}}} \cdot (D_t)^{1.25}}} \right] \geq \frac{(.60 \cdot E)}{(D_t)^{1.5}} \\ \left[\frac{(.60 \cdot E)}{(D_t)^{1.5}} \right] & \text{otherwise} \end{cases}$$

$$F_{cr} = 196.65 \text{ ksi}$$

$$F_{cr_torsion} := \min(F_{cr}, .6 \cdot F_{y_pipe})$$

$$F_{cr_torsion} = 25.2 \text{ ksi}$$

$$T_{n_pipe} := \phi_{\text{torsion}} \cdot F_{cr_torsion} \cdot C_{\text{pipe}}$$

$$T_{n_pipe} = 923.67 \text{ ft-kip}$$

AISC Spec. H3.1

Design Axial Strength

$$\phi_{\text{comp}} := .90$$

$$\lambda_c := .11 \cdot \frac{E}{F_{y_pipe}}$$

$$\lambda_c = 75.95$$

$$\lambda := \begin{cases} \text{"Noncompact"} & \text{if } D_t \geq \lambda_c \\ \text{"Slender"} & \text{otherwise} \end{cases}$$

$$\lambda = \text{"Slender"}$$

AISC Spec. B4

$$Q := \left[\frac{(.038 \cdot E)}{F_{y_pipe} \cdot D_t} \right] + \frac{2}{3}$$

$$Q = 1.3$$

AISC Spec. E7.2c

$$F_e := \frac{(\pi^2 \cdot E)}{\left(\frac{L_{\text{pipe}}}{r_{\text{pipe}}} \right)^2}$$

$$F_e = 3.79 \times 10^3 \text{ ksi}$$

AISC Equation E3-4

$$F_{cr_axial} := \begin{cases} \left[Q \cdot \left[.658 \left(Q \cdot \frac{F_{y_pipe}}{F_e} \right) \right] \cdot F_{y_pipe} \right] & \text{if } F_e \geq .44 \cdot Q \cdot F_{y_pipe} \\ (.877 \cdot F_e) & \text{if } F_e < .44 \cdot Q \cdot F_{y_pipe} \end{cases}$$

$$F_{cr_axial} = 54.35 \text{ ksi}$$

AISC Equations E7-2, E7-3

$$P_{n_s_pipe} := \phi_{\text{comp}} \cdot F_{cr_axial} \cdot A_{\text{pipe}}$$

$$P_{n_s_pipe} = 2090.85 \text{ kip}$$

AISC Equation E7-1

DESIGN OF FLEXURAL PLATE

Flexural Capacity of T-Plates Using Side-Face Blowout Capacity

Flexural Stiffener (base) Plates

- + Width of the stiffener plates
- Thickness of the stiffener plates
- Length of the stiffener plates
- Diameter of upright/embedded pipe
- Diameter of stiffeners

$$b_{flex_plate} := 2.5 \text{ in}$$

$$t_{flex_plate} := 1 \text{ in}$$

$$L_{flex_plate} := .125\pi \cdot d_{pipe}$$

$$d_{pipe} = 24 \text{ in}$$

$$d_{st} := d_{pipe} + 2 \cdot b_{flex_plate}$$

Concrete Breakout Equivalent Flexural Strength

Based on ACI 318 Appendix D

$$c_{a1} := \frac{\left[\sqrt{\left(\frac{d_{st}}{2}\right)^2 + 3.25 \cdot \left[\left(\frac{d_s}{2}\right)^2 - \left(\frac{d_{st}}{2}\right)^2\right]} - \left(\frac{d_{st}}{2}\right) \right]}{3.25}$$

$$c_{a1} = 7.05 \text{ in}$$

$$A_{tbrg} := L_{flex_plate} \cdot b_{flex_plate}$$

$$A_{tbrg} = 23.56 \text{ in}^2$$

$$N_{sb} := 200 \cdot c_{a1} \cdot \sqrt{A_{tbrg}} \cdot f_c^{.5} \cdot \text{psi}^{.5}$$

$$N_{sb} = 432.68 \text{ kip}$$

$$M_{n_blowout} := N_{sb} \cdot d_{st}$$

$$M_{n_blowout} = 1045.63 \text{ ft} \cdot \text{kip}$$

Flexural Capacity of T-Plates Using Side-Face Blowout Capacity

Flexural Capacity Using Breakout Capacity

Input

- Width of the stiffener plates
- Thickness of the stiffener plates
- Length of the stiffener plates
- Diameter of upright/embedded pipe
- Diameter of stiffeners
- Number of stiffeners

$$b_{flex_plate} := 2 \text{ in}$$

$$t_{flex_plate} = 1 \text{ in}$$

$$L_{flex_plate} := .125\pi \cdot d_{pipe}$$

$$d_{pipe} = 24 \text{ in}$$

$$d_{st} := d_{pipe} + 2 \cdot b_{flex_plate}$$

$$No_Stiff := 4$$

Concrete Breakout Equivalent Flexural Strength

Based on ACI 318 Appendix D - Design requirements for shear loading

$$\text{cover} := \frac{(d_s - d_{st})}{2} \quad \text{cover} = 10 \text{ in}$$

$$c_{a1} := \frac{\left[\sqrt{\left(\frac{d_{st}}{2}\right)^2 + 3.25 \cdot \left[\left(\frac{d_s}{2}\right)^2 - \left(\frac{d_{st}}{2}\right)^2\right]} - \left(\frac{d_{st}}{2}\right) \right]}{3.25} \quad c_{a1} = 7.33 \text{ in}$$

$$A := \frac{360 \text{ deg}}{\text{No_Stiff}} \quad A = 90 \text{ deg}$$

$$\text{chord_group} := 2 \cdot \frac{d_s}{2} \cdot \sin\left(\frac{A}{2}\right) \quad \text{chord_group} = 33.94 \text{ in}$$

$$A_{\min_group} := 2 \cdot \text{asin}\left(\frac{3.0 \cdot c_{a1} + L_{\text{flex_plate}}}{d_s}\right) \quad A_{\min_group} = 81.78 \text{ deg}$$

$$\text{Check_Group_Effect} := \begin{cases} \text{"Group Effect"} & \text{if } A \leq A_{\min_group} \\ \text{"No Group Effect"} & \text{otherwise} \end{cases} \quad \text{Check_Group_Effect} = \text{"No Group Effect"}$$

$$l_{\text{breakout}} := t_{\text{flex_plate}} + 2 \cdot 1.5 c_{a1} \quad l_{\text{breakout}} = 23 \text{ in}$$

$$A_{Vc} := l_{\text{breakout}} \cdot (3 \cdot c_{a1}) \quad A_{Vc} = 505.8 \text{ in}^2$$

$$A_{Vco} := 4.5 \cdot c_{a1}^2 \quad A_{Vco} = 241.9 \text{ in}^2$$

$$l_e := L_{\text{flex_plate}} \quad l_e = 9.42 \text{ in}$$

$$V_b := 13 \cdot \left(\frac{l_e}{t_{\text{flex_plate}}}\right)^2 \cdot \sqrt{\frac{b_{\text{flex_plate}}}{\text{in}}} \cdot \sqrt{\frac{f_c}{\text{psi}}} \cdot \left(\frac{c_{a1}}{\text{in}}\right)^{1.5} \cdot \text{lb} \quad V_b = 36.15 \text{ kip}$$

$$V_{cbg} := \left(\frac{A_{Vc}}{A_{Vco}}\right) \cdot \psi_{ec} V_e \cdot \psi_{ed} V_e \cdot \psi_{cV} \cdot V_b \quad V_{cbg} = 105.84 \text{ kip}$$

$$V_{cbg_parallel} := 2 \cdot V_{cbg} \quad V_{cbg_parallel} = 211.67 \text{ kip}$$

$$V_c := V_{cbg_parallel} \cdot \text{No_Stiff} \quad V_c = 846.68 \text{ kip}$$

$$M_{n_breakout} := V_c \cdot \left(\frac{d_{st}}{2}\right) \quad M_{n_breakout} = 987.8 \text{ ft-kip}$$

Flexural Capacity Using Breakout Capacity

$$M_{n_pipe} = 1003.95 \text{ ft}\cdot\text{kip}$$

$$M_{n_blowout} = 1045.63 \text{ ft}\cdot\text{kip}$$

$$M_{n_breakout} = 987.8 \text{ ft}\cdot\text{kip}$$

$$T_{n_pipe} = 923.67 \text{ ft}\cdot\text{kip}$$

$$T_{n_breakout_plate} = 1.37 \times 10^3 \text{ ft}\cdot\text{kip}$$

$$T_{n_blowout} = 1.81 \times 10^3 \text{ ft}\cdot\text{kip}$$

Development Length of Longitudinal Bars

Input

Longitudinal Steel

Longitudinal Steel Area

$$A_{long} = 1.27 \text{ in}^2$$

Longitudinal Steel Diameter

$$d_{long} = 1.27 \text{ in}$$

Yield Strength of Longitudinal Steel

$$f_{y_long} = 60 \text{ ksi}$$

Development Length of Longitudinal Reinforcement

$$\Psi_t := 1.0$$

ACI 318-05 12.5.2

$$\Psi_e := 1.0$$

$$\Psi_s := 1$$

$$\lambda_s := 1.0$$

ACI 318-05 12.2.3

$$\frac{Cb + Ktr}{d_{long}} = 2.5$$

$$l_{dh_long} = \left[\left(\frac{3}{40} \right) \cdot \left(\frac{f_{y_long}}{\sqrt{\frac{f_c}{psi}} \cdot psi} \right) \cdot \frac{(\Psi_t \cdot \Psi_e \cdot \Psi_s \cdot \lambda)}{\left(\frac{Cb + Ktr}{d_{long}} \right)} \right] \cdot d_{long}$$

$$l_{dh_long} := \left[\left(\frac{3}{40} \right) \cdot \left(\frac{f_{y_long}}{\sqrt{\frac{f_c}{psi}} \cdot psi} \right) \cdot \frac{(\Psi_t \cdot \Psi_e \cdot \Psi_s \cdot \lambda)}{(2.5)} \right] \cdot d_{long}$$

$$l_{dh_long} = 36.14 \text{ in}$$

ACI 318-05 12.2.3

$$l_{d_long} := l_{dh_long}$$

$$l_{d_long} = 36.14 \text{ in}$$

ACI 318-05 12.2.5

+

Development Length of Longitudinal Bars

Length of steel pipe Required

Length of Stiffeners

$$L = 18 \text{ in}$$

Length of Breakout

$$l_{\text{breakout}} := 43 \text{ in}$$

Development Length of Longitudinal Reinforcement

$$l_{d_1} := 36 \text{ in}$$

$$l_{\text{br}} := \frac{(l_{\text{breakout}} - L)}{2} \quad l_{\text{br}} = 12.5 \text{ in}$$

Required Length of steel pipe Based on Breakout and Development Length

$$l_{\text{pipe}} := l_{\text{br}} + L + l_{d_1}$$

$$l_{\text{pipe}} = 66.5 \text{ in}$$

Length of steel pipe Required

Base Connection

Plate Properties - Annular Plate

Plate diameter

$$B_p := 36 \text{ in}$$

Yield strength

$$F_{y_plate} := 50 \text{ ksi}$$

Ultimate strength

$$F_{u_plate} := 60 \text{ ksi}$$

Diameter of the bolt

$$d_{\text{bolt}} := 1.5 \text{ in}$$

Center-to-center diameter of bolts

$$d_b := 30 \text{ in}$$

Thickness of plate

$$t_{\text{plate}} := 1.5 \text{ in}$$

Bolt Properties - D1" ASTM A325

Center to Center Radius of Bolts

$$r_b := 15 \text{ in}$$

Number of Bolts

$$\text{No_Bolts} := 22$$

Yield Strength of Bolts

$$f_{y_bolt_field} := 55 \text{ ksi}$$

Ultimate Strength of Bolts

$$f_{u_bolt} := 105 \text{ ksi}$$

Radius of the pipe

$$r_p := \frac{d_{\text{pipe}}}{2} = 12 \text{ in}$$

Diameter of the bolt

$$d_{\text{bolt}} := 1.5 \text{ in}$$

Bolt Bearing Strength

$$L_c := \frac{(B_p - d_b - .5 \cdot d_{\text{bolt}})}{2}$$

$$L_c = 2.62 \text{ in}$$

$$\phi_{\text{shear}} := .75 \quad F_{u_{\text{plate}}} := 60 \text{ ksi}$$

$$\phi R_n := 1.2 \cdot F_{u_{\text{plate}}} \cdot L_c \cdot t_{\text{plate}}$$

$$\phi R_n = 283.5 \text{ kip}$$

$$R_{n_{\text{parallel}}} := 2 \cdot \phi R_n$$

$$R_{n_{\text{parallel}}} = 567 \text{ kip}$$

$$T_{n_{\text{bolt_bearing}}} := \text{No_Bolts} \cdot R_{n_{\text{parallel}}} \cdot \left(\frac{d_b}{2} \right)$$

$$T_{n_{\text{bolt_bearing}}} = 15592.5 \text{ ft} \cdot \text{kip}$$

$$\text{Check_Bolt_Bearing} := \begin{cases} \text{"Sufficient Strength"} & \text{if } T_{n_{\text{bolt_bearing}}} \geq T_{n_{\text{blowout}}} \\ \text{"Insufficient Strength"} & \text{otherwise} \end{cases}$$

+

$$\text{Check_Bolt_Bearing} = \text{"Sufficient Strength"}$$

Check Bolt Spacing

$$s_{\text{req}} := 2.67 \cdot d_{\text{bolt}} \quad s_{\text{req}} = 4 \text{ in}$$

$$s_{\text{actual}} := \frac{\pi \cdot d_b}{\text{No_Bolts}} \quad s_{\text{actual}} = 4.28 \text{ in}$$

$$\text{Check_Bolt_Spacing} := \begin{cases} \text{"Sufficient"} & \text{if } s_{\text{actual}} \geq s_{\text{req}} \\ \text{"Insufficient"} & \text{otherwise} \end{cases}$$

$$\text{Check_Bolt_Spacing} = \text{"Sufficient"}$$

Check Bolt Shear

$$A_b := \pi \cdot (.5 \cdot d_{\text{bolt}})^2 = 1.77 \text{ in}^2$$

$$F_{nv} := .4 \cdot 120 \text{ ksi} = 48 \text{ ksi}$$

$$\phi V_n := \phi_{\text{shear}} \cdot A_b \cdot F_{nv}$$

$$\phi V_n = 63.62 \text{ kip}$$

$$V_{n_{\text{parallel}}} := \phi V_n \cdot 2$$

$$V_{n_{\text{parallel}}} = 127.23 \text{ kip}$$

$$T_{\text{bolt_shear}} := \text{No_Bolts} \cdot V_{n_{\text{parallel}}} \cdot \left(\frac{d_b}{2} \right)$$

$$T_{\text{bolt_shear}} = 3498.95 \text{ ft} \cdot \text{kip}$$

$$\text{Check_Bolt_Shear} := \begin{cases} \text{"Sufficient Strength"} & \text{if } T_{\text{bolt_shear}} \geq T_{n_{\text{blowout}}} \\ \text{"Insufficient Strength"} & \text{otherwise} \end{cases}$$

$$\text{Check_Bolt_Shear} = \text{"Sufficient Strength"}$$

Weld Design

Weld Connecting Annular Plate to Pipe

$$t_{\text{pipe}} = 0.58 \text{ in}$$

$$\text{Weld Size} := 0.5 \text{ in}$$

AISC Spec. J2
Table J2.4

Along edges of plates with thickness ≥ 0.25 in.,
Max weld size = $t - 1/16$ in.

$$F_{\text{electrode}} := 70 \text{ ksi}$$

+

$$F_{\text{W}} := .6 \cdot F_{\text{electrode}}$$

AISC Spec. J2
Table J2.5

$$\text{Throat} := .707 \cdot \text{Weld Size}$$

$$R_{\text{n_weld}} := \text{Throat} \cdot F_{\text{W}}$$

$$R_{\text{n_weld}} = 14.85 \frac{\text{kip}}{\text{in}}$$

$$R_{\text{n_yield}} := .6 \cdot F_{\text{y_pipe}} \cdot t_{\text{pipe}}$$

$$R_{\text{n_yield}} = 14.64 \frac{\text{kip}}{\text{in}}$$

$$R_{\text{n_rupture}} := .45 \cdot F_{\text{u_pipe}} \cdot t_{\text{pipe}}$$

$$R_{\text{n_rupture}} = 15.16 \frac{\text{kip}}{\text{in}}$$

$$R_{\text{n}} := \min(R_{\text{n_weld}}, R_{\text{n_yield}}, R_{\text{n_rupture}})$$

$$R_{\text{n}} = 14.64 \frac{\text{kip}}{\text{in}}$$

$$R_{\text{weld}} := R_{\text{n}} \cdot \pi \cdot d_{\text{pipe}}$$

$$R_{\text{weld}} = 1.1 \times 10^3 \text{ kip}$$

$$T_{\text{weld}} := R_{\text{weld}} \cdot \frac{d_{\text{pipe}}}{2}$$

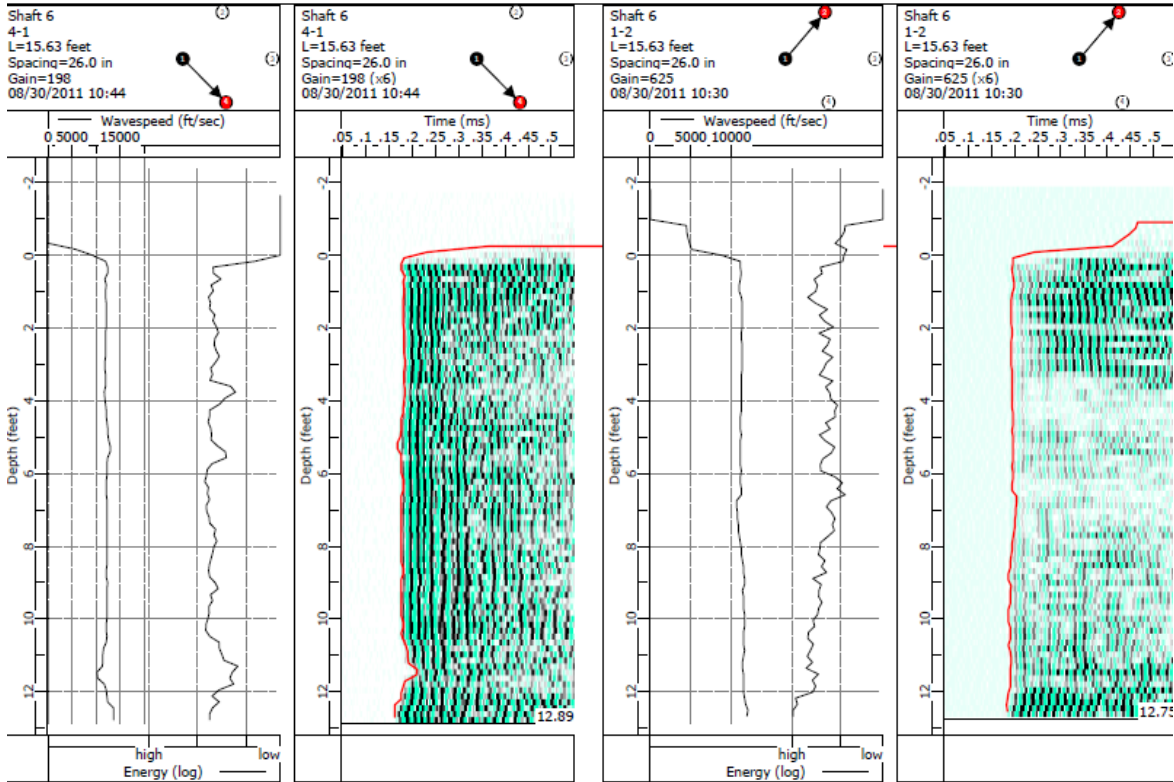
$$T_{\text{weld}} = 1103.92 \text{ ft} \cdot \text{kip}$$

$$M_{\text{weld}} := R_{\text{weld}} \cdot \frac{d_{\text{pipe}}}{2}$$

$$M_{\text{weld}} = 1103.92 \text{ ft} \cdot \text{kip}$$

▢ Base Connection

(a) TS1



(b) TS2

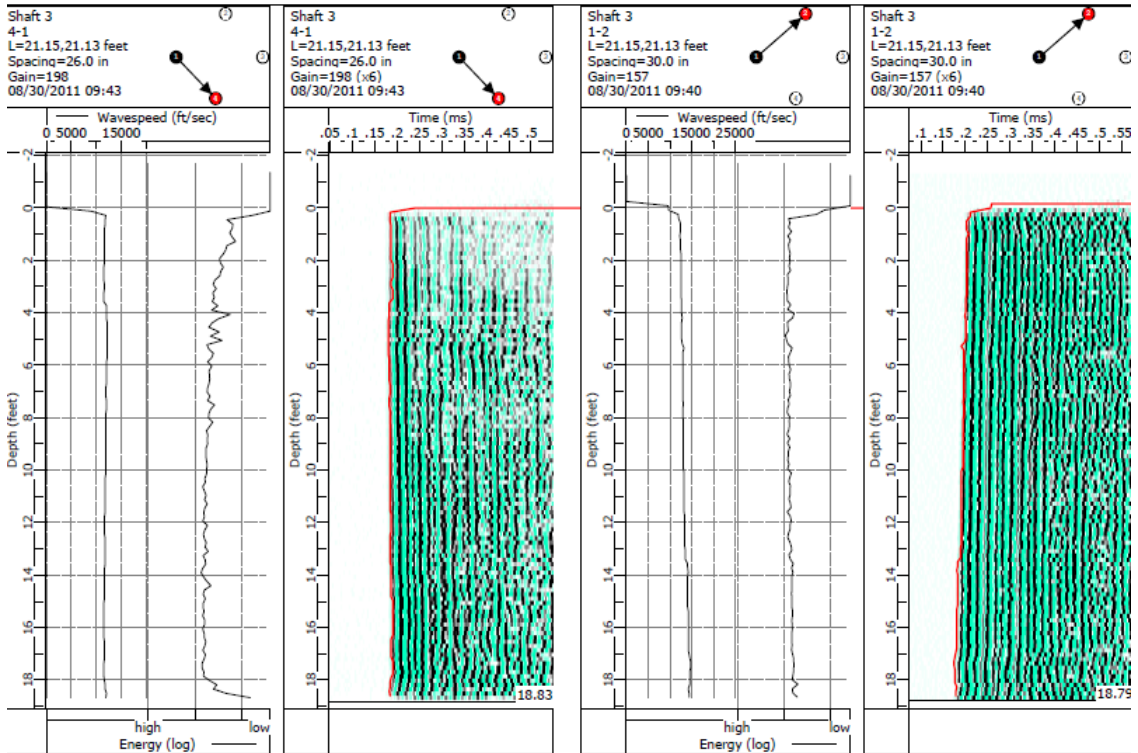


Figure B-3. CSL test results for Test shafts; (a) TS1, and (b) TS2

APPENDIX C: STRUCTURAL DESIGN OF PRECAST PILE AND CONCRETE CAP

Structural design of precast pile

Forces and Moments on foundation top

(Based on the expected torsional resistance of the pile and lateral load application at an eccentric distance of 35-ft)

$$T_u := 560 \text{kip}\cdot\text{ft}$$

$$P_n := 10.7 \text{kip}$$

$$M_x := 320 \text{kip}\cdot\text{ft}$$

$$V_x := 0.6 \text{kip}$$

$$M_z := 118 \text{kip}\cdot\text{ft}$$

$$V_z := 16 \text{kip}$$

$$M_u := \sqrt{M_x^2 + M_z^2}$$

$$M_u = 341.063 \text{kip}\cdot\text{ft}$$

$$V_u := \sqrt{V_x^2 + V_z^2}$$

$$V_u = 16.011 \text{kip}$$

▣ Pile Design - Flexural Capacity

Input

Check Flexural Capacity of pile

Width of pile

$$d_s := 28 \text{in}$$

Radius of pile

$$R_{\text{ww}} := \frac{d_s}{2} = 14 \text{in}$$

Area of shaft

$$A_s := (d_s)^2 \quad A_s = 784 \text{in}^2$$

Longitudinal Reinforcement

Number of Longitudinal Bars

$$n_{\text{long}} := 16$$

Yield Strength of Longitudinal Reinforcement

$$f_{y_long_steel} := 60 \text{ksi}$$

Longitudinal Steel Area

$$A_{\text{long_steel}} := 1 \text{in}^2$$

Number of Bars Yielded (Assumption)

$$n_{\text{long_yield}} := 9$$

Concrete strength

$$f_c := 5000 \text{psi}$$

$$\phi_{\text{flexure}} := 0.9$$

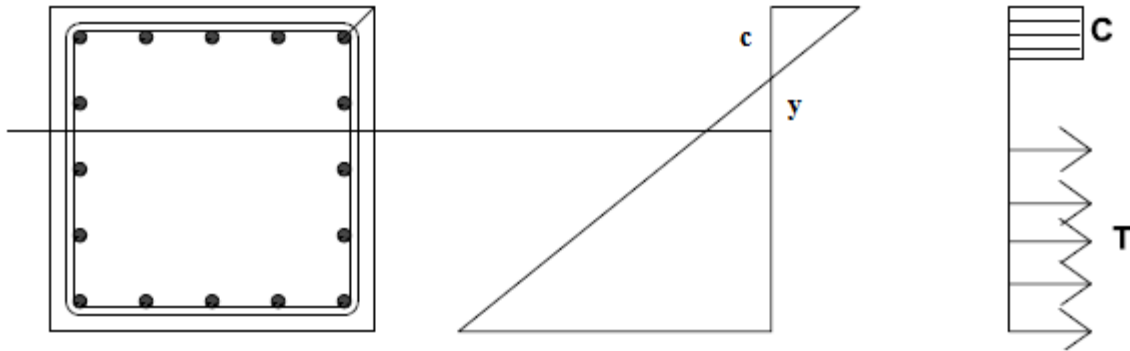


Figure C-1. ACI stress block diagram for precast pile

Calculations Using ACI Stress Block

$$\beta_1(f_c) := \begin{cases} .85 & \text{if } f_c < 4000\text{psi} \\ .65 & \text{if } f_c > 8000\text{psi} \\ \left[.85 - .05 \cdot \left[\frac{(f_c - 4000\text{psi})}{1000\text{psi}} \right] \right] & \text{if } 4000\text{psi} \leq f_c \leq 8000\text{psi} \end{cases} \quad \beta_1(f_c) = 0.8$$

ACI 10.2.7.3

$$A_{\text{comp}} := \frac{(n_{\text{long_yield}} \cdot A_{\text{long_steel}} \cdot f_{y_long_steel})}{.85 \cdot f_c} \quad A_{\text{comp}} = 127.059 \cdot \text{in}^2$$

$$a := \frac{A_{\text{comp}}}{d_s} \quad a = 4.538 \cdot \text{in}$$

$$c := \frac{a}{\beta_1(f_c)} \quad c = 5.672 \cdot \text{in}$$

$$y := .002 \cdot \frac{c}{.003} \quad y = 3.782 \cdot \text{in}$$

$$d_{\text{bar}} := \begin{pmatrix} 21.936 \\ 30.1 \\ 37.21 \\ 42.03 \end{pmatrix} \text{in} \quad d_{\text{bar}_0} = 21.936 \cdot \text{in} \quad A_{\text{long_steel}} = 1 \cdot \text{in}^2$$

$$d_{\text{bars}} := \frac{+ 14\text{in} \cdot A_{\text{long_steel}}^2 + 19.6985\text{in} \cdot A_{\text{long_steel}}^2 + 25.397\text{in} \cdot A_{\text{long_steel}}^5}{n_{\text{long_yield}} \cdot A_{\text{long_steel}}} \quad d_{\text{bars}} = 21.598 \cdot \text{in}$$

$$M_{n_pile} := \phi_{\text{flexure}} \cdot n_{\text{long_yield}} \cdot A_{\text{long_steel}} \cdot f_{y_long_steel} \cdot \left(d_{\text{bars}} - \frac{a}{2} \right) \quad M_{n_pile} = 782.828 \cdot \text{kip}\cdot\text{ft}$$

$$\text{Flexure_Check} := \begin{cases} \text{"Insufficient"} & \text{if } M_{n_pile} \leq M_u \\ \text{"Sufficient"} & \text{otherwise} \end{cases} \quad \text{Flexure_Check} = \text{"Sufficient"}$$

Check Shear Capacity of pile

Input

Gross cross-sectional area

$$A_g := d_s^2 = 784 \cdot \text{in}^2$$

Axial load

$$N_u := 0$$

Effective depth of the section

$$d := d_s$$

Area in compression

$$A_{\text{comp}} = 127.059 \cdot \text{in}^2$$

Hoop Steel Area

$$A_{\text{hoop_steel}} := 0.31 \cdot \text{in}^2$$

Hoop Steel Diameter

$$d_{\text{hoop_steel}} := 0.625 \cdot \text{in}$$

Spacing of Hoop Steel

$$s_{\text{hoop_steel}} := 2.5 \cdot \text{in}$$

Yield Strength of Hoop Steel

$$f_{y_hoop_steel} := 60 \cdot \text{ksi}$$

Centerline of Hoop Steel width

$$d_h := 24.375 \cdot \text{in}$$

$$\phi_{\text{shear}} := 0.85$$

Shear Capacity of the Concrete

$$V_c := 2 \sqrt{\frac{f_c}{\text{psi}}} \cdot \text{psi} \cdot 28 \cdot \text{in} \cdot d$$

$$V_c = 110.874 \cdot \text{kip}$$

Shear Capacity of the Steel

$$V_s := \frac{(2 \cdot A_{\text{hoop_steel}} \cdot f_{y_hoop_steel} \cdot d_h)}{s_{\text{hoop_steel}}}$$

$$V_s = 362.7 \cdot \text{kip}$$

Shear Capacity of the pile

$$V_{n_shaft} := \phi_{\text{shear}} \cdot (V_c + V_s)$$

$$V_{n_shaft} = 402.538 \cdot \text{kip}$$

$$\text{Check_Shear_Strength} := \begin{cases} \text{"Insufficient"} & \text{if } V_{n_shaft} \leq V_u \\ \text{"Sufficient"} & \text{otherwise} \end{cases}$$

$$\text{Check_Shear_Strength} = \text{"Sufficient"}$$

Check Axial Capacity of the pile

Input

Longitudinal Reinforcement

Number of Longitudinal Bars

$$n_{\text{long}} = 16$$

Yield Strength of Longitudinal Reinforcement

$$f_{y_long_steel} = 60\text{-ksi}$$

Longitudinal Steel Area

$$A_{\text{long_steel}} = 1\text{-in}^2$$

Number of Bars Yielded (Assumption)

Hoop Steel

Hoop Steel Area

$$A_{\text{hoop_steel}} = 0.31\text{-in}^2$$

Hoop Steel Diameter

$$d_{\text{hoop_steel}} = 0.625\text{-in}$$

Spacing of Hoop Steel

$$s_{\text{hoop_steel}} = 2.5\text{-in}$$

Yield Strength of Hoop Steel

$$f_{y_hoop_steel} = 60\text{-ksi}$$

Center to center distance of Hoop Steel legs

$$d_h = 24.375\text{-in}$$

$$\phi_{\text{comp}} = 0.9$$

Axial Capacity of the Shaft

Area of the tied core

$$A_c = d_h^2$$

$$P_{\text{shaft}} := f_c \cdot (A_c - n_{\text{long}} \cdot A_{\text{long_steel}}) + f_{y_long_steel} \cdot n_{\text{long}} \cdot A_{\text{long_steel}}$$

$$P_{\text{shaft}} = 3.851 \times 10^3 \cdot \text{kip}$$

$$P_{D_shaft} := \phi_{\text{comp}} P_{\text{shaft}}$$

$$P_{D_shaft} = 3465.6328 \cdot \text{kip}$$

$$\text{Check_Axial_Strength} := \begin{cases} \text{"Insufficient"} & \text{if } P_{D_shaft} \leq P_n \\ \text{"Sufficient"} & \text{otherwise} \end{cases}$$

$$\text{Check_Axial_Strength} = \text{"Sufficient"}$$

Check Torsional Capacity of the pile

Input

Area of pile

$$A_{cp} := A_s = 784 \cdot \text{in}^2$$

Perimeter of the shaft

$$p_{cp} := 4 \cdot d_s = 112 \cdot \text{in}$$

Longitudinal Reinforcement

Number of Longitudinal Bars

$$n_{\text{long}} = 16$$

Yield Strength of Longitudinal Reinforcement

$$f_{y_long_steel} = 60 \cdot \text{ksi}$$

+

Longitudinal Steel Area

$$A_{\text{long_steel}} = 1 \cdot \text{in}^2$$

Hoop Steel

Hoop Steel Area

$$A_{\text{hoop_steel}} = 0.31 \cdot \text{in}^2$$

Hoop Steel Diameter

$$d_{\text{hoop_steel}} = 0.625 \cdot \text{in}$$

Spacing of Hoop Steel

$$s_{\text{hoop_steel}} = 2.5 \cdot \text{in}$$

Yield Strength of Hoop Steel

$$f_{y_hoop_steel} = 60 \cdot \text{ksi}$$

Center to center distance of Hoop Steel legs

$$d_h = 24.375 \cdot \text{in}$$

$$\phi_{\text{torsion}} := 0.85$$

Threshold Torsion

$$T_{\text{threshold}} := \sqrt{\frac{f_c}{\text{psi}}} \cdot \text{psi} \cdot \frac{(A_{cp})^2}{p_{cp}}$$

+

$$T_{\text{threshold}} = 32.338 \cdot \text{kip-ft}$$

ACI 11.6.1a

$$\text{Neglect_Torsion} := \begin{cases} \text{"Yes"} & \text{if } \phi_{\text{torsion}} \cdot T_{\text{threshold}} \geq T_u \\ \text{"No"} & \text{otherwise} \end{cases}$$

$$\text{Neglect_Torsion} = \text{"No"}$$

Cracking Torsion

$$T_{cr} := 4 \cdot \sqrt{\frac{f_c}{\text{psi}}} \cdot \text{psi} \cdot \left(\frac{A_{cp})^2}{p_{cp}} \right)$$

$$T_{cr} = 129.353 \cdot \text{kip-ft}$$

ACI R11.6.1

Nominal Torsional Strength

$$A_o := (d_h)^2$$

$$A_t := A_{\text{hoop_steel}}$$

$$A_t = 0.31 \cdot \text{in}^2$$

$$\theta := 45 \text{deg}$$

$$T_{n_torsion} := \frac{2 \cdot A_o \cdot A_t \cdot f_{y_hoop_steel}}{s_{hoop_steel}} \cdot \cot(\theta)$$

$$\theta = 0.785$$

$$T_{n_torsion} = 736.734 \text{ kip}\cdot\text{ft}$$

$$\text{Check_Torsion_Shaft} := \begin{cases} \text{"Insufficient"} & \text{if } T_{n_torsion} \leq T_u \\ \text{"Sufficient"} & \text{otherwise} \end{cases}$$

$$\text{Check_Torsion_Shaft} = \text{"Sufficient"}$$

▣ Pile Design - Torsional Capacity

Design of Concrete cap for jet-grouted pile

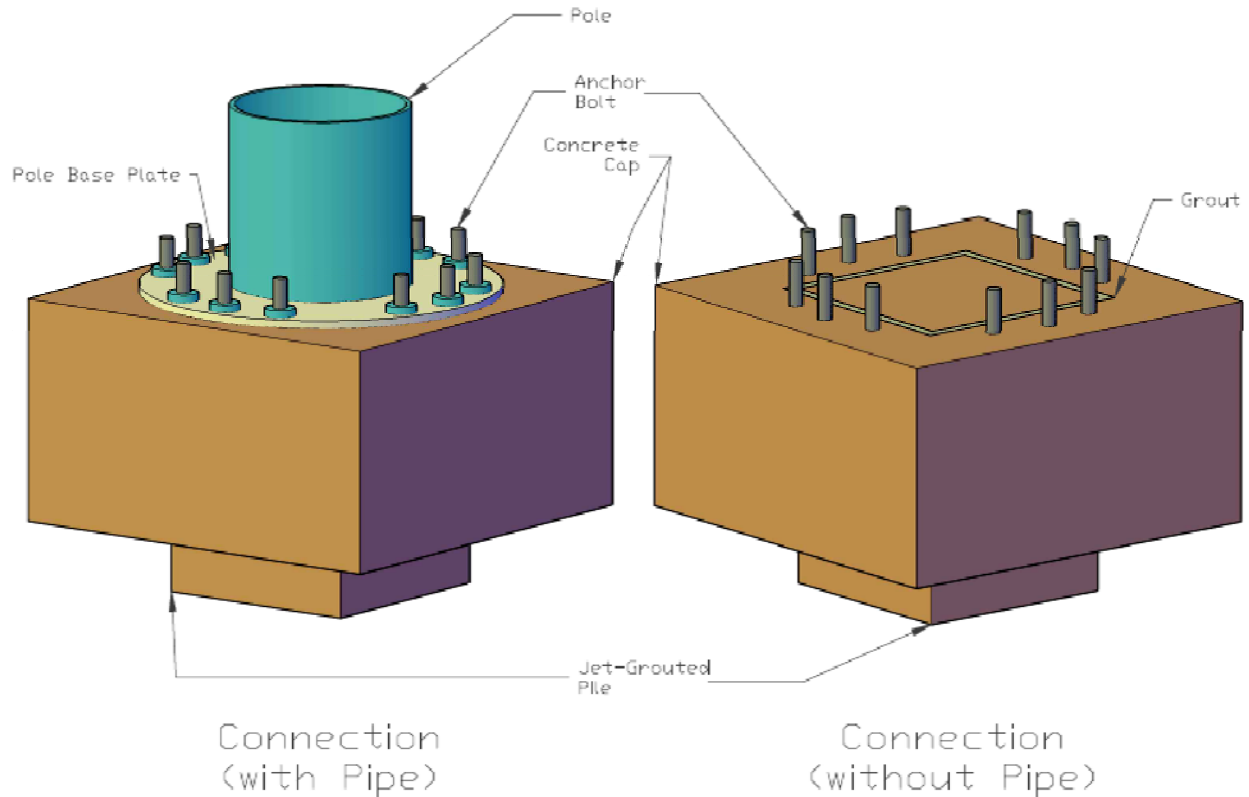


Figure C-2. Three dimensional view of concrete cap – pile connection

Forces and Moments during torsion test:

$$M_x := 320\text{kip}\cdot\text{ft}$$

$$M_y := 560\text{kip}\cdot\text{ft}$$

$$M_z := 118\text{kip}\cdot\text{ft}$$

$$V_x := 0.6\text{kip}$$

$$V_y := 8.6\text{kip}$$

$$V_z := 16\text{kip}$$

Input:

$$\#AnchorRods := 16$$

$$d_{rod} := 1.5\text{in}$$

$$A_{gross,rod} := \frac{\pi}{4} \cdot (d_{rod})^2$$

$$Diameter_{baseplate} := 50\text{in}$$

$$Diameter_{boltcircle} := 43\text{in}$$

$$I_{rod,group} := \frac{\#AnchorRods}{2} \cdot A_{gross,rod} \cdot \left(\frac{Diameter_{boltcircle}}{2} \right)^2$$

$$I_{rod,group} = 6534.91\text{in}^4$$

$$S_{rod,group} := \frac{I_{rod,group}}{\frac{Diameter_{boltcircle}}{2}}$$

$$S_{rod,group} = 303.9\text{in}^3$$

Design of Anchor bolts:

A) Bolt load

1) Using the approach given in FDOT MastArm v4.3 program

a) Using AASHTO anchor bolt CSR calculation

AASHTO 5.17

$$M_{\text{csr}} := \frac{\sqrt{(M_x)^2 + (M_z)^2}}{C_a} \quad C_a := 1 \quad M_{\text{csr}} = 341.1 \cdot \text{kip} \cdot \text{ft}$$

$$T_{\text{u.rod}} := \left(\frac{M_{\text{csr}}}{S_{\text{rod.group}}} \right) \cdot A_{\text{gross.rod}} \quad T_{\text{u.rod}} = 23.8 \cdot \text{kip}$$

$$V_{\text{csr}} := \sqrt{(V_x)^2 + (V_z)^2} \quad V_{\text{csr}} = 16.0 \cdot \text{kip}$$

$$V_{\text{u.rod}} := \frac{V_{\text{csr}}}{\# \text{AnchorRods}} + \frac{(M_y)}{\left(\frac{\text{Diameter}_{\text{boltcircle}}}{2} \right) \cdot \# \text{AnchorRods}} \quad V_{\text{u.rod}} = 20.5 \cdot \text{kip}$$

$$A_{\text{net.rod}} := \frac{\pi}{4} \cdot \left(d_{\text{rod}} - \frac{0.9743}{\frac{4}{\text{in}}} \right)^2 \quad A_{\text{net.rod}} = 1.24 \cdot \text{in}^2 \quad \text{AASHTO Eqn 5-23}$$

$$f_{\text{t.rod}} := \frac{T_{\text{u.rod}}}{A_{\text{net.rod}}} \quad f_{\text{t.rod}} = 19.192 \cdot \text{ksi}$$

$$f_{\text{v.rod}} := \frac{V_{\text{u.rod}}}{A_{\text{net.rod}}} \quad f_{\text{v.rod}} = 16.563 \cdot \text{ksi}$$

+

$$F_{y.\text{rod}} := 55 \cdot \text{ksi}$$

$$F_{\text{t.rod}} := 0.5 \cdot F_{y.\text{rod}} \quad F_{\text{t.rod}} = 27.5 \cdot \text{ksi} \quad \text{AASHTO Eqn 5-21}$$

$$F_{\text{v.rod}} := 0.3 \cdot F_{y.\text{rod}} \quad F_{\text{v.rod}} = 16.5 \cdot \text{ksi} \quad \text{AASHTO Eqn 5-22}$$

$$\text{CSR}_{\text{rod}} := \left(\frac{f_{\text{t.rod}}}{1.33 \cdot F_{\text{t.rod}}} \right)^2 + \left(\frac{f_{\text{v.rod}}}{1.33 \cdot F_{\text{v.rod}}} \right)^2 \quad \text{CSR}_{\text{rod}} = 0.845 \quad \text{AASHTO Eqn 5-24}$$

b) Using the AISC LRFD Code, 2nd Edition

(Design of bolts based on "Design Guide for Steel to Concrete Connections by Cook, Doerr & Klingner) (Research Report 1126-4F by the Bureau of Engineering Research at the Univ. of Texas at Austin)

$$T_{u,rod,old} := 1.3 \cdot T_{u,rod} \quad T_{u,rod,old} = 30.9\text{-kip}$$

$$V_{u,rod,old} := 1.3 \cdot V_{u,rod} \quad V_{u,rod,old} = 26.7\text{-kip}$$

$$A_{net,rod,old} := 0.75 \cdot \pi \cdot \left(\frac{d_{rod}}{2} \right)^2 \quad A_{net,rod,old} = 1.33\text{-in}^2$$

$$F_{u,rod} := 75\text{-ksi}$$

$$T_{s,rod} := A_{net,rod,old} \cdot F_{u,rod} \quad T_{s,rod} = 99.4\text{-kip}$$

$$\gamma := 0.5 \quad (\text{property of embedded rods}) \quad T_{n,rod} := \sqrt{T_{s,rod}^2 - \left(\frac{V_{u,rod}}{\gamma} \right)^2} \quad 0.75 \cdot T_{n,rod} = 67.9\text{-kip}$$

(if greater than actual rod tension, bolts are OK)

$$PR_{rod} := \frac{T_{u,rod,old}}{0.75 \cdot T_{n,rod}} \quad PR_{rod} = 0.456$$

II) Using ACI 318-08

Steel strength of anchor in tension (ACI 318-08, D.5.1):

The nominal strength of single anchor in tension:

$$N_{sa} := A_{net,rod} \cdot F_{u,rod} \quad N_{sa} = 92.987\text{-kip} \quad \text{ACI 318-08, D.5, Eq. D-3}$$

$$M_u := \sqrt{(1.7M_x)^2 + (1.4M_z)^2} \quad M_u = 568.5\text{-kip}\cdot\text{ft} \quad \text{load factor based on ACI 318-08, Appendix C.9.2}$$

$$T_{u,bolt} := \left(\frac{M_u}{S_{rod,group}} \right) \cdot A_{gross,rod} \quad T_{u,bolt} = 39.7\text{-kip}$$

$$\phi_{tension} := 0.8 \quad \text{ACI 318-08, Appendix D.4.5} \quad \phi_{tension} \cdot N_{sa} = 74.39\text{-kip}$$

$$\text{Check_strength_in_tension} := \begin{cases} \text{"Sufficient Strength"} & \text{if } \phi_{\text{tension}} \cdot N_{\text{sa}} \geq T_{\text{u,bolt}} \\ \text{"Insufficient Strength"} & \text{otherwise} \end{cases}$$

Check_strength_in_tension = "Sufficient Strength"

Steel strength of anchor in shear (ACI 318-08, D.6.1):

The nominal strength of anchor group:

$$V_{\text{sa}} := \# \text{AnchorRods} \cdot 0.6 \cdot A_{\text{net,rod}} \cdot F_{\text{u,rod}} \quad V_{\text{sa}} = 892.679 \cdot \text{kip} \quad \text{ACI 318-08, D.6, Eq. D-20}$$

$$V_{\text{u,total}} := 1.7V_{\text{csr}} + \frac{(1.7M_y)}{\left(\frac{\text{Diameter}_{\text{boltcircle}}}{2}\right)} \quad V_{\text{u,total}} = 558.568 \cdot \text{kip} \quad \text{load factor based on ACI 318-08, Appendix C.9.2}$$

$$\phi_{\text{shear}} := 0.75 \quad \text{ACI 318-08, Appendix D.4.5} \quad \phi_{\text{shear}} \cdot V_{\text{sa}} = 669.51 \cdot \text{kip}$$

$$\text{Check_strength_in_shear} := \begin{cases} \text{"Sufficient Strength"} & \text{if } \phi_{\text{shear}} \cdot V_{\text{sa}} \geq V_{\text{u,total}} \\ \text{"Insufficient Strength"} & \text{otherwise} \end{cases}$$

Check_strength_in_shear = "Sufficient Strength"

B) Pullout strength of anchor in tension (ACI 318-08, D.5.3):

The bearing area will be provided by welding a bearing plate at the tip of anchor bolt in accordance with American Welding Society code (AWS D1)

Net bearing area for bearing plate (ASTM A36) Reference: FDOT Design Standard Index
with a diameter = 3.1 in No: 17515

$$A_{\text{brg}} := \frac{\pi}{4} \cdot (3.1^2 - 1.5^2) \text{ in}^2 \quad A_{\text{brg}} = 5.781 \cdot \text{in}^2$$

$$f_c := 5000 \text{ psi}$$

Pullout strength of a single headed bolt in tension

$$N_p := 8 \cdot A_{\text{brg}} \cdot f_c \quad N_p = 231.221 \cdot \text{kip}$$

$$\psi_{\text{cp}} := 1$$

$$\text{Nominal pullout strength} \quad N_{\text{pn}} := \psi_{\text{cp}} \cdot N_p \quad N_{\text{pn}} = 231.221 \cdot \text{kip}$$

$$\phi_{\text{pullout}} := 0.85$$

$$\phi_{\text{pullout}} \cdot N_{\text{pn}} = 196.538\text{-kip}$$

$$\text{Tensile force on single anchor } T_{\text{u.bolt}} = 39.665\text{-kip}$$

$$\text{Check_pullout_strength} := \begin{cases} \text{"Sufficient Strength"} & \text{if } \phi_{\text{tension}} \cdot N_{\text{pn}} \geq T_{\text{u.bolt}} \\ \text{"Insufficient Strength"} & \text{otherwise} \end{cases}$$

$$\text{Check_pullout_strength} = \text{"Sufficient Strength"}$$

C) Concrete breakout strength of anchor in shear (ACI 318-08, D.6.2)

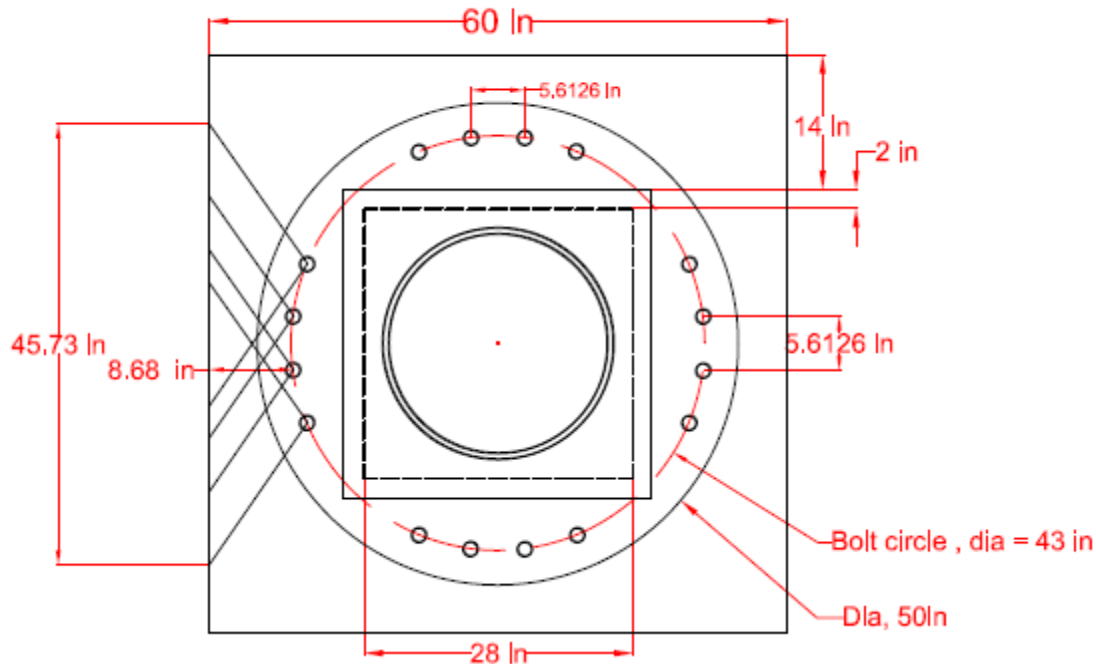


Figure C-3. Concrete breakout failure of anchors in shear

$$c_{a1} := 8.68\text{in}$$

$$A_{Vco} := 4.5 \cdot c_{a1}^2$$

$$A_{Vco} = 339.041\text{-in}^2$$

There is group effect of anchors as shown in the above figure

Therefore:

$$A_{Vc} := 4 \cdot (45.73\text{in} - 1.5 \cdot c_{a1})$$

$$A_{Vc} = 2.382 \times 10^3\text{-in}^2$$

$$l_e := 8 \cdot d_{\text{rod}}$$

$$\lambda := 1$$

$$l_e = 12\text{-in}$$

$$V_b := 7 \cdot \left(\frac{l_e}{d_{\text{rod}}} \right)^{0.2} \cdot \sqrt{\frac{d_{\text{rod}}}{\text{in}}} \cdot \lambda \cdot \sqrt{\frac{f_c}{\text{psi}}} \cdot \left(\frac{c_{a1}}{\text{in}} \right)^{1.5} \cdot \text{lbf}$$

$$V_b = 23.498\text{-kip} \quad \text{ACI 318-08, D.5, Eq. D-22}$$

$$\psi_{cV} := 1.4$$

$$\psi_{ecV} := 1.0$$

$$\psi_{edV} := 1.0$$

$$\psi_{hV} := 1.0$$

$$V_{cbg} := \left(\frac{A_{Vc}}{A_{Vco}} \right) \cdot \psi_{ecV} \cdot \psi_{edV} \cdot \psi_{cV} \cdot \psi_{hV} \cdot V_b \quad \text{ACI 318-08, D.5, Eq. D-22}$$

$$V_{cbg} = 231.086 \cdot \text{kip}$$

$$V_{cbg_parallel} := 2 \cdot V_{cbg} \quad V_{cbg_parallel} = 462.173 \cdot \text{kip} \quad \text{ACI 318-08, D.6.2.1}$$

Torsional strength:

$$\text{Torsion}_{n_breakout_ACI} := V_{cbg_parallel} \cdot \left(\frac{\text{Diameter}_{boltcircle}}{2} \right)$$

$$\text{Torsion}_{n_breakout_ACI} = 828.06 \cdot \text{kip} \cdot \text{ft}$$

$$\phi_{breakout} := 0.85 \quad \text{ACI 318-08, D.4.5}$$

$$\phi_{breakout} \cdot \text{Torsion}_{n_breakout_ACI} = 703.851 \cdot \text{kip} \cdot \text{ft}$$

D) Side-face blowout strength

ACI 318-08, D.5.4

$$N_{sb} := 160 \cdot c_{a1} \cdot \sqrt{A_{brg}} \cdot f_c^{.5} \cdot \text{psi}^{.5}$$

$$N_{sb} = 236.107 \cdot \text{kip}$$

$$\text{spacing between anchors } s_{a1} := 5.613 \text{in}$$

For multiple headed anchors:

$$N_{sbg} := \left(1 + \frac{s}{6 \cdot c_{a1}} \right) \cdot N_{sb}$$

$$N_{sbg} = 261.554 \cdot \text{kip}$$

$$\phi_{t,blowout} := 0.85 \quad \text{ACI 318-08, Appendix D.4.5}$$

$$+ \phi_{t,blowout} \cdot N_{sbg} = 222.321 \cdot \text{kip}$$

$$T_{u,\text{total}} := T_{u,\text{rod}} \cdot \frac{\#\text{AnchorRods}}{2} \quad T_{u,\text{total}} = 190.361 \cdot \text{kip}$$

$$\text{Check_strength_in_sideface_blowout} := \begin{cases} \text{"Sufficient Strength"} & \text{if } \phi_{t,\text{blowout}} \cdot N_{\text{sbg}} \geq T_{u,\text{total}} \\ \text{"Insufficient Strength"} & \text{otherwise} \end{cases}$$

Check_strength_in_sideface_blowout = "Sufficient Strength"

E) Concrete pryout strength in shear ACI 318-08, D.6.3

Actual $H_{\text{ef}} := 25\text{in}$

From the figure shown below $C_{a,\text{max}} := 22.17\text{in}$ $C_{a,\text{min}} := 8.68\text{in}$

Max. spacing between anchors $S_{\text{anch}} := 5.61\text{in}$

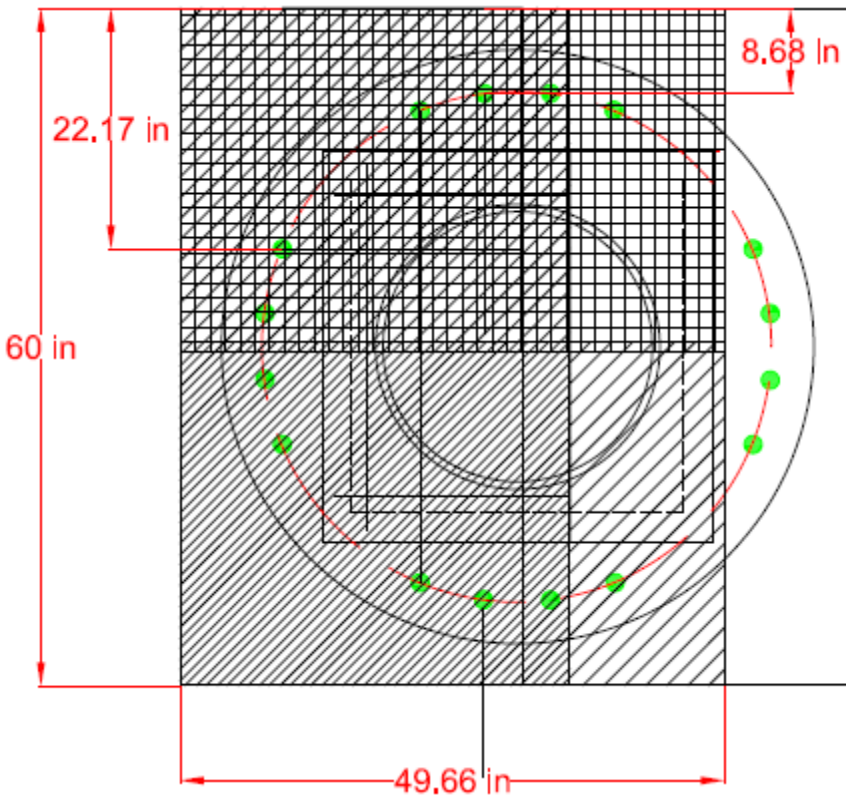


Figure C-4. Concrete pryout failure of anchors in shear

As all the edge distance are less than $1.5 h_{\text{ef}}$

Therefore $h_{\text{ef}} := \max\left(\frac{S_{\text{anch}}}{3}, \frac{C_{a,\text{max}}}{1.5}\right) \quad h_{\text{ef}} = 14.78\text{-in} \quad \text{ACI 318-08, D.5.2}$

$\psi_{cN} := 1.0$

$\psi_{ecN} := 1.0$

$$\psi_{edN} := 0.7 + 0.3 \cdot \frac{C_{a_{min}}}{h_{ef}} \quad \psi_{edN} = 0.876$$

$$\psi_{cpN} := 1.0$$

Basic concrete breakout strength of a single anchor in tension

$$N_b := k_c \cdot \lambda \cdot \left(\sqrt{\frac{f_c}{\text{psi}}} \right) \cdot \text{lb} \cdot \left(\frac{h_{ef}}{\text{in}} \right)^{1.5} \quad k_c := 24 \quad \text{ACI 318-08, D.5.2.2, Eq. D-7}$$

$$N_b = 96.429 \cdot \text{kip}$$

Projected concrete failure area of a single anchor with edge distance equal to or greater than equal to $1.5h_{ef}$:

$$A_{Nco} := 9 \cdot h_{ef}^2 \quad A_{Nco} = 1966.036 \cdot \text{in}^2 \quad \text{ACI 318-08, D.5.2.2, EQ. D-6}$$

Projected failure area of group in the present case:

$$A_{Nc} := 49.66 \text{in} \cdot 60 \text{in} \quad A_{Nc} = 2979.6 \cdot \text{in}^2$$

$$N_{cbg} := \frac{A_{Nc}}{A_{Nco}} \cdot \psi_{ecN} \cdot \psi_{edN} \cdot \psi_{ecN} \cdot \psi_{cpN} \cdot N_b \quad N_{cbg} = 128.047 \cdot \text{kip}$$

Concrete pryout strength

$$k_{cp} := 2$$

$$V_{cpg} := k_{cp} \cdot N_{cbg} \quad V_{cpg} = 256.094 \cdot \text{kip} \quad \text{ACI 318-08, D.6.3.1, EQ. D-31}$$

$$\phi_{t,pryout} := 0.85 \quad \text{ACI 318-08, Appendix D.4.5}$$

$$\phi_{t,pryout} \cdot V_{cpg} = 217.68 \cdot \text{kip}$$

$$T_{u,total} = 190.361 \cdot \text{kip}$$

$$\text{Check_strength_in_concrete_pryout} := \begin{cases} \text{"Sufficient Strength"} & \text{if } \phi_{t,pryout} \cdot V_{cpg} \geq T_{u,total} \\ \text{"Insufficient Strength"} & \text{otherwise} \end{cases}$$

$$\text{Check_strength_in_concrete_pryout} = \text{"Sufficient Strength"}$$

Reinforcement for concrete cap

A) Check Flexural Capacity of cap

Central section of the cap is considered to check flexural capacity

Longitudinal Reinforcement

Yield Strength of Longitudinal Reinforcement

$$f_{y_steel} := 60\text{ksi}$$

Longitudinal Steel Area

$$A_{steel} := 1\text{in}^2$$

Number of tensile rebars (#9 bars)

$$n_{bar_tensile} := 6$$

Concrete strength

$$f_c := 5000\text{psi}$$

$$\phi_{flexure} := 0.9$$

Calculations Using ACI Stress Block

$$\beta_1(f_c) := \begin{cases} .85 & \text{if } f_c < 4000\text{psi} \\ .65 & \text{if } f_c > 8000\text{psi} \\ \left[.85 - .05 \cdot \left[\frac{(f_c - 4000\text{psi})}{1000\text{psi}} \right] \right] & \text{if } 4000\text{psi} \leq f_c \leq 8000\text{psi} \end{cases}$$

$$\beta_1(f_c) = 0.8$$

ACI-318 10.2.7.3

$$A_{comp} := \frac{(n_{bar_tensile} \cdot A_{steel} \cdot f_{y_steel})}{.85 \cdot f_c}$$

$$A_{comp} = 84.706\text{-in}^2$$

$$a := \frac{A_{comp}}{24\text{in}} \quad a = 3.529\text{-in}$$

$$d_{bars} := 26.25\text{in}$$

$$M_{n_cap} := \phi_{flexure} \cdot n_{bar_tensile} \cdot A_{steel} \cdot f_{y_steel} \cdot \left(d_{bars} - \frac{a}{2} \right)$$

$$M_{n_cap} = 661.103\text{-kip}\cdot\text{ft}$$

$$M_{u_cap} := 1.7 \cdot \max(M_x, M_y)$$

$$M_{u_cap} = 544\text{-kip}\cdot\text{ft}$$

$$\text{Flexure_Check} := \begin{cases} \text{"Insufficient"} & \text{if } M_{n_cap} \leq M_{u_cap} \\ \text{"Sufficient"} & \text{otherwise} \end{cases}$$

$$\text{Flexure_Check} = \text{"Sufficient"}$$

Minimum flexural reinforcement

ACI 318-08, 10.5.1

$$A_{s_min} := \frac{3 \cdot \left(\frac{f_c}{\text{psi}} \right)^{0.5} \cdot \text{psi} \cdot 24 \text{in} \cdot d_{\text{bars}}}{f_{y_steel}}$$

$$A_{s_min} = 2.227 \cdot \text{in}^2$$

$$A_{s_tensile_provided} := n_{\text{bar_tensile}} \cdot A_{\text{steel}}$$

$$A_{s_tensile_provided} = 6 \cdot \text{in}^2$$

OK

B) Nominal torsional strength of cap

Hoop Steel

Hoop Steel Area

$$A_{\text{hoop_steel}} := 0.31 \text{in}^2$$

Hoop Steel Diameter

$$d_{\text{hoop_steel}} := 0.625 \text{in}$$

Spacing of Hoop Steel

$$s_{\text{hoop_steel}} := 4.46 \text{in}$$

Yield Strength of Hoop Steel

$$f_{y_hoop_steel} := 60 \text{ksi}$$

number of hoop steel per section

$$\text{num} := 4$$

Center to center distance of outer Hoop Steel bars

$$d_h := 54 \text{in}$$

$$\phi_{\text{torsion}} := 0.75$$

$$A_{\text{oh}} := (53.375 \text{in})^2$$

$$A_t := A_{\text{hoop_steel}} \quad A_t = 0.31 \text{in}^2$$

$$A_o := 0.85 \cdot A_{\text{oh}}$$

$$\theta := 45 \text{deg}$$

$$\theta = 0.785$$

$$\text{Torsion}_n := \frac{4 \cdot A_o \cdot A_t \cdot f_{y_hoop_steel}}{s_{\text{hoop_steel}}} \cdot \cot(\theta)$$

$$\text{Torsion}_n = 3.366 \times 10^3 \cdot \text{kip} \cdot \text{ft}$$

$$\phi_{\text{torsion}} \cdot \text{Torsion}_n = 2524.7 \cdot \text{kip} \cdot \text{ft}$$

$$\text{Torsion}_u := 1.7 \cdot M_y$$

$$\text{Check_Torsion_cap} := \begin{cases} \text{"Insufficient"} & \text{if } \phi_{\text{torsion}} \cdot \text{Torsion}_n \leq \text{Torsion}_u \\ \text{"Sufficient"} & \text{otherwise} \end{cases}$$

Check_Torsion_cap = "Sufficient"

Shear check for cap section

$$\text{Shear force} \quad \text{Shear} := \frac{M_y}{28\text{in}} \quad \text{Shear} = 240\text{-kip}$$

Shear Capacity of the Concrete

$$V_c := 2 \sqrt{\frac{f_c}{\text{psi}}} \cdot \text{psi} \cdot 14\text{in} \cdot 36\text{in} \quad V_c = 71.276\text{-kip}$$

Shear resistance provided by shear reinforcement

$$A_v := 2 \cdot 0.306\text{in}^2 \quad \text{spacing} := 3.05\text{in} \quad d := 23.75\text{in} \quad f_{yt} := 60\text{ksi}$$

$$V_s := \frac{A_v \cdot f_{yt} \cdot d}{\text{spacing}} \quad V_s = 285.934\text{-kip}$$

Shear Capacity of the section

$$\phi_{sr} := 0.85$$

$$V_{n_section} := \phi_{sr} \cdot (V_c + V_s)$$

$$V_{n_section} = 303.629\text{-kip}$$

$$V_{n_section} > \text{Shear}$$

C) Anchor bolt embedment

$$d_{\text{vertical_bar}} := d_{\text{hoop_steel}} = 0.625\text{-in}$$

Development length for vertical. reinforcement (#5 bars)

$$\Psi_t := 1.0$$

ACI 318-08 12.2.4

$$\Psi_e := 1.0$$

$$\Psi_s := 1$$

$$\lambda := 1.0 \quad \frac{Cb + Ktr}{d_{\text{long}}} = 2.5$$

$$l_d = \left[\left(\frac{3}{40} \right) \cdot \left(\frac{f_{y_steel}}{\lambda \cdot \sqrt{\frac{f_c}{\text{psi}} \cdot \text{psi}}} \right) \cdot \left(\frac{\Psi_t \cdot \Psi_e \cdot \Psi_s}{\left(\frac{Cb + Ktr}{d_{\text{long}}} \right)} \right) \right] \cdot d_{\text{vertical_bar}}$$

ACI 318-08 12.2.3

$$l_d := \left[\left(\frac{3}{40} \right) \cdot \left(\frac{f_{y_steel}}{\lambda \cdot \sqrt{\frac{f_c}{psi}} \cdot psi} \right) \cdot \frac{(\Psi_t \cdot \Psi_e \cdot \Psi_s)}{(2.5)} \right] \cdot d_{vertical_bar} \quad l_d = 15.91 \cdot \text{in}$$

Anchor embedment length, l_{anchor}

$C_{top} := 3\text{in}$ (clearance between top of vertical reinforcing steel and top of foundation)

$S_{anchor} := 5.3675\text{in}$ (horizontal center-to-center spacing between anchor bolt and vertical rebars)

$l_{anchor} := l_d + C_{top} + S_{anchor}$ (*NCHRP report 494*: Structural supports for Highway signs, Luminaires and Traffic signals, 2.4.5.5, Eq.6)

$l_{anchor} = 24.277 \cdot \text{in}$

$l_{anchor_provided} := 25\text{in}$

Check_embeddment := $\begin{cases} \text{"Sufficient"} & \text{if } l_{anchor_provided} \geq l_{anchor} \\ \text{"Insufficient"} & \text{otherwise} \end{cases}$

Check_embeddment = "Sufficient"

Clear cover

Clear cover to reinforcement provided for all the exposed sides of cap is 3 in as per FDOT's "Structures Design Guidelines for Load and Resistance Factor design", 2002, chapter 2, considering the site condition as "moderately aggressive".

Check for grout strength (Cementitious grout)

Tension on the cap due to factored Bending moment

$$T_{u, cap} := T_{u, bolt} \cdot \frac{\#AnchorRods}{2} \quad T_{u, cap} = 317.3 \cdot \text{kip}$$

Grout-concrete bond resistance (N_{bond})

plastic grout to hardened concrete bond strength $\tau_o := 1.9\text{ksi}$

Area of grout-concrete interface transferring tension to pile

$$A_{bond} := 30.375\text{in} \cdot 28\text{in} \quad A_{bond} = 850.5 \cdot \text{in}^2 \quad (\text{One pile-cap interface considered for area calculation})$$

$$N_{bond} := \tau_o \cdot A_{bond} \quad N_{bond} = 1615.95 \cdot \text{kip} \quad \phi_{bond} := 0.85 \quad \text{ACI 318-08, Appendix C}$$

$$\phi_{bond} \cdot N_{bond} = 1373.557 \cdot \text{kip}$$

$$T_{u.cap} < \phi_{bond} \cdot N_{bond} \quad \text{OK}$$

Tensile strength of grout

Tensile splitting strength of grout $f_t := 0.5\text{ksi}$

Tensile strength $P := f_t \cdot A_{t,bond}$ $P = 425.25\text{-kip}$ $\phi_t := 0.9$ ACI 318-08, Appendix C

$$\phi_{shear} \cdot P = 318.938\text{-kip} \quad T_{u.cap} < \phi_{shear} \cdot P \quad \text{OK}$$

Shear strength of grout

Unit shear strength of grout $s_s := 0.3\text{ksi}$ *(Considered minimum of the values reported by Moosavi et al. (2003) and Issa et al. (2003) for a portland cement grout @ 0.5 w/c ratio)*

Shear strength $S := s_s \cdot 2A_{t,bond}$ $S = 510.3\text{-kip}$ $\phi_{shear} := 0.85$

$$\phi_{shear} \cdot S = 433.755\text{-kip}$$

$$T_{u.cap} < (\phi_{shear} \cdot S) \quad \text{OK}$$

APPENDIX D: PREDICTION OF SKIN RESISTANCE OF DRILLED SHAFT

Prediction of Skin Resistance - 18 ft long x 4 ft diameter Drilled shaft (TS2)

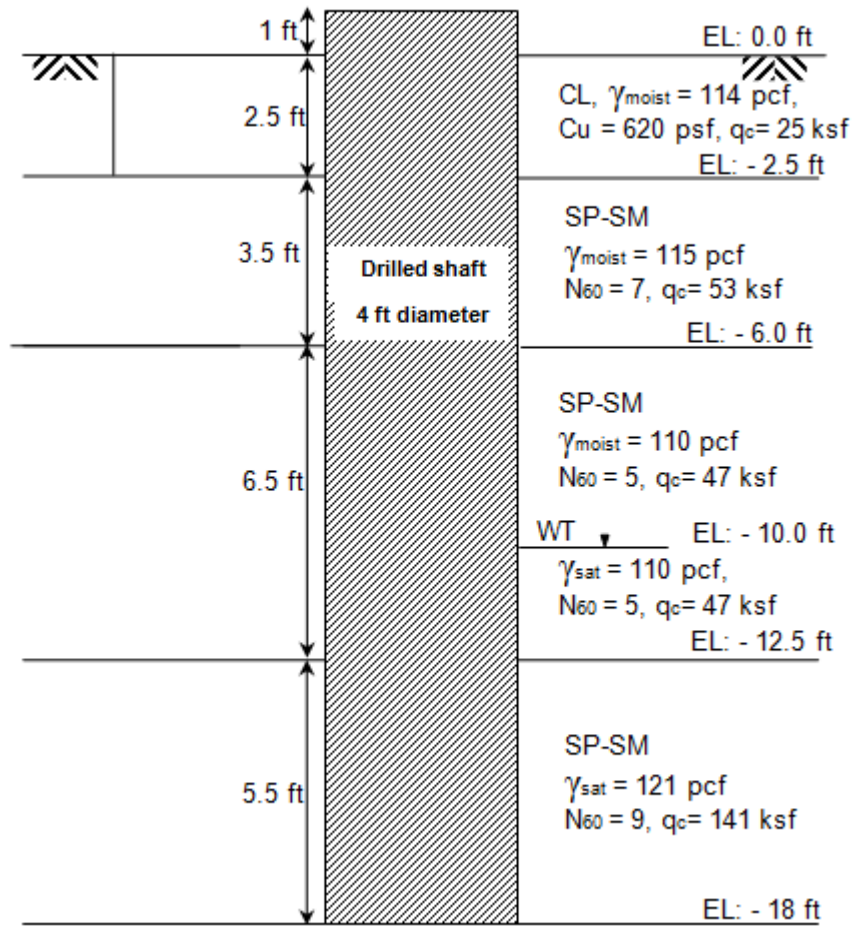


Figure D-1. Soil properties for the skin resistance prediction of TS2

Shaft diameter $D = 4$ ft

1) Depth dependent BETA (β) method or O'Neill and Hassan method

(Ref: FHWA 2010; Drilled shafts: Construction Procedures and LRFD Design Methods)

For sandy soils:

$$f_{SN} = \sigma'_v \cdot \beta$$

f_{SN} = nominal unit side resistance

β = side resistance coefficient

$$\beta = 1.5 - 0.135 \cdot \sqrt{Z} \quad \text{for } N_{60} \geq 15 \quad 0.25 \leq \beta \leq 1.2$$

$$\beta = (1.5 - 0.135 \cdot \sqrt{Z}) \cdot \frac{N_{60}}{15} \quad \text{for } N_{60} \geq 15$$

For clay: $f_{SN} = \alpha \cdot S_u$ Coefficient $\alpha := 0.55$

Calculations:

i) Skin resistance due to top 2.5 ft (EL 0.0 to -2.5)

$$S_u := 620 \quad \text{psf}$$

$$f_{SN1} := \alpha \cdot S_u \quad f_{SN1} = 341 \quad \text{psf}$$

$$Q_{s1} := \frac{(\pi \cdot D \cdot 2.5 \cdot f_{SN1})}{1000} \quad Q_{s1} = 10.713 \quad \text{kip}$$

ii) Skin resistance from EL -2.5 to -6.0)

$$N_{60} := 7 \quad Z := 4.25 \quad \text{ft}$$

$$\sigma'_v := 2.5 \cdot 114 + 1.75 \cdot 115 \quad \sigma'_v = 486.25 \quad \text{psf}$$

$$\beta := (1.5 - 0.135 \cdot \sqrt{Z}) \cdot \frac{N_{60}}{15} \quad \beta = 0.57$$

$$f_{SN2} := \sigma'_v \cdot \beta \quad f_{SN2} = 277.222 \quad \text{psf}$$

$$Q_{s2} := (\pi \cdot D \cdot 3.5 \cdot f_{SN2}) \cdot \frac{1}{1000} \quad Q_{s2} = 12.193 \quad \text{kip}$$

iii) Skin resistance from EL -6.0 to -10.0)

$$N_{60} := 5 \quad Z := 8 \quad \text{ft}$$

$$\sigma'_v := 2.5 \cdot 114 + 3.5 \cdot 115 + 2 \cdot 110 \quad \sigma'_v = 907.5 \quad \text{psf}$$

$$\beta := (1.5 - 0.135 \cdot \sqrt{Z}) \cdot \frac{N_{60}}{15} \quad \beta = 0.373$$

$$f_{SN3} := \sigma'_v \cdot \beta \quad f_{SN3} = 338.244 \quad \text{psf}$$

$$Q_{s3} := (\pi \cdot D \cdot 4 \cdot f_{SN3}) \cdot \frac{1}{1000} \quad Q_{s3} = 17.002 \quad \text{kip}$$

iv) Skin resistance from EL -10.0 to -12.5)

$$N_{60} := 5 \quad Z := 11.25 \quad \text{ft} \quad \gamma_{sat1} := 110 \quad \text{pcf} \quad \gamma_w := 62.4 \quad \text{pcf}$$

$$\gamma^I := \gamma_{sat1} - \gamma_w$$

$$\sigma'_{\text{vw}} := 2.5 \cdot 114 + 3.5 \cdot 115 + 4 \cdot 110 + 1.25 \cdot \gamma_1' \quad \sigma'_{\text{v}} = 1187 \quad \text{psf}$$

$$\beta := (1.5 - 0.135 \cdot \sqrt{Z}) \cdot \frac{N_{60}}{15} \quad \beta = 0.349$$

$$f_{\text{SN4}} := \sigma'_{\text{v}} \cdot \beta \quad f_{\text{SN4}} = 414.341 \quad \text{psf}$$

$$Q_{s4} := (\pi \cdot D \cdot 2.5 \cdot f_{\text{SN4}}) \cdot \frac{1}{1000} \quad Q_{s4} = 13.017 \quad \text{kip}$$

v) Skin resistance from EL -12.5 to -18.0)

$$N_{60} := 9 \quad Z := 15.25 \quad \text{ft} \quad \gamma_{\text{sat2}} := 121 \quad \text{pcf} \quad \gamma_2' := \gamma_{\text{sat2}} - \gamma_w$$

$$\sigma'_{\text{vw}} := 2.5 \cdot 114 + 3.5 \cdot 115 + 4 \cdot 110 + 2.5 \cdot \gamma_1' + 2.75 \cdot \gamma_2' \quad \sigma'_{\text{v}} = 1407.65 \quad \text{psf}$$

$$\beta := (1.5 - 0.135 \cdot \sqrt{Z}) \cdot \frac{N_{60}}{15} \quad \beta = 0.584$$

$$f_{\text{SN5}} := \sigma'_{\text{v}} \cdot \beta \quad f_{\text{SN5}} = 821.624 \quad \text{psf}$$

$$Q_{s5} := (\pi \cdot D \cdot 5.5 \cdot f_{\text{SN5}}) \cdot \frac{1}{1000} \quad Q_{s5} = 56.787 \quad \text{kip}$$

Total Skin resistance:

$$Q_s := Q_{s1} + Q_{s2} + Q_{s3} + Q_{s4} + Q_{s5}$$

$$Q_s = 109.711 \quad \text{kip}$$

2) BETA (β) method with separate evaluation of K and δ (Rational Method)

(Ref FHWA 2010, Drilled shafts: Construction Procedures and LRFD Design Methods)

For cohesionless soils:

$$f_{\text{SN}} = \beta \cdot \sigma'_{\text{v}}$$

$$\beta = (1 - \sin(\phi)) \cdot \left(\frac{\sigma'_p}{\sigma'_{\text{v}}} \right)^{\sin(\phi)} \cdot \tan(\phi) \leq K_p \cdot \tan(\phi)$$

β at depth less than 7.5 ft = β at 7.5 ft

$$\sigma'_p = 0.47 \cdot (N_{60})^m \cdot \text{pa} \quad \text{pa} := 2116 \quad \text{psf}$$

$$K_p = \left(\tan \left(45 + \frac{\phi}{2} \right) \right)^2$$

$$m := 0.8 \quad \text{for sandy silt to silty sand}$$

Calculations:

i) Torsional resistance due to top 2.5 ft (EL 0.0 to -2.5)

$$S_u := 620 \text{ psf}$$

$$f_{SN1} := \alpha \cdot S_u \quad f_{SN1} = 1 \text{ psf}$$

$$Q_{s1} := (\pi \cdot D \cdot 2.5 \cdot f_{SN1}) \cdot \frac{1}{1000} \quad Q_{s1} = 10.713 \text{ kip}$$

ii) Torsional resistance from EL -2.5 to -6.0)

$$N_{60} := 7 \quad Z := 4.25 \text{ ft}$$

Here z less than 7.5 ft and therefore use β corresponds to 7.5 ft

$$\sigma'_{v7.5ft} := 2.5 \cdot 114 + 3.5 \cdot 115 + 1.5 \cdot 110 \quad \sigma'_{v7.5ft} = 852.5 \text{ psf}$$

$$\phi := 31 \text{ (Degree)}$$

$$K_p := \tan^2 \left[\left(45 + \frac{\phi}{2} \right) \cdot \frac{\pi}{180} \right]^2 \quad K_p = 3.124 \quad K_p \cdot \tan \left(\phi \cdot \frac{\pi}{180} \right) = 1.877$$

$$\sigma'_p := 0.47 \cdot (N_{60})^m \cdot p_a \quad \sigma'_p = 4717.283 \text{ psf}$$

$$\beta := \min \left[\left(1 - \sin \left(\phi \cdot \frac{\pi}{180} \right) \right) \cdot \left(\frac{\sigma'_p}{\sigma'_{v7.5ft}} \right)^{\sin \left(\phi \cdot \frac{\pi}{180} \right)} \cdot \tan \left(\phi \cdot \frac{\pi}{180} \right), K_p \cdot \tan \left(\phi \cdot \frac{\pi}{180} \right) \right]$$

$$\beta = 0.703$$

$$\sigma'_{v} := 2.5 \cdot 114 + 1.75 \cdot 115 \quad \sigma'_{v} = 486.25 \text{ psf}$$

$$f_{SN2} := \sigma'_v \cdot \beta \quad f_{SN2} = 341.99 \text{ psf}$$

$$Q_{s2} := (\pi \cdot D \cdot 3.5 \cdot f_{SN2}) \cdot \frac{1}{1000} \quad Q_{s2} = 15.041 \text{ kip}$$

iii) Skin resistance from EL -6.0 to -10.0)

$$N_{60} := 5 \quad Z := 8 \text{ ft}$$

$$\sigma'_{v} := 2.5 \cdot 114 + 3.5 \cdot 115 + 2 \cdot 110 \quad \sigma'_{v} = 907.5 \text{ psf}$$

$$\phi := 31 \text{ (Degree)}$$

$$K_p := \tan\left[\left(45 + \frac{\phi}{2}\right) \cdot \frac{\pi}{180}\right]^2 \quad K_p = 3.124$$

$$\sigma'_p := 0.47 \cdot (N_{60})^m \cdot \text{pa} \quad \sigma'_p = 3604.039 \text{ psf}$$

$$\beta := \min\left[\left(1 - \sin\left(\phi \cdot \frac{\pi}{180}\right)\right) \cdot \left(\frac{\sigma'_p}{\sigma'_v}\right)^{\sin\left(\phi \cdot \frac{\pi}{180}\right)} \cdot \tan\left(\phi \cdot \frac{\pi}{180}\right), K_p \cdot \tan\left(\phi \cdot \frac{\pi}{180}\right)\right]$$

$$\beta = 0.593$$

$$f_{SN3} := \sigma'_v \cdot \beta \quad f_{SN3} = 538.03 \text{ psf}$$

$$Q_{s3} := (\pi \cdot D \cdot 4 \cdot f_{SN3}) \cdot \frac{1}{1000} \quad Q_{s3} = 27.044 \text{ kip}$$

iv) Skin resistance from EL -10.0 to -12.5)

$$N_{60} := 5 \quad Z := 11.25 \text{ ft} \quad \gamma_{sat1} := 110 \text{ pcf} \quad \gamma_w := 62.4 \text{ pcf}$$

$$\gamma_1' := \gamma_{sat1} - \gamma_w$$

$$\sigma'_v := 2.5 \cdot 114 + 3.5 \cdot 115 + 4 \cdot 110 + 1.25 \cdot \gamma_1' \quad \sigma'_v = 1187 \text{ psf}$$

$$\phi := 31 \text{ (Degree)}$$

$$K_p := \tan\left[\left(45 + \frac{\phi}{2}\right) \cdot \frac{\pi}{180}\right]^2 \quad K_p = 3.124$$

$$\sigma'_p := 0.47 \cdot (N_{60})^m \cdot \text{pa} \quad \sigma'_p = 3604.039 \text{ psf}$$

$$\beta := \min\left[\left(1 - \sin\left(\phi \cdot \frac{\pi}{180}\right)\right) \cdot \left(\frac{\sigma'_p}{\sigma'_v}\right)^{\sin\left(\phi \cdot \frac{\pi}{180}\right)} \cdot \tan\left(\phi \cdot \frac{\pi}{180}\right), K_p \cdot \tan\left(\phi \cdot \frac{\pi}{180}\right)\right]$$

$$\beta = 0.516$$

$$f_{SN4} := \sigma'_v \cdot \beta \quad f_{SN4} = 612.851 \text{ psf}$$

$$Q_{s4} := (\pi \cdot D \cdot 2.5 \cdot f_{SN4}) \cdot \frac{1}{1000} \quad Q_{s4} = 19.253 \text{ kip-ft}$$

v) Skin resistance from EL -12.5 to -18.0)

$$N_{60} := 9 \quad Z := 15.25 \text{ ft} \quad \gamma_{\text{sat2}} := 121 \text{ pcf} \quad \gamma_2' := \gamma_{\text{sat2}} - \gamma_w$$

$$\sigma_v' := 2.5 \cdot 114 + 3.5 \cdot 115 + 4 \cdot 110 + 2.5 \cdot \gamma_1' + 2.75 \cdot \gamma_2' \quad \sigma_v' = 1407.65 \text{ psf}$$

$$\phi := 34 \text{ (Degree)}$$

$$K_p := \tan \left[\left(45 + \frac{\phi}{2} \right) \cdot \frac{\pi}{180} \right]^2 \quad K_p = 3.537$$

$$\sigma_p' := 0.47 \cdot (N_{60})^m \cdot \text{pa} \quad \sigma_p' = 5767.765 \text{ psf}$$

$$\beta := \min \left[\left(1 - \sin \left(\phi \cdot \frac{\pi}{180} \right) \right) \cdot \left(\frac{\sigma_p'}{\sigma_v'} \right)^{\sin \left(\phi \cdot \frac{\pi}{180} \right)} \cdot \tan \left(\phi \cdot \frac{\pi}{180} \right), K_p \cdot \tan \left(\phi \cdot \frac{\pi}{180} \right) \right] \quad \beta = 0.654$$

$$f_{\text{SN5}} := \sigma_v' \cdot \beta \quad f_{\text{SN5}} = 920.966 \text{ psf}$$

$$Q_{s5} := (\pi \cdot D \cdot 5.5 \cdot f_{\text{SN5}}) \cdot \frac{1}{1000} \quad Q_{s5} = 63.653 \text{ kip-ft}$$

Total Skin resistance:

$$Q_s := Q_{s1} + Q_{s2} + Q_{s3} + Q_{s4} + Q_{s5}$$

$$Q_s = 135.705 \text{ kip}$$

CPT Based prediction:

Shaft diameter $D := 4 \text{ ft}$

1) Aoki and Velloso (1975)

$$f_{si} = \frac{\alpha}{F_2} \cdot q_{ci} \quad (2-18)$$

Table D-1. Aoki and Velloso's α values for different soil types

Soil Type	α (%)	Soil Type	α (%)	Soil Type	α (%)
Sand	1.4	Silt	3.0	Clay	6.0
Silty sand	2.0	Sandy silt	2.2	Sandy clay	2.4
Clayey silty sand	2.4	Clayey sandy silt	2.8	Silty sandy clay	2.8
Clayey sand	3.0	Clayey silt	3.4	Silty clayey	4.0
Silty Clayey sand	2.8	Sandy clayey silt	3.0	Sandy silty clay	3.0

$$F_2 = 6.0-7.0$$

Calculations:

i) Skin resistance due to top 2.5 ft (EL 0.0 to -2.5)

$$q_c := 25 \text{ ksf} \quad F_2 := 6 \quad \alpha := 0.06$$

$$f_{SN1} := \left(\frac{\alpha}{F_2} \right) \cdot q_c \quad f_{SN1} = 0.25 \text{ ksf}$$

$$Q_{s1} := (\pi \cdot D \cdot 2.5 \cdot f_{SN1}) \quad Q_{s1} = 7.854 \text{ kip}$$

ii) Skin resistance from EL -2.5 to -6.0

$$q_{cv} := 53 \text{ ksf} \quad F_2 := 6 \quad \alpha := 0.02$$

$$f_{SN2} := \left(\frac{\alpha}{F_2} \right) \cdot q_c \quad f_{SN2} = 0.177 \text{ ksf}$$

$$Q_{s2} := (\pi \cdot D \cdot 3.5 \cdot f_{SN2}) \quad Q_{s2} = 7.77 \text{ kip}$$

iii) Skin resistance from EL -6.0 to -10.0)

$$q_{c3} := 47 \text{ ksf} \quad F_{23} := 6 \quad \alpha_3 := 0.02$$

$$f_{SN3} := \left(\frac{\alpha}{F_2} \right) \cdot q_c \quad f_{SN3} = 0.157 \text{ ksf}$$

$$Q_{s3} := (\pi \cdot D \cdot 4 \cdot f_{SN3}) \quad Q_{s3} = 7.875 \text{ kip}$$

iv) Skin resistance from EL -10.0 to -12.5)

$$q_{c4} := 47 \text{ ksf} \quad F_{24} := 6 \quad \alpha_4 := 0.02$$

$$f_{SN4} := \left(\frac{\alpha}{F_2} \right) \cdot q_c \quad f_{SN4} = 0.157 \text{ ksf}$$

$$Q_{s4} := (\pi \cdot D \cdot 2.5 \cdot f_{SN4}) \quad Q_{s4} = 4.922 \text{ kip}$$

v) Skin resistance from EL -12.5 to -18.0)

$$q_{c5} := 141 \text{ ksf} \quad F_{25} := 6 \quad \alpha_5 := 0.02$$

$$f_{SN5} := \left(\frac{\alpha}{F_2} \right) \cdot q_c \quad f_{SN5} = 0.47 \text{ ksf}$$

$$Q_{s5} := (\pi \cdot D \cdot 5.5 \cdot f_{SN5}) \quad Q_{s5} = 32.484 \text{ kip}$$

Total Skin resistance:

$$Q_s := Q_{s1} + Q_{s2} + Q_{s3} + Q_{s4} + Q_{s5}$$

$$Q_s = 60.905 \text{ kip}$$

2) LCPC Method

$$f_{si} = \frac{q_{ci}}{\alpha_{LCPC}} \quad (2-19)$$

Table D-2. LCPC Friction coefficient

Nature of Soil	q_c/P_a	α_{LCPC}		Maximum f_s/P_a	
		IA	IB	IA	IB
Soft clay and mud	< 10	30	30	0.15	0.15
Moderately compact clay	10 to 50	40	80	0.35 (0.8)	0.35 (0.8)
Silt and loose sand	≤ 50	60	150	0.35	0.35
Compact to stiff clay and compact chalk	> 50	60	120	0.35 (0.8)	0.35 (0.8)
Soft chalk	≤ 50	100	120	0.35	0.35
Moderately compact sand and gravel	50 to 120	100	200	0.8 (1.2)	0.35 (0.8)
Weathered to fragmented chalk	> 50	60	80	1.2 (1.5)	0.8 (1.2)
Compact to very compact sand and gravel	> 120	150	300	1.2 (1.5)	0.8 (1.2)

Type IA – Plain bored piles, mud bored piles, hollow auger bored piles, cast screwed piles, piers, barrettes, and micropiles installed with low injection pressure

Type IB – Bored piles with steel casing and driven cast piles

P_a - reference stress = 100 kPa. (Bracketed value is used only in the case of careful execution and minimum soil disturbance due to construction)

$$p_a = 2.12 \text{ ksf}$$

Calculations:

i) Skin resistance due to top 2.5 ft (EL 0.0 to -2.5)

$$q_{cw} = 25 \text{ ksf}$$

$$\text{ratio} := \frac{q_c}{p_a} \quad \text{ratio} = 11.792$$

$$\alpha_{LCPC} = 40$$

$$f_{SN1} := \frac{q_c}{\alpha_{LCPC}} \quad f_{SN1} = 0.625 \text{ ksf}$$

$$\text{norm_skin} := \frac{f_{SN1}}{p_a} \quad \text{norm_skin} = 0.295$$

$$Q_{s1} := (\pi \cdot D \cdot 2.5 \cdot f_{SN1}) \quad Q_{s1} = 19.635 \text{ kip}$$

ii) Skin resistance from EL -2.5 to -6.0

$$q_{cw} = 53 \text{ ksf}$$

$$\text{ratio} := \frac{q_c}{p_a} \quad \text{ratio} = 25$$

$$\alpha_{LPC} := 60$$

$$f_{SN2} := \frac{q_c}{\alpha_{LPC}} \quad f_{SN2} = 0.883 \quad \text{ksf}$$

$$\text{norm_skin} := \frac{f_{SN2}}{p_a} \quad \text{norm_skin} = 0.417$$

Greater than 0.35, therefore,

$$f_{SN2} := 0.35 \cdot p_a$$

$$Q_{s2} := (\pi \cdot D \cdot 3.5 \cdot f_{SN2}) \quad Q_{s2} = 32.635 \quad \text{kip}$$

iii) Skin resistance from EL -6.0 to -10.0)

$$q_{cv} := 47 \quad \text{ksf}$$

$$\text{ratio} := \frac{q_c}{p_a} \quad \text{ratio} = 22.17$$

$$\alpha_{LPC} := 60$$

$$f_{SN3} := \frac{q_c}{\alpha_{LPC}} \quad f_{SN3} = 0.783 \quad \text{ksf}$$

$$\text{norm_skin} := \frac{f_{SN3}}{p_a} \quad \text{norm_skin} = 0.369$$

Greater than 0.35, therefore,

$$f_{SN3} := 0.35 \cdot p_a$$

$$Q_{s3} := (\pi \cdot D \cdot 4 \cdot f_{SN3}) \quad Q_{s3} = 37.297 \quad \text{kip}$$

iv) Skin resistance from EL -10.0 to -12.5)

$$q_{cv} := 47 \quad \text{ksf}$$

$$\text{ratio} := \frac{q_c}{p_a} \quad \text{ratio} = 22.17$$

$$\alpha_{LCPC} := 60$$

$$f_{SN4} := \frac{q_c}{\alpha_{LCPC}} \quad f_{SN4} = 0.783 \quad \text{ksf}$$

$$\text{norm_skin} := \frac{f_{SN4}}{p_a} \quad \text{norm_skin} = 0.369$$

Greater than 0.35, therefore,

$$f_{SN4} := 0.35 \cdot p_a$$

$$Q_{s4} := (\pi \cdot D \cdot 2.5 \cdot f_{SN4}) \quad Q_{s4} = 23.311 \quad \text{kip}$$

v) Skin resistance from EL -12.5 to -18.0)

$$q_{ov} := 141 \quad \text{ksf}$$

$$\text{ratio} := \frac{q_c}{p_a} \quad \text{ratio} = 66.509$$

$$\alpha_{LCPC} := 100$$

$$f_{SN5} := \frac{q_c}{\alpha_{LCPC}} \quad f_{SN5} = 1.41 \quad \text{ksf}$$

$$\text{norm_skin} := \frac{f_{SN5}}{p_a} \quad \text{norm_skin} = 0.665$$

Less than 0.80, therefore, no change

$$Q_{s5} := (\pi \cdot D \cdot 5.5 \cdot f_{SN5}) \quad Q_{s5} = 97.452 \quad \text{kip}$$

Total Skin resistance:

$$Q_s := Q_{s1} + Q_{s2} + Q_{s3} + Q_{s4} + Q_{s5}$$

$$Q_s = 210.33 \quad \text{kip}$$

3) UIUC method (Alsamman 1995)

Table D-3. UIUC equations for unit skin friction

Soil type	Ultimate unit skin f_s (tsf)
Gravelly sand / Gravel	$f_s = 0.02 q_c$ for $q_c \leq 50$ tsf $f_s = 0.0019 q_c + 0.9 \leq 1.4$ for $q_c \geq 50$ tsf
Sand / silty Sand	$f_s = 0.015 q_c$ for $q_c \leq 50$ tsf $f_s = 0.0012 q_c + 0.7 \leq 1.0$ for $q_c \geq 50$ tsf
Clay	$f_s = 0.023 (q_c - \sigma_{vc}) \leq 0.9$

Calculations:

i) Skin resistance due to top 2.5 ft (EL 0.0 to -2.5)

$$q_{cv} := 12.5 \text{ tsf}$$

$$\sigma_v := 1.25 \cdot \frac{114}{2000} \quad \sigma_v = 0.071 \quad \text{tsf}$$

$$f_{SN1} := 0.023 \cdot (q_c - \sigma_v) \quad f_{SN1} = 0.286 \quad \text{tsf}$$

$$Q_{s1} := (\pi \cdot D \cdot 2.5 \cdot f_{SN1}) \cdot 2 \quad Q_{s1} = 17.961 \text{ kip}$$

ii) Skin resistance from EL -2.5 to -6.0)

$$q_{cv} := 26.5 \text{ tsf}$$

$$f_{SN2} := 0.015 \cdot q_c \quad f_{SN2} = 0.397 \quad \text{tsf}$$

$$Q_{s2} := (\pi \cdot D \cdot 3.5 \cdot f_{SN2}) \cdot 2 \quad Q_{s2} = 34.966 \text{ kip}$$

iii) Skin resistance from EL -6.0 to -10.0)

$$q_{cv} := 23.5 \text{ tsf}$$

$$f_{SN3} := 0.015 \cdot q_c \quad f_{SN3} = 0.353 \quad \text{tsf}$$

$$Q_{s3} := (\pi \cdot D \cdot 4 \cdot f_{SN3}) \cdot 2 \quad Q_{s3} = 35.437 \text{ kip}$$

iv) Skin resistance from EL -10.0 to -12.5)

$$q_{c4} := 23.5 \text{ ksf}$$

$$f_{SN4} := 0.015 \cdot q_c \quad f_{SN4} = 0.353 \text{ tsf}$$

$$Q_{s4} := (\pi \cdot D \cdot 2.5 \cdot f_{SN4}) \cdot 2 \quad Q_{s4} = 22.148 \text{ kip}$$

v) Skin resistance from EL -12.5 to -18.0)

$$q_{c5} := 70.5 \text{ tsf}$$

$$f_{SN5} := 0.0012 \cdot q_c + 0.7 \quad f_{SN5} = 0.785 \text{ tsf}$$

$$Q_{s5} := (\pi \cdot D \cdot 5.5 \cdot f_{SN5}) \cdot 2 \quad Q_{s5} = 108.455 \text{ kip}$$

Total Skin resistance:

$$Q_s := Q_{s1} + Q_{s2} + Q_{s3} + Q_{s4} + Q_{s5}$$

$$Q_s = 218.968 \text{ kip}$$

APPENDIX E: PREDICTION OF TORSIONAL RESSITANCE OF DRILLED SHAFTS AND JET-GROUTED PILES

Prediction of torsional Resistance of TS1 (12 ft long x 4 ft diameter Drilled shaft)

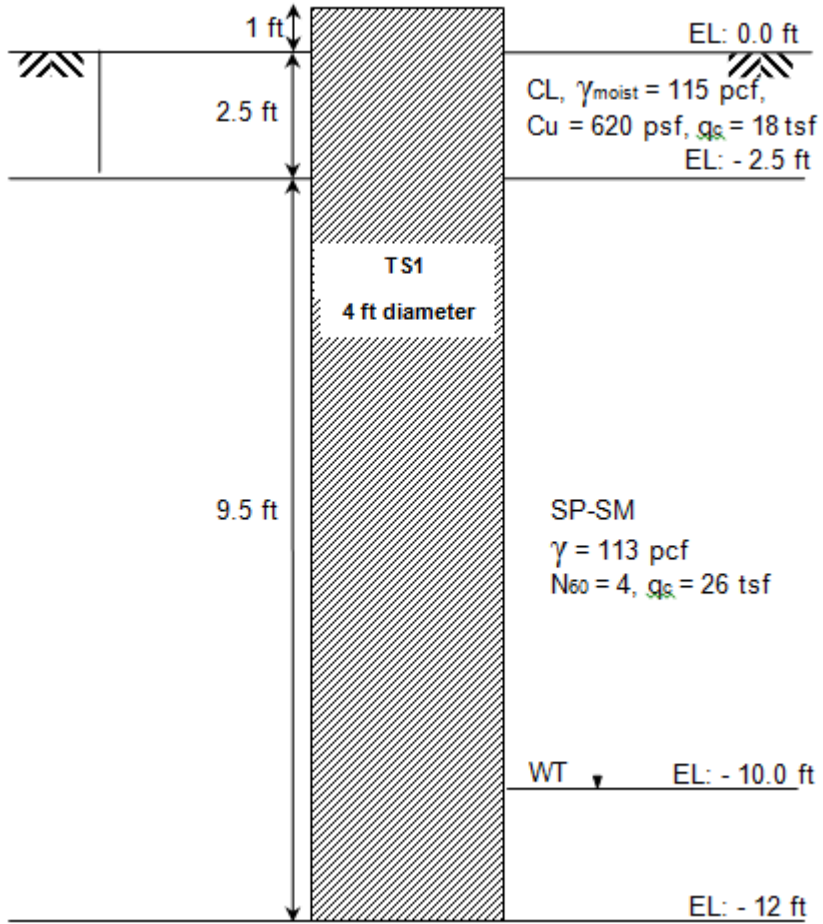


Figure E-1. Soil properties for the torsional resistance prediction of TS1

Shaft diameter $D := 4$ ft

1) Depth dependent BETA (β) method or Reese and O'Neil method
(Ref. FHWA 2010; Drilled shafts: Construction Procedures and LRFD Design Methods)

For sandy soils:

$$f_{SN} = \sigma'_v \cdot \beta$$

f_{SN} = nominal unit side resistance

β = side resistance coefficient

$$\beta = 1.5 - 0.135 \cdot \sqrt{Z} \quad \text{for } N_{60} \geq 15 \quad 0.25 \leq \beta \leq 1.2$$

$$\beta = (1.5 - 0.135 \cdot \sqrt{Z}) \cdot \frac{N_{60}}{15} \quad \text{for } N_{60} \geq 15$$

For clay:

$$f_{SN} = \alpha \cdot S_u$$

Coefficient $\alpha := 0.55$

Calculations:

i) Torsional resistance due to top 2.5 ft (EL 0.0 to -2.5)

$$S_u := 620 \text{ psf}$$

$$f_{SN1} := \alpha \cdot S_u \quad f_{SN1} = 341 \text{ psf}$$

$$T_{s1} := \frac{(\pi \cdot D \cdot 2.5 \cdot f_{SN1}) \cdot \left(\frac{D}{2}\right)}{1000} \quad T_{s1} = 21.426 \text{ kip} - \text{ft}$$

ii) Torsional resistance from EL -2.5 to -10

$$N_{60} := 4 \quad Z := 6.25 \text{ ft}$$

$$\sigma'_v := 2.5 \cdot 115 + 3.75 \cdot 113 \quad \sigma'_v = 711.25 \text{ psf}$$

$$\beta := (1.5 - 0.135 \cdot \sqrt{Z}) \cdot \frac{N_{60}}{15} \quad \beta = 0.31$$

$$f_{SN2} := \sigma'_v \cdot \beta \quad f_{SN2} = 220.488 \text{ psf}$$

$$T_{s2} := (\pi \cdot D \cdot 7.5 \cdot f_{SN2}) \cdot \left(\frac{D}{2}\right) \cdot \frac{1}{1000} \quad T_{s2} = 41.561 \text{ kip} - \text{ft}$$

iii) Torsional resistance from EL -10 to -12

$$N_{60} := 4 \quad Z := 11 \quad \text{ft}$$

$$\sigma'_v := 2.5 \cdot 115 + 7.5 \cdot 113 + 1 \cdot (113 - 62.4) \quad \sigma'_v = 1185.6 \quad \text{psf}$$

$$\beta := (1.5 - 0.135 \cdot \sqrt{Z}) \cdot \frac{N_{60}}{15} \quad \beta = 0.281$$

$$f_{SN3} := \sigma'_v \cdot \beta \quad f_{SN3} = 332.681 \quad \text{psf}$$

$$T_{s3} := (\pi \cdot D \cdot 2 \cdot f_{SN3}) \cdot \left(\frac{D}{2}\right) \cdot \frac{1}{1000} \quad T_{s3} = 16.722 \quad \text{kip} - \text{ft}$$

Total Torsional resistance:

$$T_s := T_{s1} + T_{s2} + T_{s3}$$

$$T_s = 79.709 \quad \text{kip} - \text{ft}$$

2) BETA (β) method with separate evaluation of K and δ (Rational Method)

(Ref. FHWA 2010, Drilled shafts: Construction Procedures and LRFD Design Methods)

For cohesionless soils:

$$f_{SN} = \beta \cdot \sigma'_v$$

$$\beta = (1 - \sin(\phi)) \cdot \left(\frac{\sigma'_p}{\sigma'_v}\right)^{\sin(\phi)} \cdot \tan(\phi) \leq K_p \cdot \tan(\phi)$$

β at depth less than 7.5 ft = β at 7.5 ft

$$\sigma'_p = 0.47 \cdot (N_{60})^m \cdot \text{pa} \quad \text{pa} := 2116 \quad \text{psf}$$

$$K_p = \left(\tan\left(45 + \frac{\phi}{2}\right) \right)^2$$

$$m := 0.8 \quad \text{for sandy silt to silty sand}$$

Calculations:

i) Torsional resistance due to top 2.5 ft (EL 0.0 to -2.5)

$$S_u := 620 \quad \text{psf}$$

$$f_{SN1} := \alpha \cdot S_u \quad f_{SN1} = 341 \quad \text{psf}$$

$$T_{s1} := (\pi \cdot D \cdot 2.5 \cdot f_{SN1}) \cdot \left(\frac{D}{2}\right) \cdot \frac{1}{1000} \quad T_{s1} = 21.426 \quad \text{kip}$$

ii) Torsional resistance from EL -2.5 to -10.0

$$N_{60} := 4 \quad Z := 6.25 \quad \text{ft}$$

$$\sigma'_{v,7.5} := 2.5 \cdot 115 + 5 \cdot 113 \quad \sigma'_{v,7.5} = 852.5 \quad \text{psf}$$

$$\phi := 29 \quad (\text{Degree})$$

$$K_p := \tan\left[\left(45 + \frac{\phi}{2}\right) \cdot \frac{\pi}{180}\right]^2 \quad K_p = 2.882$$

$$\sigma'_p := 0.47 \cdot (N_{60})^m \cdot \text{pa} \quad \sigma'_p = 3014.821 \quad \text{psf}$$

$$\beta := \min\left[\left(1 - \sin\left(\phi \cdot \frac{\pi}{180}\right)\right) \cdot \left(\frac{\sigma'_p}{\sigma'_{v,7.5}}\right)^{\sin\left(\phi \cdot \frac{\pi}{180}\right)} \cdot \tan\left(\phi \cdot \frac{\pi}{180}\right), K_p \cdot \tan\left(\phi \cdot \frac{\pi}{180}\right)\right]$$

$$\beta = 0.527$$

$$\sigma'_{s2} := 2.5 \cdot 115 + 3.75 \cdot 113 \quad \sigma'_{s2} = 711.25 \quad \text{psf}$$

$$f_{SN2} := \sigma'_{s2} \cdot \beta \quad f_{SN2} = 374.708 \quad \text{psf}$$

$$T_{s2} := (\pi \cdot D \cdot 7.5 \cdot f_{SN2}) \cdot \left(\frac{D}{2}\right) \cdot \frac{1}{1000} \quad T_{s2} = 70.631 \quad \text{kip} - \text{ft}$$

iii) Torsional resistance from EL -10 to -12

$$N_{60} := 4 \quad Z := 11 \quad \text{ft}$$

$$\sigma'_{v,11} := 2.5 \cdot 115 + 7.5 \cdot 113 + 1 \cdot (113 - 62.4) \quad \sigma'_{v,11} = 1185.6 \quad \text{psf}$$

$$\phi := 29 \quad (\text{Degree})$$

$$K_p := \tan\left[\left(45 + \frac{\phi}{2}\right) \cdot \frac{\pi}{180}\right]^2 \quad K_p = 2.882$$

$$\sigma'_p := 0.47 \cdot (N_{60})^m \cdot \text{pa} \quad \sigma'_p = 3014.821 \quad \text{psf}$$

$$\beta := \min\left[\left(1 - \sin\left(\phi \cdot \frac{\pi}{180}\right)\right) \cdot \left(\frac{\sigma'_p}{\sigma'_{v,11}}\right)^{\sin\left(\phi \cdot \frac{\pi}{180}\right)} \cdot \tan\left(\phi \cdot \frac{\pi}{180}\right), K_p \cdot \tan\left(\phi \cdot \frac{\pi}{180}\right)\right]$$

$$\beta = 0.449$$

$$f_{SN3} := \sigma'_v \cdot \beta \quad f_{SN3} = 532.307 \text{ psf}$$

$$T_{s3} := \left(\pi \cdot D \cdot 2 \cdot f_{SN3} \right) \cdot \left(\frac{D}{2} \right) \cdot \frac{1}{1000} \quad T_{s3} = 26.757 \text{ kip - ft}$$

Total torsional resistance:

$$T_{s} := T_{s1} + T_{s2} + T_{s3}$$

$$T_s = 118.813 \text{ kip - ft}$$

3) FDOT Re-revised OMEGA method

(Ref. FDOT Structures Manual, Vol. 9, revised in January 2013)

$$T_n = \pi \cdot D \cdot L \cdot F_s \cdot \left(\frac{D}{2} \right) + \pi \cdot \left(\frac{D}{2} \right)^2 \cdot L \cdot \gamma_{\text{conc}} \cdot \left(\frac{D}{3} \right) \cdot \mu$$

$$F_s = \sigma'_v \cdot \omega_{\text{fdot}} \quad \text{for sand}$$

$$F_{sc} = \alpha \cdot s_u \quad \text{for clay}$$

$$\mu = \tan(\phi_{\text{soil}})$$

$$\omega_{\text{fdot}} = 1.5 \cdot \left(\frac{N}{15} \right)$$

Calculations:

i) Torsional resistance due to top 2.5 ft (EL 0.0 to -2.5)

$$S_u := 620 \text{ psf}$$

$$f_{SN1} := \alpha \cdot S_u \quad f_{SN1} = 341 \text{ psf}$$

$$T_{s1} := \frac{\left(\pi \cdot D \cdot 2.5 \cdot f_{SN1} \right) \cdot \left(\frac{D}{2} \right)}{1000} \quad T_{s1} = 21.426 \text{ kip - ft}$$

ii) Torsional resistance from EL -2.5 to -10.0)

$$N_{60} := 4 \quad Z := 6.25 \text{ ft}$$

$$\sigma'_v := 2.5 \cdot 115 + 3.75 \cdot 113 \quad \sigma'_v = 711.25 \text{ psf}$$

$$f_{SN2} := \sigma'_v \cdot 1.5 \cdot \left(\frac{N_{60}}{15} \right) \quad f_{SN2} = 284.5 \text{ pcf}$$

$$T_{s2} := \left(\pi \cdot D \cdot 7.5 \cdot f_{SN2} \right) \cdot \left(\frac{D}{2} \right) \div 1000 \quad T_{s2} = 53.627 \text{ kip - ft}$$

iii) Torsional resistance from EL -10 to -12

$$\underline{N_{60}} := 4 \quad \underline{Z} := 11 \quad \text{ft}$$

$$\underline{\sigma'_v} := 2.5 \cdot 115 + 7.5 \cdot 113 + 1 \cdot (113 - 62.4) \quad \sigma'_v = 1185.6 \quad \text{psf}$$

$$\underline{f_{SN3}} := \sigma'_v \cdot 1.5 \cdot \left(\frac{N_{60}}{15} \right) \quad f_{SN3} = 474.24 \quad \text{pcf}$$

$$\underline{T_{s3}} := \left(\pi \cdot D \cdot 2 \cdot f_{SN3} \right) \cdot \left(\frac{D}{2} \right) \cdot \frac{1}{1000} \quad T_{s3} = 23.838 \quad \text{kip-ft}$$

Total Torsional resistance:

$$\underline{T_s} := T_{s1} + T_{s2} + T_{s3} \quad T_s = 98.891 \quad \text{kip-ft}$$

Torsional resistance due to tip:

$$\underline{L} := 18 \quad \text{ft} \quad \gamma_{\text{conc}} := 150 \quad \text{pcf} \quad \phi_{\text{soil}} := 29 \quad (\text{degree}) \quad \mu := \tan(\phi_{\text{soil}} \cdot \pi \div 180) \quad \mu = 0.554$$

$$T_t := \pi \left(\frac{D}{2} \right)^2 \cdot L \cdot \gamma_{\text{conc}} \cdot \left(\frac{D}{3} \right) \cdot \mu \div 1000 \quad T_t = 25.076 \quad \text{kip-ft}$$

Total torsional resistance: $T_{\text{fdot}} := T_s + T_t \quad T_{\text{fdot}} = 123.967 \quad \text{kip-ft}$

Prediction of torsional Resistance of TS2 (18 ft long x 4 ft diameter Drilled shaft)

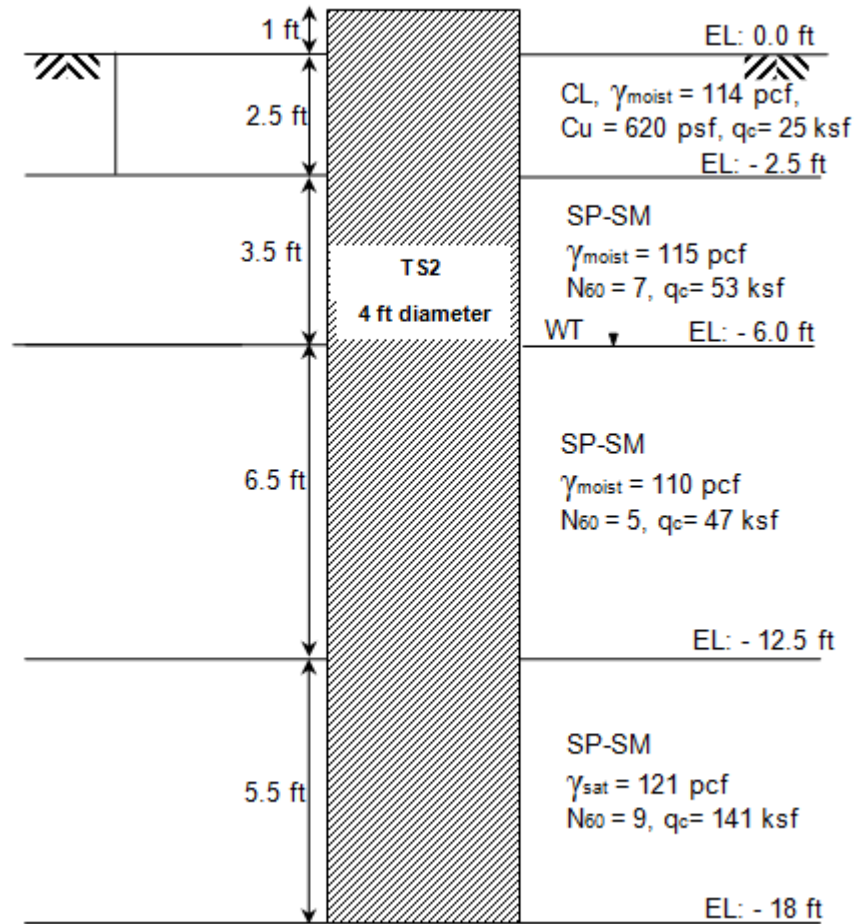


Figure E-2. Soil properties for the torsional resistance prediction of TS2

Shaft diameter $D := 4$ ft

1) Depth dependent BETA (β) method or O'Neill and Hassan method

(Ref: FHWA 2010; Drilled shafts: Construction Procedures and LRFD Design Methods)

For sandy soils:

$$f_{SN} = \sigma'_v \cdot \beta$$

f_{SN} = nominal unit side resistance

β = side resistance coefficient +

$$\beta = 1.5 - 0.135 \cdot \sqrt{Z} \quad \text{for } N_{60} \geq 15 \quad 0.25 \leq \beta \leq 1.2$$

$$\beta = (1.5 - 0.135 \cdot \sqrt{Z}) \cdot \frac{N_{60}}{15} \quad \text{for } N_{60} \geq 15$$

For clay:

$$f_{SN} = \alpha \cdot S_u$$

$$\text{Coefficient } \alpha := 0.55$$

Calculations:

i) Torsional resistance due to top 2.5 ft (EL 0.0 to -2.5)

$$S_u := 620 \text{ psf}$$

$$f_{SN1} := \alpha \cdot S_u \quad f_{SN1} = 341 \text{ psf}$$

$$T_{s1} := \frac{(\pi \cdot D \cdot 2.5 \cdot f_{SN1}) \cdot \left(\frac{D}{2}\right)}{1000} \quad T_{s1} = 21.426 \text{ kip - ft}$$

ii) Torsional resistance from EL -2.5 to -6.0

$$N_{60} := 7 \quad Z := 4.25 \text{ ft} \quad \gamma := 114 \text{ pcf}$$

$$\sigma'_v := 2.5 \cdot 114 + 1.75 \cdot 115 \quad \sigma'_v = 486.25 \text{ psf}$$

$$\beta := (1.5 - 0.135 \cdot \sqrt{Z}) \cdot \frac{N_{60}}{15} \quad \beta = 0.57$$

$$f_{SN2} := \sigma'_v \cdot \beta \quad f_{SN2} = 277.222 \text{ psf}$$

$$T_{s2} := (\pi \cdot D \cdot 3.5 \cdot f_{SN2}) \cdot \left(\frac{D}{2}\right) \cdot \frac{1}{1000} \quad T_{s2} = 24.386 \text{ kip - ft}$$

iii) Torsional resistance from EL -6.0 to -12.5

$$N_{60w} := 5 \quad Z_w := 9.25 \text{ ft}$$

$$\gamma_w := 62.4 \text{ psf} \quad \gamma_{sat1} := 110 \text{ pcf} \quad \gamma_1' := \gamma_{sat1} - \gamma_w$$

$$\sigma'_{vw} := 2.5 \cdot 114 + 3.5 \cdot 115 + 3.25 \cdot \gamma_1' \quad \sigma'_v = 842.2 \text{ psf}$$

$$\beta_w := (1.5 - 0.135 \cdot \sqrt{Z_w}) \cdot \frac{N_{60}}{15} \quad \beta = 0.363$$

$$f_{SN3} := \sigma'_v \cdot \beta \quad f_{SN3} = 305.835 \text{ psf}$$

$$T_{s3} := (\pi \cdot D \cdot 6.5 \cdot f_{SN3}) \cdot \left(\frac{D}{2}\right) \cdot \frac{1}{1000} \quad T_{s3} = 49.962 \text{ kip} - \text{ft}$$

v) Torsional resistance from EL -12.5 to -18.0

$$N_{60} := 9 \quad Z := 15.25 \text{ ft} \quad \gamma_{sat2} := 121 \text{ pcf} \quad \gamma_2' := \gamma_{sat2} - \gamma_w$$

$$\sigma_v' := 2.5 \cdot 114 + 3.5 \cdot 115 + 6.5 \cdot \gamma_1' + 2.75 \cdot \gamma_2' \quad \sigma_v' = 1158.05 \text{ psf}$$

$$\beta := (1.5 - 0.135 \cdot \sqrt{Z}) \cdot \frac{N_{60}}{15} \quad \beta = 0.584$$

$$f_{SN4} := \sigma_v' \cdot \beta \quad f_{SN4} = 675.936 \text{ psf}$$

$$T_{s4} := (\pi \cdot D \cdot 5.5 \cdot f_{SN4}) \cdot \left(\frac{D}{2}\right) \cdot \frac{1}{1000} \quad T_{s4} = 93.435 \text{ kip} - \text{ft}$$

Total Torsional resistance:

$$T_s := T_{s1} + T_{s2} + T_{s3} + T_{s4}$$

$$T_s = 189.208 \text{ kip} - \text{ft}$$

Change in torsional resistance due to water table rise by 4ft

$$\Delta t := T_s - 220 \quad (110 \text{ kips} \times D/2; \text{ See appendix D})$$

$$\Delta t = -30.792 \text{ kip} - \text{ft}$$

2) BETA (β) method with separate evaluation of K and δ (Rational Method)

(Ref: FHWA 2010, Drilled shafts: Construction Procedures and LRFD Design Methods)

+ For cohesionless soils:

$$f_{SN} = \beta \cdot \sigma_v'$$

$$\beta = (1 - \sin(\phi)) \cdot \left(\frac{\sigma_p'}{\sigma_v'}\right)^{\sin(\phi)} \cdot \tan(\phi) \leq K_p \cdot \tan(\phi)$$

β at depth less than 7.5 ft = β at 7.5 ft

$$\sigma_p' = 0.47 \cdot (N_{60})^m \cdot \text{pa} \quad \text{pa} := 2116 \text{ psf}$$

$$K_p = \left(\tan\left(45 + \frac{\phi}{2}\right) \right)^2$$

$$m := 0.8 \quad \text{for sandy silt to silty sand}$$

Calculations:

i) Torsional resistance due to top 2.5 ft (EL 0.0 to -2.5)

$$S_u := 620 \quad \text{psf}$$

$$f_{SN1} := \alpha \cdot S_u \quad f_{SN1} = 341 \quad \text{psf}$$

$$T_{s1} := \left(\pi \cdot D \cdot 2.5 \cdot f_{SN1} \right) \cdot \left(\frac{D}{2} \right) \cdot \frac{1}{1000} \quad T_{s1} = 21.426 \quad \text{kip - ft}$$

ii) Torsional resistance from EL -2.5 to -6.0

$$N_{60} := 7 \quad Z := 4.25 \quad \text{ft}$$

Here z less than 7.5 ft and therefore use β corresponds to 7.5 ft

$$\sigma'_{v7.5ft} := 2.5 \cdot 114 + 3.5 \cdot 115 + 1.5 \cdot 110 \quad \sigma'_{v7.5ft} = 852.5 \quad \text{psf}$$

$$\phi := 31 \quad (\text{Degree})$$

$$K_p := \tan^2 \left[\left(45 + \frac{\phi}{2} \right) \cdot \frac{\pi}{180} \right]^2 \quad K_p = 3.124 \quad K_p \cdot \tan \left(\phi \cdot \frac{\pi}{180} \right) = 1.877$$

$$\sigma'_p := 0.47 \cdot (N_{60})^m \cdot \text{pa} \quad \sigma'_p = 4717.283 \quad \text{psf}$$

$$\beta := \min \left[\left(1 - \sin \left(\phi \cdot \frac{\pi}{180} \right) \right) \cdot \left(\frac{\sigma'_p}{\sigma'_{v7.5ft}} \right)^{\sin \left(\phi \cdot \frac{\pi}{180} \right)} \cdot \tan \left(\phi \cdot \frac{\pi}{180} \right), K_p \cdot \tan \left(\phi \cdot \frac{\pi}{180} \right) \right]$$

$$\beta = 0.703$$

$$\sigma'_{vz} := 2.5 \cdot 114 + 1.75 \cdot 115 \quad \sigma'_{vz} = 486.25 \quad \text{psf}$$

$$f_{SN2} := \sigma'_{vz} \cdot \beta \quad f_{SN2} = 341.99 \quad \text{psf}$$

$$T_{s2} := \left(\pi \cdot D \cdot 3.5 \cdot f_{SN2} \right) \cdot \left(\frac{D}{2} \right) \cdot \frac{1}{1000} \quad T_{s2} = 30.083 \quad \text{kip - ft}$$

iii) Torsional resistance from EL -6.0 to -12.5)

$$N_{60} := 5 \quad Z := 9.25 \quad \text{ft}$$

$$\gamma_{\text{sw}} := 62.4 \text{ psf} \quad \gamma_{\text{sat1}} := 110 \text{ pcf} \quad \gamma_{\text{sw}}^1 := \gamma_{\text{sat1}} - \gamma_{\text{w}}$$

$$\sigma'_{\text{sw}} := 2.5 \cdot 114 + 3.5 \cdot 115 + 3.25 \cdot \gamma_{\text{sw}}^1 \quad \sigma'_{\text{v}} = 842.2 \text{ psf}$$

$$\phi := 31 \text{ (Degree)}$$

$$K_{\text{p}} := \tan\left[\left(45 + \frac{\phi}{2}\right) \cdot \frac{\pi}{180}\right]^2 \quad K_{\text{p}} = 3.124$$

$$\sigma'_{\text{p}} := 0.47 \cdot (N_{60})^m \cdot \text{pa} \quad \sigma'_{\text{p}} = 3604.039 \text{ psf}$$

$$\beta := \min\left[\left(1 - \sin\left(\phi \cdot \frac{\pi}{180}\right)\right) \cdot \left(\frac{\sigma'_{\text{p}}}{\sigma'_{\text{v}}}\right)^{\sin\left(\phi \cdot \frac{\pi}{180}\right)} \cdot \tan\left(\phi \cdot \frac{\pi}{180}\right), K_{\text{p}} \cdot \tan\left(\phi \cdot \frac{\pi}{180}\right)\right]$$

$$\beta = 0.616$$

$$f_{\text{SN3}} := \sigma'_{\text{v}} \cdot \beta \quad f_{\text{SN3}} = 518.894 \text{ psf}$$

$$T_{\text{SN3}} := (\pi \cdot D \cdot 6.5 \cdot f_{\text{SN3}}) \cdot \left(\frac{D}{2}\right) \cdot \frac{1}{1000} \quad T_{\text{SN3}} = 84.768 \text{ kip-ft}$$

iv) Torsional resistance from EL -12.5 to -18.0

$$N_{60} := 9 \quad Z := 15.25 \text{ ft} \quad \gamma_{\text{sat2}} := 121 \text{ pcf} \quad \gamma_{\text{sw}}^2 := \gamma_{\text{sat2}} - \gamma_{\text{w}}$$

$$\sigma'_{\text{sw}} := 2.5 \cdot 114 + 3.5 \cdot 115 + 6.5 \cdot \gamma_{\text{sw}}^2 + 2.75 \cdot \gamma_{\text{sw}}^2 \quad \sigma'_{\text{v}} = 1158.05 \text{ psf}$$

$$\phi := 34 \text{ (Degree)}$$

$$K_{\text{p}} := \tan\left[\left(45 + \frac{\phi}{2}\right) \cdot \frac{\pi}{180}\right]^2 \quad K_{\text{p}} = 3.537$$

$$\sigma'_{\text{p}} := 0.47 \cdot (N_{60})^m \cdot \text{pa} \quad \sigma'_{\text{p}} = 5767.765 \text{ psf}$$

$$\beta := \min\left[\left(1 - \sin\left(\phi \cdot \frac{\pi}{180}\right)\right) \cdot \left(\frac{\sigma'_{\text{p}}}{\sigma'_{\text{v}}}\right)^{\sin\left(\phi \cdot \frac{\pi}{180}\right)} \cdot \tan\left(\phi \cdot \frac{\pi}{180}\right), K_{\text{p}} \cdot \tan\left(\phi \cdot \frac{\pi}{180}\right)\right]$$

$$\beta = 0.73$$

$$f_{SN4} := \sigma'_v \cdot \beta \quad f_{SN4} = 845.04 \quad \text{psf}$$

$$T_{s4} := \left(\pi \cdot D \cdot 5.5 \cdot f_{SN4} \right) \cdot \left(\frac{D}{2} \right) \cdot \frac{1}{1000} \quad T_{s4} = 116.81 \quad \text{kip-ft}$$

Total Torsional resistance:

$$T_{tot} := T_{s1} + T_{s2} + T_{s3} + T_{s4}$$

$$T_s = 253.087 \quad \text{kip-ft}$$

3) FDOT's Re-revised OMEGA (ω) method (corrected for SPT)

(Ref: FDOT Structures Manual, Vol. 9)

$$T_n = \pi \cdot D \cdot L \cdot F_s \cdot \left(\frac{D}{2} \right) + \pi \left(\frac{D}{2} \right)^2 \cdot L \cdot \gamma_{conc} \cdot \left(\frac{D}{3} \right) \cdot \mu$$

$$F_s = \sigma'_v \cdot \omega_{fdot} \quad \text{for sand}$$

$$F_{sc} = \alpha \cdot s_u \quad \text{for clay}$$

$$\mu = \tan(\phi_{soil})$$

$$\omega_{fdot} = 1.5 \cdot \left(\frac{N}{15} \right)$$

Calculations:

i) Torsional resistance due to top 2.5 ft (EL 0.0 to -2.5)

$$S_u := 620 \quad \text{psf}$$

$$f_{sc} := \alpha \cdot S_u \quad f_{sc} = 341 \quad \text{psf}$$

$$T_{n1} := \left(\pi \cdot D \cdot 2.5 \cdot f_{sc} \right) \cdot \left(\frac{D}{2} \right) \div 1000 \quad T_{n1} = 21.426 \quad \text{kip-ft}$$

ii) Torsional resistance from EL -2.5 to -6.0

$$N_{60} := 7 \quad Z := 4.25 \quad \text{ft}$$

$$\sigma'_v := 2.5 \cdot 114 + 1.75 \cdot 115 \quad \sigma'_v = 486.25 \quad \text{psf}$$

$$F_{s1} := \sigma'_v \cdot 1.5 \cdot \left(\frac{N_{60}}{15} \right) \quad F_{s1} = 340.375 \quad \text{pcf}$$

$$T_{n2} := \left(\pi \cdot D \cdot 3.5 \cdot F_{s1} \right) \cdot \left(\frac{D}{2} \right) \div 1000 \quad T_{n2} = 29.941 \quad \text{kip-ft}$$

iii) Torsional resistance from EL -6.0 to -12.5

$$N_{60} := 5 \quad Z := 9.25 \text{ ft} \quad \gamma_{\text{sat1}} := 110 \text{ pcf} \quad \gamma_w := 62.4 \text{ pcf}$$

$$\gamma_1' := \gamma_{\text{sat1}} - \gamma_w$$

$$\sigma_v' := 2.5 \cdot 114 + 3.5 \cdot 115 + 3.25 \cdot \gamma_1' \quad \sigma_v' = 842.2 \text{ psf}$$

$$F_{s2} := \sigma_v' \cdot 1.5 \cdot \left(\frac{N_{60}}{15} \right) \quad F_{s2} = 421.1 \text{ pcf}$$

$$T_{n3} := \left(\pi \cdot D \cdot 6.5 \cdot F_{s2} \right) \cdot \left(\frac{D}{2} \right) \div 1000 \quad T_{n3} = 68.792 \text{ kip-ft}$$

iv) Torsional resistance from EL -12.5 to -18.0)

$$N_{60} := 9 \quad Z := 15.25 \text{ ft} \quad \gamma_{\text{sat2}} := 121 \text{ pcf} \quad \gamma_2' := \gamma_{\text{sat2}} - \gamma_w$$

$$\sigma_v' := 2.5 \cdot 114 + 3.5 \cdot 115 + 6.5 \cdot \gamma_1' + 2.75 \cdot \gamma_2' \quad \sigma_v' = 1158.05 \text{ psf}$$

$$F_{s3} := \sigma_v' \cdot 1.5 \cdot \left(\frac{N_{60}}{15} \right) \quad F_{s3} = 1.042 \times 10^3 \text{ pcf}$$

$$T_{n4} := \left(\pi \cdot D \cdot 5.5 \cdot F_{s3} \right) \cdot \left(\frac{D}{2} \right) \div 1000 \quad T_{n4} = 144.07 \text{ kip-ft}$$

Total Torsional resistance due to skin friction:

$$T_{\text{skin}} := T_{n1} + T_{n2} + T_{n3} + T_{n4}$$

$$T_s = 264.228 \text{ kip-ft}$$

Torsional resistance due to tip:

$$L := 18 \text{ ft} \quad \gamma_{\text{conc}} := 150 \text{ pcf} \quad \phi_{\text{soil}} := 34 \text{ (degree)}$$

$$\mu := \tan(\phi_{\text{soil}} \cdot \pi \div 180) \quad \mu = 0.675$$

$$T_t := \pi \left(\frac{D}{2} \right)^2 \cdot L \cdot \gamma_{\text{conc}} \cdot \left(\frac{D}{3} \right) \cdot \mu \div 1000 \quad T_t = 30.514 \text{ kip-ft}$$

Total torsional resistance:

$$T_{\text{fdot}} := T_s + T_t \quad T_{\text{fdot}} = 294.742 \text{ kip-ft}$$

Prediction of torsional Resistance of TS3 (18 ft long x 4 ft diameter Drilled shaft)

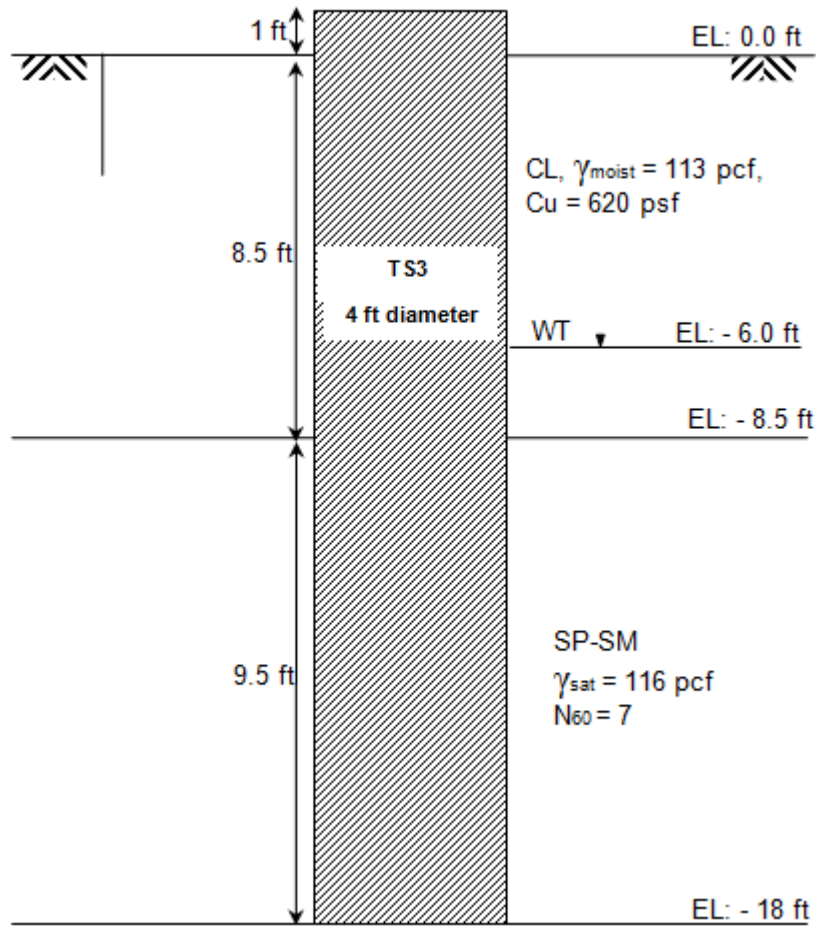


Figure E-3. Soil properties for the torsional resistance prediction of TS3

1) Depth dependent BETA(β) method or O'Neill and Hassan method

For sandy soils:

$$f_{SN} = \sigma'_v \cdot \beta$$

f_{SN} = nominal unit side resistance

β = side resistance coefficient

$$\beta = 1.5 - 0.135 \cdot \sqrt{Z} \quad \text{for } N_{60} \geq 15 \quad 0.25 \leq \beta \leq 1.2$$

$$\beta = (1.5 - 0.135 \cdot \sqrt{Z}) \cdot \frac{N_{60}}{15} \quad \text{for } N_{60} \geq 15$$

For clay:

$$f_{SN} = \alpha \cdot S_u$$

Coefficient $\alpha = 0.55$

Calculations:

i) Torsional resistance due to top 8.5 ft (EL 0.0 to 8.5)

$$S_u := 620 \text{ psf}$$

$$f_{SN1} := \alpha \cdot S_u \quad f_{SN1} = 341 \text{ psf}$$

$$T_{s1} := \frac{(\pi \cdot D \cdot 8.5 \cdot f_{SN1}) \cdot \left(\frac{D}{2}\right)}{1000} \quad T_{s1} = 72.847 \text{ kip} - \text{ft}$$

ii) Torsional resistance from EL -8.5 to -18)

$$N_{60} := 7 \quad Z := 13.25 \text{ ft}$$

$$\sigma'_v := 6 \cdot 113 + 2.5 \cdot (113 - 62.4) + 4.75 \cdot (116 - 62.4) \quad \sigma'_v = 1059.1 \text{ psf}$$

$$\beta := (1.5 - 0.135 \cdot \sqrt{Z}) \cdot \frac{N_{60}}{15} \quad \beta = 0.471$$

$$f_{SN2} := \sigma'_v \cdot \beta \quad f_{SN2} = 498.494 \text{ psf}$$

$$T_{s2} := (\pi \cdot D \cdot 9.5 \cdot f_{SN2}) \cdot \left(\frac{D}{2}\right) \cdot \frac{1}{1000} \quad T_{s2} = 119.021 \text{ kip} - \text{ft}$$

Total Torsional resistance:

$$T_s := T_{s1} + T_{s2}$$

$$T_s = 191.868 \text{ kip} - \text{ft}$$

2) BETA (β) method with separate evaluation of K and δ (Rational Method)

(Ref: FHWA 2010, Drilled shafts: Construction Procedures and LRFD Design Methods)

For cohesionless soils:

$$f_{SN} = \beta \cdot \sigma'_v$$

$$\beta = (1 - \sin(\phi)) \cdot \left(\frac{\sigma'_p}{\sigma'_v}\right)^{\sin(\phi)} \cdot \tan(\phi) \leq K_p \cdot \tan(\phi)$$

β at depth less than 7.5 ft = β at 7.5 ft

$$\sigma'_p = 0.47 \cdot (N_{60})^m \cdot \text{pa} \quad \text{pa} := 2116 \text{ psf}$$

$$K_p = \left(\tan\left(45 + \frac{\phi}{2}\right) \right)^2$$

$$m := 0.8 \quad \text{for sandy silt to silty sand}$$

Calculations:

i) Torsional resistance due to top 8.5 ft (EL 0.0 to -8.5)

$$S_u := 620 \quad \text{psf}$$

$$f_{SN1} := \alpha \cdot S_u \quad f_{SN1} = 341 \quad \text{psf}$$

$$T_{s1} := \left(\pi \cdot D \cdot 8.5 \cdot f_{SN1} \right) \cdot \left(\frac{D}{2} \right) \cdot \frac{1}{1000} \quad T_{s1} = 72.847 \quad \text{kip}$$

ii) Torsional resistance from EL -8.5 to -18.0

$$N_{60} := 7 \quad Z := 13.25 \quad \text{ft}$$

$$\sigma'_v := 6 \cdot 113 + 2.5 \cdot (113 - 62.4) + 4.75 \cdot (116 - 62.4) \quad \sigma'_v = 1059.1 \quad \text{psf}$$

$$\phi := 32 \quad (\text{Degree})$$

$$K_p := \tan \left[\left(45 + \frac{\phi}{2} \right) \cdot \frac{\pi}{180} \right]^2 \quad K_p = 3.255$$

$$\sigma'_p := 0.47 \cdot (N_{60})^m \cdot \text{pa} \quad \sigma'_p = 4717.283 \quad \text{psf}$$

$$\beta := \min \left[\left(1 - \sin \left(\phi \cdot \frac{\pi}{180} \right) \right) \cdot \left(\frac{\sigma'_p}{\sigma'_v} \right)^{\sin \left(\phi \cdot \frac{\pi}{180} \right)} \cdot \tan \left(\phi \cdot \frac{\pi}{180} \right), K_p \cdot \tan \left(\phi \cdot \frac{\pi}{180} \right) \right]$$

$$\beta = 0.648$$

$$f_{SN2} := \sigma'_v \cdot \beta \quad f_{SN2} = 686.573 \quad \text{psf}$$

$$T_{s2} := \left(\pi \cdot D \cdot 9.5 \cdot f_{SN2} \right) \cdot \left(\frac{D}{2} \right) \cdot \frac{1}{1000} \quad T_{s2} = 163.927 \quad \text{kip - ft}$$

Total torsional resistance:

$$T_{s} := T_{s1} + T_{s2}$$

$$T_s = 236.774 \quad \text{kip - ft}$$

3) FDOT Re-revised OMEGA method

(Ref FDOT Structures Manual, Vol. 9, revised in January 2013)

$$T_n = \pi \cdot D \cdot L \cdot F_s \cdot \left(\frac{D}{2} \right) + \pi \left(\frac{D}{2} \right)^2 \cdot L \cdot \gamma_{\text{conc}} \cdot \left(\frac{D}{3} \right) \cdot \mu$$

$$F_s = \sigma_v \cdot \omega_{fdot} \quad \text{for sand}$$

$$F_{sc} = \alpha \cdot s_u \quad \text{for clay}$$

$$\mu = \tan(\phi_{soil})$$

$$\omega_{fdot} = 1.5 \cdot \left(\frac{N}{15} \right)$$

Calculations:

i) Torsional resistance due to top 8.5 ft (EL 0.0 to -8.5)

$$S_u := 620 \quad \text{psf}$$

$$f_{SN1} := \alpha \cdot S_u \quad f_{SN1} = 341 \quad \text{psf}$$

$$T_{s1} := \frac{(\pi \cdot D \cdot 8.5 \cdot f_{SN1}) \cdot \left(\frac{D}{2} \right)}{1000} \quad T_{s1} = 72.847 \quad \text{kip-ft}$$

ii) Torsional resistance from EL -8.5 to -18)

$$N_{60} := 7 \quad Z := 13.25 \quad \text{ft}$$

$$\sigma'_v := 6 \cdot 113 + 2.5 \cdot (113 - 62.4) + 4.75 \cdot (116 - 62.4) \quad \sigma'_v = 1059.1 \quad \text{psf}$$

$$f_{SN2} := \sigma'_v \cdot 1.5 \cdot \left(\frac{N_{60}}{15} \right) \quad f_{SN2} = 741.37 \quad \text{pcf}$$

$$T_{s2} := (\pi \cdot D \cdot 9.5 \cdot f_{SN2}) \cdot \left(\frac{D}{2} \right) \div 1000 \quad T_{s2} = 177.01 \quad \text{kip-ft}$$

Total Torsional resistance:

$$T_{s1} := T_{s1} + T_{s2}$$

$$T_s = 249.858 \quad \text{kip-ft}$$

Torsional resistance due to tip:

$$L := 18 \quad \text{ft} \quad \gamma_{conc} := 150 \quad \text{pcf} \quad \phi_{soil} := 32 \quad (\text{degree})$$

$$\mu := \tan(\phi_{soil} \cdot \pi \div 180) \quad \mu = 0.625$$

$$T_t := \pi \left(\frac{D}{2} \right)^2 \cdot L \cdot \gamma_{conc} \cdot \left(\frac{D}{3} \right) \cdot \mu \div 1000 \quad T_t = 28.268 \quad \text{kip-ft}$$

Total torsional resistance:

$$T_{fdot} := T_s + T_t$$

$$T_{fdot} = 278.126 \quad \text{kip-ft}$$

Torsional resistance prediction for Jet-grouted Piles

Table E-1. Torsional resistance using K_g method

Pile	Grout zone	Zone length $H(ft)$	Depth to middle of zone (ft)	Initial vertical eff. stress at middle σ'_{vo} (psf)	K_g at middle Fig.2-6	Grouted vertical eff. stress $\sigma'_{vg}=K_g \sigma'_{vo}$ (psf)	$\delta - \phi$	f_s (psf) (Eq. 2-2) ($\delta - \phi$)	A_s Surface area (ft ²)	Radius of grout zones (ft)	T_s Torsional resistance (kip-ft) ($\delta - \phi$)	Total (kip-ft) ($\delta - \phi$)
JP1	Top	7	6.5	717.3	2.33 ^a	1671.3	23.8° - 34°	1035-1758	83.84	1.916	167-282	450-768
	Bottom	7	14	1305.6	2 ^b	2611.2	25.2° - 36°	1752-3012	84.29	1.916	283-486	
JP2	Top	7	6.5	730.0	2.33 ^a	1700.9	23.8° - 34°	1053-1789	83.39	1.916	167-287	456-783
	Bottom	7	14	1331.4	2 ^b	2662.8	25.2° - 36°	1787-3072	85.77	1.916	289-496	

^a From Figure 2-6 for $\phi = 34^\circ$

^b Extrapolated from Figure 2-6 for $\phi = 36^\circ$

Table E-2. Torsional resistance using pressuremeter data

Pile	Grout zone	Zone length $H(ft)$	δ	Horizontal stress after grouting, σ_h (psi) Fig. 6-16	$f_s = \sigma_h \tan(\delta)$ (psf)	A_s Surface area (ft ²)	Radius of grout zones (ft)	T_s Torsional resistance (kip)	Total (kip-ft)
JP1	Top	7	23.8°	22	1397	83.84	1.916	224	772
	Bottom	7	25.2°	50	3388	84.29	1.916	548	
JP2	Top	7	23.8°	16	1016	83.39	1.916	163	598
	Bottom	7	25.2°	39	2643	85.77	1.916	435	

Table E-3. Torsional resistance using sustained tip grout pressures

Pile	Tip grout pressure (psi)	Effective tip area (in ²)	Skin resistance (kip)	Radius of grout zones (<i>ft</i>)	Torsional resistance (kip-ft)
JP1	290	1231	357	1.916	684
JP2	280-300	1231	345-369	1.916	661-707